**Title**
Crucial Connections: Plant Cell-Cell Communication by Plasmodesmata is affected by Signaling among the Organelles



**Author**
Runkel, Anne Mary

**Publication Date**
2016

Peer reviewed|Thesis/dissertation

# Crucial Connections: Plant Cell-Cell Communication by Plasmodesmata is affected by Signaling among the Organelles

By

Anne Mary Runkel

A dissertation submitted in partial satisfaction of the

requirements for the degree of

Doctor of Philosophy

in

Plant Biology

in the

Graduate Division

of the

University of California, Berkeley

Committee in charge:

Professor Patricia C. Zambryski, Chair
Professor Jennifer C. Fletcher
Professor Sarah C. Hake
Professor Gian Garriga

Summer 2016

Crucial Connections: Plant Cell-Cell Communication by Plasmodesmata is affected by Signaling among the Organelles



by

Anne Mary Runkel

Abstract

Crucial Connections: Plant Cell-Cell Communication by Plasmodesmata is affected by Signaling among the Organelles

by

Anne Mary Runkel

Doctor of Philosophy in Plant Biology

University of California, Berkeley

Professor Patricia Zambryski, Chair

Plant cells transport molecules through small channels called plasmodesmata (PD); these nanoscopic channels are ~30-50 nm in diameter and cross through cellulosic walls to connect neighboring cells. PD regulate the movement of key developmental factors (e.g. transcription factors, small RNAs, and hormones) from cell to cell, which influence the formation of new organs, cell types, embryos, and the meristem. Mutants that affect PD transport were identified indirectly, in screens for defective developmental processes (e.g. stomata formation or root development), and in screens directed at finding PD transport mutants.

The genes identified in mutant screens for altered PD transport encode proteins that do not localize to PD. These genes that affect PD transport include *INCREASED SIZE EXCLUSION LIMIT* (*ISE*) *1* and *ISE2*, which encode RNA helicase proteins that localize to mitochondria and plastids, respectively; *GFP ARRESTED TRAFFICKING 1* (*GAT1*), which encodes a plastid-localized thioredoxin; *CHAPERONIN CONTAINING TCP1 8* (*CCT8*), which encodes a cytoplasmic chaperonin subunit; and *DECREASED SIZE EXCLUSION LIMIT 1* (*DSE1*), which encodes a WD40-repeat protein found in the cytoplasm and nucleus.

Loss of *DSE1* causes decreased PD transport both in *Arabidopsis thaliana* embryos and in the leaves of a distantly related eudicot species *Nicotiana benthamiana*. Through transcriptome analysis, we demonstrate here that DSE1 affects the expression of seed maturation and abscisic acid (ABA) response genes and that ABA INSENSITIVE 5 (ABI5), a key ABA transcription factor, reduces cell-cell transport. Further, *dse1* embryos have reduced PD frequency, suggesting that the PD transport phenotype observed in this mutant is due to fewer PD in the cell wall.

We characterize a new PD mutant *ise3* that was identified in a screen for mutants with increased PD transport in *A. thaliana* embryos. *ISE3* encodes a SEL1-like repeat mitochondrial protein and we show that this protein interacts with an EMBRYO DEFECTIVE-mitochondrial-PPR-domain-containing protein in Bimolecular Fluorescence

Complementation. Loss of the *N. benthamiana* orthologs of *ISE3* or its interactor, *ISE3 INTERACTING PROTEIN 1* (*IPR1*), cause increased PD transport in leaves. We also show that ISE3, like ISE1 affects the expression of genes involved in reactive oxygen species (ROS) regulation and show that loss of *ISE3* or *IPR1* cause increased $H_2O_2$ production. These results support findings that ROS can regulate PD transport, and further suggest that the mitochondria and the plastids signal to the nucleus (through 'retrograde signaling') to coordinate nuclear gene expression and PD transport, in a pathway called 'organelle-nucleus-PD signaling', or ONPS. This thesis supports the growing body of evidence that intercellular transport is driven by critical intracellular signals and processes.

Retrograde signalling pathways require signal exchange among the organelles and the nucleus, and a putative pathway for this exchange is through "stromules," which are stroma-filled tubular extensions of plastids. Herein we describe the first identified signal transduction pathways initiated by the plastid that are linked to stromule formation. We show that stromule frequency is affected by light cues as well as by ROS and the redox status of the chloroplast. Finally, we demonstrate that isolated chloroplasts can make stromules, indicating that the plastid drives the formation of these tubule structures, which may be involved in intracellular signalling.

For my grandfather, who taught me to love plants and books.

## TABLE OF CONTENTS

## LIST OF FIGURES

## LIST OF FIGURES

(continued from previous page)

**Chapter 4: Chloroplasts extend stromules independently and in response to internal redox signals**

## LIST OF TABLES

## ACKNOWLEDGMENTS

This thesis work was possible because I had the support of many generous people, and I would like to point out those who made a lasting impact on me and who were integral to the completion of this project.

Foremost, I express my most sincere gratitude to my advisor Professor Patricia Zambryski and members of her research team, past and present. I would like to acknowledge the undergraduate researchers in the Zambryski lab, particularly Mary Ahern, and thank her for contributions to results herein.

Many thanks go to my thesis committee member Professor Sarah Hake, who, in addition to being a member of my thesis committee, provided guidance throughout my time at Berkeley, as the chair of my qualifying exam and as my graduate research rotation advisor. My thanks go to Professor Jennifer Fletcher, a member of my thesis committee, qualifying exam committee, and my advisor as a graduate student instructor. My thanks go to Professor Gian Garriga, a member of my thesis committee and qualifying exam committee, who provided insightful input on my work, with a perspective outside of the Plant and Microbial Biology Department. My thanks go to Professor Robert Fischer, who was my graduate research rotation advisor, my advisor as a graduate student instructor, and who provided valuable input on my research.

Thank you to my past research mentors, especially Professor David Sands and Professor Jeremy Ward, who were integral in supporting my development as a scientist.

Thank you to the Plant and Microbial Biology Department, with special thanks to Rocio Sanchez, the department's outstanding graduate advisor.

I would like to thank Denise Schichnes and Steven Ruzin of the College of Natural Resources Biological Imaging Facility who were an incredible resource and who provided support for the fluorescence microscopy results. My thanks go to Reena Zalpuri and Kent McDonald of the Electron Microscopy Lab for providing training and support for the transmission electron microscopy results. My thanks go to Minyong Chung, the Vincent J. Coates Genomics Sequencing Laboratory at UC Berkeley, and the California Institute for the Quantitative Biosciences (QB3) for their support and funding to conduct the RNA-sequencing results.

Thank you to the National Science Foundation for supporting my graduate research through a Graduate Research Fellowship. Thank you to the Daniel Arnon Fellowship Foundation and the Arnon family for providing funding support during my first year of graduate research.

My deepest thanks go to my loved ones and friends. Their support made this possible.

## CURRICULUM VITAE

**Education**

- University of CA, Berkeley – Ph.D. in Plant Biology (2011 - 2016)
- Middlebury College – B.A. in Biology**,** *summa cum laude* (2011)

**Experience**

- Thesis Research Student – Middlebury College (2010 - 2011)
- Visiting Researcher – University of MT, Bozeman and Maseno, Kenya (2011)
- Researcher – University of MT, Bozeman (2009)

**Teaching**

- Graduate Student Instructor – University of CA, Berkeley (2013 & 2015)
- Laboratory and Lecture Teaching Assistant – Middlebury College (2009 - 2010)

**Outreach Work**

- Bay Area Scientists in Schools (BASIS) – teaching (2011 - 2016)
- NSF-CAREER Grant Educational Outreach Grant – teaching (2010 - 2011)

**Selected Fellowships and Awards**

- National Science Foundation Graduate Research Fellow (2013 - 2016)
- Daniel Arnon Fellowship (2011 - 2012)
- Outstanding Graduate Student Instructor Awards (2014)
- Janet C. Curry '49 award in Biological Sciences (2011)
- Priscilla (Kay) Beck '52 Botanical Fellowship (2009)

**Selected Publications**

Brunkard JO†, Runkel AM†, [†co-first authors], and Zambryski PC (2015) Chloroplasts extend stromules independently in response to internal redox signals. *Proc Natl Acad Sci USA* **112**, 10044-9.

Brunkard JO†, Runkel AM†, [†co-first authors], and Zambryski PC (2015) Comment on “A promiscuous intermediate underlies the evolution of LEAFY DNA binding specificity.” *Science* **347**, 621.

Brunkard JO, Runkel AM, and Zambryski PC (2015) The cytosol must flow: intercellular transport through plasmodesmata. *Curr Opin Cell Biol* **35**, 13-20.

Buescher EM, Moon J, Runkel AM, Hake S, and Dilkes BP (2014) Natural variation at *sympathy for the ligule* controls penetrance of the semidominant *Liguleless narrow-R* mutation in *Zea mays*. *G3* **4**, 2297-06.

Brunkard JO, Burch-Smith TM, Runkel AM, and Zambryski PC (2015) Investigating plasmodesmata genetics with virus-induced gene silencing and an *Agrobacterium*-mediated GFP movement assay. *Methods Mol Biol* **1217**, 185-98.

Brunkard JO, Runkel AM, and Zambryski PC (2013) Plasmodesmata dynamics are coordinated by intracellular signaling pathways. *Curr Opin Plant Biol* **16**, 614-20.

**Selected Presentations**

Runkel, AM…Zambryski, PC (2015) “Developmental transitions in embryogenesis uncover a new pathway regulating plasmodesmata.” Presentation: American Society of Plant Biologists Conference, *Plant Biology*, Minneapolis, MN, USA.

Runkel, AM…Zambryski, PC (2014) “DSE1 interactors and a transcriptome identify a new pathway regulating plasmodesmata transport.” Poster: EMBO Conference, *Intercellular Communication in Plant Development and Disease*, Strasbourg, FR.

## Chapter 1: Introduction – a tale of plasmodesmata and organelles

**Content partially derived from publications:**

**Brunkard JO, Runkel AM, and Zambryski PC** (2013) Plasmodesmata dynamics are coordinated by intracellular signaling pathways. *Curr Opin Plant Biol* **16**, 614-620.

**Brunkard JO, Runkel AM, and Zambryski PC** (2015a) The cytosol must flow: intercellular transport through plasmodesmata. *Curr Opin Cell Biol* **35**, 13-20.

## Plasmodesmata structure

Plant cells, unlike animal cells, are separated by cellulosic walls. Cell walls create structural integrity and a barrier to pathogens, but they also pose a challenge for the movement of micro and macromolecules among cells. Plant cells transport molecules through small channels in the cell wall called plasmodesmata (PD).

Transmission electron microscopy (TEM) imaging reveal the structure of PD; these nanoscopic channels are ~30-50 nm in diameter and cross through the cell wall to connect neighboring cells (**Fig. 1A**) (reviewed in **Burch-Smith and Zambryski, 2012**). A few basic structural components make up PD: the cytosolic sleeve, where most molecules move between cells; the plasma membrane that is continuous between the connected cells; and strands of tightly compressed endoplasmic reticulum (ER) that make up the 'desmotubule' in the center of PD (**Fig. 1B**). While many PD simply cross the cell wall as a simple channel, some PD form branched, twinned, and complex structures (**Fig. 1A**) (**Burch-Smith and Zambryski, 2010; Burch-Smith et al., 2011a; Oparka et al., 1999**). Additional cellular components have been observed in PD, including cytoskeletal proteins (e.g. actin and myosin) (**White and Barton, 2011**), and a number of recently discovered PD localized proteins (**Table 1; Burch-Smith et al., 2012**). The function of PD localized proteins is the subject of ongoing research.

**Table 1. Recently discovered plasmodesmal localized proteins**

| Protein Name[1] | Protein Function | Reference |
|---|---|---|
| β-1,6-N-ACETYLGLUCOSAMINYL TRANSFERASE-LIKE ENZYME (GnTL) | Glycosyltransferase-like protein | (**Zalepa-King and Citovsky, 2013**) |
| CLAVATA1 (CLV1), ARABIDOPSIS CRINKLY4 (ACR4), STRUBBELIG (SUB), QUIRKY(QKY) | Receptor-like kinase | (**Stahl et al., 2013; Vaddepalli et al., 2014)** |
| GLUCAN SYNTHASE-LIKE 12 (GSL12) | Putative callose synthase, negatively regulates PD transport | (**Zavaliev et al., 2011; Vatén et al., 2011**) |
| LYSIN MOTIF DOMAIN-CONTAINING GPI-ANCHORED PROTEIN 2 (LYM2) | Receptor-like protein, negatively regulates PD transport in response to chitin | (**Amari et al., 2010; Faulkner et al., 2013**) |
| NETWORKED 1A (NET1A) | Actin-binding protein | (**Deeks et al., 2012**) |
| PD GERMIN-LIKE PROTEIN 1, 2 (PDGLP1,2) | Positively regulate PD transport | (**Ham et al., 2012**) |
| RETICULONS 3, 6 (RTNLB3,6) | Associate with the ER in the desmotubule of PD | (**Knox et al., 2015; Kriechbaumer et al., 2015**) |

[1] **Burch-Smith and Zambryski** (**2012**) describe additional proteins and cellular components of PD.

## Plasmodesmata function

How is plasmodesmatal transport regulated?

PD can transport small (e.g., sugars, ions, hormones) and large molecules (e.g., proteins and RNAs) (**Chaiwanon et al., 2016; Furuta et al., 2012; Wu and Gallagher, 2012; Xu et al., 2011**), and the movement of molecules through PD depends primarily on 1. the aperature of the PD, 2. the number of PD in the cell wall, 3. the size of the molecules to be transported, which is also linked to cytoplasmic streaming, and 4.

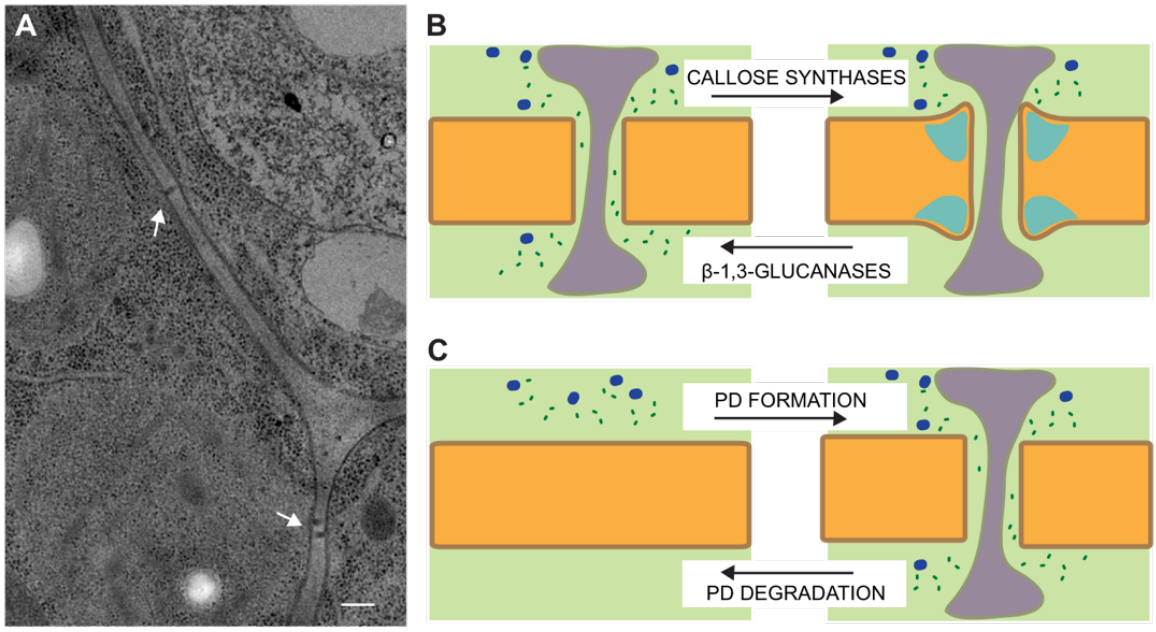


**Fig. 1. PD are nanoscopic channels that connect neighboring cells.** (**A**) TEM of PD in the plant cell wall. A simple PD (top) and a twinned PD (bottom) are noted by white arrows. (scale = 0.2 μm). (**B, left**) The cytosol (light green) is shown on either side of two neighboring cells. The cytosolic sleeve (light green) is where most molecules transport from cell to cell, and is the open area between the cell wall (wall is orange, with plasma membrane brown) and the tightly compressed desmotubule (purple). (**B, left**) PD can transport small (dark green dots) and large molecules (blue dots); smaller molecules move more readily through PD than larger molecules. (**B, right**) PD aperture is thought to be regulated by callose deposition (teal) in the cell wall surrounding PD. (**B**) Callose synthases promote callose formation and reduce PD transport, and β-1,3-glucanases degrade callose and increase PD transport. (**C, left**) The number of PD in the cell wall influence the ability for molecules to move between neighboring cells. Without PD, the molecules (dark green and blue dots) cannot move cell to cell. (**C, right**) With PD in the cell wall, molecules can move. (**C**) PD formation can occur during cell division and also after cell division. PD degradation can occur when specific cells need to be isolated.

sequestration or subcellular targeting of molecules (**Burch-Smith and Zambryski, 2012; Calderwood et al., 2016; Crawford and Zambryski 2000; Pickard, 2003; Rim et al., 2011**). Only certain proteins – such as viral proteins – are targeted to PD and move through cells in a directed manner (**Deng et al., 2015**; **Heinlein, 2015; Niehl and Heinlein, 2011**). Certain protein-protein interactions may be involved in regulating PD transport, as shown for CHAPERONIN CONTAINING TCP1 (CCT8), a chaperonin subunit, that is required for proper folding of the KNOTTED (KN1) transcription factor (TF) after KN1 moves through PD (**Xu et al., 2011; Fichtenbauer et al., 2012**). Generally, molecules move through PD without facilitation; however, and we describe these basic PD regulatory mechanisms here.

Presumably, PD with a wider diameter allow larger and more molecules to move cell to cell. PD aperture is regulated by callose deposition in the cell wall surrounding PD, and callose synthases promote callose formation at PD, thus reducing cell-cell transport (**Fig. 1B**) (**Botha et al., 2000; De Storme and Geelen, 2014; Lee et al., 2011; Vatén et al., 2011; Zavaliev et al., 2011**). Degradation of callose at PD is mediated by β-1,3-glucanases and results in increased PD transport (**Levy et al., 2007**).

Another mechanism regulating PD transport is the number of PD in the cell wall, which is regulated by PD formation and degradation (**Fig. 1C**). PD formation can occur during cell division (primary PD) and also after cell division (secondary PD) (**Burch-Smith and Zambryski, 2012; Burch-Smith et al., 2011a**). Secondary PD are necessary to form the connections between cells that are not the progeny of a cell division, such as the cells between the radial layers of the root. PD degradation is less generalized but can occur when specific cell types, such as stomata, need to be isolated.

To date, a few *Arabidopsis thaliana* mutants have been shown to alter PD formation. Two mutants with increased PD transport *increased size exclusion limit* (*ise*) *1* and *ise2* have higher proportions of twinned and branched PD in embryos (**Burch-Smith and Zambryski, 2010; Kim et al., 2002; Stonebloom et al., 2009**). A mutant with decreased PD transport *decreased size exclusion limit* (*dse1*) has fewer twinned and branched PD and reduced PD frequency in embryos (**Thesis Chapter 2; Xu et al., 2012**). A different mutant screen identified *gfp arrested trafficking* (*gat1*) with reduced PD transport; *gat1* does not affect PD frequency, but displays more branched and occluded PD in the root (**Benitez-Alfonso et al., 2009**).

Molecules themselves can affect cell-cell transport; smaller molecules move more readily through PD than larger molecules (**Fig. 1B**), which is at least in part related to cytoplasmic streaming (**Pickard, 2003**). Studies with heterologous fluorescent proteins, such as GFP, and large fluorescent dyes show that large molecules can move from cell to cell, and that the rate of movement is largely dependent on the size of the molecule (**Brunkard et al., 2015b; Crawford and Zambryski, 2001; Kim et al., 2002; Kim et al., 2005a; Kim et al., 2005b; Oparka et al., 1999; Roberts et al., 1997; Wu et al., 2003**).

Subcellular targeting and sequestration can also affect how specific molecules traffic through PD. Since nearly all plant cells are connected by PD, most molecules — including proteins — should be able to move cell to cell, so how are proteins retained, especially those that are necessary for a specific function in one cell or tissue? One mechanism is subcellular targeting or sequestration, which occurs when proteins are targeted to a part of the cell (e.g. nucleus, plastid, mitochondria, or ER). For example, the SHORT ROOT TF regulates root endodermis specification and it becomes trapped in the nucleus after association with the protein SCARECROW before it moves to a neighboring cell through PD (**Cui et al., 2007; Schiefelbein et al., 2014**). Similarly, when TRANSPARENT TESTA GLABRA 1 (TTG1), which is essential for trichome patterning, associates with GLABRA 3 (GL3), it becomes trapped in the nucleus (**Bouyer et al., 2008; Balkunde et al., 2011**).

Plasmodesmatal transport controls plant development

PD play a critical role in plant tissue formation and patterning, including the formation of new organs, cell types, embryos, and the meristem (**Benitez-Alfonso et al., 2013; Daum et al., 2014; Giannoutsou et al., 2013; Gisel et al., 1999; Gisel et al., 2002; Kim et al., 2002; Kim et al., 2005a; Kim et al., 2005b; Maule et al., 2013; Otero et al., 2016; Rinne and van der Schoot, 1998; Sanger and Lee, 2014; Vatén et al., 2011**), which is largely because PD regulate the movement of key developmental factors (e.g. TFs, small RNAs, and hormones) (**Furuta et al., 2012; Molnar et al., 2011; Gallagher et al., 2014**). In fact, TF movement through PD appears to be the rule rather than the exception (**Chen et al., 2013; Cui et al., 2007; Lee et al., 2006; Rim et al., 2011**; **Schiefelbein et al., 2014; Wu and Gallagher, 2011; Wu and Gallagher, 2012**). Since PD traffic developmental regulators, several screens for mutants with defective developmental processes have found weak mutant alleles of genes that affect PD. The role of PD in stomatal formation and root tissue and organ differentiation is well supported and is described here.

Genetic screens for defective stomatal complex formation found two mutants: *chorus* and *kobito1* that both have increased PD transport, allowing the TF SPEECHLESS (SPCH) to traffic out of a differentiating guard cell and initiate spurious stomatal formation (**Guseman et al., 2010; Kong et al., 2012; Pillitteri and Torii, 2012**). *chorus* is a weak recessive allele of *GLUCAN SYNTHASE-LIKE* (*GSL8*), a gene that encodes a putative callose synthase (**Guseman et al., 2010; Chen et al., 2009; Zavaliev et al., 2011**). Loss of *GSL8* results in very little callose accumulation at PD and, subsequently, increased PD transport (**Guseman et al., 2010**). *kobito1* mutants do not show defects in callose deposition at PD, instead, *kobito1* is involved in cellulose biosynthesis during cell expansion, and is an *abscisic acid (ABA) insensitive* (*abi*) mutant (**Brocard-Gifford et al., 2004**; **Kong et al., 2012; Pagant et al., 2002**).

In a screen for *A. thaliana* mutants with root stele developmental defects, a dominant mutation (*cals3-d*) in *GSL12*, which like *GSL8,* encodes a putative callose synthase, was found to increase callose deposition specifically in the cell wall surrounding PD. *cals3-d* decreases PD transport and prevents intercellular movement of the SHORT-

ROOT TF and a regulatory small RNA, miRNA156 (**Carlsbecker et al., 2010; Vatén et al., 2011**).

The formation of lateral root organs is also affected by PD transport; during lateral root organogenesis, PD transport into the emerging lateral root becomes more and more restricted as callose accumulates at the PD separating the lateral root from the main root axis (**Benitez-Alfonso et al., 2013; Maule et al., 2013**). Loss of *β-1,3 glucanases* (*PDBGs*) cause ectopic lateral root formation, and overexpression of *PDBGs* decrease lateral root formation (**Benitez-Alfonso et al., 2013**). Cellular isolation, caused by callose at PD, presumably allows the plant hormone auxin to accumulate in the lateral root primordia and initiate organogenesis (**Han et al., 2014; Maule et al., 2013**), possibly through cooperation/antagonism with other hormones like ABA and cytokinin (**Petricka et al., 2012; Shkolnik-Inbar and Bar-Zvi, 2010**).

**Intracellular signaling affects intercellular signaling**

In the last decade, mutant screens identified genes regulating PD transport. The first screen found altered movement of fluorescent tracers in *embryo defective* (*emb*) mutants, reasoning that any mutant with strong effects on PD transport would exhibit severely disrupted development (**Kim et al., 2002**). From this screen, *ise1*, *ise2*, and *dse1* have been characterized (**Burch-Smith and Zambryski, 2010; Burch-Smith et al., 2011b; Kim et al., 2002; Stonebloom et al., 2009**; **Xu et al., 2012**). Other genetic screens searched for mutants with decreased protein movement, and led to the characterization of two PD mutants: *gat1* and *cct8* (**Benitez-Alfonso et al., 2009; Xu et al., 2011; Fichtenbauer et al., 2012**).

Unexpectedly, none of the genes identified from these mutant screens encode proteins that localize to PD. ISE1 and ISE2 are RNA helicases that localize to mitochondria and plastids, respectively; DSE1 is a WD40-repeat protein found in the cytoplasm and nucleus that affects the expression of seed maturation and ABA response genes (**Thesis Chapter 2**); GAT1 is a plastid-localized thioredoxin; and CCT8 is a cytoplasmic chaperonin subunit. A newly characterized PD regulatory gene *ISE3* encodes a protein that is also not found at PD, but localizes instead in the mitochondria (**Thesis Chapter 3**).

There must be extensive signaling among organelles, the nucleus, and PD to coordinate intercellular transport. Many of the PD mutants identified to date contribute to a single narrative: PD function and formation are strongly affected by intracellular signals involving the mitochondria and plastids (**Fig. 2**). Beyond dramatically increasing PD transport and affecting PD formation (**Burch-Smith et al., 2010; Burch-Smith et al., 2011b**), loss of *ISE1* or *ISE2* also affects the expression of thousands of genes, many of which encode chloroplast proteins. Loss of *ISE3* also increases PD transport and affects the expression of nuclear and organellar genes (**Thesis Chapter 3**). Furthermore, although DSE1 is not found in the plastid or mitochondria, it affects the expression of genes involved in the ABA response pathway, a signaling pathway that is

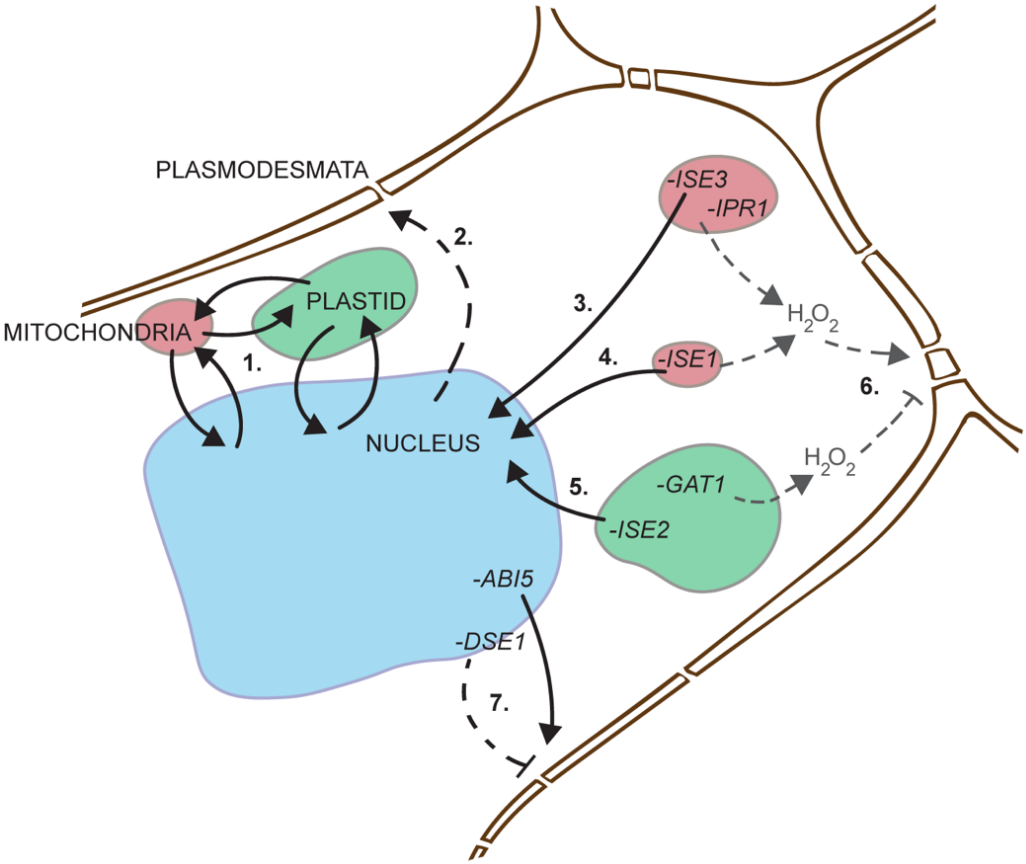


**Fig. 2. Cell-cell transport is driven by many proteins that do not localize at PD.** (**1**) Retrograde and anterograde signaling (arrows) coordinate organelles and the nucleus (**Kleine and Leister, 2016; Kleine et al., 2009**). (**2**) The nucleus affects the function of PD through unknown mechanisms (dotted arrow). (**3-5**) ISE1 is a mitochondrial protein, ISE2 is a plastid protein, and ISE3 is a mitochondrial protein; all affect the expression of nuclear genes encoding proteins that target to these organelles (**Burch-Smith et al., 2011b;** and results herein). (**6**) $H_2O_2$, affects PD transport (**Rutschow et al., 2011**; **Stonebloom et al., 2012**), and loss (shown with "-") of *ISE1*, *ISE3*, *IPR1*, or *GAT1* result in excessive $H_2O_2$ that may be generated by their respective organelles and may explain their PD transport phenotypes (**Benitez-Alfonso et al., 2009; Rutschow et al., 2011**; **Stonebloom et al., 2009; Stonebloom et al., 2012; Thesis Chapter 3**). (**7**) Loss (shown with "-") of *DSE1* affects the expression of nuclear-encoded genes, including the transcription factor ABI5, and loss of *DSE1* and *ABI5* signal (unknown) events to affect PD transport (**Thesis Chapter 2**). [Figure in **Thesis Chapter 3** – **Runkel AM†, Xu M†, Goodman HM, Zambryski PC** (in prep 2016) Loss of *ISE3,* a mitochondrial SEL1-like protein, increases plant cell-cell communication.]

involved in retrograde signaling (**Bobik and Burch-Smith, 2015; Kleine and Leister, 2016; León et al., 2013**).

Changes in the redox states of mitochondria or chloroplasts serve as upstream signals to rapidly alter PD transport (**Stonebloom et al., 2012**). Without the mitochondrial genes *ISE1* or *ISE3,* the reactive oxygen species (ROS) hydrogen peroxide ($H_2O_2$) over accumulates (**Stonebloom et al., 2009; Thesis Chapter 3**). Loss of the plastid *THIOREDOXIN-M3* (*gat1*) also leads to $H_2O_2$ accumulation, but *gat1* strongly reduces PD transport (**Benitez-Alfonso et al., 2009**). The origin of ROS (the mitochondria versus the plastids) and/or the concentration of $H_2O_2$ differentially affect PD transport (**Rutschow et al., 2011; Stonebloom et al., 2012**). $H_2O_2$ acts as a retrograde signaling molecule – for organelles to communicate with the nucleus (**Kleine and Leister, 2016; Kleine et al., 2009**) – which in turn may induce gene expression to affect PD transport. Disruptions in chloroplast or mitochondrial homeostasis trigger signal transduction pathways that affect nuclear gene expression, and likely, in turn affect PD transport (**Fig. 2**); this pathway is called 'organelle-nucleus-plasmodesmata signaling', or ONPS (**Burch-Smith and Zambryski, 2012; Bobik and Burch-Smith, 2015**; **Burch-Smith et al., 2011b**).

**How do organelles communicate with the nucleus to coordinate cellular functions?**

Retrograde signalling pathways rely on a fundamental missing link: the method for signal exchange among the organelles and the nucleus. How do the mitochondria and the plastids communicate with the nucleus to coordinate cellular functions? A putative route for signals to move between the plastids and the nucleus is through "stromules," which are stroma-filled tubular extensions of the plastids (**Caplan et al. 2015; Hanson and Sattarzadeh, 2011; Köhler et al., 1997**). Interestingly, the other two organelles primarily involved in ROS generation (a retrograde signal) produce stromule-like structures: matrixules of the mitochondria and peroxules of the peroxisomes (**Foyer and Noctor, 2007**).

Stromules have been observed in every cell type and in all land plant species investigated to date (**Natesan et al., 2005**), and such strong evolutionary conservation suggests stromules likely have a function. Other than a hypothesized role in intracellular signalling, however, stromules have no known function. Many conditions have been tested to perturb plant cells in attempts to alter stromule dynamics (an overview of conditions tested for altering stromule frequency are reported in **Table 2**). To date, stromule frequency is known to change in response to abiotic stress, plant hormone treatments and to massive disruption of whole-cell function. The strongest evidence for stromule involvement in cellular signaling was data collected by multiple groups showing that stromules could be affected by light (**Gray et al., 2012; Schattat et al., 2012**). We tested if light-sensing mechanisms within the chloroplast itself could be responsible for changes in stromule frequency, and found the first identified signal transduction pathways initiated by the chloroplast that are linked to stromule formation (**Fig. 3; Thesis Chapter 4**).

## Table 2. Physiological, chemical, or genetic effects on stromule frequency.

| Effect on Stromules | Testing | Treatment | Tissue | Reference[1] |
|---|---|---|---|---|
| Increase | Light/dark conditions | Daytime in 12h/12h day light cycle | *Arabidopsis thaliana* epidermis | **(Schattat, et al., 2012)** |
| | | Transition from constant light to constant dark | *Nicotiana tabacum* chloroplasts and *Triticum aestivum* leucoplasts | **(Gray et al., 2012)** |
| | Sugars | Sucrose or glucose | *A. thaliana* epidermis and *A. thaliana* mesophyll chloroplasts | **(Schattat and Klösgen, 2011)** |
| | Oxidizing agent | $H_2O_2$ | *T. aestivum* root hair leucoplasts; *Nicotiana benthamiana* chloroplasts and *A. thaliana* chloroplasts | **(Gray et al., 2012) (Caplan et al., 2015)** |
| | Temperature | Warm | *N. tabacum* chloroplasts | **(Gray et al., 2012; Holzinger et al. 2007)** |
| | Osmoticants | Mannitol | *T. aestivum* root hair leucoplasts | **(Gray et al., 2012)** |
| | | Polyethylene glycol 4000 | *N. tabacum* chloroplasts | **(Gray et al., 2012)** |
| | Salts | Sodium chloride (100 mM) or Potassium chloride (200 mM) | *N. tabacum* hypocotyl epidermis chloroplasts and *T. aestivum* root hair leucoplasts | **(Gray et al., 2012)** |
| | Plant hormones | Abscisic acid | *N. tabacum* chloroplasts | **(Gray et al., 2012)** |
| | | Ethylene (ACC) | *N. tabacum* chloroplasts and *T. aestivum* root hair leucoplasts | **(Gray et al., 2012)** |
| | | Methyl jasmonate | *T. aestivum* root hair leucoplasts | **(Gray et al., 2012)** |
| | | Cytokinin produced by *A. tumefaciens* GV3101::pMP90 | *N. benthamiana* chloroplasts; *N. tabacum* chloroplasts | **(Erickson et al. 2014; Schattat, et al., 2012)** |
| | | INA (SA analog) | *Nicotiana benthamiana* chloroplasts and *A. thaliana* chloroplasts | **(Caplan et al., 2015)** |
| | Physical disruption to leaf | Leaf detached for 4 hours | *N. tabacum* chloroplasts | **(Gray et al., 2012)** |
| Decrease | Light/dark conditions | Nighttime | *A. thaliana* epidermis | **(Schattat and Klösgen, 2011)** |
| | | Etiolated seedlings exposed to white, red, or far-red light | *N. tabacum* transition from etioplast to chloroplast | **(Gray et al., 2012)** |
| | Temperature | Cold | *N. tabacum* chloroplasts | **(Gray et al., 2012; Holzinger et al. 2007)** |
| | Plant hormones | Salicylic acid | *N. tabacum* chloroplasts and *T. aestivum* root hair leucoplasts | **(Gray et al., 2012)** |
| | | Silver nitrate (inhibitor of ethylene action) | *N. tabacum* chloroplasts and *T. aestivum* root hair leucoplasts | **(Gray et al., 2012)** |
| | Translation inhibitor (cytosol) | Cycloheximide | *A. thaliana* epidermis (only considered leucoplasts) | **(Schattat and Klösgen, 2011)** |
| | Cytoskeleton inhibitors | RNAi of myosin XI, BDM, Latrunculin B, Cytochalasin D | *N. benthamiana* epidermis chloroplasts | **(Natesan et al. 2009)** |
| | Fruit ripening inhibitor | *ripening inhibitor* mutant | *S. lycopersicum* fruit inner mesocarp amyloplasts | **(Waters et al., 2004)** |
| No effect | Sugars | Fructose | *A. thaliana* epidermis (only considered leucoplasts) | **(Schattat and Klösgen, 2011)** |
| | Osmoticants | Mannitol or sorbitol | *A. thaliana* epidermis (only considered leucoplasts) | **(Schattat and Klösgen, 2011)** |
| | Plant hormones (ABA inhibitor) | Abamine or norflurazon | *T. aestivum* root hair leucoplasts | **(Gray et al., 2012)** |
| | Translation inhibitor (plastid) | Streptomycin or Spectinomycin | *A. thaliana* epidermis (only considered leucoplasts) | **(Schattat and Klösgen, 2011)** |
| | | Lincomycin or Erythromycin, | *N. tabacum* chloroplasts | **(Gray et al., 2012)** |
| | Translation inhibitor (cytosol) | Anisomycin, or Cycloheximide | *N. tabacum* chloroplasts | **(Gray et al., 2012)** |
| | Cytoskeleton inhibitors | APM or Oryzalin | *N. benthamiana* epidermis chloroplasts | **(Natesan et al. 2009)** |

[1] Quantitative studies of stromule frequencies, and of data collected using plastid-targeted florescent proteins with *in planta* (not cell culture) approaches.

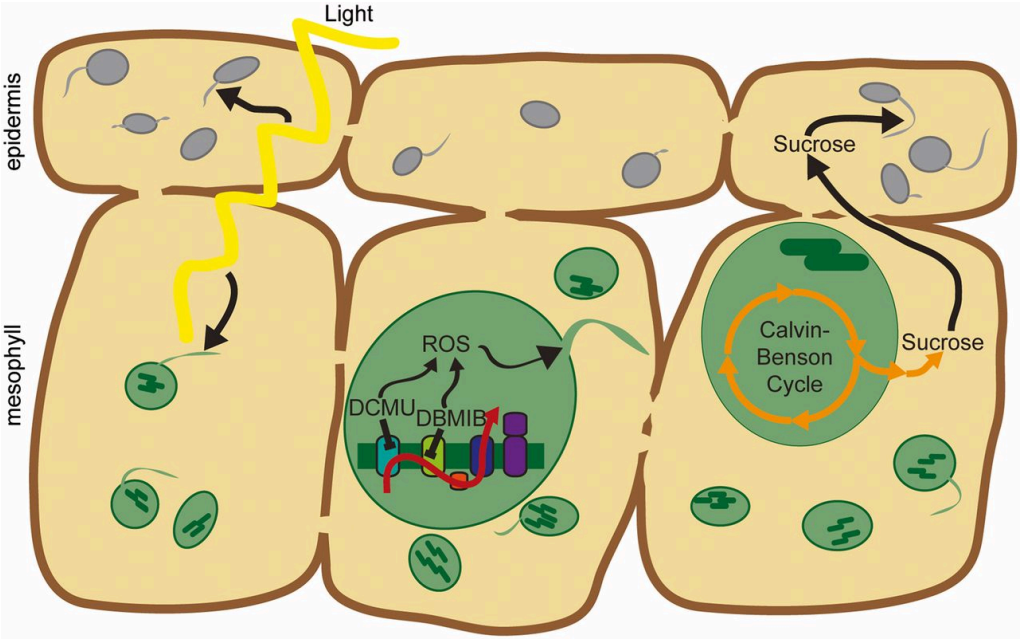


**Fig. 3. Stromules are initiated by signals within the chloroplast.** (Left) Stromule frequency increases in the light (daytime) in both chloroplasts and leucoplasts. (Center) ROS generated from the pETC trigger stromule formation in chloroplasts. (Right) Sucrose promotes stromule formation in leucoplasts, but not chloroplasts. Sucrose is synthesized in the cytosol from products of the Calvin–Benson cycle in chloroplasts and then moves into neighboring heterotrophic pavement cells via plasmodesmata. For simplicity of presentation, only photosynthetic mesophyll cells are shown (and not photosynthetic guard cells), because there is no evidence suggesting that stromules in these cell types behave differently. [Figure in **Thesis Chapter 4** and published in **Brunkard JO**[†]**, Runkel AM**[†]**, Zambryski PC** (2015) Chloroplasts extend stromules independently and in response to internal redox signals. *Proc Natl Acad Sci USA.* **112**, 10044-10049.]

**Overview of thesis chapters**

**Thesis Chapter 2:** The cytoplasmic WD40 repeat protein DSE1 is involved in one or more cellular pathways that affect PD transport, and at least in part, DSE1 controls the number of PD that form. The *dse1* transcriptome and comparisons to the transcriptomes of phenotypically-similar *leafy cotyledon* mutants and the *ise1* and *ise2* mutants suggest that *DSE1* is involved in pathways regulated by abscisic acid (ABA). ABA regulation of PD transport was hinted at before (**Brocard-Gifford et al., 2004; Han and Kim 2016; Kong et al., 2012; Moore-Gordon et al., 1998; Shkolnik-Inbar and Bar-Zvi, 2010**), and we show that ABI5, one of the major ABA transcription factors, reduces cell-cell transport.

**Thesis Chapter 3:** A newly identified PD mutant *ise3* causes increased PD transport. ISE3, like ISE1, is a mitochondrial localized protein. An EMB-mitochondrial-PPR-domain-containing protein interacts with ISE3 in bimolecular fluorescence complementation, and loss of the *Nicotiana benthamiana* orthologs of *ISE3* or its interactor, *ISE3 INTERACTING PROTEIN 1* (*IPR1*), cause increased PD transport in leaves and loss of these genes also cause increased $H_2O_2$ production. Further, a transcriptome analysis of *ise3* mutant embryos suggest ISE3 is involved in reactive oxygen species (ROS) regulation. These data provide further support for an emerging hypothesis that ROS can regulate PD transport.

**Thesis Chapter 4:** Plastids are capable of generating stromules through internal signalling pathways. Stromule frequency is driven by light cues as well as by ROS and the redox status of the chloroplast. Further, the by-product of photosynthesis, sucrose, induced stromules in non-photosynthetic leucoplast plastids. Finally, we discovered that isolated chloroplasts could make stromules, indicating that the plastid drives the formation of its own tubule structures.

## REFERENCES

**Amari K, Boutant E, Hofmann C, Schmitt-Keichinger C, Fernandez-Calvino L, Didier P, Lerich A, Mutterer J, Thomas CL, Heinlein M, et al.** (2010) A family of plasmodesmal proteins with receptor-like properties for plant viral movement proteins. *PLoS Path* **6**, 1-10.

**Balkunde R, Bouyer D, and Hülskamp M** (2011) Nuclear trapping by GL3 controls intercellular transport and redistribution of TTG1 protein in *Arabidopsis*. *Development* **138**, 5039-5048.

**Benitez-Alfonso Y, Cilia M, San Roman A, Thomas C, Maule A, Hearn S, and Jackson D** (2009) Control of *Arabidopsis* meristem development by thioredoxin-dependent regulation of intercellular transport. *Proc Natl Acad Sci USA* **106**, 3615-3620.

**Benitez-Alfonso Y, Faulkner C, Pendle A, Miyashima S, Helariutta A, and Maule A** (2013) Symplastic intercellular connectivity regulates lateral root patterning. *Dev Cell* **26**,136-147.

**Bobik K, and Burch-Smith TM** (2015) Chloroplast signaling within, between and beyond cells. *Front Plant Sci* **6**, 781.

**Botha CEJ, Cross RHM, Bel AJE, and Peter CI** (2000) Phloem loading in the sucrose-export-defective (SXD-1) mutant maize is limited by callose deposition at plasmodesmata in bundle sheath—vascular parenchyma interface. *Protoplasma* **214**, 65-72.

**Bouyer D, Geier F, Kragler F, Schnittger A, Pesch M, Wester K, Balkunde R, Timmer J, Fleck C, and Hülskamp M** (2008) Two-dimensional patterning by a trapping/depletion mechanism: the role of TTG1 and GL3 in *Arabidopsis* trichome formation. *PLoS Biol* **6**, e141.

**Brocard-Gifford I, Lynch TJ, Garcia ME, Malhotra B, and Finkelstein RR** (2004) The *Arabidopsis thaliana ABSCISIC ACID-INSENSITIVE8* locus encodes a novel protein mediating abscisic acid and sugar responses essential for growth. *Plant Cell* **16**, 406-421.

**Brunkard JO, Burch-Smith TM, Runkel AM, and Zambryski PC** (2015b) Investigating plasmodesmata genetics with virus-induced gene silencing and an *Agrobacterium*-mediated GFP movement assay. *Methods Mol Biol* **1217**, 185-198.

**Burch-Smith TM, and Zambryski PC** (2010) Loss of INCREASED SIZE EXCLUSION LIMIT (ISE)1 or ISE2 increases the formation of secondary plasmodesmata. *Curr Biol* **20**, 989-993.

**Burch-Smith TM, and Zambryski PC** (2012) Plasmodesmata paradigm shift: Regulation from without versus within. *Annu Rev Plant Biol* **63**, 239-260.

**Burch-Smith TM, Stonebloom S, Xu M, and Zambryski PC** (2011a) Plasmodesmata during development: re-examination of the importance of primary, secondary, and branched plasmodesmata structure versus function. *Protoplasma* **248**, 61-74.

**Burch-Smith TM, Brunkard JO, Choi YG, and Zambryski PC** (2011b) Organelle-nucleus cross-talk regulates plant intercellular communication via plasmodesmata. *Proc Natl Acad Sci USA* **108**, 1451-1460.

**Calderwood A, Kopriva S, and Morris RJ** (2016) Transcript abundance explains mRNA mobility data in *Arabidopsis thaliana*. *Plant Cell* **28**, 610-605.

**Caplan JL, Kumar AS, Park E, Padmanabhan MS, Hoban K, Modla S, Czymmek K, and Dinesh-Kumar SP** (2015) Chloroplast stromules function during innate immunity. *Dev Cell* **34**, 45-57.

**Carlsbecker A, Lee JY, Roberts, CJ, Dettmer J, Lehesranta S, Zhou J, Lindgren O, Moreno-Risueno MA, Vatén A, Thitamadee S, et al.** (2010) Cell signalling by microRNA165/6 directs gene dose-dependent root cell fate. *Nature* **465**, 316-321.

**Chaiwanon J, Wang W, Zhu JY, Oh E, and Wang ZY** (2016) Information integration and communication in plant growth regulation. *Cell* **164**, 1257-1268.

**Chen H, Ahmad M, Rim Y, Lucas WJ, and Kim J-Y** (2013) Evolutionary and molecular analysis of Dof transcription factors identified a conserved motif for intercellular protein trafficking. *New Phytol* **198**, 1250-1260.

**Chen XY, Liu L, Lee E, Han X, Rim Y, Chu H, Kim SW, Sack F, and Kim JY** (2009) The *Arabidopsis* callose synthase gene *GSL8* is required for cytokinesis and cell patterning. *Plant Physiol* **150**, 105-113.

**Crawford KM, and Zambryski PC** (2000) Subcellular localization determines the availability of non-targeted proteins to plasmodesmatal transport. *Curr Biol* **10**, 1032-1040.

**Crawford KM, and Zambryski PC** (2001). Non-targeted and targeted protein movement through plasmodesmata in leaves in different developmental and physiological states. *Plant Physiol*, **125,** 1802-1812.

**Cui H, Levesque MP, Vernoux T, Jung JW, Paquette AJ, Gallagher KL, Wang JY, Blilou I, Scheres B, and Benfey PN** (2007) An evolutionarily conserved mechanism delimiting SHR movement defines a single layer of endodermis in plants. *Science* **316**, 421-425.

**Daum G, Medzihradszky A, Suzaki T, and Lohmann JU** (2014) A mechanistic framework for noncell autonomous stem cell induction in *Arabidopsis*. *Proc Natl Acad Sci USA* **111**,14619-14624.

**De Storme N, and Geelen D** (2014) Callose homeostasis at plasmodesmata: molecular regulators and developmental relevance. *Front Plant Sci* **5**, 138.

**Deeks MJ, Calcutt JR, Ingle EKS, Hawkins TJ, Chapman S, Richardson AC, Mentlak DA, Dixon MR, Cartwright F, Smertenko AP, et al.** (2012) A superfamily of actin-binding proteins at the actin-membrane nexus of higher plants. *Curr Biol* **22**, 1595-1600.

**Deng P, Wu Z, and Wang A** (2015) The multifunctional protein CI of potyviruses plays interlinked and distinct roles in viral genome replication and intercellular movement. *Virol J* **12**, 141.

**Erickson JL, Ziegler J, Guevara D, Abel S, Klösgen RB, Mathur J, Rothstein SJ, and Schattat MH** (2014) Agrobacterium-derived cytokinin influences plastid morphology and starch accumulation in *Nicotiana benthamiana* during transient assays. *BMC Plant Biol* **14**, 127.

**Faulkner C, Petutschnig E, Benitez-Alfonso Y, Beck M, and Robatzek S** (2013) LYM2-dependent chitin perception limits molecular flux via plasmodesmata. *Proc Natl Acad Sci USA* **110**, 9166-9170.

**Fichtenbauer D, Xu XM, Jackson D, and Kragler F** (2012) The chaperonin CCT8 facilitates spread of tobamovirus infection. *Plant Signal & Behav* **7**, 318-321.

**Foyer CH, and Noctor G** (2007) Shape-shifters building bridges? Stromules, matrixules and metabolite channelling in photorespiration. *Trends Plant Sci* **12**, 381-383.

**Furuta K, Lichtenberger R, and Helariutta Y** (2012) The role of mobile small RNA species during root growth and development. *Curr Opin Cell Biol* **24**, 211-216.

**Gallagher KL, Sozzani R, and Lee CM** (2014) Intercellular protein movement: deciphering the language of development. *Annu Rev Cell Dev Biol*, **30** 207-233.

**Giannoutsou E, Sotiriou P, Apostolakos P, and Galatis B** (2013) Early local differentiation of the cell wall matrix defines the contact sites in lobed mesophyll cells of Zea mays. *Ann Bot* **112**, 1067-1081.

**Gisel A, Barella S, Hempel FD, and Zambryski PC** (1999) Temporal and spatial regulation of symplastic trafficking during development in *Arabidopsis thaliana* apices. *Development* **126**, 1879-1889.

**Gisel A, Hempel FD, Barella S, and Zambryski P** (2002) Leaf-to-shoot apex movement of symplastic tracer is restricted coincident with flowering in *Arabidopsis*. *Proc Natl Acad Sci USA* **99**, 1713-1717.

**Gray JC, Hansen MR, Shaw DJ, Graham K, Dale R, Smallman P, Natesan SK, and Newell CA** (2012) Plastid stromules are induced by stress treatments acting through abscisic acid. *Plant J* **69**, 387-398.

**Guseman JM, Lee JS, Bogenschutz NL, Peterson KM, Virata RE, Xie B, Kanaoka MM, Hong Z, and Torii KU** (2010) Dysregulation of cell-to-cell connectivity and stomatal patterning by loss-of-function mutation in *Arabidopsis chorus* (*glucan synthase-like 8*). *Development* **137**, 1731-1741.

**Ham B-K, Li G, Kang B-H, Zeng F, and Lucas WJ** (2012) Overexpression of *Arabidopsis* plasmodesmata germin-like proteins disrupts root growth and development. *Plant Cell* **24**, 3630-3648.

**Han X, and Kim JY** (2016) Integrating hormone- and micromolecule-mediated signaling with plasmodesmal communication. *Mol Plant* **9**, 46-56.

**Han X, Hyun TK, Zhang M, Kumar R, Koh EJ, Kang BH, Lucas WJ, and Kim JY.** (2014) Auxin-callose-mediated plasmodesmal gating is essential for tropic auxin gradient formation and signaling *Dev Cell*, **28** 132-146.

**Hanson MR, and Sattarzadeh A** (2011) Stromules: Recent insights into a long neglected feature of plastid morphology and function. *Plant Physiol* **155**, 1486-1492.

**Heinlein M** (2015) Plasmodesmata: channels for viruses on the move. In *Plasmodesmata: Methods and Protocols* (ed. Manfred Heinlein), pp. 25-54. Springer International Publishing, New York.

**Holzinger A, Buchner O, Lütz C, and Hanson MR** (2007) Temperature-sensitive formation of chloroplast protrusions and stromules in mesophyll cells of *Arabidopsis thaliana*. *Protoplasma* **230**, 23-30.

**Kim I, Hempel FD, Sha K, Pfluger J, and Zambryski PC** (2002) Identification of a developmental transition in plasmodesmatal function during embryogenesis in *Arabidopsis thaliana*. *Development* **129**, 1261-1272.

**Kim I, Cho E, Crawford K, Hempel FD, and Zambryski PC** (2005a) Cell-to-cell movement of GFP during embryogenesis and early seedling development in *Arabidopsis*. *Proc Natl Acad Sci USA* **102**, 2227-2231.

**Kim I, Kobayashi K, Cho E, and Zambryski PC** (2005b) Subdomains for transport via plasmodesmata corresponding to the apical-basal axis are established during *Arabidopsis* embryogenesis. *Proc Natl Acad Sci USA* **102**, 11945-11950.

**Kleine T, and Leister D** (2016) Retrograde signaling: Organelles go networking. *Biochim Biophys Acta* **1857**, 1313-1325.

**Kleine T, Maier UG, and Leister D** (2009) DNA transfer from organelles to the nucleus: the idiosyncratic genetics of endosymbiosis. *Annu Rev Plant Biol* **60**, 115-138.

**Knox K, Wang P, Kriechbaumer V, Tilsner J, Frigerio L, Sparkes I, Hawes C, and Oparka KJ** (2015) Putting the squeeze on plasmodesmata: a role for reticulons in primary plasmodesmata formation. *Plant Physiol* **168**, 1563-1572.

**Köhler RH, Cao J, Zipfel WR, Webb WW, and Hanson MR** (1997) Exchange of protein molecules through connections between higher plant plastids. *Science* **276**, 2039-2042.

**Kong D, Karve R, Willet A, Chen MK, Oden J, and Shpak ED** (2012) Regulation of plasmodesmatal permeability and stomatal patterning by the glycosyltransferase-like protein KOBITO1. *Plant Physiol* **159**, 156-168.

**Kriechbaumer V, Botchway SW, Slade SE, Knox K, Frigerio L, Oparka K, and Hawes C** (2015) Reticulomics: protein-Protein interaction studies with two plasmodesmata-localized reticulon family proteins identify binding partners enriched at plasmodesmata, endoplasmic reticulum, and the plasma membrane. *Plant Physiol* **169**, 1933-1945.

**Lee J-Y, Colinas J, Wang JY, Mace D, Ohler U, and Benfey PN** (2006) Transcriptional and posttranscriptional regulation of transcription factor expression in *Arabidopsis* roots. *Proc Natl Acad Sci USA* **103**, 6055-6060.

**Lee J-Y, Wang X, Cui W, Sager R, Modla S, Czymmek K, Zybaliov B, van Wijk K, Zhang C, Lu H, et al.** (2011) A plasmodesmata-localized protein mediates crosstalk between cell-to-cell communication and innate immunity in *Arabidopsis*. *Plant Cell* **23**, 3353-3373.

**León P, Gregorio J, and Cordoba E** (2013) ABI4 and its role in chloroplast retrograde communication. *Front Plant Sci* **3**, 304.

**Levy A, Erlanger M, Rosenthal M, and Epel BL** (2007) A plasmodesmata-associated beta-1,3-glucanase in *Arabidopsis*. *Plant J* **49**, 669-682.

**Maule A, Gaudioso-Pedraza R, and Benitez-Alfonso Y.** (2013) Callose deposition and symplastic connectivity are regulated prior to lateral root emergence. *Commun Integr Biol* **6**, e26531.

**Molnar A, Melnyk C, and Baulcombe DC** (2011) Silencing signals in plants, a long journey for small RNAs. *Genome Biol* **12**, 215.

**Moore-Gordon CS, Cowan AC, Bertling I, Botha, CEJ, and Cross RHM** (1998) Symplastic solute transport and Avocado fruit development: a decline in cytokinin/ABA ratio is related to appearance of the Hass small fruit variant. *Plant Cell Physiol* **39**, 1027-1038.

**Natesan SK, Sullivan JA, and Gray JC** (2005) Stromules: A characteristic cell-specific feature of plastid morphology. *J Exp Bot* **56**, 787-797.

**Natesan SK, Sullivan JA, and Gray JC** (2009) Myosin XI is required for actin-associated movement of plastid stromules. *Mol Plant* **2**, 1262-1272.

**Niehl A, and Heinlein M** (2011) Cellular pathways for viral transport through plasmodesmata. *Protoplasma* **248**, 75-99.

**Oparka KJ, Roberts AG, Boevink P, Santa Cruz S, Roberts I, Pradel KS, Imlau A, Kotlizky G, Sauer N, and Epel B** (1999) Simple, but not branched, plasmodesmata allow the nonspecific trafficking of proteins in developing tobacco leaves. *Cell* **97**, 743-754.

**Otero S, Helariutta Y, and Benitez-Alfonso Y** (2016) Symplastic communication in organ formation and tissue patterning. *Curr Opin Plant Biol* **29**, 21-28.

**Pagant S, Bichet A, Sugimoto K, Lerouxel O, Desprez T, Mccann M, Lerouge P, Vernhettes S, and Höfte H** (2002) *KOBITO1* encodes a novel plasma membrane protein necessary for normal synthesis of cellulose during cell expansion in *Arabidopsis*. *Plant Cell* **14**, 2001-2013.

**Petricka JJ, Winter CM, and Benfey PN** (2012) Control of *Arabidopsis* root development. *Annu Rev Plant Biol* **63**, 563-590.

**Pickard WF** (2003) The role of cytoplasmic streaming in symplastic transport. *Plant Cell Environ* **26**, 1-15.

**Pillitteri LJ, and Torii KU** (2012) Mechanisms of stomatal development. *Ann Rev Plant Biol* **63**, 591-614.

**Rim Y, Huang L, Chu H, Han X, Cho WK, Jeon CO, Kim HJ, Hong J-C, Lucas WJ, and Kim JY** (2011) Analysis of *Arabidopsis* transcription factor families revealed extensive capacity for cell-to-cell movement as well as discrete trafficking patterns. *Mol Cells* **32**, 519-526.

**Rinne PL, and van der Schoot C** (1998) Symplasmic fields in the tunica of the shoot apical meristem coordinate morphogenetic events. *Development* **125**, 1477-1485.

**Roberts AG, Santz Cruz S, Roberts IM, Prior DAM, Turgeon R, and Oparka KJ** (1997) Phloem unloading in sink leaves of *Nicotiana benthamiana*: comparison of a fluorescent solute with a fluorescent virus. *Plant Cell*, **9** 1381-1396.

**Runkel AM, Brunkard JO, Ahern, MA, Xu, M, and Zambryski PC** (*submitted and under review*, 2016) The *dse1* transcriptome reveals that ABI5 down-regulates plasmodesmatal transport.

**Rutschow HL, Baskin TI, and Kramer EM** (2011) Regulation of solute flux through plasmodesmata in the root meristem. *Plant Physiol* **155**, 1817-1826.

**Sanger R, and Lee JY** (2014) Plasmodesmata in integrated cell signalling: insights from development and environmental signals and stresses. *J Exp Bot* **65**, 6337-6358.

**Schattat MH, and Klösgen RB** (2011) Induction of stromule formation by extracellular sucrose and glucose in epidermal leaf tissue of *Arabidopsis thaliana*. *BMC Plant Biol* **11**, 115.

**Schattat MH, Klösgen RB, and Mathur J** (2012) New insights on stromules: Stroma filled tubules extended by independent plastids. *Plant Signal Behav* **7**, 1132-1137.

**Schiefelbein J, Huang L, and Zheng X** (2014) Regulation of epidermal cell fate in *Arabidopsis* roots: the importance of multiple feedback loops. *Front Plant Sci,* doi: 10.3389/fpls.2014.00047.

**Shkolnik-Inbar D, and Bar-Zvi D** (2010) ABI4 mediates abscisic acid and cytokinin inhibition of lateral root formation by reducing polar auxin transport in *Arabidopsis*. *Plant Cell* **22**, 3560-3573.

**Stahl Y, Grabowski S, Bleckmann A, Kühnemuth R, Weidtkamp-Peters S, Pinto KG, Kirschner GK, Schmid JB, Wink RH, Hülsewede A, et al.** (2013) Moderation of *Arabidopsis* root stemness by CLAVATA1 and ARABIDOPSIS CRINKLY4 receptor kinase complexes. *Curr Biol* **23**, 362-371.

**Stonebloom S, Burch-Smith T, Kim I, Meinke D, Mindrinos M, and Zambryski P** (2009) Loss of the plant DEAD-box protein ISE1 leads to defective mitochondria and increased cell-to-cell transport via plasmodesmata. *Proc Natl Acad Sci USA* **106**, 17229-17234.

**Stonebloom S, Brunkard JO, Cheung AC, Jiang K, Feldman LJ, and Zambryski PC** (2012) Redox states of plastids and mitochondria differentially regulate intercellular transport via plasmodesmata. *Plant Physiol* **158**, 190-199.

**Vaddepalli P, Herrmann A, Fulton L, Oelschner M, Hillmer S, Stratil TF, Fastner A, Hammes UZ, Ott T, Robinson DG, and Schneitz K** (2014) The C2-domain protein

QUIRKY and the receptor-like kinase STRUBBELIG localize to plasmodesmata and mediate tissue morphogenesis in *Arabidopsis thaliana*. *Development* **141**, 4139-4148.

**Vatén A, Dettmer J, Wu S, Stierhof Y-D, Miyashima S, Yadav SR, Roberts CJ, Campilho A, Bulone V, Lichtenberger R, et al.** (2011) Callose biosynthesis regulates symplastic trafficking during root development. *Dev Cell* **21**, 1144-1155.

**Waters MT, Fray RG, and Pyke KA** (2004) Stromule formation is dependent upon plastid size, plastid differentiation status and the density of plastids within the cell. *Plant J* **39**, 655-667.

**White RG, and Barton DA** (2011) The cytoskeleton in plasmodesmata: a role in intercellular transport? *J Exp Bot*, **62**, 5249-5266.

**Wu S, and Gallagher KL** (2011) Mobile protein signals in plant development. *Curr Opin Plant Biol* **14**, 563-570.

**Wu S, and Gallagher KL** (2012) Transcription factors on the move. *Curr Opin Plant Biol* **15**, 645-651.

**Wu X, Dinneny JR, Crawford KM, Rhee Y, Citovsky V, Zambryski PC, and Weigel D** (2003) Modes of intercellular transcription factor movement in the *Arabidopsis* apex. *Development* **130**, 3735-3745.

**Xu M, Cho E, Burch-Smith TM, and Zambryski PC** (2012) Plasmodesmata formation and cell-to-cell transport are reduced in *decreased size exclusion limit 1* during embryogenesis in *Arabidopsis*. *Proc Natl Acad Sci USA* **109**, 5098-5103.

**Xu XM, Wang J, Xuan Z, Goldshmidt A, Borrill PG, Hariharan N, Kim JY, and Jackson D** (2011) Chaperonins facilitate KNOTTED1 cell-to-cell trafficking and stem cell function. *Science* **26**, 1141-1144.

**Zalepa-King L, and Citovsky V** (2013) A plasmodesmal glycosyltransferase-like protein. *PLoS One* **8**, e58025.

**Zavaliev R, Ueki S, Epel BL, and Citovsky V** (2011) Biology of callose (β-1,3-glucan) turnover at plasmodesmata. *Protoplasma* **248**, 117-130.

## Chapter 2: The *dse1* transcriptome reveals that ABI5 down-regulates plasmodesmatal transport

**Submitted for publication as:**

**Runkel AM, Brunkard JO, Ahern, MA, Xu, M, and Zambryski PC** (*submitted and under review*, 2016) The *dse1* transcriptome reveals that ABI5 down-regulates plasmodesmatal transport.

## ABSTRACT

Plant cells use plasmodesmata (PD) to transport key developmental signals, including transcription factors, RNA, sugars, and hormones, from cell to cell. Loss of *DECREASED SIZE EXCLUSION LIMIT 1* (*DSE1*) causes reduced PD transport, limits PD number, and results in various phenotypic abnormalities. An analysis of the *dse1* transcriptome and comparisons to the transcriptomes of phenotypically-similar *leafy cotyledon* mutants suggest that *DSE1* is involved in developmental pathways regulated by abscisic acid (ABA). Directly applying ABA or overexpressing the ABA response transcription factor *ABSCISIC ACID INSENSITIVE 5 (ABI5)* reduce PD transport. In further support, silencing expression of *ABI5* causes increased PD transport. ABA and other hormones may act as key signals to mediate the reduction of PD transport during late embryogenesis, and could affect PD function or formation throughout plant development.

## INTRODUCTION

Cell-to-cell communication in land plants requires channels that traverse the cell wall, called plasmodesmata (PD). PD form cytoplasmic connections between neighboring cells, allowing for transport of small (e.g., sugars, ions, hormones) and large molecules (e.g., proteins and RNAs) through the symplast (**Brunkard et al., 2015a; Calderwood et al., 2016; Chaiwanon et al., 2016; Rim et al., 2011; Sanger and Lee, 2014; Wu and Gallagher, 2012; Xu et al., 2011**). PD are lined with membranes: the plasma membrane, continuous along the cell wall, forms the outer limit of the channel, and tightly compressed strands of endoplasmic reticulum (the desmotubule) form the axial center. Molecules move from cell to cell in between these two membranes in a region called the “cytosolic sleeve”.

Regulation of PD transport drives key developmental processes in the plant. PD affect the spatial regulation of gene expression by permitting or restricting movement of signaling molecules to control organogenesis, meristem organization, and embryo development (**Benitez-Alfonso et al., 2013; Brunkard et al., 2015a; Daum et al., 2014; Gisel et al., 1999; Gisel et al., 2002; Kim et al., 2002; Kim et al., 2005a; Kim et al., 2005b; Rinne and van der Schoot, 1998; Sanger and Lee, 2014; Vatén et al., 2011**).

PD transport is thought to be controlled by PD in three ways: 1) transient restrictive or expansive processes at PD that alter rates of transport, 2) *de novo* formation of PD permitting increased transport between cells, and 3) PD degradation, which may be less generalized but can occur when specific cell types need to become isolated, as seen in guard cells. One process that restricts PD transport is known, and is caused by callose deposition in the cell wall surrounding PD that presumably occludes PD (**De Storme and Geelen, 2014; Vatén et al., 2011**; **Zavaliev et al., 2011**). Callose deposition is countered by β-1,3-glucanases that remove callose and lead to PD opening (**Levy et al., 2007**). The mechanisms driving the formation of PD are not well understood; PD can form during cell division (primary PD) and also after cell division (secondary PD),

which is critical to form connections between cells that are not the progeny of a cell division (**Burch-Smith and Zambryski, 2012)**, such as between the radial layers of cells in roots.

Three genes identified in a screen for *emb* mutants with altered PD transport during embryogenesis in *Arabidopsis thaliana* are currently associated with changes to PD formation: two genes are involved in the restriction of PD transport, *INCREASED SIZE EXCLUSION LIMIT 1* (*ISE1*) and *ISE2*, and one gene is involved in promoting PD transport, *DECREASED SIZE EXCLUSION LIMIT 1* (*DSE1*) (**Brunkard et al., 2013**; **Burch-Smith and Zambryski, 2010**; **Kim et al., 2002; Stonebloom et al., 2009; Xu et al., 2012**). These PD mutants were identified based on their enhanced or reduced ability to transport symplastic dyes during a key transition in embryo development, when PD transport changes to become increasingly restricted at the WT torpedo stage of embryo development (**Kim et al., 2002**). The PD transport phenotype in *dse1* embryos is incredibly severe, as even 0.5 kilodalton symplastic dyes cannot move between cells (**Xu et al., 2012**). Null mutants of all three alleles are embryo lethal, attesting to the essential functions of their encoded products.

ISE1, ISE2, and DSE1 proteins are not localized at PD. Instead, ISE1 is an RNA helicase localized to the mitochondria (**Stonebloom et al., 2009**), ISE2 is an RNA helicase found in the chloroplast (**Burch-Smith et al., 2011b**), and DSE1 is a protein containing repeated WD40 motifs (also called Trp-Asp motifs) that is found in the nucleus and cytosol (**Xu et al., 2012**). All three proteins are required for regulation of PD transport in embryos of *A. thaliana* and in the leaves of a distantly related eudicot species, *Nicotiana benthamiana*. Thus, PD function is likely exquisitely sensitive to intracellular signals resulting from defects in different critical cellular processes (**Burch-Smith and Zambryski, 2012**).

A study of the transcriptomes of *ise1* and *ise2* implicated both ISE1 and ISE2 in the regulation of photosynthesis-associated nuclear gene expression and chloroplast biogenesis, and suggested the 'organelle-nucleus-plasmodesmata signaling' (ONPS) pathway (**Burch-Smith and Zambryski, 2012; Burch-Smith et al., 2011b; Brunkard et al., 2013**). The mechanism by which DSE1 regulates PD, however, is unknown.

*DSE1* was first identified as *TANMEI* (*TAN)* in a screen for embryo defective (*emb*) mutants and was compared to the *leafy cotyledon* (*lec*) mutants *lec1*, *lec2*, and *fusca 3* (*fus3*) (**Keith et al., 1994; Meinke et al., 1994; Stone et al., 2001; West et al., 1994**) due to numerous phenotypic similarities, including ectopic trichome formation on cotyledons, anthocyanin accumulation in embryos, and desiccation intolerance (**Yamagishi et al., 2005**). Despite strong phenotypic similarity, crosses of *tan* to *lec1*, *lec2*, or *fus3* did not reveal epistasis, but instead revealed synergistic effects, suggesting that these genes operate in distinct but ultimately overlapping pathways to regulate embryogenesis (**Yamagishi et al., 2005**). A final incarnation of the *tan/dse1* mutant was identified as *aluminum tolerant 2* (*alt2*) in a suppressor screen for an aluminum hypersensitive mutant (**Nezames et al., 2012**). The *alt2-1* mutation is a weak

mutant allele of *DSE1* that interferes with normal root growth inhibition and fails to induce the cell cycle inhibitor CyclinB1;1 under aluminum stress.

Proteins with repeated WD40 motifs (WDRs), like DSE1, are involved in many molecular pathways in the cell, and are often platforms for protein complex assembly (**Mishra et al., 2012; Stirnimann et al., 2010**). WDRs are involved in hundreds of protein interactions in plants; *A. thaliana* contains 237 proteins with four or more WD40 motifs, and a single WDR protein can participate in multiple complexes (**Ramsay and Glover, 2005; van Nocker and Ludwig, 2003**).

To identify genetic players in *DSE1* signaling, we used comparative transcriptomics to study the *dse1* transcriptome in comparison to transcriptomes of *ise1*, *ise2*, and the *lec* mutants (**Burch-Smith et al., 2011b; Yamamoto et al., 2014**). The results show that DSE1 is required for the normal progression of embryo development, as *dse1* precociously expresses late embryogenesis specific genes. This transcriptional response found in *dse1* correlates with the known reduction of PD transport in wild type (WT) late embryogenesis (**Kim et al., 2002; Kim et al., 2005a; Kim et al., 2005b**). Notably, the abscisic acid (ABA) pathway is altered in *dse1*, and a key ABA transcription factor ABSCISIC ACID INSENITIVE 5 (ABI5) restricts PD transport, suggesting that ABA signaling may regulate PD transport.

## RESULTS

### Transcriptome analysis of *dse1*

The transcriptome of *dse1* reveals alterations in 759 protein-coding genes, 7 transposable elements, and 1 pseudogene (**Fig. 1A, Table S1**). We utilized MapMan and Gene Ontology (GO) analyses that provide well-accepted outputs for interpreting transcriptome-wide changes in gene expression (**Klie and Nikoloski, 2012; Usadel et al., 2005**). Both analyses revealed that *dse1* has significant transcriptional alterations in two major areas: late embryogenesis developmental pathways regulated by abscisic acid (ABA) and photosynthesis.

Unlike the *ise1* and *ise2* mutants, *dse1* showed dramatically induced expression of genes associated with late embryogenesis and response to ABA, including those encoding LATE EMBRYOGENESIS ABUNDANT PROTEINS (LEA) and seed storage proteins; see bins 33, 33.2, 35.1.22, and 17.1, which include the ABA-response and LEA genes (**Table 1**). Conspicuously, some LEA and seed storage protein genes are also the top up-regulated genes in the *dse1* transcriptome (over 100-fold induction, **Table S2**; LEA genes were annotated as in **Hundertmark and Hincha, 2008**). Additionally, *dse1* has an up-regulated gene encoding a critical ABA biosynthesis protein, NINE-CIS-EPOXYCAROTENOID DIOXYGENASE 6 (NCED6) (**Finkelstein, 2013; Lefebvre et al., 2006**) (**Table S1**). A "biological process" GO analysis of the up-regulated genes in the *dse1* transcriptome also indicated a dramatic enrichment of LEA genes in GO categories related to dehydration, dormancy, and response to ABA (see all GO enrichments of *dse1* up-regulated genes in **Table S3**).

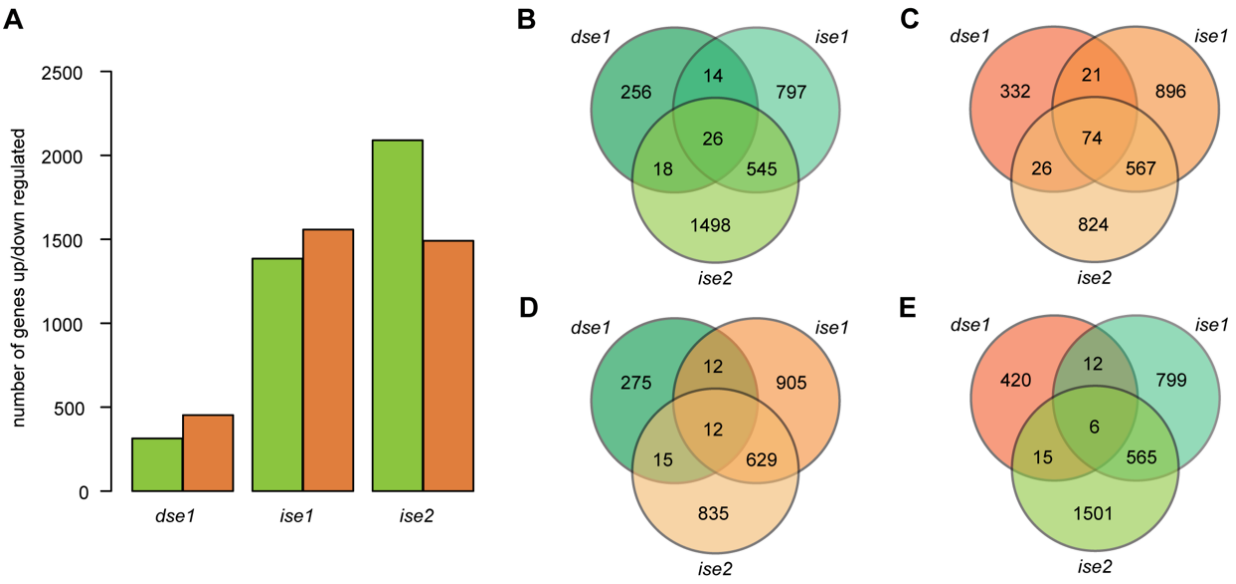


**Fig. 1. Comparison of the *dse1* transcriptome to *ise1* and *ise2* transcriptomes.** Genes reported for each transcriptome are those with twofold or greater altered expression compared with WT samples, with p-value < 0.05. (**A**) In total, the *dse1* transcriptome has 767 genetic regions with altered expression when compared to WT (759 protein-coding genes, and 8 transposons and/or pseudogenes) with 314 up-regulated (green bar) and 453 down-regulated (orange bar). The transcriptome of *ise1* has 2,940 genetic regions affected (2,788 protein-coding genes, 30 non-protein-coding RNAs, and 122 transposons and/or pseudogenes) with 1,382 up-regulated and 1,558 down-regulated. The *ise1* and *ise2* transcriptome data is from **Burch-Smith et al. (2011b)**, using the same transcriptome methods used here for the *dse1* transcriptome. The *ise2* transcriptome has 3,578 genetic regions (3,408 protein-coding genes, 23 non-protein-coding RNAs, and 147 transposons and/or pseudogenes) showing altered expression, with 2,087 up-regulated and 1,491 down-regulated. (**B**) *dse1*, *ise1*, and *ise2* share 26 similarly up-regulated genes. *ise1* and *ise2* share 571 up-regulated genes, while *dse1* and each *ise* mutant share < 50 overlapping genes. (**C**) *dse1*, *ise1*, and *ise2* share 74 similarly down-regulated genes. (**D**) Twelve genes are up-regulated in *dse1* and down-regulated in the *ise* mutants. (**E**) *dse1* has 6 down-regulated genes that are up-regulated in the *ise* mutants.

**Table 1. MapMan analysis of significantly overrepresented pathways in the *dse1* transcriptome, including photosynthesis, ABA metabolism, and late embryogenesis development.**

| Bin | MapMan category name | # of genes | p-value[1] |
|---|---|---|---|
| 1 | Photosynthesis | 49 | 1.78e-08 |
| 1.1 | Photosynthesis: lightreaction | 32 | 9.08e-05 |
| 1.1.1 | Photosynthesis: lightreaction - photosystem II | 15 | 1.38e-02 |
| 1.1.1.2 | Photosynthesis: lightreaction - photosystem II - photosystem II polypeptide subunits | 10 | 3.39e-02 |
| 17 | Hormone metabolism | 28 | 2.40e-03 |
| 17.1 | Hormone metabolism: abscisic acid | 10 | 3.29e-02 |
| 33 | Development | 28 | 2.06e-02 |
| 33.2 | Development - late embryogenesis abundant | 9 | 1.03e-03 |
| 35.1.22 | Not assigned: no ontology - late embryogenesis abundant domain-containing protein | 6 | 9.33e-03 |

[1] Adjusted p-value (Wilcoxon Rank-Sum Test with a Benjamini Hochberg correction for false discovery rate).

Numerous photosynthesis and chloroplast-related genes are affected in the *dse1* transcriptome (**Table 1 and Table S4**), which is unsurprising, since *dse1* mutants are chlorotic (**Xu et al., 2012**); however, these transcriptional changes are not likely the cause of the decreased PD transport phenotype in *dse1*. In fact, most *emb* lines are chlorotic (lacking chlorophyll) (*emb* database: http://www.seedgenes.org/) (**McElver et al., 2001; Patton et al., 1991**), but these do not have a PD phenotype (**Kim et al., 2002**). *ise1* and *ise2* mutants exhibit reduced expression of more photosynthesis-associated nuclear genes (**Burch-Smith et al., 2011b**), as expected because *ISE1* and *ISE2* encode organelle-targeted proteins, so organelle function is directly impacted in those mutants.

There are also genes that are misregulated in *dse1* that encode components of the cell wall or the endoplasmic reticulum (ER), which might be involved in regulating PD function, given that PD cross the cell wall and PD contain ER. β-*1,3-GLUCANASE 3* (*BG3*), which is up-regulated in *dse1*, encode*s* an enzyme that increases PD transport by reducing callose accumulation. The up-regulation of *BG3*, and a lack of other callose-related genes exhibiting altered expression in the *dse1* transcriptome, however, suggests that *dse1* does not appear to decrease PD transport by altering transcription of genes involved in callose metabolism. Some of the other possible PD related genes affected in the *dse1* transcriptome are discussed in the transcriptomic comparisons below.

### Transcriptomes of *dse1* versus other embryo defective mutants

*dse1* versus *ise1* and *ise2* mutants

We compared the previously published *ise1* and *ise2* transcriptomes (**Burch-Smith et al., 2011b**) to the *dse1* transcriptome to find misexpressed genes that may be involved in PD regulation. If *ise1* and *ise2* affect PD regulation through the same genetic pathway(s) as *dse1*, but have opposite PD phenotypes, we might expect that the

expression of genes involved in PD regulation would be affected oppositely between *dse1* and *ise1/2*. We identified all similarly as well as oppositely regulated genes in these mutants (**Fig. 1, Table S5, and Table 2**). All 18 oppositely affected genes are listed in **Table 2** and the 100 similarly regulated genes are listed in **Table S5**. The oppositely expressed genes in the PD mutant transcriptomes include 12 genes that are up-regulated in *dse1* and down-regulated in *ise1* and *ise2,* and 6 genes that are down-regulated in *dse1* and up-regulated in *ise1* and *ise2* (**Fig. 1D-E**).

Remarkably, 8 of the 12 genes up-regulated in *dse1* and down-regulated in the *ise1/2* mutants are normally expressed during late embryogenesis and many are ABA induced (**Table 2**). A ninth gene, *OXIDATION-RELATED ZINC FINGER 2* (*OZF2*), encodes a transcription factor that causes ABA hypersensitivity when overexpressed (**Lee et al., 2012**).

Also of note, three of the 18 differentially regulated genes encode proteins that may play a role in PD regulation as they are predicted to modify cell wall components or the ER: AT5G15780 is a putative extensin that belongs to a superfamily of cell wall modification enzymes (**Wolf et al., 2012**), AT2G01610 is a member of the pectinesterase inhibitors, and *BETA GLUCOSIDASE 18* (*BGLU18*) is a component of ER bodies (**Table 2**).

**Table 2. Genes oppositely expressed in *dse1* and the *ise* mutant transcriptomes.**

| Locus[1] | gene symbol or gene description[1] | *dse1* | *ise1* | *ise2* |
|---|---|---|---|---|
| AT1G03880 | *CRUCIFERIN 2* (*CRU2*)† | 2.9 | -2.5 | -2.3 |
| AT1G04560 | AWPM-19-like family protein† | 31.4 | -14 | -3.3 |
| AT1G52400 | *BETA GLUCOSIDASE 18* (*BGLU18*) | 2.7 | -4.3 | -4.5 |
| AT1G52690 | *LATE EMBRYOGENESIS ABUNDANT 7* (LEA7) † | 3.2 | -3.3 | -2.9 |
| AT2G36640 | *EMBRYONIC CELL PROTEIN 63* (*ECP63*) † | 5 | -7.3 | -10.6 |
| AT3G12145 | *FLOR1* (*FLR1*) | 2.1 | -6.5 | -2.4 |
| AT4G02280 | *SUCROSE SYNTHASE 3* (*SUS3*) † | 5 | -3.4 | -2.4 |
| AT4G29190 | *OXIDATION-RELATED ZINC FINGER 2* (*OZF2*) | 2.2 | -3.1 | -2.9 |
| AT5G01670 | NAD(P)-linked oxidoreductase superfamily protein† | 3.4 | -2.2 | -2.5 |
| AT5G03860 | *MALATE SYNTHASE* (*MLS*) † | 2.6 | -12.3 | -5.9 |
| AT5G15780 | Pollen Ole e 1 allergen and extensin family protein | 2.2 | -4.1 | -16 |
| AT5G22470 | NAD+ ADP-ribosyltransferases† | 3.6 | -6.4 | -3.2 |
| AT1G16390 | *ORGANIC CATION/CARNITINE TRANSPORTER 3* (*OCT3*) | -3.4 | 2.4 | 3.3 |
| AT1G28700 | Nucleotide-diphospho-sugar transferase family protein | -4.7 | 2.9 | 5.2 |
| AT2G01610 | Plant invertase/pectin methylesterase inhibitor superfamily protein | -2.5 | 3.1 | 3.9 |
| AT4G33600 | unknown protein | -4.6 | 3.2 | 2.5 |
| AT5G10230 | *ANNEXIN 7* (*ANNAT7*) | -2.4 | 3 | 3.4 |
| AT5G12460 | Protein of unknown function (DUF604) | -2.3 | 3.4 | 5.1 |

[1] Gene locus, symbols, and descriptions are annotated from the TAIR database at http://www.arabidopsis.org/. Gene symbols are capitalized and italicized, but if no gene symbol has been annotated, an abbreviated description of the gene is provided (full gene descriptions for each gene can be found at TAIR).
† Genes are ABA induced and are expressed in the later stages of seed development, according to AtGenExpress annotation (**Schmid et al., 2005**).

*dse1* versus the *lec* mutants

Given the previously described similarities among *tan* (*dse1*), *lec1*, *lec2*, and *fus3* (**Yamagishi et al., 2005**), we next sought to compare the *dse1* transcriptome to the recently published *lec1*, *lec2*, and *fus3* transcriptomes (**Yamamoto et al., 2014**). These mutants were all originally identified in genetic screens for embryo development dysfunction. *dse1* and *fus3* mutant embryos share similar phenotypes: both exhibit anthocyanin accumulation at the shoot apical meristem (**Meinke et al., 1994; Xu et al., 2012**), ectopic trichomes on cotyledons, desiccation intolerant seeds (**To et al., 2006; Xu et al., 2012; Yamagishi et al., 2005**), and the formation of embryonic leaf primordia (**Fig. S1**; **Table S6**). Transcriptome data from *lec1*, *lec2,* and *fus3* were collected by **Yamamoto et al.** (**2014**), using the Affymetrix ATH1 Genome Array (ATH1 array), which provides data on fewer genes than the Affymetrix Tiling Array (used here), but provides comparable results on levels of gene expression (**Laubinger et al., 2008**; **Matsui et al., 2008**). When comparing *dse1* or the *ise* mutant transcriptomes to the *lec1, lec2,* or *fus3* transcriptomes herein, we excluded genes unique to the tiling array (**Table S7**). **Table S7** also shows transcriptomes from WT embryos at 12 and 16 days after fertilization (DAF) (**Yamamoto et al., 2014**). For all comparisons we considered WT 8 DAF embryos as "control"; the 8 DAF embryos from **Yamamoto et al.** (**2014**) matched the morphological stage of the control embryos in our transcriptome study of *dse1* (note that the control embryos in our transcriptome included WT and heterozygote *dse1* embryos).

We compared the similarities of up- or down-regulated genes in *dse1* and the *lec* mutants and discovered that *fus3* shows the highest percentage of gene overlap with *dse1* (**Fig. 2B-D**). Approximately 40 percent of the *dse1* transcriptome overlaps with genes in the *fus3* transcriptome (the overlapping genes in the *dse1* and *fus3* transcriptomes divided by the total genes affected in *dse1* transcriptome (**Fig. 2A-B**)). *lec1* and *lec2* overlap with the *dse1* transcriptome to somewhat lesser but nonetheless highly significant degrees, 26 and 21 percent, respectively.

*DSE1* and the *LEC* genes operate in overlapping pathways to regulate embryogenesis, but are not epistatic (**Yamagishi et al., 2005**), so we sought to identify any potential diverging pathways between *dse1* and the *lec* mutant most similar, *fus3.* The 26 differentially regulated genes between *dse1* and *fus3* are shown in **Table S8** and **Figure S2B-C**. *dse1* shows an induction of a few seed storage genes that are, in contrast, down-regulated in *fus3* including four 2S albumin superfamily proteins and *CRUCIFERIN 2* (*CRU2*). Three of the differentially regulated genes encode proteins related to hormone signaling. *NCED6*, involved in ABA biosynthesis, and *ZINC FINGER OF ARABIDOPSIS THALIANA 6* (*ZAT6*), known to regulate SA and redox regulation (**Shi et al., 2014**), are both transcriptionally induced in *dse1* and reduced in *fus3*. A gene encoding a protein that attenuates jasmonic acid response, *JASMONATE-ZIM-DOMAIN PROTEIN 10* (*JAZ10*) (**Moreno et al., 2013**) is induced in *fus3* and reduced in *dse1*. Overall, however, the similarities between *dse1* and *fus3* are much more apparent than their differences.

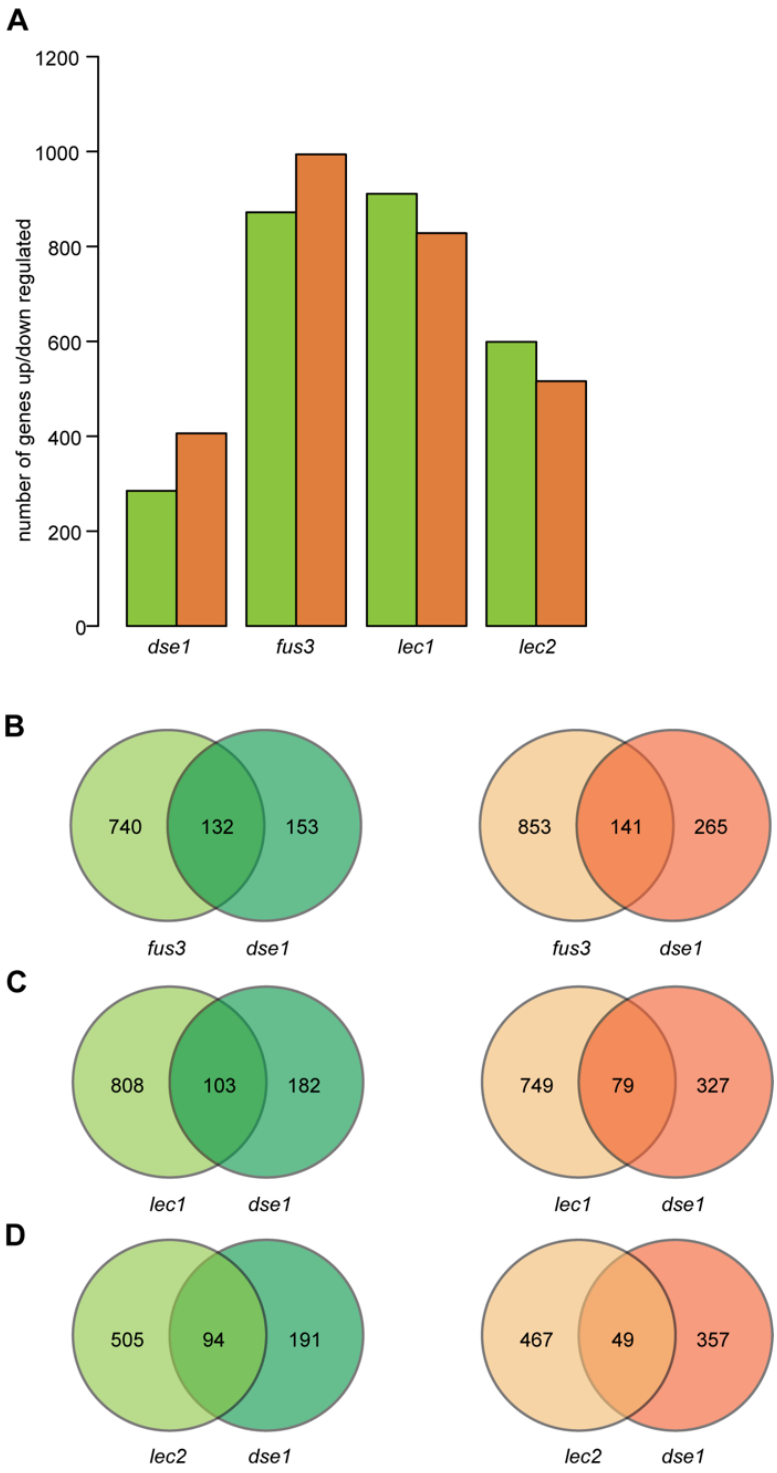
A
1200
1000
800
600
400
200
0
number of genes up/down regulated
dse1
fus3
lec1
lec2
B
740
132
153
fus3
dse1
853
141
265
fus3
dse1
C
808
103
182
lec1
dse1
749
79
327
lec1
dse1
D
505
94
191
lec2
dse1
467
49
357
lec2
dse1

(continued on previous page)

**Fig. 2. *dse1* and *lec* mutants show transcriptional overlap.** (**A**) Total number of up (green bars) or down (orange bars) regulated genes in each of the *dse1* and *lec* transcriptomes. The *lec* transcriptome data was collected by **Yamamoto et al.** (**2014**) using the ATH1 array. For comparisons of *dse1* and the *lec* mutants, the *dse1* transcriptome has been limited to only include genes that are also on the ATH1 array (using the ATH1 array genes, the *dse1* transcriptome has 691 affected genes). (**B**) The Venn diagram (left) shows similarly up-regulated genes in the *dse1* and *fus3* transcriptomes, with overlapping genes in the center, and the Venn diagram (right) shows similarly down-regulated genes in the *dse1* and *fus3* transcriptomes. *fus3* shows the most transcriptional overlap with the *dse1* transcriptome (hypergeometric test, p-value = 6.3e-117, representation factor = 4.7), (**C**) compared to *lec1* (hypergeometric test, p-value = 5.78e-51, representation factor = 3.4), or (**D**) *lec2* (hypergeometric test, p-value = 7.9e-50, representation factor = 4.1).

In contrast, we also tested if the transcriptomes of *ise1* or *ise2* showed any overlap with the *fus3* transcriptome. We found 30 similarly up-regulated genes among the three mutants and 79 similarly down-regulated genes between *fus3* and the *ise1* and *ise2* mutants (**Fig. 2, Table S9**). The up-regulated genes produced the "biological process" GO enrichments "hexose transmembrane transport" (GO:0035428), "glucose transport" (GO:0015758), "glucose import" (GO:0046323), and "carbohydrate transport" (GO:0008643), suggesting that the *ise* and *fus3* mutants could have some related sugar transport defects. There are 81 oppositely regulated genes between the two *ise* mutants and *fus3* (26 genes down-regulated in the *ise* mutants and up-regulated in *fus3* as well as 55 genes up-regulated in the *ise* mutants and down-regulated in *fus3*). Generally, the *ise* and *fus* mutant transcriptome comparison, however, reveals little relationship between the mutants, suggesting they are involved in distinct pathways, as predicted by their different developmental phenotypes.

**Transcriptomes of *dse1* versus WT embryos**

The *dse1* transcriptome suggests it is a precociously aged embryo due to up-regulation of late embryogenesis genes and other genes expressed during late stages of embryogenesis (**Le et al., 2010; Righetti et al., 2015; Schmid et al., 2005**). To test whether late embryogenesis genes are precociously expressed in the *dse1* mutant, we compared the differentially expressed genes between *dse1* and WT embryos with the genes that are differentially expressed between 12 days after fertilization (DAF) and 8 DAF embryos (the "12 DAF transcriptome") and genes that are differentially expressed between 16 DAF and 8 DAF (the "16 DAF transcriptome") (from **Yamamoto et al. (2014)**). Many genes overlap between *dse1* and these aging embryos (**Fig. S3A and B**) and relatively few genes are oppositely regulated between the *dse1* transcriptome and the 12 DAF or 16 DAF transcriptomes (**Table S7, Fig. S3C and D**).

Many genes encoding LEA proteins are up-regulated in *dse1* and in the 12 DAF and 16 DAF embryo transcriptomes (**Table S2 and S7**), as well as LEA-like genes including *KIN1* (AT5G15960), *KIN2* (AT5G15970) and AT1G22600. *ABI5* is also up-regulated in all three transcriptomes (*dse1*, 12 DAF, and 16 DAF). Additional genes encoding proteins that are induced by ABA or involved in ABA-response are also up-regulated in the three transcriptomes: *OIL BODY-ASSOCIATED PROTEIN 1A* (*OBAP1A*), *HVA22 HOMOLOGUE B* (*HVA22B*), *LOW-TEMPERATURE-INDUCED 65* (*LTI65*), a AWPM-19-like family protein (AT1G04560), *ZINC-FINGER PROTEIN 2* (*ZF2*), and a gene that encodes a known negative regulator of ABA response (*ABA-HYPERSENSITIVE GERMINATION 1* or *AHG1*). A few genes encoding ABA-associated proteins were up-regulated in *dse1* and in the 16 DAF transcriptome, but were not up-regulated in the 12 DAF transcriptome, including *DRE-BINDING PROTEIN 2A* (*DREB2A*), and *LOW-TEMPERATURE-INDUCED 78* (*LTI78*), as well as a *LEA* gene (AT2G18340). *fus3* also has many of these LEA and ABA-associated protein genes up-regulated in its transcriptome.

Notably, the *dse1* transcriptome also identified numerous genes not found in the 12 DAF or 16 DAF transcriptomes that encode proteins that may be expressed in later

stages of embryo development. Some of the 173 genes up-regulated in *dse1,* but not overlapping in the up-regulated genes in the 12 DAF or 16 DAF transcriptomes (**Fig. S3A**), encode typical late embryo proteins such as LEA and seed-storage proteins: four 2S albumin superfamily proteins, SENESCENCE-ASSOCIATED GENE 21 (SAG21), and a number of LEA (**Table S2 and S7**). Genes encoding ABA-response proteins that also induced in *dse1* (compared to 12 DAF or 16 DAF embryos) including *ABSCISIC ACID RESPONSIVE ELEMENTS-BINDING FACTOR 3* (*ABF3*) and *ABA INSENSITIVE 1* (*ABI1*), note that ABI1 negatively regulates ABA response. Genes encoding proteins induced by ABA such as *CRU2*, *HVA22 HOMOLOGUE D* (*HVA22D*), *HOMEOBOX 7 (HB-7)*, *MYC2*, and *MYB DOMAIN PROTEIN 60* (*MYB60*) are also induced in *dse1* but not in the 12 DAF or 16 DAF transcriptomes.

Genes encoding cell wall and ER-associated proteins are up-regulated in the *dse1* transcriptome, but not in the 12 DAF or 16 DAF transcriptomes (**Fig. S3A**). Genes encoding cell wall proteins include pectin modifying proteins (AT1G67750 and AT5G20860), *EXTENSIN 3* (*EXT3*), another extensin family protein (AT2G16630), *EXPANSIN A14* (*EXPA14*), and XYLOGLUCAN ENDOTRANSGLUCOSYLASE/HYDROLASE (XTH) proteins (XTH19, XTH4, and XTH5). Other genes encoding hormone-related proteins, particularly JA-associated proteins, are up-regulated in *dse1*, but not in the 12 DAF or 16 DAF transcriptomes, such as *ZAT6* (SA related), *CORONATINE INDUCED 1* (*CORI3*), *SULFOTRANSFERASE 16* (*SOT16*), *JASMONATE RESISTANT 1* (*JAR1*). Genes encoding ER body proteins, which are induced by JA (**Matsushima et al., 2002**), are also found in *dse1* and not the WT transcripts. These ER body genes were also up-regulated in the *lec* transcriptomes and are discussed in **Yamamoto et al.** (**2014**). Genes that encode ER body-associated proteins found in *dse1* include *NAI2*, *PYK10*, *BGLU18*, *BGLU21*, *BGLU22*, *JACALIN-RELATED LECTIN 31* (*JAL31*), *JAL33*, *JAL34*, *GDSL LIPASE-LIKE PROTEIN 22* (*GLL22*), a TRAF-like family protein (AT5G26280), and *PYK10-BINDING PROTEIN 1* (*PBP1*).

**Hormones and PD transport**

Direct application of phytohormones affects PD transport

The hormone response genes identified in the *dse1* transcriptome may be involved in the reduced PD transport phenotype of *dse1*. We tested if direct application of ABA, gibberellic acid ($GA_3$), or jasmonic acid (JA) affected PD transport. We also tested salicylic acid (SA) as a positive control for our method, since SA is known to affect PD transport and PD structure (**Fitzgibbon et al., 2013; Wang et al., 2013**). PD transport was monitored by a cell-to-cell movement assay of transiently expressed GFP in leaves of *N. benthamiana* (**Brunkard et al., 2015b**). Hormones were applied onto leaf surfaces by an aqueous spray. Previous studies used a spray approach to apply either ABA, GA, or SA at 100 μM (**Choi and Hwang et al., 2011; Wang et al., 2013**; **Xu et al., 2013**), and we used this concentration for all hormones analyzed here. At the concentration tested, ABA, JA, and SA caused a significant reduction in PD transport (Wilcoxon rank sum test, $n \geq 84$, p-value < 0.002), but $GA_3$ did not (Wilcoxon rank sum test, $n \geq 84$, p-

value > 0.6) (**Fig. 3**). This simple assay indicates that hormone treatments can alter PD transport, although the mechanism(s) underlying the observed alterations are unknown.

Genetic perturbation of ABI5 signaling affects PD transport

To further test our hypothesis that ABA can regulate PD transport, we genetically tested if one of the key ABA transcription factors, ABSCISIC ACID INSENSITIVE 5 (ABI5, AT2G36270 (**Finkelstein, 2013; Finkelstein and Lynch 2000; Finkelstein et al., 2005**), which is up-regulated in the *dse1* transcriptome, affects PD transport. To acutely over-express *ABI5*, we used a high inoculum of *Agrobacterium* carrying a construct to express *ABI5* under the control of a dual 35S CaMV promoter (over-expression vector pMDC32 described in **Curtis and Grossniklaus** (**2003**). To control for any impact such a high inoculum might have on PD transport, we used a similar high inoculum of *Agrobacterium* carrying a construct to express β-*GLUCURONIDASE* (*GUS*) under the same promoter. The results show that ectopic expression of *ABI5* in leaves of *N. benthamiana* by *Agrobacterium* infiltration caused significantly reduced PD transport compared to the *GUS* control (Wilcoxon rank sum test, n ≥ 98, p-value < 1.0e-6) (**Fig. 4**). In support, loss of the *ABI5 N. benthamiana* ortholog by virus-induced gene silencing (VIGS) (**Fig. S4**) caused a significant increase in PD transport compared to the control (Wilcoxon rank sum test, n ≥ 96, p-value < 1.0e-15) (**Fig. 4**).

### *dse1* has fewer PD per cell wall length

How is PD transport restricted in *dse1*? Previously, *dse1* was shown to have a lower frequency of twinned and branched PD (**Xu et al., 2012**). The frequency of twinned and branched PD is positively correlated with PD transport levels in young tissues (**Burch-Smith and Zambryski, 2010; Burch-Smith et al., 2011a**) and may indicate increased formation of secondary PD in the cell wall (**Burch-Smith and Zambryski, 2012**). Here we counted the number of PD per cell wall length in T.E.M. images of a *dse1* embryo, compared to a same staged WT or heterozygous embryo, in two separate experiments. *dse1* has significantly fewer PD per cell wall length; *dse1* embryos had 0.13 PD per μm cell wall (119 PD / 920 μm) and WT/heterozygous embryos had 0.32 PD per μm cell wall (523 PD / 1620 μm) (**Fig. 5A**; **Fig. S5**). The decreased PD frequency is not simply due to excessive cell expansion, as the sizes of cells in *dse1* and WT embryos are similar (**Fig. 5B**).

## DISCUSSION

### Reduced PD formation in *dse1*

Previous studies with *ise1* and *ise2* revealed that mutations in nuclear genes encoding mitochondrial or chloroplast targeted RNA helicases both disrupt chloroplast biogenesis and result in increased PD transport. Lack of essential RNA helicases likely causes alterations in inter-organelle and organelle-nuclear signaling that in turn affect PD transport and formation (**Burch-Smith and Zambryski, 2012; Burch-Smith et al., 2011b; Brunkard et al., 2013**). This organelle-nuclear-plasmodesmata-signaling

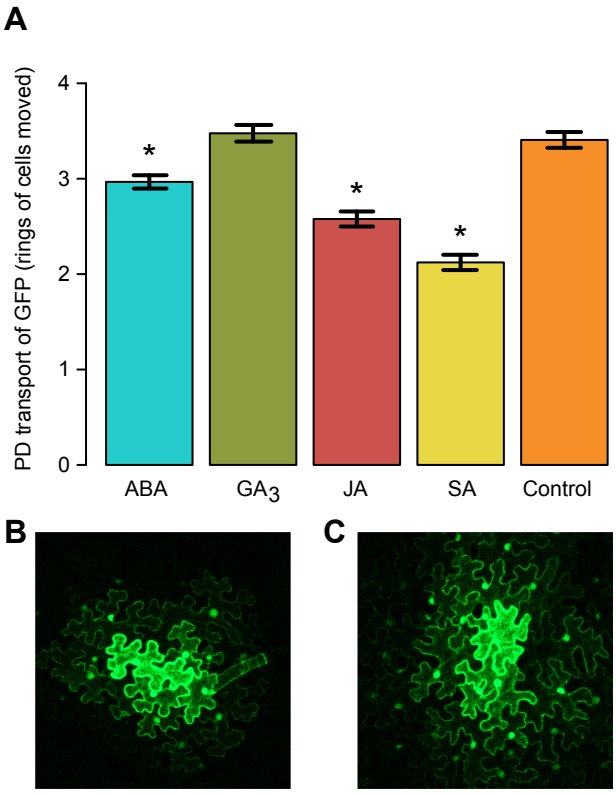


**Fig. 3. Direct application of ABA, JA, and SA affects PD transport.** (**A**) Exogenous application of plant hormones on the leaves of *N. benthamiana* affects the movement of transiently expressed GFP in the leaf epidermis. ABA, JA, and SA caused a significant reduction in PD transport (Wilcoxon rank sum two-tailed test, ABA: n = 90, GA: n = 84, JA: n = 90, SA: n = 106, control: n = 91, 11 plants per treatment (ABA, GA, SA) and 10 plants per treatment (JA and control), 4 separate experiments, *p-value ≤ 0.002), but $GA_3$ did not (p-value > 0.6). Error bars indicate ± SE. (**B**) Example GFP movement assay in a leaf of *N. benthamiana* treated with SA. (**C**) Example GFP movement assay in a leaf that was not treated with hormones (control). PD transport is assessed by the number of rings of cells expressing GFP move away from the initially transfected cell in the middle.

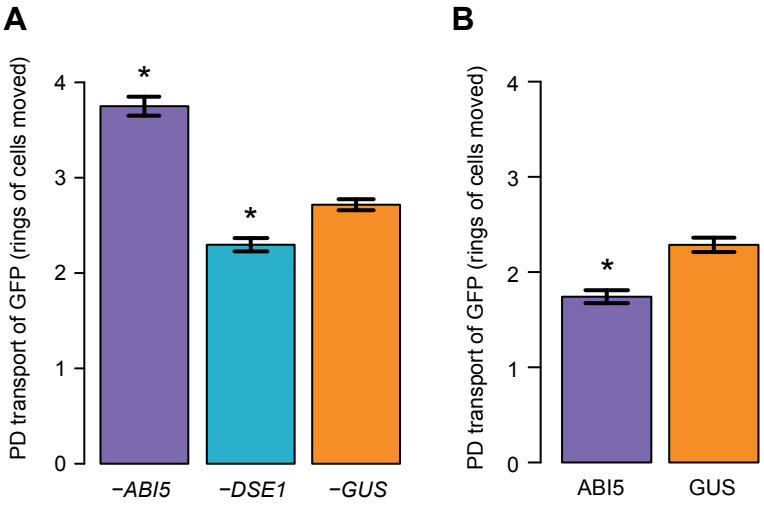


**Fig. 4. Genetic perturbation of ABA signaling affects PD transport.** (**A**) Silencing *N. benthamiana ABI5*, a transcription factor involved in the ABA response pathway, causes increased PD transport of transiently expressed GFP; loss of *N. benthamiana DSE1* causes reduced PD transport. A gene not encoded by the *N. benthamiana* genome, *GUS*, is used as the negative control (Wilcoxon rank sum two-tailed test, *-ABI5*: n = 96 (9 plants), *-DSE1*: n = 128 (7 plants), control: n = 187 (15 plants), 5 separate experiments *p-value < 1.0e-5). (**B**) Agroinfiltration to cause transient overexpression of *A. thaliana ABI5* in leaves of *N. benthamiana* caused reduced PD transport compared to agroinfiltration causing transient overexpression of *GUS* (Wilcoxon rank sum two-tailed test, GUS: n = 98 and ABI5 n = 112, 7 plants per treatment, 3 separate experiments, *p-value < 1.0e-6). Error bars indicate ± SE. PD transport is assessed by the number of rings of cells expressing GFP move away from the initially transfected cell in the middle.

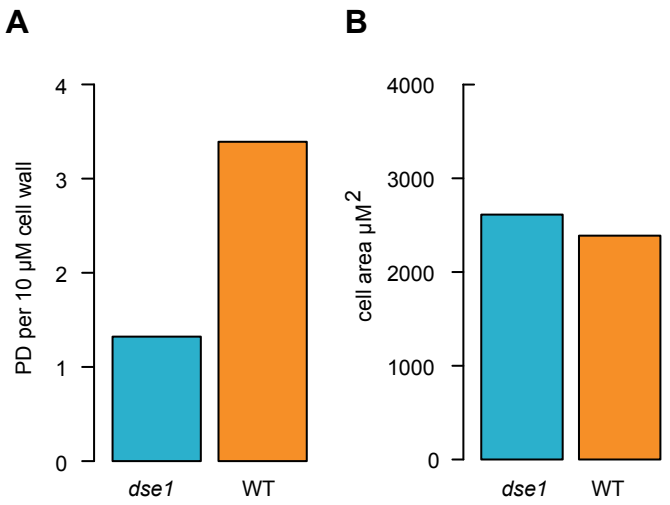


**Fig. 5. *dse1* has fewer PD per cell wall length.** (**A**) Cell wall length and PD number were measured and counted in TEM images of *dse1* embryos and WT/heterozygous embryos of a similar stage; fewer PD per cell wall length were found in the *dse1* mutant. 119 PD / 920 µm were counted in the *dse1* embryos and 523 PD /1620 µm were counted in the WT/heterozygous embryos (PD per cell wall length were counted in two embryos of each genotype). (**B**) We measured the areas of cells in similarly staged *dse1* and WT embryos, with two embryos of each genotype (38 cells of each genotype).

(ONPS) pathway challenges the notion that PD regulation must occur *at* PD, and instead suggests that many components of the plant cell control cell-to-cell transport. Here we show that the WD40 repeat protein DSE1 is involved in one or more cellular pathways that affect PD transport, at least in part by controlling the number of PD that form.

The present analyses do not reveal *how* PD formation might be directly controlled, other than revealing a few “suspects" that are altered in expression (including genes encoding cell wall modifying enzymes). Notably, our results further support that regulation of critical cellular pathways, as shown in our studies with *ise1* and *ise2,* affect PD formation/function.

**Comparative transcriptome studies of *emb* mutants**

*dse1* and the *ise1*/*2* transcriptomes are unique; *dse1* expresses many genes that are associated with late embryo development and seed maturation, while some of these genes are down-regulated in *ise1* and *ise2*. Perhaps these disparate transcriptional profiles are related to the opposing PD phenotypes seen in *dse1* and *ise1/2*.

*dse1* has many phenotypic similarities to the *lec* mutants, especially to *fus3*. *dse1* showed a strong transcriptional relationship to each of the *lec* mutants, with the most significant overlap with *fus3.* Many of the genetic pathways affected in both *dse1* and *fus3* could explain their shared phenotypic characteristics. The synergistic role that these two genes play in establishing the proper timing of embryo development and seed maturation could be elucidated in further studies of the genes unique or differentially regulated between these two mutants.

**ABA response pathway affected in *dse1***

The *dse1* transcriptome implicates this PD mutant in the ABA response pathway, which is generally associated with late stages of embryogenesis. The most highly up-regulated genes in the *dse1* transcriptome encode LEA and other seed storage proteins, and most of these LEA are transcriptionally induced in response to ABA in WT. For instance, *LATE EMBRYOGENESIS ABUNDANT 1* (*EM1*), as well as *LATE EMBRYOGENESIS ABUNDANT 6* (*GEA6*), are both transcriptionally activated by ABA and ABI5 (**Bies et al., 1998; Carles et al., 2002; Delseny et al., 2001; Finkelstein, 2010; Lopez-Molina et al., 2002**). Many of the ABA-related genes induced in *dse1* are ABA-signaling or response genes, but it is also notable that a key ABA biosynthesis enzyme involved in seed dormancy, NCED6, (**Finkelstein, 2013; Lefebvre et al., 2006; Seo and Koshiba, 2002**), is also transcriptionally up-regulated in *dse1*. Our results suggest that, in wild-type plants, DSE1 restricts the ABA-regulated seed maturation program, perhaps by repressing *ABI5* expression. In the *dse1* mutant, without this repression, ABI5 might decrease PD transport, as observed in *N. benthamiana* leaves.

**Hormones alter PD function**

While PD are channels that allow hormone movement between cells (reviewed in **Burch-Smith and Zambryski, 2016**; **Brunkard et al., 2015a**), plant hormones have rarely been recognized as regulators of PD themselves, with the exception of recent studies on SA and auxin (**Benitez-Alfonso et al., 2013; Fitzgibbon et al., 2013, Han and Kim, 2016; Wang et al., 2013**).

In this study, sprayed application of ABA to leaves reduced PD transport. ABA has been previously indirectly linked to the regulation of PD transport. The *kobito1* mutant is an ABA insensitive mutant with increased stomatal clustering due to increased PD transport (**Kong et al., 2012**). Furthermore, one study in avocado (*Persea americana*) indicated that ABA affected PD structure, causing increased electron-dense material at the opening of PD (**Han and Kim 2016; Moore-Gordon et al., 1998**). Crosstalk among the other plant hormones may be involved in ABA affecting PD transport.

Here, JA also reduced PD transport when applied to leaves. JA impacts many pathways that could, in turn, impact PD transport; as examples, JA is involved in repressing growth, initiating defense responses, initiating oxidative stress-tolerance genes, and affecting expression of photosynthesis-related genes (**Attaran et al., 2014; Creelman and Mullet, 1995; Jung et al., 2007).** Alternatively, since JA is highly interconnected to other plant hormones (**Devoto and Turner, 2003; Ellis et al., 2002; Nagpal et al., 2005; Turner et al., 2002**), the decrease in PD transport following JA application may be caused by hormone crosstalk.

We show that key regulators of ABA biosynthesis and downstream signaling are induced in *dse1* suggesting that alterations in ABA signaling affect PD transport. *ABI5* expression and genes regulated by the ABI5 transcription factor are strongly up-regulated in the *dse1* mutant. Additionally, over-expression or silencing expression of *ABI5* demonstrate that ABI5 can restrict PD transport in leaves. Several hormones likely regulate PD transport and further study of plant hormones, PD, and plant development will elucidate the specific roles hormones play in controlling cell-cell communication through PD.

**Figure 6** summarizes our results to date on *emb* mutants that affect PD formation. WT embryos undergo a down-regulation in PD transport at the mid-torpedo stage of embryogenesis (**Kim et al., 2002; Kim et al., 2005a; Kim et al., 2005b**) and we identified *ise1, ise2*, and *dse1* mutants with increased or decreased PD transport at this stage. Previous transcriptome analyses of *ise1* and *ise2* revealed these mutants were immature with a significant lack of expression of genes for chloroplast biogenesis (**Burch-Smith et al., 2011b**). In direct contrast, *dse1* prematurely expresses genes associated with mature embryos. We hypothesize that *dse1* embryos have precocious expression of genes involved in the seed maturation process, and concomitant reduced PD transport normally associated with later stages of embryogenesis. Thus, the WT DSE1 WD40 repeat protein may play an important role(s) either in restricting late

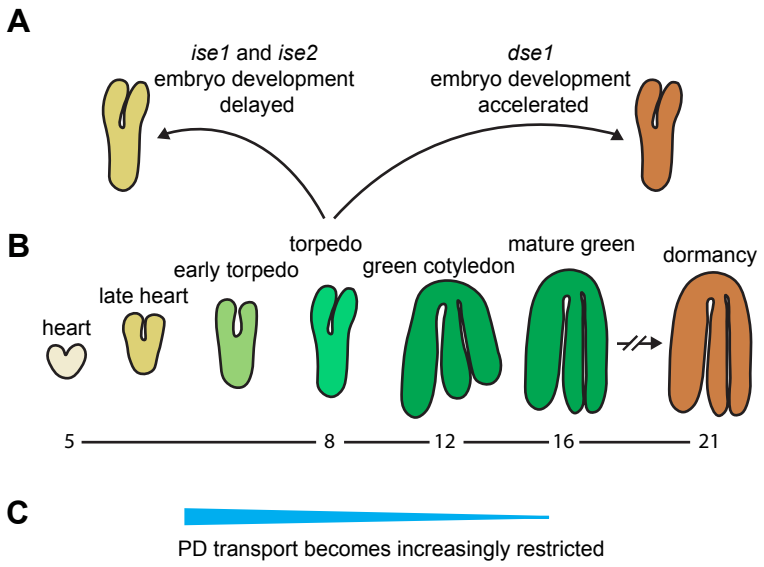


**Fig. 6. *dse1* mutant embryos prematurely express late development genes and have precociously restricted PD transport.** (**A**) *dse1* transcriptionally expresses an abundance of genes associated with late embryo development (brown). In contrast, *ise1* and *ise2* are delayed in embryo development, with a strong reduction in gene expression associated with chloroplast development (cream). (**B**) *A. thaliana* embryos develop through stages, with chlorophyll greening (intensity of green color) increasing from the heart stage until the mature green stage before the seed enters dormancy (brown) (**Mansfield and Briarty, 1990; Nambara et al.,1995**; **Raz et al., 2001**). Numbers represent the approximate day after fertilization (DAF) of the WT embryo. (**C**) As *A. thaliana* embryos develop from early torpedo to the green cotyledon stage, PD transport becomes increasingly restricted. PD transport in *dse1* is strongly reduced, whereas, *ise1* and *ise2* have increased PD transport compared to WT.

embryo specific gene expression, or enhancing expression of genes essential for early embryo development.

## MATERIALS AND METHODS

### *dse1* transcriptome

Tiling array analysis

The *dse1* tissue collection and transcriptome analysis were carried out as described (**Burch-Smith et al., 2011b**). *dse1* or sibling WT seeds at the mid-torpedo stage of embryogenesis were collected from siliques of *dse1*/+ heterozygous plants. WT embryos were collected ~8 DAF and *dse1* embryos were collected at ~12 DAF as described (**Burch-Smith et al., 2011b**). Throughout the text we refer to genes by names in the TAIR database, otherwise we give the gene TAIR locus.

Confirmation of transcriptome using RT-qPCR

Expression of a clathrin reference gene and 9 other genes affected in the transcriptome were assessed by reverse transcription followed by reverse transcriptase quantitative PCR (RT-qPCR) (**Fig. S6**) as in (**Burch-Smith et al., 2011b**). The RT-qPCR primers were designed using the AtRTPrimer program at http://pombe.kaist.ac.kr/AtRTPrimer/ (**Han and Kim, 2006**) with a target size of 100 base pair (bp) and a melting temperature of 65°C (**Table S10**). Three technical replicates were performed for each reaction. WT and *dse1* tiling array results were compared to the RT-qPCR results with a Pearson's product-moment correlation.

Analysis of genes and pathways

MapMan (http://mapman.gabipd.org/) software version 10.0, the TAIR9 pathways, and a Benjamini Hochberg correction for false discovery were used to identify the significantly affected processes in *dse1* (**Usadel et al., 2005**). PANTHER Overrepresentation Test for Gene Ontology at http://pantherdb.org/ (release 2015-04-30, GO Ontology database released 2016-05-20), complete biological processes, molecular processes, and cellular component GO analyses were conducted using Bonferroni correction (**Mi et al., 2013; Mi et al., 2016**).

### Comparative transcriptomics

The limma package was used to import the normalized transcriptomes and to calculate the differentially expressed genes using GEO2R at http://www.ncbi.nlm.nih.gov/geo/geo2r/ (R 3.2.3, Biobase 2.30.0, GEOquery 2.36.0, limma 3.26.8, data downloaded on May 20, 2016) with Benjamini & Hochberg correction for false discovery rate (**Barrett et al., 2013**). Only genes that had an adjusted p-value < 0.05 (identified with one-way ANOVA) and a fold change of ≥ 2 were included in further analysis. As the **Yamamoto et al.** (**2014**) transcriptomes were analyzed by the ATH1

array (ATH1-121501 Annotations, Release 32, http://www.affymetrix.com/), comparisons of the *lec1, lec2,* or *fus3* mutants, 12 DAF, or 16 DAF transcriptomes to the *dse1* or *ise* transcriptomes included genes only in the ATH1 array. Additional details of the methods used for comparative transcriptomics in **Supplementary Materials and Methods**.

**Propidium iodide staining**

*A. thaliana* plants were grown at 22°C under 16-hours-light/8-hours-dark and 100 µmol photons $m^{-2}s^{-1}$. WT and *dse1* embryos were extracted from their seed coats, and stained using 10 µL of 1 mg/mL propidium iodide (ThermoFisher Scientific, 0046880) in ½ Murashige and Skoog (MS) (Caisson Laboratories, MSP01-50LT) liquid medium for 2 minutes, transferred to ½ MS, placed on a slide with ½ MS, and imaged using a Zeiss LSM 710 confocal microscope, with 543-nm laser, collecting emissions from 592 to 630 nm.

**PD movement assays**

Movement assays, *Agrobacterium* methods, and imaging methods were performed as described (**Brunkard et al., 2015b**). *N. benthamiana* plants were grown at room temperature under 16-hours-light/8-hours-dark and 100 µmol of photons $m^{-2}s^{-1}$ of light. Wilcoxon rank sum tests were performed to compare the treatments and controls.

**Hormone treatments**

The fourth leaf (counting from the most recently emerged leaf downwards) of four-week old *N. benthamiana* plants was infiltrated with *Agrobacterium tumefaciens* (carrying a construct to express 1X-GFP) at an OD600 of 1.0e-4 as described (**Brunkard et al., 2015b**). Twenty-four hours later, the plants were randomly assigned to separate treatment groups and 5 mL of 100 µM of one hormone (Sigma-Aldrich catalog numbers as follows: ABA-A1049, GA-G7645, JA-J2500, SA-S3007) or water control was applied, via a spray bottle, to one plant, covering all of the leaves (including the leaf infiltrated to express GFP). The spray treatment was repeated 4 hours after the first spray to ensure full coverage of the leaves. The hormones were made in 1,000X stock and diluted to 100 µM in water. After 48 hours, the same region of each leaf was imaged.

**Overexpression of ABI5**

*ABI5* was cloned from *A. thaliana* seedling cDNA (ThermoFisher Scientific/Invitrogen, 18080051) with the primers, forward: 5'-caccATGGTAACTAGAGAAACGAAGTTGAC-3' and reverse: 5'-GAGTGGACAACTCGGGTTCCTCAT-3' and Gateway® cloned (ThermoFisher Scientific/Invitrogen K240020 and 11791-020) into the pMDC32 overexpression vector (**Curtis and Grossniklaus, 2003**) to make pMDC32-*AtABI5*. As a control, pMDC32-*GUS* was Gateway® cloned from the pENTR™-*GUS* plasmid (ThermoFisher Scientific/Invitrogen, 11791-020) into the pMDC32 overexpression vector. Constructs were confirmed by sequencing, transformed into *Agrobacterium*

(GV3101), and confirmed by colony PCR. The fourth leaf (counting from the most recently emerged leaf downwards) of four-week old plants was simultaneously infiltrated with *A. tumefaciens* (carrying a construct to express 1X-GFP) at an OD600 of 1.0e-4 and *A. tumefaciens* (carrying a construct to express ABI5 or the control overexpression construct) at an OD600 of 0.1. After 48 hours, the same region of each leaf was imaged.

### Virus Induced Gene Silencing

pTRV2-*NbDSE1* (**Xu et al., 2012**) and pTRV2-*GUS* (pYC1) (**Stonebloom et al., 2009**) were designed previously. Details of *NbABI5* Virus Induced Gene Silencing (VIGS) construct design in **Supplementary Materials and Methods**. Movement assays, *Agrobacterium* methods, VIGS, and imaging methods were performed as described (**Brunkard et al., 2015b**). *N. benthamiana* plants were grown at room temperature under 16-hours-light/8-hours-dark under 100 µmol photons $m^{-2}s^{-1}$. The fourth leaf (counting from the most recently emerged leaf downwards) of five week old silenced plants was infiltrated with *A. tumefaciens* (carrying a construct to express 1X-GFP) at an OD600 of 1.0e-4. Silencing of *NbABI5* was confirmed with RT-qPCR and details of these methods are in **Supplementary Materials and Methods**

### Transmission Electron Microscopy

Transmission Electron Microscopy (TEM) imaging was carried out as in (**Burch-Smith and Zambryski, 2010**; **Xu et al., 2012**). Imaging data from one embryo in **Xu et al.** (**2012**), previously used to find the proportion of twinned/branched PD, and data from a second experiment, published here, were used as replicates. The proportion of PD per cell wall was calculated for two embryos of each genotype (WT/heterozygous or *dse1*) at the late torpedo stage of embryo development. The area of cells in two embryos of each genotype were measured and compared.

## ACKNOWLEDGEMENTS

This work initially was funded by the National Institutes of Health (NIH) Grant GM45244 (to P.C.Z.). A.M.R. and J.O.B. were supported by predoctoral fellowships from the National Science Foundation. J.O.B. was also supported by a NIH Genetics Training Grant. We thank D. Schichnes and S. E. Ruzin of the CNR Biological Imaging Facility at the University of California, Berkeley; fluorescence microscopy imaging reported in this publication was supported in part by the NIH S10 program under award number 1S10RR026866-01. The content is solely the responsibility of the authors and does not necessarily represent the official views of the NIH.

## REFERENCES

**Attaran E, Major IT, Cruz JA, Rosa BA, Koo AJ, Chen J, Kramer DM, He SY, and Howe GA** (2014) Temporal dynamics of growth and photosynthesis suppression in response to jasmonate signaling. *Plant Physiol* **165**, 1302-1314.

**Barrett T, Wilhite SE, Ledoux P, Evangelista C, Kim IF, Tomashevsky M, Marshall KA, Phillippy KH, Sherman PM, Holko M, et al.** (2013) NCBI GEO: archive for functional genomics data sets--update. *Nucleic Acids Res* **41**, D991-D995.

**Benitez-Alfonso Y, Faulkner C, Pendle A, Miyashima S, Helariutta Y, and Maule A** (2013) Symplastic intercellular connectivity regulates lateral root patterning. *Dev Cell* **26**, 136-147.

**Bies N, Aspart L, Carles C, Gallois P, and Delseny M** (1998) Accumulation and degradation of Em proteins in *Arabidopsis thaliana*: evidence for post-transcriptional controls. *J Exp Bot* **49**, 1925-1933.

**Brunkard JO, Runkel AM, and Zambryski PC** (2013) Plasmodesmata dynamics are coordinated by intracellular signaling pathways. *Curr. Opin. Plant Biol* **16**, 614-620.

**Brunkard JO, Runkel AM, and Zambryski PC** (2015a) The cytosol must flow: intercellular transport through plasmodesmata. *Curr. Opin. Cell Biol* **35**, 13-20.

**Brunkard JO, Burch-Smith TM, Runkel AM, and Zambryski PC** (2015b) Investigating plasmodesmata genetics with virus-induced gene silencing and an *Agrobacterium*-mediated GFP movement assay. *Methods Mol Biol* **1217**, 185-198.

**Burch-Smith TM, and Zambryski PC** (2010) Loss of *INCREASED SIZE EXCLUSION LIMIT (ISE)1* or *ISE2* increases the formation of secondary plasmodesmata. *Curr Biol* **20**, 989-993.

**Burch-Smith TM, and Zambryski PC** (2012) Plasmodesmata paradigm shift: regulation from without versus within. *Annu Rev Plant Biol* **63**, 239-260.

**Burch-Smith TM, and Zambryski PC** (2016) Regulation of plasmodesmal transport and modification of plasmodesmata during development and following infection by viruses and viral proteins. In *Plant-Virus Interactions* (ed. Tatjana Kleinow), pp. 87-122. Springer International Publishing Switzerland.

**Burch-Smith TM, Stonebloom S, Xu M, and Zambryski PC** (2011a) Plasmodesmata during development: re-examination of the importance of primary, secondary, and branched plasmodesmata structure versus function. *Protoplasma* **248**, 61-74.

**Burch-Smith TM, Brunkard JO, Choi YG, and Zambryski PC** (2011b) Organelle-nucleus cross-talk regulates plant intercellular communication via plasmodesmata. *Proc Natl Acad Sci USA* **108**, 1451-1460.

**Calderwood A, Kopriva S, and Morris RJ** (2016) Transcript abundance explains mRNA mobility data in *Arabidopsis thaliana*. *Plant Cell* **28**, 610-605.

**Carles C, Bies-Etheve N, Aspart L, Léon-Kloosterziel KM, Koornneef M, Echeverria M, and Delseny M** (2002) Regulation of *Arabidopsis thaliana* Em genes: role of ABI5. *Plant J* **30**, 373-383.

**Chaiwanon J, Wang W, Zhu JY, Oh E, and Wang ZY** (2016) Information integration and communication in plant growth regulation. *Cell* **164**, 1257-1268.

**Choi DS, and Hwang BK** (2011). Proteomics and functional analyses of pepper abscisic acid-responsive 1 (ABR1), which is involved in cell death and defense signaling. *Plant Cell* **23**, 823-842.

**Creelman RA, and Mullet JE** (1995) Jasmonic acid distribution and action in plants: regulation during development and response to biotic and abiotic stress. *Proc Natl Acad Sci USA* **92**, 4114-4119.

**Curtis MD, and Grossniklaus U** (2003) A Gateway cloning vector set for high-throughput functional analysis of genes *in planta*. *Plant Physiol* **133**, 462-469.

**Daum G, Medzihradszky A, Suzaki T, and Lohmann JU** (2014) A mechanistic framework for noncell autonomous stem cell induction in *Arabidopsis*. *Proc Natl Acad Sci USA* **111**,14619-14624.

**De Storme N, and Geelen D** (2014) Callose homeostasis at plasmodesmata: molecular regulators and developmental relevance. *Front Plant Sci* **5**, 138.

**Delseny M, Bies-Etheve N, Carles C, Hull G, Vicient C, Raynal M, Grellet F, and Aspart L** (2001) Late embryogenesis abundant (LEA) protein gene regulation during *Arabidopsis* seed maturation. *J. Plant Physiol* **158**, 419-427.

**Devoto A, and Turner JG** (2003) Regulation of jasmonate-mediated plant responses in *Arabidopsis*. *Ann Bot* **92**, 329-337.

**Ellis C, Karafyllidis I, Wasternack C, and Turner JG** (2002) The *Arabidopsis* mutant *cev1* links cell wall signaling to jasmonate and ethylene responses. *Plant Cell* **14**, 1557-1566.

**Finkelstein R** (2010) The role of hormones during seed development and germination. In *Plant Hormones* (ed. Davies, P.J.), pp. 549-573. Springer Netherlands.

**Finkelstein R** (2013) Abscisic acid synthesis and response. In *The Arabidopsis Book*. edition 11, e0166.

**Finkelstein RR, and Lynch TJ** (2000) The *Arabidopsis* abscisic acid response gene *ABI5* encodes a basic leucine zipper transcription factor. *Plant Cell* **12**, 599-609.

**Finkelstein R, Gampala SS, Lynch TJ, Thomas TL, and Rock CD** (2005) Redundant and distinct functions of the ABA response loci *ABA-INSENSITIVE(ABI)5* and *ABRE-BINDING FACTOR (ABF)3*. *Plant Mol Biol* **59**, 253-267

**Fitzgibbon J, Beck M, Zhou J, Faulkner C, Robatzek S, and Oparka K** (2013) A developmental framework for complex plasmodesmata formation revealed by large-scale imaging of the *Arabidopsis* leaf epidermis. *Plant Cell* **25**, 57-70.

**Gisel A, Barella S, Hempel FD, and Zambryski PC** (1999) Temporal and spatial regulation of symplastic trafficking during development in *Arabidopsis thaliana* apices. *Development* **126**, 1879-1889.

**Gisel A, Hempel FD, Barella S, and Zambryski P** (2002) Leaf-to-shoot apex movement of symplastic tracer is restricted coincident with flowering in *Arabidopsis*. *Proc Natl Acad Sci USA* **99**, 1713-1717.

**Han S, and Kim D** (2006) AtRTPrimer: database for *Arabidopsis* genome-wide homogeneous and specific RT-PCR primer-pairs. *BMC Bioinformatics* **7**, 179.

**Han X, and Kim JY** (2016) Integrating hormone- and micromolecule-mediated signaling with plasmodesmal communication. *Mol Plant* **9**, 46-56.

**Hundertmark M, and Hincha DK** (2008) LEA (late embryogenesis abundant) proteins and their encoding genes in *Arabidopsis thaliana*. *BMC Genomics* **9**, 118.

**Jung C, Lyou SH, Yeu S, Kim MA, Rhee S, Kim M, Lee JS, Choi YD, and Cheong JJ** (2007) Microarray-based screening of jasmonate-responsive genes in *Arabidopsis* thaliana. *Plant Cell Rep* **26**, 1053-1063.

**Keith K, Kraml M, Dengler NG, and McCourt P** (1994) *fusca3*: A heterochronic mutation affecting late embryo development in *Arabidopsis*. *Plant Cell* **6**, 589-600.

**Kim I, Hempel FD, Sha K, Pfluger J, and Zambryski PC** (2002) Identification of a developmental transition in plasmodesmatal function during embryogenesis in *Arabidopsis thaliana*. *Development* **129**, 1261-1272.

**Kim I, Cho E, Crawford K, Hempel FD, and Zambryski PC** (2005a) Cell-to-cell movement of GFP during embryogenesis and early seedling development in *Arabidopsis*. *Proc Natl Acad Sci USA* **102**, 2227-2231.

**Kim I, Kobayashi K, Cho E, and Zambryski PC** (2005b) Subdomains for transport via plasmodesmata corresponding to the apical-basal axis are established during *Arabidopsis* embryogenesis. *Proc Natl Acad Sci USA* **102**, 11945-11950.

**Klie S, and Nikoloski Z** (2012) The choice between MapMan and Gene Ontology for automated gene function prediction in plant science. *Frontiers in Genetics* **3**, 115.

**Kong D, Karve R, Willet A, Chen MK, Oden J, and Shpak ED** (2012) Regulation of plasmodesmatal permeability and stomatal patterning by the glycosyltransferase-like protein KOBITO1. *Plant Physiol* **159**, 156-68.

**Laubinger S, Zeller G, Henz SR, Sachsenberg T, Widmer CK, Naouar N, Vuylsteke M, Schölkopf B, Rätsch G, and Weigel D** (2008) At-TAX: a whole genome tiling array resource for developmental expression analysis and transcript identification in *Arabidopsis thaliana*. *Genome Biol* **9**, R112.

**Le BH, Cheng C, Bui AQ, Wagmaister JA, Henry KF, Pelletier J, Kwong L, Belmonte M, Kirkbride R, Horvath S, et al.** (2010) Global analysis of gene activity during *Arabidopsis* seed development and identification of seed-specific transcription factors. *Proc Natl Acad Sci USA* **107**, 8063-8070.

**Lee SJ, Jung HJ, Kang H, and Kim SY** (2012) *Arabidopsis* zinc finger proteins AtC3H49/AtTZF3 and AtC3H20/AtTZF2 are involved in ABA and JA responses. *Plant Cell Physiol* **53**, 673-686.

**Lefebvre V, North H, Frey A, Sotta B, Seo M, Okamoto M, Nambara E, and Marion-Poll A** (2006) Functional analysis of *Arabidopsis NCED6* and *NCED9* genes indicates that ABA synthesized in the endosperm is involved in the induction of seed dormancy. *Plant J* **45**, 309-319.

**Levy A, Erlanger M, Rosenthal M, and Epel BL** (2007) A plasmodesmata-associated beta-1,3-glucanase in *Arabidopsis*. *Plant J* **49**, 669-82.

**Liu D, Shi L, Han C, Yu J, Li D, and Zhang Y** (2012) Validation of reference genes for gene expression studies in virus-infected *Nicotiana benthamiana* using quantitative real-time PCR. *PLoS ONE*, **7**, e46451.

**Lopez-Molina L, Mongrand S, McLachlin DT, Chait BT, and Chua NH** (2002) ABI5 acts downstream of ABI3 to execute an ABA-dependent growth arrest during germination. *Plant J* **32**, 317–328.

**Mansfield SG, and Briarty LG** (1990) Early embryogenesis in *Arabidopsis thaliana* .II. The developing embryo. *Can J Bot* **69**, 461-476

**Matsui A, Ishida J, Morosawa T, Mochizuki Y, Kaminuma E, Endo TA, Okamoto M, Nambara E, Nakajima M, Kawashima M, et al.** (2008) *Arabidopsis* transcriptome

analysis under drought, cold, high-salinity and ABA treatment conditions using a tiling array. *Plant Cell Physiol* **49**, 1135-1149.

**Matsushima R, Hayashi Y, Kondo M, Shimada T, Nishimura M, and Hara-Nishimura I** (2002) An endoplasmic reticulum-derived structure that is induced under stress conditions in *Arabidopsis. Plant Physiol* **130**, 1807-1814.

**McElver J, Tzafrir I, Aux G, Rogers R, Ashby C, Smith K, Thomas C, Schetter A, Zhou Q, Cushman MA, et al.** (2001) Insertional mutagenesis of genes required for seed development in *Arabidopsis thaliana*. *Genetics* **159**, 1751-63.

**Meinke DW, Franzmann LH, Nickle TC, and Yeung EC** (1994) *Leafy Cotyledon* mutants of *Arabidopsis*. *Plant Cell* **6**, 1049-1064.

**Mi H, Muruganujan A, Casagrande JT, and Thomas PD** (2013) Large-scale gene function analysis with the PANTHER classification system. *Nat Protoc* **8**, 1551-1566.

**Mi H, Poudel S, Muruganujan A, Casagrande JT, and Thomas PD** (2016) PANTHER version 10: expanded protein families and functions, and analysis tools. *Nucleic Acids Res* **44**, 336-342.

**Mishra AK, Puranik S, and Prasad M** (2012) Structure and regulatory networks of WD40 protein in plants. *J Plant Biochem Biot* **21**, 32-39.

**Moore-Gordon CS, Cowan AC, Bertling I, Botha, CEJ, and Cross RHM** (1998) Symplastic solute transport and Avocado fruit development: a decline in cytokinin/ABA ratio is related to appearance of the Hass small fruit variant. *Plant Cell Physiol* **39**, 1027-1038.

**Moreno JE, Shyu C, Campos ML, Patel LC, Chung HS, Yao J, He SY, and Howe GA** (2013) Negative feedback control of jasmonate signaling by an alternative splice variant of JAZ10. *Plant Physiol* **162**, 1006-1017.

**Nagpal P, Ellis CM, Weber H, Ploense SE, Barkawi LS, Guilfoyle TJ, Hagen G, Alonso JM, Cohen JD, Farmer EE, et al.** (2005) Auxin response factors ARF6 and ARF8 promote jasmonic acid production and flower maturation. *Development* **132**, 4107-4118.

**Nambara E, Keith K, McCourt P, and Naito S** (1995) A regulatory role for the *ABI3* gene in the establishment of embryo maturation in *Arabidopsis thaliana. Development* **121**, 629-636.

**Nezames CD, Sjogren CA, Barajas JF, and Larsen PB** (2012) The *Arabidopsis* cell cycle checkpoint regulators TANMEI/ALT2 and ATR mediate the active process of aluminum-dependent root growth inhibition. *Plant Cell* **24**, 608-621.

**Patton DA, Franzmann LH, and Meinke DW** (1991) Mapping genes essential for embryo development in *Arabidopsis thaliana*. *Mol Gen Genet* **227**, 337-47.

**Ramsay NA, and Glover BJ** (2005) MYB-bHLH-WD40 protein complex and the evolution of cellular diversity. *Trends Plant Sci* **10**, 63-70.

**Raz V, Bergervoet JH, and Koornneef M** (2001) Sequential steps for developmental arrest in *Arabidopsis* seeds. *Development* **128**, 243-252.

**Righetti K, Vu JL, Pelletier S, Vu BL, Glaab E, Lalanne D, Pasha A, Patel RV, Provart NJ, Verdier J, et al.** (2015) Inference of longevity-related genes from a robust coexpression network of seed maturation identifies regulators linking seed storability to biotic defense-related pathways. *Plant Cell* **27**, 2692-2708.

**Rim Y, Huang L, Chu H, Han X, Cho WK, Jeon CO, Kim HJ, Hong JC, Lucas WJ, and Kim JY** (2011) Analysis of *Arabidopsis* transcription factor families revealed extensive capacity for cell-to-cell movement as well as discrete trafficking patterns. *Mol Cells* **32**, 519-526.

**Rinne PL, and van der Schoot C** (1998) Symplasmic fields in the tunica of the shoot apical meristem coordinate morphogenetic events. *Development* **125**, 1477-1485.

**Sanger R, and Lee JY** (2014) Plasmodesmata in integrated cell signalling: insights from development and environmental signals and stresses. *J Exp Bot* **65**, 6337-6358.

**Schmid M, Davison TS, Henz SR, Pape UJ, Demar M, Vingron M, Schölkopf B, Weigel D, and Lohmann JU** (2005) A gene expression map of *Arabidopsis thaliana* development. *Nat Genet* **37**, 501–506.

**Seo M, and Koshiba T** (2002) Complex regulation of ABA biosynthesis in plants. *Trends Plant Sci* **7**, 41-48.

**Shi H, Wang X, Ye T, Chen F, Deng J, Yang P, Zhang Y, and Chan Z** (2014). The cysteine2/histidine2-type transcription factor ZINC FINGER OF ARABIDOPSIS THALIANA6 modulates biotic and abiotic stress responses by activating salicylic acid-related genes and C-REPEAT-BINDING FACTOR genes in *Arabidopsis*. *Plant Physiol* **165**, 1367-1379.

**Stirnimann CU, Petsalaki E, Russell RB, and Müller CW** (2010) WD40 proteins propel cellular networks. *Trends Biochem Sci* **35**, 565-574.

**Stone SL, Kwong LW, Yee KM, Pelletier J, Lepiniec L, Fischer RL, Goldberg RB, and Harada JJ** (2001) LEAFY COTYLEDON2 encodes a B3 domain transcription factor that induces embryo development. *Proc Natl Acad Sci USA* **98**, 11806-11811.

**Stonebloom S, Burch-Smith T, Kim I, Meinke D, Mindrinos M, and Zambryski P** (2009) Loss of the plant DEAD-box protein *ISE1* leads to defective mitochondria and increased cell-to-cell transport via plasmodesmata. *Proc Natl Acad Sci USA* **106**, 17229-17234.

**To A, Valon C, Savino G, Guilleminot J, Devic M, Giraudat J, and Parcy F** (2006) A network of local and redundant gene regulation governs *Arabidopsis* seed maturation. *Plant Cell* **18**, 1642-1651.

**Turner JG, Ellis C, and Devoto A** (2002) The jasmonate signal pathway. *Plant Cell* **14**, S153–S164.

**Usadel B, Nagel A, Thimm O, Redestig H, Blaesing OE, Palacios-Rojas N, Selbig J, Hannemann J, Piques MC, Steinhauser D, et al.** (2005) Extension of the visualization tool MapMan to allow statistical analysis of arrays, display of corresponding genes, and comparison with known responses. *Plant Physiol* **138**, 1195-11204.

**van Nocker S, and Ludwig P** (2003) The WD-repeat protein superfamily in *Arabidopsis*: conservation and divergence in structure and function. *BMC Genomics* **4**, 50.

**Vatén A, Dettmer J, Wu S, Stierhof YD, Miyashima S, Yadav SR, Roberts CJ, Campilho A, Bulone V, Lichtenberger R, et al.** (2011) Callose biosynthesis regulates symplastic trafficking during root development. *Dev Cell* **21**, 1144-1155.

**Wang X, Sager R, Cui W, Zhang C, Lu H, and Lee JY** (2013) Salicylic acid regulates plasmodesmata closure during innate immune responses in *Arabidopsis*. *Plant Cell* **25**, 2315-2329.

**West M, Yee KM, Danao J, Zimmerman JL, Fischer RL, Goldberg RB, and Harada JJ** (1994) LEAFY COTYLEDON1 is an essential regulator of late embryogenesis and cotyledon identity in *Arabidopsis*. *Plant Cell* **6**, 1731-1745.

**Wolf S, Hématy K, and Höfte H** (2012) Growth control and cell wall signaling in plants. *Ann Review Plant Biol* **63**, 381-407.

**Wu S, and Gallagher KL** (2012) Transcription factors on the move. *Curr Opin Plant Biol* **15**, 645-651.

**Xu M, Cho E, Burch-Smith TM, and Zambryski PC** (2012) Plasmodesmata formation and cell-to-cell transport are reduced in *decreased size exclusion limit 1* during embryogenesis in *Arabidopsis*. *Proc Natl Acad Sci USA* **109**, 5098-5103.

**Xu XM, Wang J, Xuan Z, Goldshmidt A, Borrill PG, Hariharan N, Kim JY, and Jackson D** (2011) Chaperonins facilitate KNOTTED1 cell-to-cell trafficking and stem

cell function. *Science* **26**, 1141-1144.

**Xu H, Iwashiro R, Li T, and Harada T** (2013) Long-distance transport of *Gibberellic Acid Insensitive* mRNA in *Nicotiana benthamiana*. *BMC Plant Biol* **13**, 165.

**Yamagishi K, Nagata N, Yee KM, Braybrook SA, Pelletier J, Fujioka S, Yoshida S, Fischer RL, Goldberg RB, and Harada JJ** (2005) *TANMEI/EMB2757* encodes a WD repeat protein required for embryo development in *Arabidopsis*. *Plant Physiol* **139**, 163-73.

**Yamamoto A, Yoshii M, Murase S, Fujita M, Kurata N, Hobo T, Kagaya Y, Takeda S, and Hattori T** (2014) Cell-by-cell developmental transition from embryo to post-germination phase revealed by heterochronic gene expression and ER-body formation in *Arabidopsis leafy cotyledon* mutants. *Plant Cell Physiol* **55**, 2112-2125.

**Zavaliev R, Ueki S, Epel BL, and Citovsky V** (2011) Biology of callose (β-1,3-glucan) turnover at plasmodesmata. *Protoplasma* **248**, 117-130.

## SUPPLEMENTARY MATERIALS

### Supplementary Figures

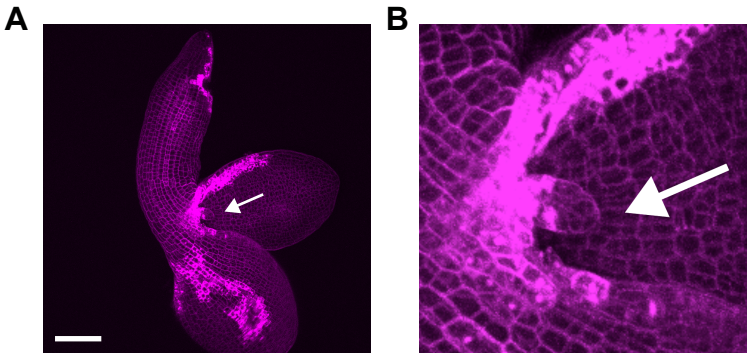


**Fig. S1. Leaf primordium on *dse1* embryos is similar to the *lec* mutants.** (**A**) A late walking stick stage *dse1* mutant embryo with a leaf primordium (white arrow), occasionally found on late walking stick and older *dse1* embryos. (Scale bar: 100 μm.) (**B**) Close up of leaf primordium on *dse1* embryo.

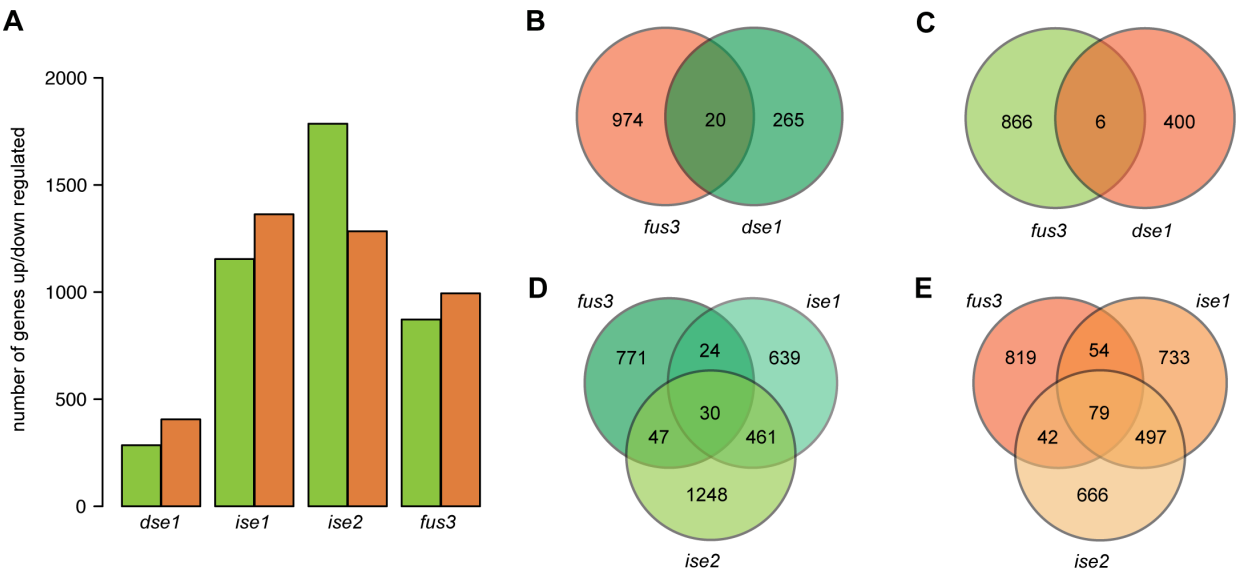


**Fig. S2. The *fus3* transcriptome compared to the *dse1* and *ise* transcriptomes.** (**A**) Total number of up (green bars) or down-regulated (orange bars) genes in *dse1*, *ise1*, *ise2*, and *fus3* transcriptomes. The *dse1*, *ise1*, and *ise2* transcriptomes were limited to genes on the ATH1 array, to match the same genes assayed in the *fus3* transcriptome *fus3* data from **Yamamoto et al.** (**2014**). (**B**) There are 20 overlapping genes in the Venn diagram of *dse1* up-regulated and *fus3* down-regulated genes. (**C**) Venn diagram showing 6 overlapping genes between *dse1* down-regulated genes and *fus3* up-regulated genes. The 273 similarly regulated genes between *dse1* and *fus3* are shown in **Fig. 2**. (**D**) There are 30 similarly up-regulated genes in *fus3* and the two *ise* mutants. (**E**) There are 79 similarly down-regulated genes in *fus3* and the two *ise* mutants. There are 81 oppositely regulated genes between the two *ise* mutants and *fus3*; all individual genes can be found in **Table S7**.

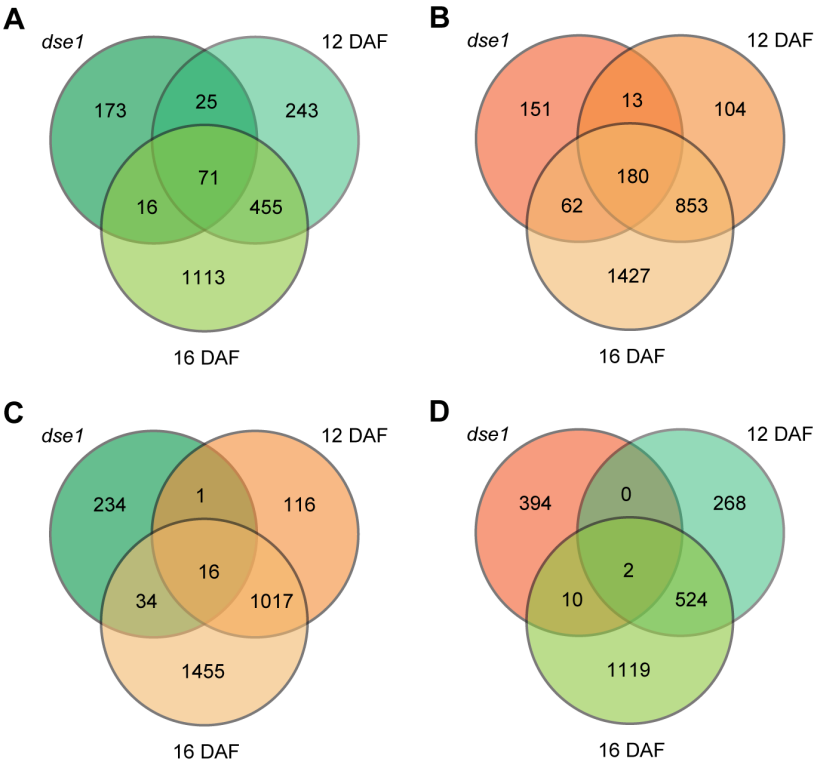


**Fig. S3. The *dse1* transcriptome compared to the 12 DAF and 16 DAF WT transcriptomes.** The *dse1* transcriptome was limited to genes on the ATH1 array, to match the same genes assayed in the 12 DAF and 16 DAF WT embryo transcriptomes (12 DAF and 16 DAF data collected by **Yamamoto et al.** (**2014**) using the ATH1 array). (**A**) Venn diagram of up-regulated genes in *dse1* and 12 DAF and 16 DAF WT embryo transcriptomes. (**B**) Venn diagram of down-regulated genes in *dse1* and 12 DAF and 16 DAF WT embryo transcriptomes. (**C**) Venn diagram of up-regulated genes in *dse1* and down-regulated genes in 12 DAF and 16 DAF WT embryo transcriptomes. (**D**) Venn diagram of down-regulated genes in *dse1* and up-regulated genes in 12 DAF and 16 DAF WT embryo transcriptomes.

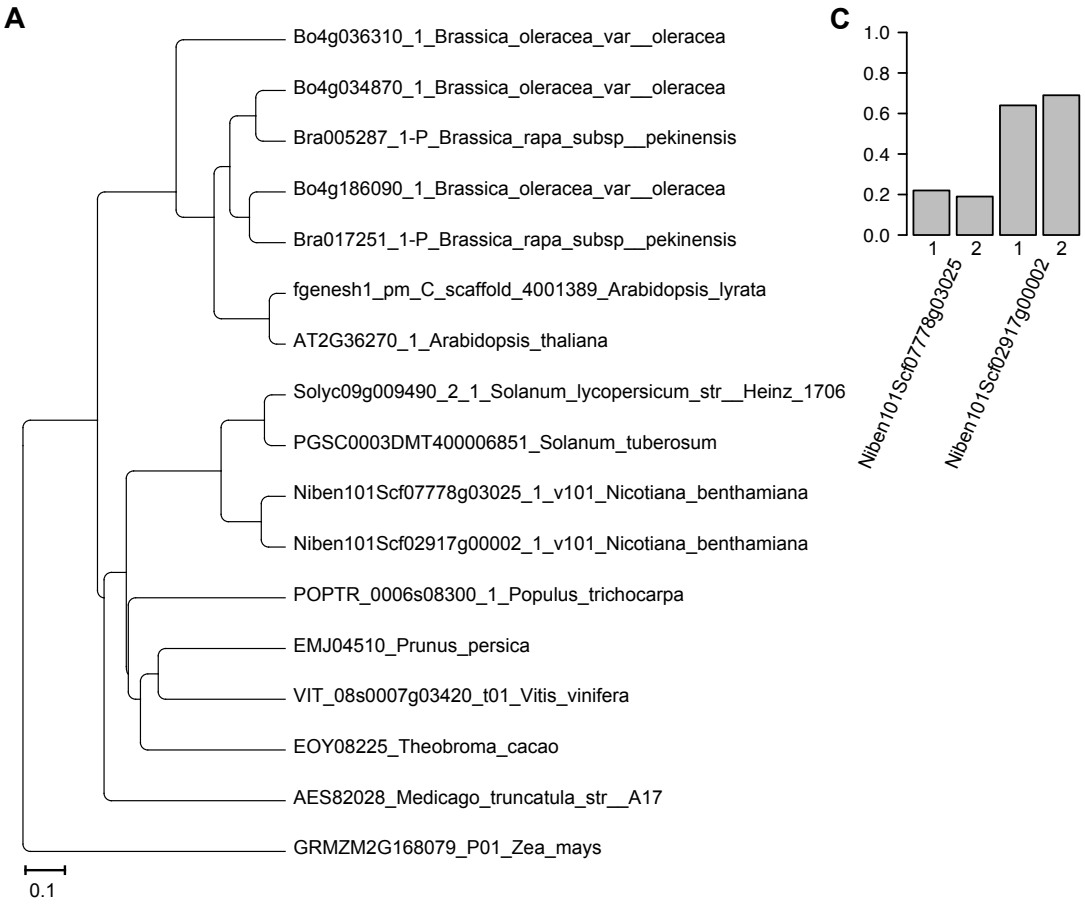


**B**

```
NbABI5_VIGS_trigger      ------------------------------------------ccaagcccacacgcacgc
Niben101Scf07778g03025.1 tatggatgaattccttaacagcatttggactgctgaagaaaaccaagcccacacgcacgc
Niben101Scf02917g00002.1 tatggatgaattccttaacagcatttggactgctgaagaaaatcaagcccacgcacacgc
                                                          .*********.*.*****

NbABI5_VIGS_trigger      gcatgcccatgctgcgcatgggcacggacacgggcacgcgcattctcatgctcatagcca
Niben101Scf07778g03025.1 gcatgcccatgctgcgcatgggcacggacacgggcacgcgcattctcatgctcatagcca
Niben101Scf02917g00002.1 ccatgcccatgccgcgcat------------aggcacgcgcattctcatgctcatagcca
                          ***********.******           .****************************

NbABI5_VIGS_trigger      ggcaccaagtgcaggggaagccactagcacgccacattttgcaataggacagagcaatgt
Niben101Scf07778g03025.1 ggcaccaagtgcaggggaagccactagcacgccacattttgcaataggacagagcaatgt
Niben101Scf02917g00002.1 ggcaccaagtacaggggaagccactagcacaccacattttgcgataggacagagcaatgt
                         **********.******************.***********.*****************

NbABI5_VIGS_trigger      ttcaatggagaaagctattgccaagcagccaagcctgccaagacagggttctcttacgct
Niben101Scf07778g03025.1 ttcaatggagaaagctattgccaagcagccaagcctgccaagacagggttctcttacgct
Niben101Scf02917g00002.1 tccaatggagaaagctattgccaagcagccaagcttgccaaggcagggttctcttacact
                         *.*********************************.*******.**************.**

NbABI5_VIGS_trigger      tccggaacctttatgtcggaaaactgtggatgaagtttggtcagaaattcataagagcca
Niben101Scf07778g03025.1 tccggaacctttatgtcggaaaactgtggatgaagtttggtcagaaattcataagagcca
Niben101Scf02917g00002.1 tccggaacctttgtgtcgaaaaactgtggatgaagtttggtcagaaattcataagagcca
                         ************.******.****************************************

NbABI5_VIGS_trigger      aaaagagcaacatcagaataacgggagcagtgtcccggacacgggtaattccgctcaacg
Niben101Scf07778g03025.1 aaaagagcaacatcagaataacgggagcagtgtcccggacacgggtaattccgctcaacg
Niben101Scf02917g00002.1 aaaagagcaacatcagaataatgggagcagtgtccaggacacgggtaattctgctcaacg
                         **********************.************* ***************.********

NbABI5_VIGS_trigger      acaggttacatttggtgaaatgacactcgagga---------------------------
Niben101Scf07778g03025.1 acaggttacatttggtgaaatgacactcgaggatttcttggtgaaagcaggggtagtacg
Niben101Scf02917g00002.1 acaggtcacatttggtgaaatgacactcgaggatttcttggtgaaagcaggggtagtacg
                         ******.*************************
```

(continued from previous page)

**Fig. S4. VIGS trigger design for *ABI5* in *N. benthamiana*.** *ABI5* orthologs were found through Ensembl Plants, and any *N. benthamiana* proteins with alignments to the *A. thaliana* ABI5 protein (BLAST through SolGenomics) were identified. Protein sequences were aligned by MAFFT (L-INS-i with 100 bootstrap values) to produce gene trees with Archaeopteryx. (**A**) According to this gene tree, there are two *ABI5* genes in the *N. benthamiana* genome, which is not surprising, because *N. benthamiana* is the descendent of an allotetraploid, and often has two homeologues of each gene in its genome. (**B**) An alignment of the two genes (cDNA) with the designed pTRV2-*NbABI5* trigger shows that the VIGS construct is highly similar to both copies of the *N. benthamiana ABI5* gene (Niben101Scf07778g03025 and Niben101Scf02917g00002). (**C**) Gene silencing of *NbABI5* was confirmed with RT-qPCR. Three biological replicates *NbABI5* silenced plants and three control plants were each tested with primer set 1 for each *ABI5* ortholog and verified with two separate biological replicates and primer set 2 for each ortholog. Expression level was calculated according to an endogenous reference gene and relative to the VIGS control calibrator = $2^{-\Delta\Delta Ct}$. Expression level shown in bar graph is relative to VIGS control (proportional to 1.0).

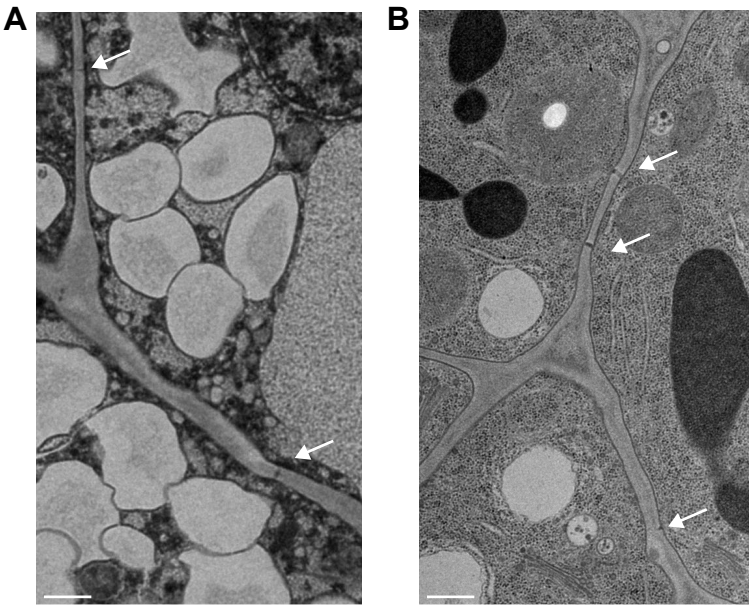


**Fig. S5. TEM of WT and *dse1* embryos.** (**A**) WT image. (**B**) *dse1* image. (Scale bars: 0.5 μm.) Arrows indicate location of PD in cell wall.

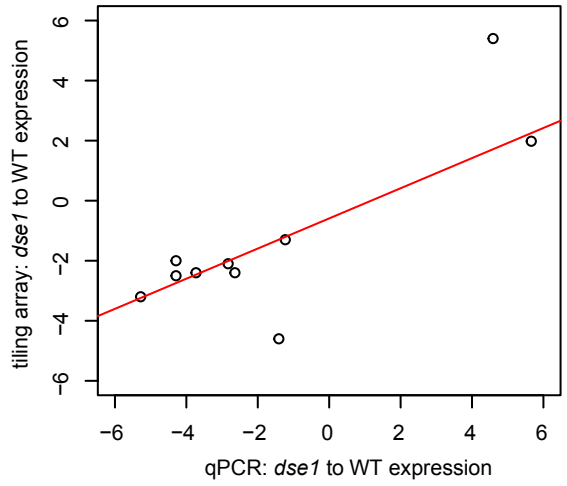


**Fig. S6. Quantitative PCR confirmed the *dse1* tiling array results.** Expression levels of 10 genes altered in expression in the *dse1* transcriptome were assayed independently by RT-qPCR and the results from each analysis were plotted against each other (Pearson's product-moment correlation, three technical replicates were performed for each reaction, t = 2.897, df = 9, p-value < 0.008, cor = 0.69).

## Supplementary Materials and Methods

Comparative transcriptomics

The ATH1 probe annotation was downloaded from Affymetrix at http://www.affymetrix.com/catalog/131416/AFFY/Arabidopsis+ATH1+Genome+Array#1_3 on May 20, 2016.

The *lec1, lec2,* or *fus3* mutant transcriptomes corresponding to 12 DAF were used for comparisons with the corresponding WT 8 DAF; *fus3* mutant was in Col-0 background and *lec1* and *lec2* mutants were in Ws background as described (**Yamamoto et al., 2014**). The WT 12 DAF or WT 16 DAF transcriptomes compared to the WT 8 DAF transcriptome were in the Col-0 background.

Hypergeometric probabilities for transcriptome comparisons were calculated as described (**Fury et al., 2006**) using R (3.2.3) and were confirmed with a hypergeometric probability program that also calculates a gene overlap representation factor for transcriptomes (conducted on May 23, 2016, program at http://nemates.org/MA/progs/overlap_stats.html and program's statistics information at http://nemates.org/MA/progs/representation.stats.html).

R (3.2.3) was used to create Venn diagrams and bar graphs in the comparative transcriptome studies.

Virus Induced Gene Silencing

Details on construct design

The protein sequence of the *A. thaliana ABI5* gene from TAIR (http://www.arabidopsis.org/) was used to BLAST the *N. benthamiana* genome (v1.0.1) at https://solgenomics.net/ (**Bombarely et al., 2012**) using an e-value threshold of 10 and BLOSUM62 substitution matrix. Any protein matches were used to construct gene trees, along with ortholog protein sequences collected from Ensembl Plants (release 30 - December 2015) at http://plants.ensembl.org/ (**Vilella et al., 2009**) to identify *N. benthamiana* orthologs of the gene of interest (**Fig. S4A**). Gene trees were made with MAFFT (v7.273) alignments (**Katoh et al., 2005**), with the highly accurate L-INS-i method, with 100 bootstrap values, and the gene tree design program Archaeopteryx (version 0.9901, 2014-10-14, based on forester 1.038). The VIGS trigger was designed to silence only the orthologs of *ABI5* by selectively finding regions specific to the gene of interest, but not overlapping with related homologs. The trigger was used as a BLAST query against the *N. benthamiana* genome (predicted cDNA v1.0.1) using an e-value threshold of 10 and BLOSUM62 substitution matrix to check for any off-target genes, and selected to not have any off-target sequence matches >18 bp. The constructs were checked again to be orthologs of *A. thaliana*, with BLAST in TAIR.

The *ABI5* VIGS trigger was cloned from *N. benthamiana* genotype Nb-1 cDNA (RNA extraction: Sigma-Aldrich, STRN250-1KT; DNase treatment: NEB, M0303S; first-strand cDNA synthesis: ThermoFisher Scientific/Invitrogen, 18080051; RNase H treatment: ThermoFisher Scientific/Invitrogen: 18021071), and restriction cloned (NEB, NcoI and XmaI) into pYL156 (empty TRV2 vector). The pTRV2-*NbABI5* construct was cloned with the primers, forward: 5'-gagccatggCCAAGCCCACACGC-3' and reverse: 5'-caacccgggTCCTCGAGTGTCATTTCACC-3'. The VIGS triggers were aligned with the *N. benthamiana* genome (v1.0.1) sequence and the cloned cDNA sequence (**Fig. S4B**).

The cloned trigger was used as a BLAST query against the *N. benthamiana* genome (predicted cDNA v1.0.1) using an e-value threshold of 10 and BLOSUM62 substitution matrix to check for any off-target genes. No off-target sequence matches >18 bp were identified with the final cloned pTRV2-*NbABI5* construct.

Details of RT-qPCR for VIGS

Silencing of *NbABI5* was confirmed with RT-qPCR, with three biological replicates of pTRV2-*NbABI5* silenced plants and three biological replicates of pTRV2-*GUS* VIGS plants as controls (**Fig. S4C**). Gene silencing of *NbABI5* was tested using two primer sets for each *N. benthamiana ABI5* ortholog, as well as primers for a verified reference gene (primers in **Table S10**; **Liu et al., 2012**). Gene silencing was approximately 80 percent for the *N. benthamiana ABI5* ortholog Niben101Scf07778g03025 (relative expression level = $2^{-\Delta\Delta Ct}$ = 0.22 for primer set 1 and 0.19 for primer set 2) and approximately 30 percent for the *ABI5* ortholog Niben101Scf02917g00002 (relative expression level = $2^{-\Delta\Delta Ct}$ = 0.64 for primer set 1 and 0.69 for primer set 2).

The fourth leaf of three biological replicates (separate plants) were ground with a mortar and pestle in liquid $N_2$. Total RNA was extracted following manufactures protocol (Sigma-Aldrich, STRN250-1KT) and genomic DNA was removed with DNase treatment (NEB, M0303S). First-strand cDNA was made following manufactures protocol from 3 µg of RNA (ThermoFisher Scientific/Invitrogen, 18080051), treated with RNaseH (ThermoFisher Scientific/Invitrogen: 18021071), and diluted 1:1.

Primers were designed to amplify a sequence less than 150 bp and were synthesized by Elim Biopharmaceuticals, Inc. (**Table S10**). Primers were used at 0.5 µM final concentration with DyNAmo HS SYBR Green master mix (ThermoFisher Scientific, F410L), 1.5 µL cDNA (~5.5 ng/µL cDNA) in the qPCR reaction. Three biological replicates *NbABI5* silenced plants and three control plants were each tested with primer set 1 for each *ABI5* ortholog (**Fig. S4**; **Table S10**) and verified with two separate biological replicates and primer set 2 for each ortholog. Thermocycling conditions were 95°C for 15 min, then 40 cycles of 94°C for 10 s, 60°C for 30 s, 72°C for 30 s, and a final extension of 72°C for for 2 min. A melt curve was followed starting at 72°C and ramping up to 95°C in 0.5°C increments. iCycler and Ct values were calculated with iQ5 (Bio-Rad; http://www.bio-rad.com). Expression level was calculated according to the endogenous reference gene (**Liu et al., 2012**) and relative to the VIGS control calibrator = $2^{-\Delta\Delta Ct}$.

**Supplementary Materials References**

**Bombarely A, Rosli HG, Vrebalov J, Moffett P, Mueller LA, and Martin GB** (2012) A draft genome sequence of *Nicotiana benthamiana* to enhance molecular plant-microbe biology research. *Mol Plant Microbe Interact* **25**, 1523-1530.

**Fury W, Batliwalla F, Gregersen PK, and Li W** (2006) Overlapping probabilities of top ranking gene lists, hypergeometric distribution, and stringency of gene selection criterion. *Conf Proc IEEE Eng Med Biol Soc* **1**, 5531-5534.

**Katoh K, Kuma K, Toh H, and Miyata T** (2005) MAFFT version 5: improvement in accuracy of multiple sequence alignment. *Nucleic Acids Res* **33**, 511-518.

**Liu D, Shi L, Han C, Yu J, Li D, and Zhang Y** (2012) Validation of reference genes for gene expression studies in virus-infected *Nicotiana benthamiana* using quantitative real-time PCR. *PLoS ONE* **7**, e46451.

**Vilella AJ, Severin J, Ureta-Vidal A, Heng L, Durbin R, and Birney E** (2009) EnsemblCompara GeneTrees: Complete, duplication-aware phylogenetic trees invertebrates. *Genome Res* **19**, 327-335.

**Yamamoto A, Yoshii M, Murase S, Fujita M, Kurata N, Hobo T, Kagaya Y, Takeda S, and Hattori T** (2014) Cell-by-cell developmental transition from embryo to post-germination phase revealed by heterochronic gene expression and ER-body formation in *Arabidopsis leafy cotyledon* mutants. *Plant Cell Physiol* **55**, 2112-2125.

## Supplementary Tables

Note: Supplementary Tables 1 and 7 are in two separate documents due to size, and are available upon request.

## Table S2. Twenty-one of the 51 Late Embryogenesis Abundant (LEA) protein encoding genes are up-regulated in the *dse1* transcriptome.

| Locus[1, 2] | Gene symbol[2] | *dse1*_Tiling | *ise1*_Tiling | *ise2*_Tiling |
|---|---|---|---|---|
| AT1G01470 | *LATE EMBRYOGENESIS ABUNDANT 14 (LEA14)* | - | - | -2.1 |
| AT1G02820 | *LATE EMBRYOGENESIS ABUNDANT 3 (LEA3)* | - | - | - |
| AT1G03120 | *RESPONSIVE TO ABSCISIC ACID 28 (RAB28)* | - | - | -4.6 |
| AT1G20440 | *COLD-REGULATED 47 (COR47)* | - | - | -2.6 |
| AT1G20450 | *EARLY RESPONSIVE TO DEHYDRATION 10 (ERD10)* | - | - | -2.2 |
| AT1G32560 | *LATE EMBRYOGENESIS ABUNDANT 4-1 (AtLEA4-1)* | 4.7 | -16.5 | - |
| AT1G52690 | *LATE EMBRYOGENESIS ABUNDANT 7 (LEA7)* | 3.2 | -3.3 | -2.9 |
| AT1G54410 | | - | - | - |
| AT1G72100 | | 12 | - | - |
| AT1G76180 | *EARLY RESPONSE TO DEHYDRATION 14 (ERD14)* | - | - | - |
| AT2G03740 | | - | - | - |
| AT2G03850 | | - | 4.5 | 5.9 |
| AT2G18340 | | 4.1 | - | - |
| AT2G21490 | *DEHYDRIN LEA (LEA)* | 8.1 | - | - |
| AT2G23110 | | - | - | - |
| AT2G23120 | | 6.2 | - | - |
| AT2G33690 | | - | - | - |
| AT2G35300 | *LATE EMBRYOGENESIS ABUNDANT 18 (LEA18)* | 24.4 | - | - |
| AT2G36640 | *EMBRYONIC CELL PROTEIN 63 (ECP63)* | 5 | -7.3 | -10.6 |
| AT2G40170 | *LATE EMBRYOGENESIS ABUNDANT 6 (GEA6)* | 11.5 | - | - |
| AT2G41260 | *(M17)* | - | - | - |
| AT2G41280 | *(M10)* | - | - | - |
| AT2G42530 | *COLD REGULATED 15B (COR15B)* | - | - | - |
| AT2G42540 | *COLD-REGULATED 15A (COR15A)* | - | - | - |
| AT2G42560 | | 19.7 | 2.3 | - |
| AT2G44060 | | - | - | - |
| AT2G46140 | | - | - | - |
| AT3G02480 | | 74.5 | - | - |
| AT3G15670 | | 108.9 | - | - |
| AT3G17520 | | 114 | - | - |
| AT3G22490 | | - | - | - |
| AT3G22500 | *LATE EMBRYOGENESIS ABUNDANT PROTEIN ECP31 (ATECP31)* | - | - | - |
| AT3G50970 | *LOW TEMPERATURE-INDUCED 30 (LTI30)* | - | - | 2.8 |
| AT3G50980 | *DEHYDRIN XERO 1 (XERO1)* | 3.8 | - | 8.9 |
| AT3G51810 | *LATE EMBRYOGENESIS ABUNDANT 1 (EM1)* | 213.4 | - | - |

| | | | | |
|---|---|---|---|---|
| AT3G53040 | | 18.8 | - | - |
| AT3G53770 | | - | - | - |
| AT4G02380 | *SENESCENCE-ASSOCIATED GENE 21 (SAG21)* | 3.5 | - | - |
| AT4G13230 | | - | - | - |
| AT4G13560 | *UNFERTILIZED EMBRYO SAC 15 (UNE15)* | - | - | - |
| AT4G15910 | *DROUGHT-INDUCED 21 (DI21)* | - | - | - |
| AT4G21020 | | 9.5 | - | - |
| AT4G36600 | | - | - | - |
| AT4G38410 | | - | - | - |
| AT4G39130 | | - | - | - |
| AT5G06760 | *LATE EMBRYOGENESIS ABUNDANT 4-5 (LEA4-5)* | 87.6 | - | - |
| AT5G27980 | | - | - | - |
| AT5G44310 | | 10.7 | - | -6.3 |
| AT5G53260 | | - | -5.1 | -28.6 |
| AT5G53270 | | - | - | - |
| AT5G66400 | *RESPONSIVE TO ABA 18 (RAB18)* | 12.9 | - | - |

[1] LEA protein encoding genes in the *Arabidopsis* genome were identified in **Hundertmark and Hincha, 2008**.
[2] TAIR annotation.

## Table S3. A GO analysis of the up-regulated genes in the *dse1* _Tiling transcriptome.

| GO biological process complete | Ref (#) | Found (#) | Expected (#) | Enrichment | Fold | p-value |
|---|---|---|---|---|---|---|
| S-glycoside catabolic process (GO:0016145) | 27 | 5 | 0.3 | up | 16.42 | 3.06E-02 |
| glucosinolate catabolic process (GO:0019762) | 27 | 5 | 0.3 | up | 16.42 | 3.06E-02 |
| glycosinolate catabolic process (GO:0019759) | 27 | 5 | 0.3 | up | 16.42 | 3.06E-02 |
| S-glycoside metabolic process (GO:0016143) | 59 | 8 | 0.67 | up | 12.02 | 9.10E-04 |
| glucosinolate metabolic process (GO:0019760) | 59 | 8 | 0.67 | up | 12.02 | 9.10E-04 |
| glycosinolate metabolic process (GO:0019757) | 59 | 8 | 0.67 | up | 12.02 | 9.10E-04 |
| response to water deprivation (GO:0009414) | 168 | 22 | 1.9 | up | 11.61 | 1.80E-13 |
| response to water (GO:0009415) | 171 | 22 | 1.93 | up | 11.41 | 2.57E-13 |
| response to cold (GO:0009409) | 185 | 16 | 2.09 | up | 7.67 | 1.19E-06 |
| response to temperature stimulus (GO:0009266) | 274 | 20 | 3.09 | up | 6.47 | 1.62E-07 |
| response to abscisic acid (GO:0009737) | 302 | 22 | 3.41 | up | 6.46 | 1.88E-08 |
| response to osmotic stress (GO:0006970) | 334 | 24 | 3.77 | up | 6.37 | 2.77E-09 |
| response to salt stress (GO:0009651) | 306 | 20 | 3.45 | up | 5.79 | 1.07E-06 |
| response to alcohol (GO:0097305) | 342 | 22 | 3.86 | up | 5.7 | 1.94E-07 |
| response to inorganic substance (GO:0010035) | 536 | 30 | 6.05 | up | 4.96 | 2.18E-09 |
| response to lipid (GO:0033993) | 417 | 23 | 4.7 | up | 4.89 | 1.36E-06 |
| response to acid chemical (GO:0001101) | 676 | 37 | 7.63 | up | 4.85 | 8.24E-12 |
| sulfur compound metabolic process (GO:0006790) | 260 | 13 | 2.93 | up | 4.43 | 2.03E-02 |
| secondary metabolic process (GO:0019748) | 323 | 16 | 3.64 | up | 4.39 | 2.23E-03 |
| response to oxygen-containing compound (GO:19017( | 879 | 40 | 9.92 | up | 4.03 | 2.19E-10 |
| response to abiotic stimulus (GO:0009628) | 1121 | 50 | 12.65 | up | 3.95 | 2.73E-13 |
| response to endogenous stimulus (GO:0009719) | 996 | 37 | 11.24 | up | 3.29 | 5.93E-07 |
| response to hormone (GO:0009725) | 924 | 34 | 10.42 | up | 3.26 | 4.17E-06 |
| response to organic substance (GO:0010033) | 1148 | 41 | 12.95 | up | 3.17 | 1.91E-07 |
| response to chemical (GO:0042221) | 1682 | 54 | 18.97 | up | 2.85 | 7.89E-09 |
| response to stress (GO:0006950) | 2171 | 57 | 24.49 | up | 2.33 | 3.79E-06 |
| multicellular organism development (GO:0007275) | 1510 | 37 | 17.03 | up | 2.17 | 1.72E-02 |
| single-multicellular organism process (GO:0044707) | 1552 | 38 | 17.51 | up | 2.17 | 1.31E-02 |
| multicellular organismal process (GO:0032501) | 1652 | 40 | 18.63 | up | 2.15 | 9.54E-03 |
| anatomical structure development (GO:0048856) | 1684 | 40 | 19 | up | 2.11 | 1.49E-02 |
| single-organism developmental process (GO:0044767) | 1732 | 41 | 19.54 | up | 2.1 | 1.23E-02 |
| developmental process (GO:0032502) | 1758 | 41 | 19.83 | up | 2.07 | 1.75E-02 |
| response to stimulus (GO:0050896) | 3894 | 82 | 43.92 | up | 1.87 | 1.79E-05 |
| Unclassified (UNCLASSIFIED) | 8013 | 90 | 90.39 | down | 1 | 0.00E+00 |

| GO cellular component complete | Ref (#) | Found (#) | Expected (#) | Enrichment | Fold | p-value |
|---|---|---|---|---|---|---|
| plasmodesma (GO:0009506) | 658 | 21 | 7.42 | up | 2.83 | 1.06E-02 |

| | | | | | | |
|---|---|---|---|---|---|---|
| symplast (GO:0055044) | 658 | 21 | 7.42 | up | 2.83 | 1.06E-02 |
| cell-cell junction (GO:0005911) | 660 | 21 | 7.44 | up | 2.82 | 1.10E-02 |
| cell junction (GO:0030054) | 660 | 21 | 7.44 | up | 2.82 | 1.10E-02 |
| extracellular region (GO:0005576) | 2288 | 58 | 25.81 | up | 2.25 | 2.18E-06 |
| Unclassified (UNCLASSIFIED) | 6192 | 76 | 69.85 | up | 1.09 | 0.00E+00 |
| intracellular organelle (GO:0043229) | 14047 | 120 | 158.45 | down | 0.76 | 2.49E-03 |
| organelle (GO:0043226) | 14047 | 120 | 158.45 | down | 0.76 | 2.49E-03 |
| intracellular membrane-bounded organelle (GO:00432 | 13824 | 118 | 155.94 | down | 0.76 | 3.23E-03 |
| membrane-bounded organelle (GO:0043227) | 13824 | 118 | 155.94 | down | 0.76 | 3.23E-03 |

| **GO molecular function complete** | **Ref (#)** | **Found (#)** | **Expected (#)** | **Enrichment** | **Fold** | **p-value** |
|---|---|---|---|---|---|---|
| Unclassified (UNCLASSIFIED) | 7768 | 85 | 87.62 | down | 0.97 | 0.00E+00 |

## Table S4. A GO analysis of the down-regulated genes in the *dse1*_Tiling transcriptome.

| GO biological process complete | Ref (#) | Found (#) | Expected (#) | Enrichment | Fold | p-value |
|---|---|---|---|---|---|---|
| protoporphyrinogen IX biosynthetic process (GO:000678 | 9 | 5 | 0.15 | up | 33.69 | 9.65E-04 |
| protoporphyrinogen IX metabolic process (GO:0046501) | 9 | 5 | 0.15 | up | 33.69 | 9.65E-04 |
| chlorophyll biosynthetic process (GO:0015995) | 25 | 9 | 0.41 | up | 21.83 | 1.13E-06 |
| heme biosynthetic process (GO:0006783) | 15 | 5 | 0.25 | up | 20.22 | 1.14E-02 |
| porphyrin-containing compound biosynthetic process (G | 31 | 9 | 0.51 | up | 17.61 | 7.17E-06 |
| heme metabolic process (GO:0042168) | 18 | 5 | 0.3 | up | 16.85 | 2.73E-02 |
| chlorophyll metabolic process (GO:0015994) | 33 | 9 | 0.54 | up | 16.54 | 1.22E-05 |
| tetrapyrrole biosynthetic process (GO:0033014) | 33 | 9 | 0.54 | up | 16.54 | 1.22E-05 |
| porphyrin-containing compound metabolic process (GO: | 43 | 9 | 0.71 | up | 12.69 | 1.15E-04 |
| tetrapyrrole metabolic process (GO:0033013) | 44 | 9 | 0.73 | up | 12.4 | 1.39E-04 |
| photosynthesis (GO:0015979) | 133 | 21 | 2.19 | up | 9.58 | 4.43E-11 |
| photosynthesis, light reaction (GO:0019684) | 60 | 9 | 0.99 | up | 9.1 | 1.80E-03 |
| pigment biosynthetic process (GO:0046148) | 74 | 9 | 1.22 | up | 7.38 | 9.70E-03 |
| pigment metabolic process (GO:0042440) | 88 | 9 | 1.45 | up | 6.2 | 3.77E-02 |
| cofactor biosynthetic process (GO:0051188) | 145 | 13 | 2.39 | up | 5.44 | 2.44E-03 |
| cofactor metabolic process (GO:0051186) | 247 | 18 | 4.07 | up | 4.42 | 4.82E-04 |
| response to light stimulus (GO:0009416) | 422 | 21 | 6.96 | up | 3.02 | 1.98E-02 |
| response to radiation (GO:0009314) | 442 | 21 | 7.29 | up | 2.88 | 3.89E-02 |
| Unclassified (UNCLASSIFIED) | 8013 | 157 | 132.13 | up | 1.19 | 0.00E+00 |

| GO cellular component complete | Ref (#) | Found (#) | Expected (#) | Enrichment | Fold | p-value |
|---|---|---|---|---|---|---|
| photosystem II oxygen evolving complex (GO:0009654) | 15 | 5 | 0.25 | up | 20.22 | 2.64E-03 |
| chloroplast thylakoid lumen (GO:0009543) | 54 | 16 | 0.89 | up | 17.97 | 1.08E-12 |
| plastid thylakoid lumen (GO:0031978) | 54 | 16 | 0.89 | up | 17.97 | 1.08E-12 |
| thylakoid lumen (GO:0031977) | 60 | 17 | 0.99 | up | 17.18 | 3.00E-13 |
| photosystem I (GO:0009522) | 21 | 5 | 0.35 | up | 14.44 | 1.31E-02 |
| thylakoid part (GO:0044436) | 271 | 58 | 4.47 | up | 12.98 | 3.98E-42 |
| photosynthetic membrane (GO:0034357) | 239 | 51 | 3.94 | up | 12.94 | 1.04E-36 |
| thylakoid membrane (GO:0042651) | 238 | 50 | 3.92 | up | 12.74 | 1.24E-35 |
| chloroplast thylakoid membrane (GO:0009535) | 224 | 47 | 3.69 | up | 12.72 | 2.37E-33 |
| plastid thylakoid membrane (GO:0055035) | 224 | 47 | 3.69 | up | 12.72 | 2.37E-33 |
| plastoglobule (GO:0010287) | 43 | 9 | 0.71 | up | 12.69 | 2.64E-05 |
| chloroplast thylakoid (GO:0009534) | 298 | 62 | 4.91 | up | 12.62 | 1.70E-44 |
| plastid thylakoid (GO:0031976) | 298 | 62 | 4.91 | up | 12.62 | 1.70E-44 |
| photosystem II (GO:0009523) | 39 | 8 | 0.64 | up | 12.44 | 1.67E-04 |
| thylakoid (GO:0009579) | 341 | 66 | 5.62 | up | 11.74 | 1.28E-45 |
| photosystem (GO:0009521) | 54 | 10 | 0.89 | up | 11.23 | 1.52E-05 |

| | | | | | | |
|---|---|---|---|---|---|---|
| organelle subcompartment (GO:0031984) | 521 | 63 | 8.59 | up | 7.33 | 9.53E-32 |
| chloroplast stroma (GO:0009570) | 426 | 47 | 7.02 | up | 6.69 | 1.65E-21 |
| plastid stroma (GO:0009532) | 440 | 47 | 7.26 | up | 6.48 | 6.16E-21 |
| chloroplast part (GO:0044434) | 858 | 90 | 14.15 | up | 6.36 | 7.27E-42 |
| plastid part (GO:0044435) | 874 | 90 | 14.41 | up | 6.24 | 3.10E-41 |
| chloroplast envelope (GO:0009941) | 414 | 35 | 6.83 | up | 5.13 | 3.51E-12 |
| plastid envelope (GO:0009526) | 424 | 35 | 6.99 | up | 5.01 | 6.98E-12 |
| organelle envelope (GO:0031967) | 718 | 35 | 11.84 | up | 2.96 | 8.77E-06 |
| envelope (GO:0031975) | 719 | 35 | 11.86 | up | 2.95 | 9.07E-06 |
| chloroplast (GO:0009507) | 2957 | 132 | 48.76 | up | 2.71 | 2.01E-24 |
| plastid (GO:0009536) | 3002 | 132 | 49.5 | up | 2.67 | 8.30E-24 |
| intracellular organelle part (GO:0044446) | 3101 | 100 | 51.13 | up | 1.96 | 1.74E-08 |
| organelle part (GO:0044422) | 3109 | 100 | 51.27 | up | 1.95 | 2.00E-08 |
| Unclassified (UNCLASSIFIED) | 6192 | 141 | 102.1 | up | 1.38 | 0.00E+00 |
| cellular_component (GO:0005575) | 20492 | 299 | 337.9 | down | 0.88 | 6.09E-03 |
| nucleus (GO:0005634) | 7656 | 69 | 126.24 | down | 0.55 | 5.19E-08 |
| mitochondrion (GO:0005739) | 2913 | 25 | 48.03 | down | 0.52 | 4.19E-02 |

| **GO molecular function complete** | **Ref (#)** | **Found (#)** | **Expected (#)** | **Enrichment** | **Fold** | **p-value** |
|---|---|---|---|---|---|---|
| Unclassified (UNCLASSIFIED) | 7768 | 155 | 128.09 | up | 1.21 | 0.00E+00 |
| nucleotide binding (GO:0000166) | 2516 | 19 | 41.49 | down | 0.46 | 4.99E-02 |
| nucleoside phosphate binding (GO:1901265) | 2516 | 19 | 41.49 | down | 0.46 | 4.99E-02 |
| small molecule binding (GO:0036094) | 2613 | 19 | 43.09 | down | 0.44 | 1.83E-02 |
| anion binding (GO:0043168) | 2322 | 15 | 38.29 | down | 0.39 | 9.99E-03 |
| carbohydrate derivative binding (GO:0097367) | 1996 | 11 | 32.91 | down | 0.33 | 6.24E-03 |
| purine ribonucleoside triphosphate binding (GO:003563 | 1890 | 10 | 31.16 | down | 0.32 | 7.09E-03 |
| ATP binding (GO:0005524) | 1743 | 9 | 28.74 | down | 0.31 | 1.32E-02 |
| purine ribonucleoside binding (GO:0032550) | 1937 | 10 | 31.94 | down | 0.31 | 3.97E-03 |
| purine nucleoside binding (GO:0001883) | 1937 | 10 | 31.94 | down | 0.31 | 3.97E-03 |
| ribonucleoside binding (GO:0032549) | 1941 | 10 | 32.01 | down | 0.31 | 3.78E-03 |
| nucleoside binding (GO:0001882) | 1941 | 10 | 32.01 | down | 0.31 | 3.78E-03 |
| purine ribonucleotide binding (GO:0032555) | 1954 | 10 | 32.22 | down | 0.31 | 3.21E-03 |
| purine nucleotide binding (GO:0017076) | 1956 | 10 | 32.25 | down | 0.31 | 3.13E-03 |
| ribonucleotide binding (GO:0032553) | 1977 | 10 | 32.6 | down | 0.31 | 2.41E-03 |
| adenyl ribonucleotide binding (GO:0032559) | 1807 | 9 | 29.8 | down | 0.3 | 5.94E-03 |
| adenyl nucleotide binding (GO:0030554) | 1809 | 9 | 29.83 | down | 0.3 | 5.79E-03 |
| phosphotransferase activity, alcohol group as acceptor ( | 906 | 2 | 14.94 | down | < 0.2 | 4.16E-02 |
| kinase activity (GO:0016301) | 1078 | 2 | 17.78 | down | < 0.2 | 3.07E-03 |
| transferase activity, transferring phosphorus-containing g | 1243 | 2 | 20.5 | down | < 0.2 | 2.37E-04 |

## Table S5. Genes that are similarly affected in the *dse1* , *ise1* , and *ise2* transcriptomes.

| Locus (1) | Gene description (1) | Gene symbol (1) | *dse1*_Tiling | *ise1* _Tiling | *ise2* _Tiling |
|---|---|---|---|---|---|
| AT1G08990 | plant glycogenin-like starch ir | *PLANT GLYCOGENIN-LIKE* | 2.8 | 3.8 | 3.6 |
| AT1G17030 | unknown protein; FUNCTION | | 2.7 | 6.2 | 3.2 |
| AT1G19200 | Protein of unknown function ( | | 2.6 | 4.2 | 2.6 |
| AT1G23410 | Ribosomal protein S27a / Ubi | | 3.2 | 9.3 | 7.6 |
| AT1G28470 | NAC domain containing prote | *NAC DOMAIN CONTAINING* | 4.1 | 2.3 | 2.1 |
| AT2G06850 | endoxyloglucan transferase ( | *XYLOGLUCAN ENDOTRAN* | 6.1 | 4.8 | 6.9 |
| AT3G03650 | embryo sac development arre | *EMBRYO SAC DEVELOPMI* | 2.9 | 6.8 | 4.5 |
| AT3G07390 | isolated from differential scre | *AUXIN-INDUCED IN ROOT* | 2.2 | 3.9 | 2.8 |
| AT3G10890 | Glycosyl hydrolase superfami | | 5 | 2.5 | 3.6 |
| AT3G15950 | Similar to TSK-associating pr | *(NAI2)* | 10 | 5.1 | 4.9 |
| AT3G16400 | Encodes a nitrile-specifier pro | *NITRILE SPECIFIER PROTI* | 8 | 5 | 11.5 |
| AT3G22400 | Encodes lipoxygenase5 (LOX | *(LOX5)* | 15.5 | 2 | 3.6 |
| AT3G23000 | Encodes a serine/threonine p | *CBL-INTERACTING PROTE* | 2.2 | 3.1 | 4 |
| AT4G01070 | the glycosyltransferase (UGT | *(GT72B1)* | 2.6 | 2.4 | 2.3 |
| AT4G16640 | Matrixin family protein; FUNC | | 6.2 | 2.1 | 3.2 |
| AT4G21990 | Encodes a protein disulfide is | *APS REDUCTASE 3 (APR3)* | 2.9 | 4.2 | 2 |
| AT4G25000 | Predicted to be secreted prot | *ALPHA-AMYLASE-LIKE (AM* | 2.7 | 2.1 | 2.9 |
| AT4G29110 | unknown protein; FUNCTION | | 6.1 | 7.8 | 5.7 |
| AT4G30290 | Encodes a xyloglucan endotr | *XYLOGLUCAN ENDOTRAN* | 2.6 | 50.3 | 15 |
| AT4G30530 | Encodes a gamma-glutamyl p | *GAMMA-GLUTAMYL PEPTI* | 2.3 | 3 | 6.9 |
| AT4G37690 | Galactosyl transferase GMA1 | | 3 | 7 | 4.2 |
| AT5G01040 | putative laccase, knockout m | *LACCASE 8 (LAC8)* | 2.6 | 2.1 | 2.8 |
| AT5G06720 | Encodes a peroxidase with di | *PEROXIDASE 2 (PA2)* | 4.8 | 3.6 | 4.5 |
| AT5G07530 | encodes a glycine-rich protei | *GLYCINE RICH PROTEIN 1* | 3.1 | 8.1 | 14.6 |
| AT5G14130 | Peroxidase superfamily prote | | 2.4 | 2.9 | 2 |
| AT5G64060 | NAC domain containing prote | *NAC DOMAIN CONTAINING* | 2 | 2.4 | 3.4 |
| AT1G01320 | Tetratricopeptide repeat (TPF | | -2 | -4 | -3.7 |
| AT1G03130 | Encodes a protein predicted I | *PHOTOSYSTEM I SUBUNIT* | -2.8 | -3.1 | -10.4 |
| AT1G03457 | RNA-binding (RRM/RBD/RNF | | -2.1 | -2.2 | -2.3 |
| AT1G03630 | Encodes for a protein with pr | *PROTOCHLOROPHYLLIDE* | -7.7 | -2.4 | -6.6 |
| AT1G09750 | Eukaryotic aspartyl protease | | -2.3 | -9.1 | -40.5 |
| AT1G12900 | glyceraldehyde 3-phosphate | *GLYCERALDEHYDE 3-PHO* | -3.2 | -2.8 | -13.3 |
| AT1G15820 | Lhcb6 protein (Lhcb6), light h | *LIGHT HARVESTING COMF* | -3.3 | -5.5 | -3.9 |
| AT1G17810 | beta-tonoplast intrinsic protei | *BETA-TONOPLAST INTRIN* | -2.1 | -5.3 | -4.2 |
| AT1G19715 | Mannose-binding lectin supe | | -2.1 | -3 | -2.9 |
| AT1G19720 | Pentatricopeptide repeat (PP | | -2.8 | -4.2 | -5.7 |
| AT1G20020 | Encodes a leaf-type ferredoxi | *FERREDOXIN-NADP(+)-OX* | -4.6 | -3.2 | -2.9 |

| | | | | | |
|---|---|---|---|---|---|
| AT1G20340 | recombination and DNA-dam | *DNA-DAMAGE-REPAIR/TOI* | -2.3 | -15.7 | -6.4 |
| AT1G21500 | unknown protein; Has 29 Bla | | -3.2 | -7.5 | -5.1 |
| AT1G22430 | GroES-like zinc-binding dehy | | -2.6 | -10.2 | -2.4 |
| AT1G25440 | B-box type zinc finger protein | | -3.2 | -4.3 | -5.3 |
| AT1G26680 | transcriptional factor B3 famil | | -4 | -2.9 | -3.1 |
| AT1G31920 | Tetratricopeptide repeat (TPF | | -2.3 | -5.2 | -3.8 |
| AT1G32060 | phosphoribulokinase (PRK); I | *PHOSPHORIBULOKINASE* | -2.4 | -3.1 | -6.4 |
| AT1G32470 | Single hybrid motif superfami | | -11.4 | -4.3 | -3.2 |
| AT1G60970 | SNARE-like superfamily prote | | -2.8 | -2.3 | -3.1 |
| AT1G76110 | HMG (high mobility group) bc | | -2.7 | -5.2 | -5 |
| AT2G03590 | Encodes a member of a class | *UREIDE PERMEASE 1 (UP* | -3.8 | -2.4 | -6.7 |
| AT2G03750 | P-loop containing nucleoside | | -10.7 | -3.7 | -3.3 |
| AT2G05160 | CCCH-type zinc fingerfamily | | -3.6 | -5.3 | -10.6 |
| AT2G05310 | unknown protein; FUNCTION | | -2.2 | -2.2 | -2.1 |
| AT2G23260 | UDP-glucosyl transferase 84I | *UDP-GLUCOSYL TRANSFE* | -4 | -57.8 | -7.9 |
| AT3G01480 | Encodes a chloroplast cyclop | *CYCLOPHILIN 38 (CYP38)* | -3.9 | -3.4 | -3.5 |
| AT3G05625 | Tetratricopeptide repeat (TPF | | -3.2 | -2.3 | -3.6 |
| AT3G08940 | Lhcb4.2 protein (Lhcb4.2, prc | *LIGHT HARVESTING COMF* | -3.5 | -6.9 | -8.3 |
| AT3G09580 | FAD/NAD(P)-binding oxidore | | -3.2 | -2.9 | -3.6 |
| AT3G10200 | S-adenosyl-L-methionine-dep | | -3.9 | -2.3 | -4.2 |
| AT3G10405 | unknown protein; FUNCTION | | -4.3 | -2.4 | -4.1 |
| AT3G13790 | Encodes a protein with invert | *(ATBFRUCT1)* | -2.6 | -4 | -2.7 |
| AT3G14415 | Aldolase-type TIM barrel fami | | -3.7 | -2.1 | -2.2 |
| AT3G14420 | Aldolase-type TIM barrel fami | | -3.7 | -2.2 | -2.2 |
| AT3G18890 | NAD(P)-binding Rossmann-fo | *TRANSLOCON AT THE INN* | -3.7 | -2.6 | -2.1 |
| AT3G21055 | Encodes photosystem II 5 kD | *PHOTOSYSTEM II SUBUNI* | -2.2 | -2.8 | -3.8 |
| AT3G23700 | Nucleic acid-binding proteins | | -3.4 | -4.1 | -2.2 |
| AT3G25690 | actin binding protein required | *CHLOROPLAST UNUSUAL* | -3.1 | -2.7 | -2.3 |
| AT3G26650 | Encodes one of the two subu | *GLYCERALDEHYDE 3-PHO* | -2.5 | -2.4 | -4.7 |
| AT3G29030 | Encodes an expansin. Namin | *EXPANSIN A5 (EXPA5)* | -2.3 | -3 | -2.7 |
| AT3G54090 | Encodes a fructokinase-like p | *FRUCTOKINASE-LIKE 1 (FL* | -3.1 | -3.5 | -2.6 |
| AT4G03050 | Transcriptional silent in leaf ti | *(AOP3)* | -2.7 | -2.5 | -2.2 |
| AT4G04640 | One of two genes (with ATPC | *(ATPC1)* | -2.3 | -2.4 | -2.7 |
| AT4G09010 | Encodes a thylakoid lumen pi | *THYLAKOID LUMEN 29 (TL* | -3.4 | -4.5 | -4.6 |
| AT4G09160 | SEC14 cytosolic factor family | | -2.1 | -2.3 | -3.1 |
| AT4G14540 | nuclear factor Y, subunit B3 ( | *NUCLEAR FACTOR Y, SUB* | -9.2 | -3.3 | -4.9 |
| AT4G16980 | arabinogalactan-protein famil | | -8.2 | -8.5 | -7.9 |
| AT4G17810 | C2H2 and C2HC zinc fingers | | -4.7 | -5.5 | -12.7 |
| AT4G21280 | Encodes the PsbQ subunit of | *PHOTOSYSTEM II SUBUNI* | -3.3 | -3.2 | -3 |
| AT4G24660 | homeobox protein 22 (HB22) | *HOMEOBOX PROTEIN 22 (* | -2.9 | -5.6 | -10.3 |

| | | | | |
|---|---|---|---|---|
| AT4G25080 | Encodes a protein with methy | *MAGNESIUM-PROTOPORF* | -3.8 | -3.1 | -4 |
| AT4G27440 | light-dependent NADPH:protc | *PROTOCHLOROPHYLLIDE* | -4 | -18.5 | -18.6 |
| AT4G27700 | Rhodanese/Cell cycle control | | -3.6 | -4 | -4.2 |
| AT4G29060 | embryo defective 2726 (emb2 | *EMBRYO DEFECTIVE 2726* | -2.8 | -3.2 | -2.2 |
| AT4G31760 | Peroxidase superfamily prote | | -3 | -2.2 | -4.4 |
| AT4G34830 | Encodes MRL1, a conserved | *MATURATION OF RBCL 1 (* | -2.2 | -2.5 | -2.6 |
| AT5G01530 | light harvesting complex phot | *LIGHT HARVESTING COMF* | -2 | -6 | -3.4 |
| AT5G02160 | unknown protein; FUNCTION | | -5.6 | -3.9 | -4.3 |
| AT5G06690 | Encodes a thioredoxin (WCR | *WCRKC THIOREDOXIN 1 (* | -6.4 | -3 | -4.4 |
| AT5G08030 | Encodes a member of the gly | *GLYCEROPHOSPHODIEST* | -3 | -4.5 | -9.5 |
| AT5G08050 | FUNCTIONS IN: molecular_f | | -4.4 | -5.4 | -4.5 |
| AT5G08280 | Encodes a protein with porph | *HYDROXYMETHYLBILANE* | -2 | -3.2 | -4.5 |
| AT5G09640 | encodes a serine carboxypep | *SERINE CARBOXYPEPTIDA* | -2.3 | -2.9 | -2.1 |
| AT5G09660 | encodes a microbody NAD-d | *PEROXISOMAL NAD-MALA* | -4.9 | -3.5 | -2.8 |
| AT5G13630 | Encodes magnesium chelata | *GENOMES UNCOUPLED 5* | -2.1 | -2.3 | -4.7 |
| AT5G14910 | Heavy metal transport/detoxif | | -2.1 | -2.3 | -2.7 |
| AT5G15240 | Transmembrane amino acid t | | -2.6 | -2.9 | -4 |
| AT5G16370 | acyl activating enzyme 5 (AA | *ACYL ACTIVATING ENZYM* | -2 | -9.8 | -2.1 |
| AT5G18660 | Encodes a protein with 3,8-di | *PALE-GREEN AND CHLOR* | -3.1 | -2.2 | -2.8 |
| AT5G19220 | Encodes the large subunit of | *ADP GLUCOSE PYROPHOS* | -8.4 | -2.2 | -4 |
| AT5G19940 | Plastid-lipid associated protei | | -2.6 | -8.5 | -9 |
| AT5G22300 | encodes a nitrilase isomer. Tl | *NITRILASE 4 (NIT4)* | -2.1 | -2.8 | -2.8 |
| AT5G23060 | Encodes a chloroplast-locali | *CALCIUM SENSING RECEF* | -2.6 | -2.3 | -4.6 |

(1) TAIR annotation.

**Table S6. Phenotypic similarities among *dse1* and *lec* mutants.**

| Phenotype[1] | WT | *dse1* | *fus3* | *lec1* | *lec2* |
|---|---|---|---|---|---|
| Chlorophyll accumulation in dry seed | no | no | no | yes | yes |
| Area of anthocyanin accumulation in embryo | none | shoot apical meristem | shoot apical meristem | cotyledon margins | top half of cotyledons |
| Embryo hypocotyl shape | normal | normal | normal | shortened | shortened |
| Ectopic trichomes on cotyledons of embryo | no | yes | yes | yes | yes |
| Leaf primordia on embryo[2] | no | yes | yes | yes | yes |
| Highest expression of WT gene in embryo[3] | - | mature green ~16 DAF | walking stick ~9 DAF | heart ~5 DAF | heart ~5 DAF |

[1] Phenotypes of the *lec* and *dse1* mutant alleles (**Keith et al., 1994**; **Meinke et al., 1994; Stone et al., 2001**; **To et al., 2006**; **West et al., 1994; Xu et al., 2012**; **Yamagishi et al., 2005**).
[2] *dse1* mutant embryos can form leaf primordia, as shown here (**Fig. S1**).
[3] The approximate embryo stage when *LEC1, LEC2,* and *FUS3* gene expression (**Yamamoto et al., 2014**) or *DSE1* gene expression (**Yamagishi et al., 2005**) is highest in WT embryos.

## Table S8. Differentially regulated genes in *dse1* and *fus3* transcriptomes.

| Locus (1) | Gene description (1) | Gene symbol (1) | *dse1*_ ATH1 | *fus3*_ATH1 |
|---|---|---|---|---|
| AT1G03880 | Protein is tyrosine-phosphorylated ar | *CRUCIFERIN 2 (CRU2)* | 2.9 | -3.6 |
| AT1G07440 | NAD(P)-binding Rossmann-fold supe | | -3.2 | 2 |
| AT1G72230 | Cupredoxin superfamily protein; FUN | | 4.2 | -2.8 |
| AT1G73290 | serine carboxypeptidase-like 5 (scpl5 | *SERINE CARBOXYPEPTIDASE-LIKE* | 3.4 | -3.5 |
| AT1G78860 | curculin-like (mannose-binding) lectir | | -2.7 | 4.4 |
| AT2G24762 | Encodes a member of the GDU (glut | *GLUTAMINE DUMPER 4 (GDU4)* | 8 | -2.1 |
| AT2G38380 | Peroxidase superfamily protein; FUN | | 11.4 | -2.3 |
| AT2G38390 | Peroxidase superfamily protein; FUN | | 2.9 | -2.3 |
| AT2G48130 | Bifunctional inhibitor/lipid-transfer pro | | 4.8 | -3.2 |
| AT2G48140 | embryo sac development arrest 4 (E | *EMBRYO SAC DEVELOPMENT ARR* | 3.5 | -2.3 |
| AT3G02940 | Encodes a putative transcription fact | *MYB DOMAIN PROTEIN 107 (MYB10* | 6.7 | -3.1 |
| AT3G22600 | Bifunctional inhibitor/lipid-transfer pro | | 12.4 | -3.1 |
| AT3G22620 | Bifunctional inhibitor/lipid-transfer pro | | 10 | -3 |
| AT3G24220 | A member of gene NCED-related ge | *NINE-CIS-EPOXYCAROTENOID DIO* | 2.3 | -3.6 |
| AT3G50770 | calmodulin-like 41 (CML41); FUNCT | *CALMODULIN-LIKE 41 (CML41)* | 3.7 | -3.6 |
| AT3G57240 | encodes a member of glycosyl hydro | *BETA-1,3-GLUCANASE 3 (BG3)* | 2.4 | -5.1 |
| AT3G63160 | FUNCTIONS IN: molecular_function | *OUTER ENVELOPE PROTEIN 6 (OE* | -2.5 | 3 |
| AT4G26370 | antitermination NusB domain-contair | | -2.4 | 2.4 |
| AT4G36610 | alpha/beta-Hydrolases superfamily p | | 5.7 | -3.7 |
| AT5G01870 | Predicted to encode a PR (pathogen | | 3.6 | -2.8 |
| AT5G04340 | putative c2h2 zinc finger transcriptior | *ZINC FINGER OF ARABIDOPSIS TH* | 6 | -2.6 |
| AT5G08250 | Cytochrome P450 superfamily protei | | 2.2 | -2.2 |
| AT5G13220 | Plants overexpressing At5g13220.3, | *JASMONATE-ZIM-DOMAIN PROTEI* | -2.5 | 2.4 |
| AT5G39210 | Encodes a protein of the chloroplasti | *CHLORORESPIRATORY REDUCTIO* | -2.9 | 3 |
| AT5G41040 | Encodes a feruloyl-CoA transferase i | | 23.1 | -2.2 |
| AT5G43770 | proline-rich family protein; FUNCTIO | | 3.3 | -2 |

(1) TAIR annotation.

## Table S9. Similarly regulated genes in *ise* and *fus3* transcriptomes.

| Locus (1) | Gene description (1) | Gene symbol (1) | *ise1* _ATH1 | *ise2*_ATH1 | *fus3*_ATH1 |
|---|---|---|---|---|---|
| AT1G03457 | RNA-binding (RRM/RBD/I | | -2.2 | -2.3 | -2.7 |
| AT1G03880 | Protein is tyrosine-phosph | *CRUCIFERIN 2 (CRU2)* | -2.5 | -2.3 | -3.6 |
| AT1G03890 | RmlC-like cupins superfar | | -3.5 | -5.7 | -2.7 |
| AT1G09500 | similar to Eucalyptus gunr | | -3.9 | -2.6 | -5 |
| AT1G10640 | Pectin lyase-like superfan | | -3.3 | -7.6 | -4.3 |
| AT1G11580 | methylesterase PCR A (P | *METHYLESTERASE PCR* | 2.4 | 2.3 | 5 |
| AT1G12600 | UDP-N-acetylglucosamine | | -2.1 | -2.3 | -4.1 |
| AT1G12900 | glyceraldehyde 3-phospha | *GLYCERALDEHYDE 3-PH* | -2.8 | -13.3 | -2.1 |
| AT1G16490 | Member of the R2R3 fact | *MYB DOMAIN PROTEIN 5* | -11.5 | -3.4 | -3.8 |
| AT1G19330 | unknown protein; FUNCTI | | -3.7 | -2.1 | -4 |
| AT1G21500 | unknown protein; Has 29 | | -7.5 | -5.1 | -2.4 |
| AT1G22170 | Phosphoglycerate mutase | | -2.5 | -3.2 | -3.6 |
| AT1G22710 | Encodes for a high-affinity | *SUCROSE-PROTON SYM* | -2.1 | -3.6 | -3.6 |
| AT1G23410 | Ribosomal protein S27a / | | 9.3 | 7.6 | 2.8 |
| AT1G25510 | Eukaryotic aspartyl protea | | -3.1 | -2.8 | -3.2 |
| AT1G26680 | transcriptional factor B3 fa | | -2.9 | -3.1 | -5.9 |
| AT1G30515 | unknown protein; FUNCTI | | -4.6 | -4.6 | -3.4 |
| AT1G32060 | phosphoribulokinase (PRI | *PHOSPHORIBULOKINASE* | -3.1 | -6.4 | -3 |
| AT1G33700 | Beta-glucosidase, GBA2 t | | -3.1 | -2.8 | -5.7 |
| AT1G54740 | Protein of unknown functi | | -4.9 | -4.7 | -2.4 |
| AT1G60970 | SNARE-like superfamily p | | -2.3 | -3.1 | -6.2 |
| AT1G74310 | Encodes ClpB1, which be | *HEAT SHOCK PROTEIN 1* | -6.4 | -2.5 | -2.2 |
| AT1G76110 | HMG (high mobility group | | -5.2 | -5 | -3.7 |
| AT2G01210 | Leucine-rich repeat protei | | -2.7 | -3.8 | -2.3 |
| AT2G01770 | Encodes an iron transport | *VACUOLAR IRON TRANS* | -6.4 | -4.3 | -4.8 |
| AT2G03750 | P-loop containing nucleos | | -3.7 | -3.3 | -2.8 |
| AT2G03980 | GDSL-like Lipase/Acylhyd | | 2.9 | 3.8 | 2.3 |
| AT2G06850 | endoxyloglucan transfera | *XYLOGLUCAN ENDOTRA* | 4.8 | 6.9 | 5.5 |
| AT2G21510 | DNAJ heat shock N-termi | | -11.7 | -12.6 | -2.3 |
| AT2G23010 | serine carboxypeptidase-l | *SERINE CARBOXYPEPTI* | 9.4 | 3.9 | 5 |
| AT2G23260 | UDP-glucosyl transferase | *UDP-GLUCOSYL TRANSF* | -57.8 | -7.9 | -2.9 |
| AT2G23600 | Encodes a protein shown | *ACETONE-CYANOHYDRI* | -6 | -7.9 | -2.2 |
| AT2G30580 | Encodes a C3HC4 RING- | *DREB2A-INTERACTING P* | -2.3 | -2.6 | -2.9 |
| AT2G34710 | Dominant PHB mutations | *PHABULOSA (PHB)* | -3.2 | -2.3 | -2.5 |
| AT2G36190 | cwINV4 appears to functi | *CELL WALL INVERTASE 4* | -5.8 | -2.4 | -2.3 |
| AT2G41400 | Pollen Ole e 1 allergen an | | 9.7 | 8.2 | 4.5 |
| AT2G44460 | beta glucosidase 28 (BGL | *BETA GLUCOSIDASE 28 (* | 2.7 | 2.5 | 3.2 |
| AT3G01540 | RNA HELICASE DRH1 | *DEAD BOX RNA HELICAS* | 2.4 | 2.1 | 2.2 |

| | | | | | |
|---|---|---|---|---|---|
| AT3G02730 | thioredoxin F-type 1 (TRX | *THIOREDOXIN F-TYPE 1* | -2.4 | -3.2 | -2.2 |
| AT3G03590 | SWIB/MDM2 domain sup | | -2.7 | -2.4 | -3.1 |
| AT3G03770 | Leucine-rich repeat protei | | -4.5 | -2.5 | -2.3 |
| AT3G10010 | Encodes a protein with DI | *DEMETER-LIKE 2 (DML2)* | -2.5 | -2.2 | -3.5 |
| AT3G10190 | Calcium-binding EF-hand | | 2.3 | 3.7 | 2.5 |
| AT3G10200 | S-adenosyl-L-methionine- | | -2.3 | -4.2 | -2.2 |
| AT3G12060 | Encodes a member of the | *TRICHOME BIREFRINGEI* | -2.7 | -3.4 | -2.9 |
| AT3G12203 | serine carboxypeptidase-l | *SERINE CARBOXYPEPTII* | -4.9 | -2.2 | -3.1 |
| AT3G13510 | Protein of Unknown Funct | | -2.7 | -2.2 | -2.4 |
| AT3G15680 | Ran BP2/NZF zinc finger- | | -2.3 | -2.2 | -2 |
| AT3G15820 | Functions as phosphatidy | *REDUCED OLEATE DESA* | -2.9 | -2.1 | -5.2 |
| AT3G15950 | Similar to TSK-associating | *(NAI2)* | 5.1 | 4.9 | 7.3 |
| AT3G16400 | Encodes a nitrile-specifier | *NITRILE SPECIFIER PRO* | 5 | 11.5 | 4.4 |
| AT3G16470 | JA-responsive gene | *JASMONATE RESPONSIV* | 9 | 8.5 | 5.7 |
| AT3G16950 | encodes a plastid lipoamid | *LIPOAMIDE DEHYDROGE* | -7.4 | -2.8 | -3.3 |
| AT3G18890 | NAD(P)-binding Rossman | *TRANSLOCON AT THE IN* | -2.6 | -2.1 | -2.4 |
| AT3G21055 | Encodes photosystem II 5 | *PHOTOSYSTEM II SUBUN* | -2.8 | -3.8 | -2.1 |
| AT3G21250 | member of MRP subfamily | *ATP-BINDING CASSETTE* | 5.8 | 2.9 | 2.3 |
| AT3G25160 | ER lumen protein retaining | | -2.9 | -3.1 | -7.4 |
| AT3G25690 | actin binding protein requi | *CHLOROPLAST UNUSUA* | -2.7 | -2.3 | -2.2 |
| AT3G25930 | Adenine nucleotide alpha | | -3.7 | -2.3 | -4.3 |
| AT3G29030 | Encodes an expansin. Na | *EXPANSIN A5 (EXPA5)* | -3 | -2.7 | -6.4 |
| AT3G49260 | IQ-domain 21 (iqd21); FU | *IQ-DOMAIN 21 (iqd21)* | -5.5 | -4.1 | -2.4 |
| AT4G00260 | maternal effect embryo ar | *MATERNAL EFFECT EMB* | -4.9 | -2.6 | -2.4 |
| AT4G02330 | Encodes a pectin methyle | *(ATPMEPCRB)* | 4.2 | 3.6 | 2.6 |
| AT4G03050 | Transcriptional silent in le | *(AOP3)* | -2.5 | -2.2 | -6.3 |
| AT4G05180 | Encodes the PsbQ subun | *PHOTOSYSTEM II SUBUN* | -3.7 | -6.4 | -2.6 |
| AT4G09160 | SEC14 cytosolic factor far | | -2.3 | -3.1 | -2.5 |
| AT4G14540 | nuclear factor Y, subunit E | *NUCLEAR FACTOR Y, SU* | -3.3 | -4.9 | -2.9 |
| AT4G14770 | TESMIN/TSO1-like CXC 2 | *TESMIN/TSO1-LIKE CXC 2* | -6.7 | -2.1 | -2.6 |
| AT4G15160 | Bifunctional inhibitor/lipid- | | 4.8 | 2.3 | 2 |
| AT4G15620 | Uncharacterised protein fa | | -4.1 | -14.2 | -4.4 |
| AT4G16480 | Encodes a high affinity H+ | *INOSITOL TRANSPORTEI* | -2.6 | -2.9 | -2.1 |
| AT4G24480 | Protein kinase superfamily | | 3.2 | 2.1 | 3.6 |
| AT4G27460 | Cystathionine beta-synthas | *CBS DOMAIN CONTAININ* | -3.4 | -8.5 | -3.8 |
| AT4G27560 | UDP-Glycosyltransferase | | 3.4 | 3.9 | 3.3 |
| AT4G27700 | Rhodanese/Cell cycle con | | -4 | -4.2 | -2.2 |
| AT4G28570 | Long-chain fatty alcohol d | | 2.2 | 2.1 | 2.5 |
| AT4G29240 | Leucine-rich repeat (LRR) | | -2.5 | -3.3 | -2.2 |
| AT4G30290 | Encodes a xyloglucan enc | *XYLOGLUCAN ENDOTRA* | 50.3 | 15 | 6.4 |

| | | | | | |
|---|---|---|---|---|---|
| AT4G30520 | Encodes SARK (SENESC | *SENESCENCE-ASSOCIA* | -2.9 | -6 | -2.6 |
| AT4G31760 | Peroxidase superfamily p | | -2.2 | -4.4 | -2.6 |
| AT4G34131 | UDP-glucosyl transferase | *UDP-GLUCOSYL TRANSF* | 2.1 | 2.6 | 3.6 |
| AT4G34135 | The At4g34135 gene enc | *UDP-GLUCOSYLTRANSF* | 3.7 | 2.3 | 3.6 |
| AT4G34520 | Encodes KCS18, a memb | *3-KETOACYL-COA SYNTH* | -6.7 | -2.2 | -4.3 |
| AT4G36250 | Encodes a putative aldeh | *ALDEHYDE DEHYDROGE* | 2.9 | 6.5 | 5.1 |
| AT4G36280 | Histidine kinase-, DNA gy | | -6.8 | -4.1 | -3.5 |
| AT4G38370 | Phosphoglycerate mutase | | -2.4 | -2.2 | -2.2 |
| AT4G39500 | member of CYP96A | *CYTOCHROME P450, FAM* | 3.7 | 9 | 2.5 |
| AT5G01040 | putative laccase, knockou | *LACCASE 8 (LAC8)* | 2.1 | 2.8 | 3.7 |
| AT5G02160 | unknown protein; FUNCTI | | -3.9 | -4.3 | -2.3 |
| AT5G03795 | Exostosin family protein; l | | -2.1 | -3 | -5.2 |
| AT5G04660 | encodes a protein with cyl | *CYTOCHROME P450, FAM* | -4.1 | -3.4 | -3.2 |
| AT5G07030 | Eukaryotic aspartyl protea | | -3.8 | -5 | -3.1 |
| AT5G07190 | Gene is expressed prefer | *SEED GENE 3 (ATS3)* | -2.7 | -3.6 | -4.8 |
| AT5G07530 | encodes a glycine-rich pro | *GLYCINE RICH PROTEIN* | 8.1 | 14.6 | 2.1 |
| AT5G08030 | Encodes a member of the | *GLYCEROPHOSPHODIES* | -4.5 | -9.5 | -4.4 |
| AT5G09640 | encodes a serine carboxy | *SERINE CARBOXYPEPTIL* | -2.9 | -2.1 | -5.8 |
| AT5G13330 | encodes a member of the | *RELATED TO AP2 6L (Rap* | 2.9 | 6 | 2.6 |
| AT5G15240 | Transmembrane amino ac | | -2.9 | -4 | -3 |
| AT5G16240 | Plant stearoyl-acyl-carrier | | -3.3 | -3.1 | -3.2 |
| AT5G16400 | Encodes an f-type thiored | *THIOREDOXIN F2 (TRXF2* | -2.2 | -2.4 | -2 |
| AT5G19220 | Encodes the large subunit | *ADP GLUCOSE PYROPHO* | -2.2 | -4 | -2.6 |
| AT5G19580 | glyoxal oxidase-related pr | | 3 | 3.8 | 2.4 |
| AT5G20420 | chromatin remodeling 42 | *CHROMATIN REMODELIN* | -2.8 | -4.4 | -2.4 |
| AT5G22300 | encodes a nitrilase isome | *NITRILASE 4 (NIT4)* | -2.8 | -2.8 | -2.7 |
| AT5G25110 | member of AtCIPKs | *CBL-INTERACTING PROT* | 2.6 | 3.4 | 2.1 |
| AT5G25190 | encodes a member of the | *ETHYLENE AND SALT INL* | 6.9 | 10 | 4.9 |
| AT5G27360 | Encodes a sugar-porter fa | *(SFP2)* | -11.3 | -2.1 | -4.4 |
| AT5G64080 | Bifunctional inhibitor/lipid- | *XYLOGEN PROTEIN 1 (XY* | -2.9 | -3.5 | -2.5 |
| AT5G64100 | Peroxidase superfamily p | | 6.8 | 5.4 | 5.1 |

(1) TAIR annotation.

## Table S10. Quantitative PCR primers used for verification of the *dse1* transcriptome or VIGS gene silencing.

| Name | Gene Locus (F/R) | Sequence 5' - 3' | Purpose | Notes |
|---|---|---|---|---|
| AR_001 | At1g70070_R | CAACCAGCTAATTCATCCGGATTTG | *dse1* transcriptome | |
| AR_002 | At1g70070_F | TGCCATTGTTTTGGATGAGGTTCAC | *dse1* transcriptome | |
| AR_003 | At5g22330_R | TGTCACGGCCATTCATTTTCGCTAC | *dse1* transcriptome | |
| AR_004 | At5g22330_F | ATAGCCATTCGTGCGCAAGTTGAAG | *dse1* transcriptome | |
| AR_005 | At5g67630_R | CAATTTGTTCCCGGACTTCTGATCG | *dse1* transcriptome | |
| AR_006 | At5g67630_F | CAGTGCCCTGAAGGTGAGTTGC | *dse1* transcriptome | |
| AR_007 | At2g39190_R | TGGGCCCAAATGTAGCATGGTTT | *dse1* transcriptome | |
| AR_008 | At2g39190_F | TGTCGTTGCCTTTAGGCTTCTCG | *dse1* transcriptome | |
| AR_009 | At2g29940_R | GTGACAAGTCCCACAAATCCAACCT | *dse1* transcriptome | |
| AR_010 | At2g29940_F | TGCGGATCCTTCAGCTTTATGCAG | *dse1* transcriptome | |
| AR_011 | At3g54210_R | CCACCACCGTCAACAATTTTGAATC | *dse1* transcriptome | |
| AR_012 | At3g54210_F | TTCTCGCCGTCCGGTTACTCTTC | *dse1* transcriptome | |
| AR_013 | At1g76470_R | GGGCCTATAATGACAGACGGACAGA | *dse1* transcriptome | |
| AR_014 | At1g76470_F | GGACGAGGATTGTTGGTCAGACAC | *dse1* transcriptome | |
| AR_015 | At1g12900_R | GTGGCTCGCATCTAACAACCTTTG | *dse1* transcriptome | |
| AR_016 | At1g12900_F | AGCCATGAAGATACGATCATCAGCA | *dse1* transcriptome | |
| AR_017 | At1g61520_R | ATGCTAGCCATCTTGGCTCAATGAA | *dse1* transcriptome | |
| AR_018 | At1g61520_F | GCAAGGAGCCAACAGACCATTGTG | *dse1* transcriptome | |
| AR_019 | At1g54010_R | ACCGCAACCATAAGCATCATGTGTC | *dse1* transcriptome | |
| AR_020 | At1g54010_F | TGCATCAGCTCCTTTCCAATTCACC | *dse1* transcriptome | |
| AR_021 | At5g57920_R | GCAACACTGAATCATTCTCCGCATT | *dse1* transcriptome | |
| AR_022 | At5g57920_F | TTCTGGTGGGAGGCAAATCTAACAC | *dse1* transcriptome | |
| AR_023 | At5g58250_R | CACGCTCACCGAAGTAACGGAGA | *dse1* transcriptome | |
| AR_024 | At5g58250_F | CAGCTACCTCCATCGAGCAACAGT | *dse1* transcriptome | |
| AR_025 | At4g33600_R | CGTGATTTTGATGTCTCGGACAAGC | *dse1* transcriptome | |
| AR_026 | At4g33600_F | ATCACAGCGACTTACGGTCAGAACA | *dse1* transcriptome | |
| AR_027 | At3g26650_R | TAAGCTTGGCCTCAGTCACACCTTT | *dse1* transcriptome | |
| AR_028 | At3g26650_F | CTGAATTCTCAGGATTGCGAAGCTC | *dse1* transcriptome | |
| AR_029 | At5g46630_R | TCTGACGCACAGGACAATTCCCTA | *dse1* transcriptome | |
| AR_030 | At5g46630_F | TGGCTGCTTCCGCCATCTATTTTC | *dse1* transcriptome | |
| AR_031 | At1g13320_R | GGCCGTATCATGTTCTCCACAACC | *dse1* transcriptome | |
| AR_032 | At1g13320_F | GGGATCCGAGATCACATGTTCCA | *dse1* transcriptome | |
| AR_298 | Niben101Scf04495g02005_F | GGCACTCACAAACGTCTATTTC | VIGS gene silencing | (Liu et al., 2012) |
| AR_299 | Niben101Scf04495g02005_R | ACCTGGGAGGCATCCTGCTTAT | VIGS gene silencing | (Liu et al., 2012) |
| AR_300 | Niben101Scf07778g03025_F | GGGATGAGGAGGAGTTTGAGTTG | VIGS gene silencing | primer set 1 |
| AR_301 | Niben101Scf07778g03025_R | CGGACATTTGTTCTTCGCTGGTC | VIGS gene silencing | primer set 1 |
| AR_302 | Niben101Scf02917g00002_F | GAGAGGGATGAGGAGAAGTTTGAG | VIGS gene silencing | primer set 1 |

| | | | |
|---|---|---|---|
| AR_303 | Niben101Scf02917g00002_R | CCGATGAGCTACTTCTGTCTTTG | VIGS gene silencing primer set 1 |
| AR_304 | Niben101Scf07778g03025_F | CACGGGTAATTCCGCTCAACG | VIGS gene silencing primer set 2 |
| AR_305 | Niben101Scf07778g03025_R | GTACAGGGGCAGTTGCATTCTCC | VIGS gene silencing primer set 2 |
| AR_306 | Niben101Scf02917g00002_F | CAGAATAATGGGAGCAGTGTCCAG | VIGS gene silencing primer set 2 |
| AR_307 | Niben101Scf02917g00002_R | CTGTTGAGGAGGTGCAGGGG | VIGS gene silencing primer set 2 |

## Chapter 3: Loss of *ISE3,* a mitochondrial SEL1-like protein, increases plant cell-cell communication

**Content in prep for publication as:**

**Runkel AM[†], Xu M[†], Goodman HM, and Zambryski PC** (*in prep*, 2016)

[†] A.M.R. and M.X. contributed equally to this work

## ABSTRACT

An embryo defective mutant of *Arabidopsis thaliana*, *increased size exclusion limit 3* (*ise3*), causes increased plasmodesmata (PD) transport during the mid-torpedo stage of embryogenesis. The *ise3* mutation occurs in AT2G25570 and results in a single amino acid change from glycine to glutamic acid in a predicted SEL1-like repeat protein. ISE3 is localized in the mitochondria and interacts with a mitochondrial pentatricopeptide repeat (PPR) domain protein, *ISE3 INTERACTING PROTEIN 1* (*IPR1*), encoded by AT1G04590. ISE3 affects PD transport in adult plants, as silencing the expression of the *Nicotiana benthamiana ISE3* ortholog (*NbISE3*) also causes increased PD transport in leaves. Silencing the gene encoding IPR1 in *N. benthamiana* (*NbIPR1*) also increases cell-cell transport. To discover the genetic pathways affected in *ise3*, we analyzed its transcriptome. *ise3* exhibits changes in gene expression related to cell wall restructuring, phenylpropanoid biosynthesis, and reactive oxygen species (ROS) homeostasis. Loss of *ISE3* likely alters cellular homeostasis and retrograde signaling that ultimately affects cell-cell transport, perhaps through ROS signaling. Silencing of *NbISE3* and *NbIPR1* causes excessive production of hydrogen peroxide ($H_2O_2$), a ROS that has previously been shown to affect PD transport.

## INTRODUCTION

Organelle-nucleus communication is essential for regulating myriad processes in the plant cell, and recent findings implicate intercellular communication in a pathway called 'organelle-nucleus-plasmodesmata signaling' (ONPS) (**Burch-Smith et al., 2011a; Burch-Smith et al., 2011b; Burch-Smith and Zambryski, 2012; Brunkard et al., 2013; Brunkard et al., 2015a**). Mitochondrial and chloroplast proteins can affect the transport of molecules from cell-to-cell via plasmodesmata (PD) (**Benitez-Alfonso et al., 2009; Botha et al., 2000; Burch-Smith et al., 2011b; Provencher et al., 2001; Stonebloom et al., 2009**), and changes in the redox status of either of these organelles can also affect PD transport (**Stonebloom et al., 2012**).

PD are small channels that span the cellulosic wall of plant cells and allow signaling and movement of micro and macromolecules among neighboring cells (**Brunkard et al., 2015a; Calderwood et al., 2016; Rim et al., 2011; Wu and Gallagher, 2012; Xu et al., 2011**). PD are composed of membranes; the outer limits of PD are plasma membranes (PM), and the axial center of PD contains tightly compressed strands of endoplasmic reticulum (ER). The space between the PM and ER membranes is the "cytosolic sleeve" that forms a direct conduit between the cytoplasts of adjacent cells, and functions as the major passageway for molecules to move cell-to-cell through PD.

PD transport is driven by PD number, PD aperture, and the size and characteristics of potential transportable molecules. To date, our lab has studied three *Arabidopsis thaliana* mutants *increased size exclusion limit* (*ise*)*1*, *ise2*, and *decreased size exclusion limit* (*dse1*) that either increase or decrease PD transport, respectively; notably, these mutants all alter PD formation (**Burch-Smith and Zambryski, 2010; Burch-Smith et al., 2011b; Kim et al., 2002; Stonebloom et al., 2009; Xu et al.,**

**2012**). PD aperture, and consequent transport, is proposed to be modified by callose deposition in the cell wall surrounding PD (**De Storme and Geelen, 2014; Levy et al., 2007; Vatén et al., 2011; Zavaliev et al., 2011**), but the *ise1*, *ise2*, and *dse1* mutants do not seem to affect callose at PD.

Due to the integral nature of PD in cell-cell signaling, the regulation of PD is deeply connected to developmental and physiological processes in the plant. PD transport is highly regulated during embryo development, transitioning from extensive macromolecular transport in early stages to minimal transport in later stages (**Brunkard et al., 2013**; **Burch-Smith and Zambryski, 2010**; **Kim et al., 2002; Kim et al., 2005a; Kim et al., 2005b; Stonebloom et al., 2009; Xu et al., 2012**). PD transport undergoes precisely timed increases or decreases during the formation of new organs, cell types, and the development of the meristem (**Benitez-Alfonso et al., 2013; Brunkard et al., 2015a; Daum et al., 2014; Giannoutsou et al., 2013; Gisel et al., 1999; Gisel et al., 2002; Maule et al., 2013; Rinne and van der Schoot, 1998; Sanger and Lee, 2014; Vatén et al., 2011**). Further, physiological processes such as the exchange of energy and metabolites as well as plant defense responses are regulated by the transport of molecules via PD (**Bilska and Sowinski, 2010; Burch-Smith and Zambryski, 2016; Faulkner et al., 2013; Lee et al., 2011; Tilsner et al., 2016**).

Communication among PD, plastids, and mitochondria is required, as energy metabolism must be coordinated with intercellular signaling. Signaling between mitochondria and/or plastids to the nucleus, called “retrograde signaling”, is essential to control the expression of nuclear-encoded organellar proteins (**Kleine et al., 2009**). The nucleus then controls gene expression of the organelles through “anterograde signaling” (**Kleine and Leister, 2016**). Retrograde signaling can involve many different pathways and molecules, including reactive oxygen species (ROS) (**Kleine and Leister, 2016**).

Mitochondria produce ROS, which primarily include hydrogen peroxide ($H_2O_2$) and superoxide made during ATP synthesis (**Apel and Hirt, 2004**). ROS affect the function of the mitochondrial electron transport chain (mETC) as well as many other processes in the cell. ROS generated by the mitochondria affect other intracellular compartments via retrograde signaling, hormone signaling, pathogen response, and the cell death response (**Dietz et al., 2016; Huang et al., 2016; Kleine and Leister, 2016**). Notably, increasing mitochondrial ROS leads to increased intercellular transport (**Stonebloom et al., 2012**).

In mutant screens to identify genes regulating PD transport, none of the genes recovered encode proteins that localize to PD. Instead, the proteins localize to mitochondria (ISE1), chloroplasts (ISE2 and GFP ARRESTED TRAFFICKING (GAT1)), and the nucleus/cytoplasm (DSE1 and CHAPERONIN CONTAINING TCP1 8 (CCT8)) (**Benitez-Alfonso et al., 2009; Burch-Smith et al., 2011b; Fichtenbauer et al., 2012; Kim et al., 2002; Stonebloom et al., 2009; Xu et al., 2011; Xu et al., 2012**). ISE1, ISE2, and GAT1 all affect ROS production and/or the oxidation state of the chloroplasts or mitochondria. Here we characterize another *A. thaliana* mutant *ise3* that exhibits

increased cell-to-cell transport and encodes a small mitochondrial localized protein with SEL1-like repeats.

## RESULTS

### *ise3* exhibits increased PD transport

*ise3* is an *Arabidopsis thaliana embryo defective* (*emb*) mutant (**McElver et al., 2001; Patton et al., 1991**) that we identified using a previous screen for altered PD transport (**Kim et al., 2002**). *ise3* continues to transport 10 kDa fluorescent dextrans during the torpedo stage of embryo development compared to WT embryos (**Fig. 1A-B**). The *ise3-1* mutation was identified with mapped-based cloning and sequencing to the genetic locus AT2G25570 and confirmed with complementation. A single nucleotide mutation causes an amino acid change from a glycine to glutamic acid at amino acid position 134 in the ISE3 protein (**Fig. 1C-E**). ISE3 is a predicted SEL1-like repeat (SLR) protein with four SEL1 domains (**Alva et al., 2016; Karpenahalli et al., 2007**), and the *ise3-1* mutation occurs in the third SEL1 repeat (**Fig. 1E**). To our knowledge, ISE3 has never been studied in plants. In other organisms, SLR proteins often form macromolecular complexes that act in signal transduction pathways (**Mittl and Schneider-Brachert, 2007**), but little is known about their roles in plants.

### ISE3 is located in the mitochondria and interacts with another mitochondrial protein

ISE3 is a predicted mitochondrial protein, and when ISE3 is tagged with the fluorescent protein GFP, it localizes to the mitochondria (**Figs. 2 and S1A**) (**Emanuelsson et al., 2000**). Since SLR proteins can act as protein adaptors, we searched for mitochondrial proteins that might interact with ISE3 and have a necessary role in embryo development. We identified *emb* mutants (*emb* database: http://www.seedgenes.org/) that encode mitochondrial localized proteins, and studied several candidates: COENZYME Q 3 (EMB 3002), SURF1 (EMB 3121), ATCCMH, and a PPR domain containing protein (AT1G04590, of which the *emb* phenotype was confirmed with exon insertion lines). We also tested a predicted ClpP protease family protein (AT4G16800) for interaction with ISE3, which is not classified as an EMB, but may be involved in mitochondrial protein quality control. These mitochondrial WT encoded proteins were tested with WT ISE3 using a Bimolecular Fluorescence Complementation (BiFC) assay for possible interaction. As mitochondrial targeting requires an N-terminal signal sequence, all constructs had the fluorescent tags at the C-terminus. ISE3 produced a BiFC with only one of the tested candidate proteins, AT1G04590, which we name *ISE3 INTERACTING PROTEIN 1* (*IPR1*) (**Fig. 3A-B**).

TargetP (**Emanuelsson et al., 2000**) predicts IPR1 is a mitochondrial protein (**Fig. S1B**) and the RNA expression profile of *ISE3* and *IPR1* are similar according to AtGenExpress annotation (**Schmid et al., 2005**), indicating that these proteins may be co-expressed. In control experiments, neither protein (with its respective half of YFP) induced fluorescence when expressed alone (**Fig. 3C-F**). We tested if the single amino

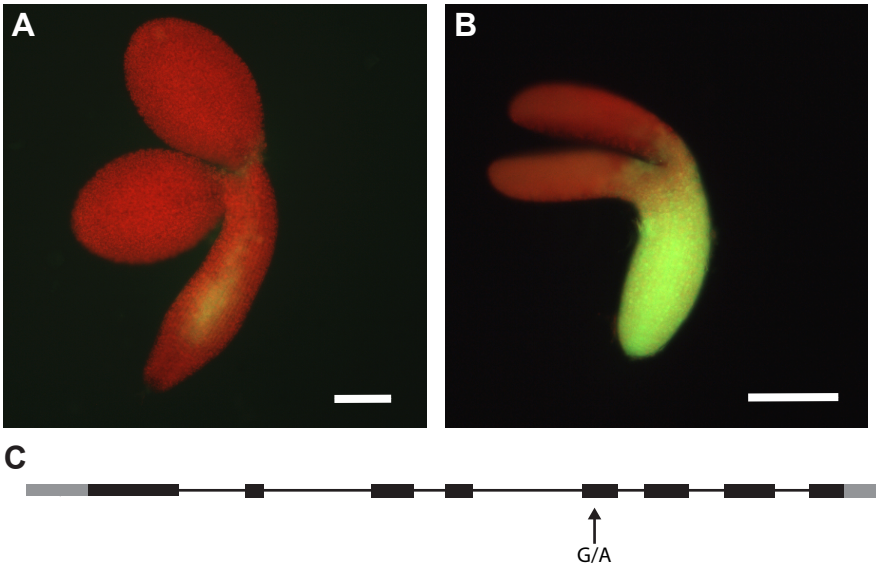


C




D

```
WT   ACATGGGTAATGCAGATGCTCAATATGAGCTAGGGTGTCGTTTAAGAGTCGAGgtcaggct
ise3 ACATGGGTAATGCAGATGCTCAATATGAGCTAGAGTGTCGTTTAAGAGTCGAGgtcaggct
     ********************************.**************************
```

E

| Repeat | Begin | Alignment from ISE3 | End | P-value |
|---|---|---|---|---|
| SEL1 | 54 | EVERVIDYCELNDRRLIPLLRGAKENFELALEADNL | 89 | 4.0e-03 |
| SEL1 | 92 | HARYWLSKLHLKYHVPGACKAVGAALLVEAADMGNA | 127 | 6.7e-04 |
| SEL1 | 128 | DAQYELGCRLRVENDHVQSDQQAFHYIENAVDQLHP | 163 | 2.1e-09 |
| SEL1 | 164 | GALYLLGIVYLTGDCVKQDVDSAIWCFHRASEKGHA | 199 | 6.7e-15 |

**Fig. 1. A mutation in AT2G25570 causes increased PD transport.** (**A**) WT embryos at the mid-to-late torpedo stage of embryo development cannot load a 10-kDa fluorescein (F)-conjugated dextran dye, by contrast, (**B**) *ise3* mutant embryos can move this dye from cell-to-cell. (Scale bars: 100 μm.) (**C**) *ise3* was mapped to the gene AT2G25570, (**D**) and was identified as a G to A mutation (black arrow), which would cause a single amino acid change from glycine (G) at amino acid position 134 to glutamic acid (E). (**E**) TPRpred (**Alva et al., 2016; Karpenahalli et al., 2007**) predicts ISE3 is a SEL1-like protein with a probability of 100% (p = 5.1e-24). The *ise3* mutation falls within the third SEL1-like repeat (black arrow).

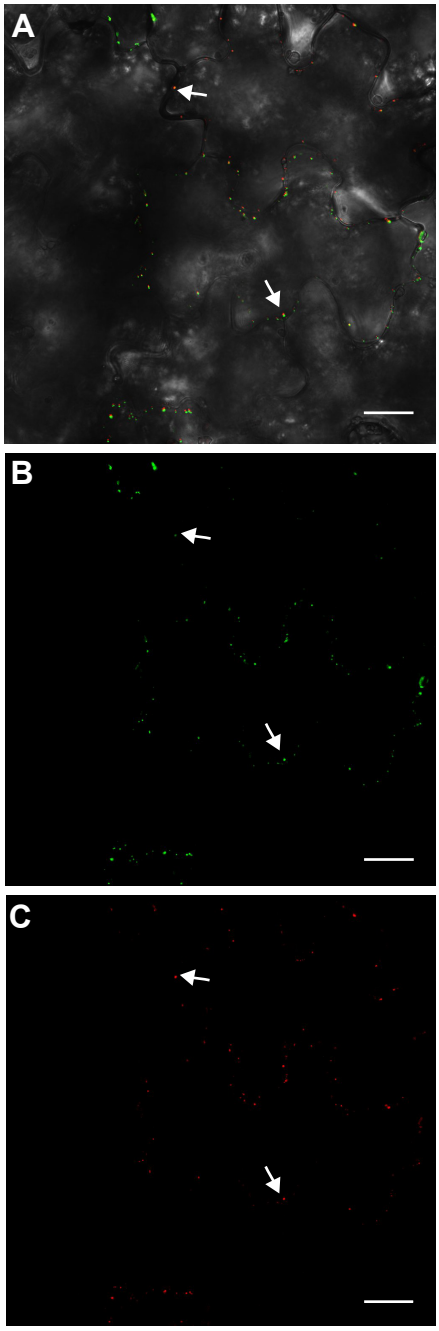


**Fig. 2. ISE3 is localized in the mitochondria.** (**A**) Composite image of transmitted light, GFP fluorescence from ISE3-GFP (green), and mitoCFP (red). Co-localization examples indicated by white arrows. (**B**) GFP fluorescence (green) from ISE3-GFP alone. (**C**) mitoCFP fluorescence (red) alone. (Scale bars: 25 μm.)

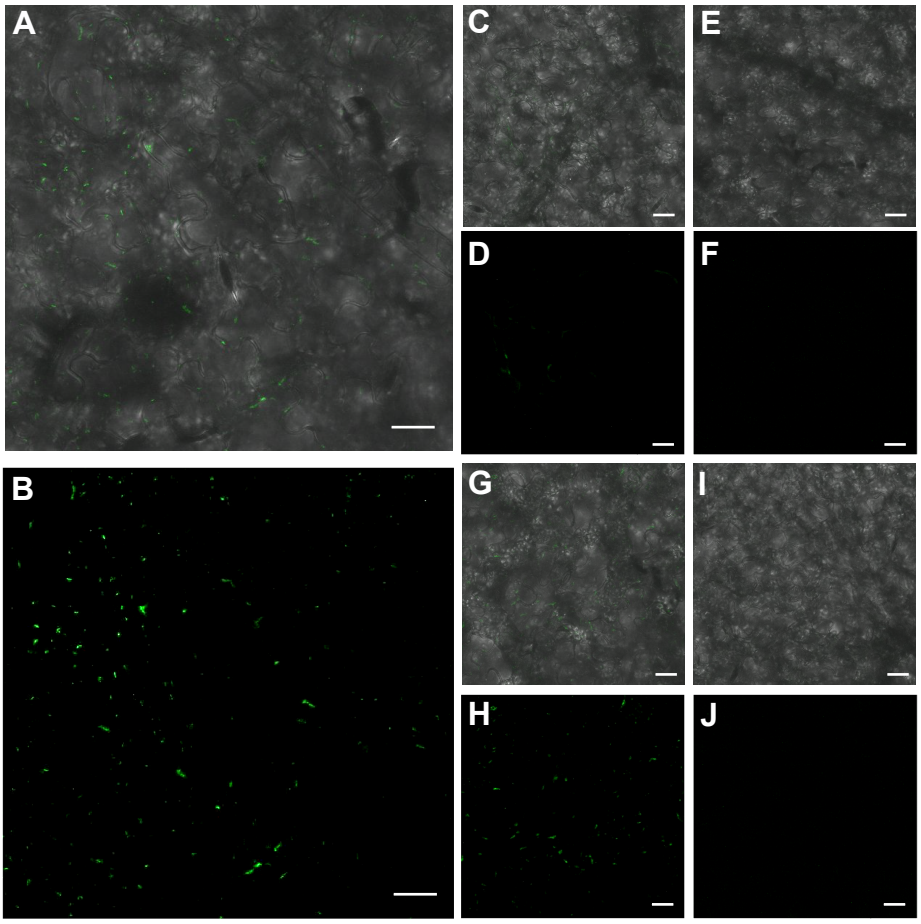


**Fig. 3. ISE3 interacts with AT1G04590, ISE3 INTERACTING PROTEIN 1 (IPR1), but does not interact with ISE1.** (**A**) Composite image of transmitted light and YFP fluorescence from BiFC interaction between ISE3-cYFP and IPR1-nYFP. (**B**) YFP fluorescence from BiFC interaction between ISE3-cYFP and IPR1-nYFP. (**C**) Composite image of transmitted light and no YFP fluorescence from ISE3-cYFP alone. (**D**) no YFP fluorescence from ISE3-cYFP alone. (**E**) Composite image of transmitted light and no YFP fluorescence from IPR1-nYFP alone. (**F**) no YFP fluorescence from IPR1-nYFP alone. (**G**) Composite image of transmitted light and YFP fluorescence from BiFC interaction between ISE3-G134E-cYFP and IPR1-nYFP. (**H**) YFP fluorescence from BiFC interaction between ISE3-G134E-cYFP and IPR1-nYFP. (**I**) Composite image of transmitted light and no YFP fluorescence from ISE3-cYFP and ISE1-nYFP alone. (**J**) no YFP fluorescence from ISE3-cYFP and ISE1-nYFP. (Scale bars: 25 μm.)

acid change in *ise3-1* affected the BiFC of ISE3 with IPR1. The mutation, however, did not eliminate the BiFC reaction (**Fig. 3G-H**). We also tested if ISE3 interacted with the mitochondrial localized ISE1; however, no BiFC was observed (**Fig. 3I-J**).

ISE3 and IPR1 contain similar protein domains. TPRpred (**Karpenahalli et al., 2007; Mitchell et al. 2015**) predicts that IPR1 contains four PPR motifs in the C-terminal half of the protein (**Fig. S1C)**. PPR and SLR and tetratricopeptide repeat (TPR) proteins are solenoid proteins with alpha-helical repeat structures containing either 34 (TRP), 35 (PPR) or 36 (SLR) amino acid repeats (**Karpenahalli et al., 2007**; **Mittl and Schneider-Brachert, 2007**).

**Virus Induced Gene Silencing of *N. benthamiana ISE3* or *IPR1* increase PD transport**

To identify orthologs of *ISE3* and *IPR1* in *N. benthamiana,* gene trees were made from available genomes (**Bombarely et al., 2012; Kersey et al., 2016**). Orthologs of *ISE3* and *IPR1* can be found in land plants (**Figs. S2A and S3A**), but not in organisms outside of plants in the Ensembl Genomes database (**Kersey et al., 2016**). Silencing the expression of the *N. benthamiana ISE3* (**Fig. S2**) or *IPR1* (**Fig. S3**) with Virus Induced Gene Silencing (VIGS) causes increased PD transport of transiently expressed GFP compared to the VIGS GUS control (Wilcoxon rank sum two-tailed test, $n \geq 59$, p-value < 1.0e-5) (**Fig. 4**).

**Transcriptome analysis of *ise3***

The transcriptome of *ise3* reveals 638 up-regulated and 123 down-regulated genetic loci (**Fig. 5A, Table S1**) These changes in gene expression were assessed with Gene Ontology (GO) and MapMan (**Klie and Nikoloski, 2012; Usadel et al., 2005**) to identify their affected biological pathways. In particular, we found alterations in gene expression of nuclear-encoded mitochondrial proteins, proteins related to oxidative stress (likely related to ROS), cell wall restructuring, phenylpropanoid biosynthesis, and photosynthesis (**Tables S2, S3, and S4**).

Upregulated nuclear-encoded mitochondrial proteins include genes that encode proteins involved in the mETC: *NAD(P)H DEHYDROGENASE B3* (*NDB3*)*, NDB4, ALTERNATIVE OXIDASE 1A* (*AOX1A), ALTERNATIVE NAD(P)H DEHYDROGENASE 1* (*NDA1*)*,* and *SUCCINATE DEHYDROGENASE 2-3* (*SDH2-3*) (**Table S1**)*.* A gene encoding a key mitochondrial import protein, *TRANSLOCASE OF INNER MITOCHONDRIAL MEMBRANE 23-3* (*TIM23-3*) is also up-regulated in *ise3* (**Table S1**)*.*

As ISE3 is a mitochondrial protein that affects the expression of nuclear-encoded mitochondrial genes, we were interested if changes in expression of proteins involved in retrograde signaling pathways might be affected in the *ise3* mutant. Indeed, the transcriptome suggests *ise3* over expresses genes that encode proteins involved in ROS response (**Table S1**). Six genes encoding PEROXIDASE family proteins are up-regulated in *ise3* (*PA2, PER64, AT5G14130, AT2G38380, AT1G68850,* and

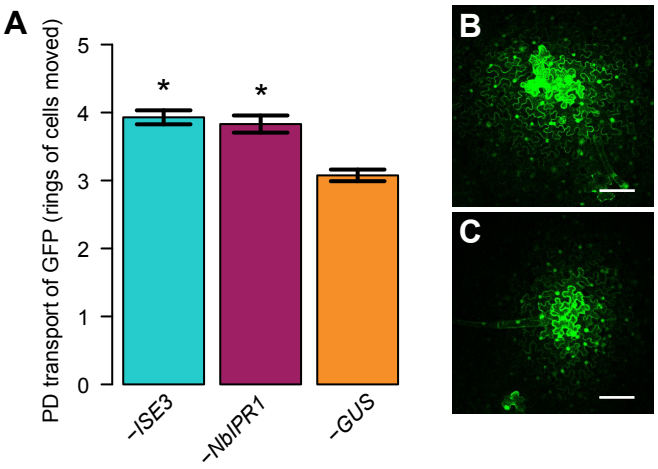


**Fig. 4. VIGS of *NbISE3* or *NbIPR1* increases PD transport in leaves.** (**A**) Silencing *N. benthamiana ISE3* or *IPR1* cause increased PD transport of transiently expressed GFP compared to the VIGS GUS control (Wilcoxon rank sum two-tailed test, GUS: n = 93, *NbISE3*: n = 71, *NbIPR1*: n = 59, ≥7; plants per treatment; 3 separate experiments; *p-value < 1.0e-5). Error bars indicate ± SE. (**B**) GFP movement following silencing of *NbISE3* and (**C**) GFP movement following silencing of *GUS* control. PD transport is assessed by the number of rings of cells expressing GFP that move away from the initially transfected cell in the middle. (Scale bars = 100 μm.)

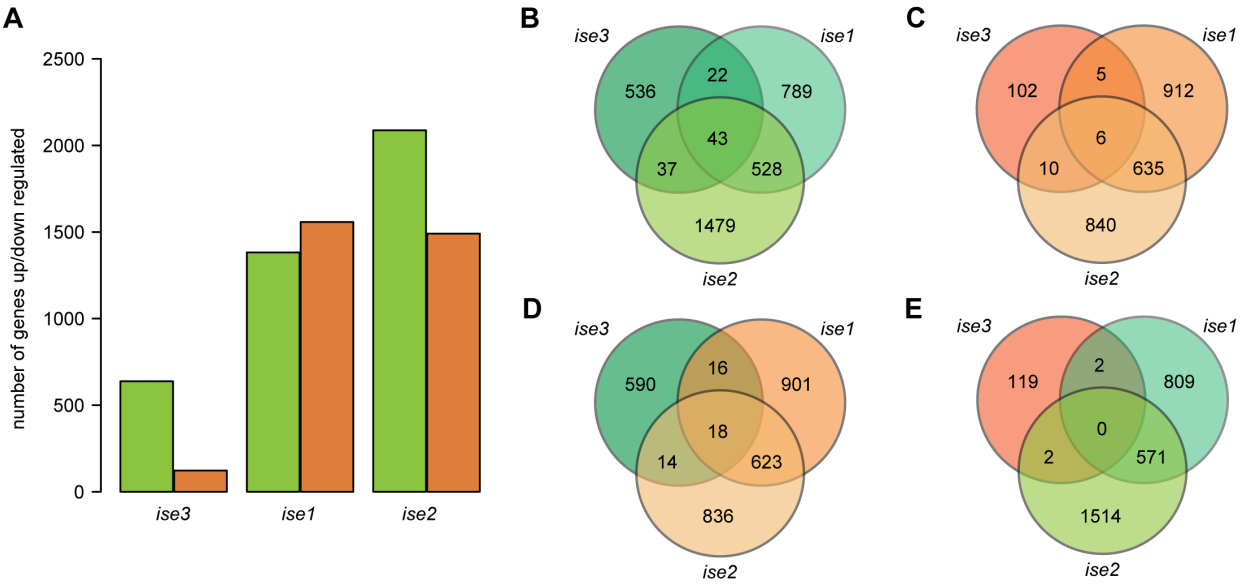


**Fig. 5. Comparison of the *ise3* transcriptome to *ise1* and *ise2* transcriptomes.** Transcriptomes include genes that have twofold or greater altered expression compared with WT samples and a p-value < 0.05. (**A**) In total, the *ise3* transcriptome has 638 up-regulated (green bar) and 123 down-regulated genetic loci (orange bar). The *ise1* and *ise2* transcriptome data is from **Burch-Smith et al.** (**2011b**). The transcriptome of *ise1* has altered expression of 1,382 up-regulated and 1,558 down-regulated genetic loci. The *ise2* transcriptome has 2,087 up-regulated and 1,491 down-regulated genetic loci with altered expression (**B**) *ise1*, *ise2*, and *ise3* share 43 similarly up-regulated genes, and (**C**) 6 similarly down-regulated genes. (**D**) Comparing the differentially expressed genes in the *ise* mutants, 18 genes are up-regulated in *ise3* and down-regulated in the *ise1* and *ise2* mutants and (**E**) no down-regulated genes in *ise3* are up-regulated in both the *ise1* and *ise2* mutants.

*AT4G36430*), with another one down-regulated (*AT2G24800*). Three *PURPLE ACID PHOSPHATASE* proteins (*PAP8, PAP21, and PAP22*), which are part of a gene family implicated in ROS metabolism (**Kaija et al., 2002; Ravichandran et al., 2015; Veljanovski et al., 2006**) are also induced in *ise3*. *RESPIRATORY BURST OXIDASE HOMOLOG A* (*RBOHA*), involved in $H_2O_2$ production (**Yoshioka et al., 2003**), is also strongly induced (+11 fold). The transcriptome also shows induced expression of genes that encode proteins of a gene family involved in another retrograde signaling pathway, the *WRKY DNA-BINDING PROTEINS* (**Kleine and Leister, 2016; Van Aken et al., 2009; Van Aken et al., 2013**): *WRKY23, 24, 25, 26, 28, 33, 43, 47, 48, 56, and 70*.

Other genes that might affect PD transport in *ise3* encode proteins involved in cell wall biosynthesis or restructuring; a number of extensin family genes show induced transcription in *ise3*: *EXTENSIN 3* (*EXT3*), *AT2G41400, AT2G41390, AT5G05020*, and *EXTENSIN PROLINE-RICH 1* (*EPR1*). The *ise3* transcriptome also has four *ARABINOGALACTAN PROTEIN* genes with altered expression, three up-regulated (*AGP2, 5, 14*) and one down-regulated (*AGP19*) (**Table S1**).

The other up-regulated genes in *ise3* suggest an enrichment in the phenylpropanoid biosynthesis and secondary metabolite pathways (**Tables S1 and S2**). The phenylpropanoid pathway is required for the production of monolignols – the basic components of lignins – as well as hydroxycinnamic acids, flavonoids, and coumarins (**Boerjan et al., 2003; D'Auria and Gershenzon 2005; Fraser and Chapple, 2011**). Genes up-regulated in *ise3* encode proteins likely involved in the lignin biosynthetic process, which include: *PHENYLALANINE AMMONIA-LYASE 4* (*PAL4*) that encodes a protein with possible involvement in lignin and salicylic acid (SA) accumulation, as well as *PINORESINOL REDUCTASE 2* (*PRR2*)*, CINNAMOYL COA REDUCTASE* (*CCR2*)*, 4-COUMARATE:COA LIGASE 2* (*4CL2*)*, BETA-GLUCOSIDASE 45* (*BGLU45*)*,* four *LACCASE* genes (*LAC3, 5, 12, and 16*)*,* and the *PEROXIDASE* family protein genes mentioned earlier (**Barros et al., 2015; Chapelle et al., 2012; Huang et al. 2010; Nakatsubo et al., 2008; Vogt, 2010; Zhou et al., 2010**). Lignins and these other secondary metabolites might be involved in signaling pathways and/or affecting the cell wall structure (**Hückelhoven, 2007; Pollastri and Tattini, 2011**) to alter PD transport. Alternatively, these transcriptional effects, like the others mentioned here, could be the side effect of, or feedback caused by, altered PD transport in *ise3.*

In terms of other known proteins that affect PD transport, the *ise3* transcriptome does not indicate a change in expression of *CALLOSE SYNTHASES* (*CalS*) or *β-1,3-GLUCANASES* (*BG*) involved in callose deposition at PD (**Table S1**) (**De Storme and Geelen, 2014; Levy et al., 2007; Vatén et al., 2011; Zavaliev et al., 2011**). Perhaps of interest, *PLASMODESMATA-LOCATED PROTEIN 4* (*PDLP4*), a gene that encodes a PD localized protein that promotes the movement of viruses is strongly induced (+9.8 fold) in *ise3* (**Amari et al., 2010**).

There are a number of processes that affect transcriptional regulation of the mitochondrial genome (**Millar et al., 2008**), such as RNA editing, so a transcriptome study on RNA abundance may not entirely reflect the mitochondrial transcriptional

profile of *ise3*; however, it is notable that 10 genes encoded by the mitochondria are up-regulated in *ise3*: *ORF143, 106E, 105E, 105A, 105B, 116, 110B, 122C, 240B, CYTOCHROME C BIOGENESIS 382* (*CCB382*)*, and ATP SYNTHASE SUBUNIT 1* (*ATP1*) (**Table S1**). ATP1 is part of the ATP synthase complex and responds to oxidative stress (**Busi et al., 2011; Moghadam et al., 2013**).

**Comparison of *ise3* to PD mutant transcriptomes**

We compared the previously published *ise1*, *ise2,* and *dse1* transcriptomes, which were analyzed using *A. thaliana* Tiling microarrays (**Burch-Smith et al., 2011b; Runkel et al., *submitted and under review***), to the *ise3* transcriptome, which was analyzed with RNA-sequencing (herein) to find shared misexpressed genes that may be involved in PD regulation (the entire *ise1, ise2, ise3*, and *dse1* transcriptomes are shown in **Table S1** and similarly regulated genes among *ise1*, *ise2*, and *ise3* are in **Table S5**). While RNA sequencing and tiling arrays will introduce slightly different biases, most gene expression levels are well correlated with these two methods (**Agarwal et al., 2010**).

If there was an obvious transcriptional change that explained the PD transport phenotype in all four of the PD mutants, we might find genes that were similarly up- or down-regulated in all three of the *ise* mutants and expressed oppositely in *dse1*, however, no genes fit this pattern (**Table S5**). Generally, the *ise3* transcriptome shows some overlap with *ise1* and *ise2* (**Fig. 5B-C**) with very few oppositely expressed genes (**Fig. 5D-E**). While *ise1* and *ise2* have a statistically significant transcriptional overlap ($p < 1.0e-300$, representation factor = 3.1), however, *ise3* does not significantly overlap with *ise1* or *ise2* ($p > 0.4$, representation factor = 1). While there was not significant overlap of individual genes among the *ise* mutants, three similarly regulated genetic pathways were observed among the three *ise* mutant transcriptomes: cell wall restructuring, photosynthesis, and ROS metabolism.

The *ise1*, *ise2*, and *ise3* transcriptomes misexpress a number of genes that encode proteins involved in cell wall restructuring (**Burch-Smith et al., 2011b; Cosgrove, 2005; Wolf et al., 2012;** results herein). The *ise1* and *ise2* transcriptomes generally show a down-regulation of genes encoding expansin proteins, and *ise3* also follows this trend with a down-regulation of *EXPANSIN A3* (*EXP3*) and *EXPANSIN B1* (*EXPB1*). Also shared among the *ise* mutants is a down-regulation of many genes that encode proteins involved in pectin synthesis and metabolism. In the *ise3* transcriptome, the genes encoding *PECTIN METHYLESTERASE 5* (*PME5*), a pectin methylesterase inhibitor superfamily protein (*AT1G11590*), and three pectin lyase-like superfamily proteins (*AT1G10640, AT1G11590, AT4G00872*) are down-regulated. An extensin family protein gene (*AT2G41400*) is strongly up-regulated in all three *ise* mutants (+9.7, +8.2, and +12.3 fold in *ise1, 2*, and *3* respectively); other EXTENSIN genes affected in *ise3* were mentioned earlier. Many genes encoding XYLOGLUCAN ENDOTRANSGLYCOSYLASE/HYDROLASE (XTH) or XTH-related (XTR) proteins are induced in expression in *ise1* and *ise2.* In *ise3 XTR6* is up-regulated, although, this particular *XTR* is down-regulated in *ise1* and *ise2*.

Like *ise1, ise2,* and *dse1,* many of the down-regulated genes in the *ise3* transcriptome, are connected to photosynthesis, which is not surprising as most *emb* mutants are chlorotic (**McElver et al., 2001; Patton et al., 1991**). Some of the key photosynthesis genes affected in *ise3* include: *PHOTOSYNTHETIC NDH SUBCOMPLEX B 3* (*PnsB3*)*, PHOTOSYSTEM I LIGHT HARVESTING COMPLEX GENE 6* (*LHCA6*)*, PHOTOSYSTEM II LIGHT HARVESTING COMPLEX GENE 2.3* (*LHCB2.3*)*, PROTOCHLOROPHYLLIDE OXIDOREDUCTASE C* (*POR C*)*, RUBISCO SMALL SUBUNIT 2B* (*RBCS2B*)*, RUBISCO SMALL SUBUNIT 3B* (*RBCS3B*)*, CHLORORESPIRATORY REDUCTION 7* (*CRR7*)*,* and *NON-PHOTOTROPIC HYPOCOTYL 3* (*NPH3*).

Finally, some of the similarly regulated genes among the three *ise* mutant transcriptomes are involved in ROS metabolism. PAP8 and PAP21, mentioned earlier, are up-regulated in all three *ise* mutants. Additionally, the peroxidase superfamily protein *AT5G14130* and *PEROXIDASE 2* (*PA2*) are up-regulated in the *ise* and *dse1* mutants. *AOX1A*, *NDB3,* and *NDB4* are induced in both *ise2* and *ise3*. Loss of *ISE1* or *ISE2* produces altered oxidation states in the mitochondria and plastid (**Stonebloom et al., 2009; Stonebloom et al., 2012**). **Burch-Smith et al.** (**2011b**) describes the ROS metabolism genes affected specifically in *ise1* and *ise2* in more detail. Here we also show that more $H_2O_2$ was detected using a 3,3-diaminobenzidine (DAB) stain in *N. benthamaina* leaves silenced for *NbISE3* or *NbIPR1* compared to the control (**Fig. 6**).

## DISCUSSION

The *ise3* mutation affects the *A. thaliana* gene AT2G25570 and causes increased PD transport in embryos. Loss of the *N. benthamiana ISE3* ortholog also causes increased PD transport in leaves indicating that ISE3 is necessary for restricting PD transport not only in developing embryos but also in leaves of a distantly related eudicot species.

ISE3 is a mitochondrial protein; it is predicted to localize to the mitochondria using cellular localization prediction software (**Emanuelsson et al., 2000**) and co-localizes with a mitochondrial marker in transient expression assays. SLR proteins, like ISE3, are often involved in forming macromolecular complexes, so we tested if five mitochondrial proteins, which are involved in critical aspects of mitochondrial function, interacted with ISE3. ISE3 produced a BiFC with an EMB-mitochondrial-PPR-domain-containing protein, we name IPR1.

PPR proteins generally bind protein ligands or nucleic acids (**Barkan and Small, 2014; Prikryl et al., 2011; Zhang et al., 2015**). In plants, there has been a dramatic expansion of these proteins, and most are involved in RNA regulation in the chloroplast or the mitochondria (**Barkan and Small, 2014; Bentolila et al., 2013; Lurin et al., 2004**). One well known PPR is required for plastid-to-nucleus retrograde regulation: *GENOMES UNCOUPLED 1* (*GUN1*). The loss of *GUN1*, however, does not appear to affect the expression of specific plastid transcripts but rather plays a more general role in retrograde signaling (**Barkan and Small, 2014; Koussevitzky et al., 2007; Woodson et al., 2013**). Potentially, IPR1 along with ISE3 regulate the expression of

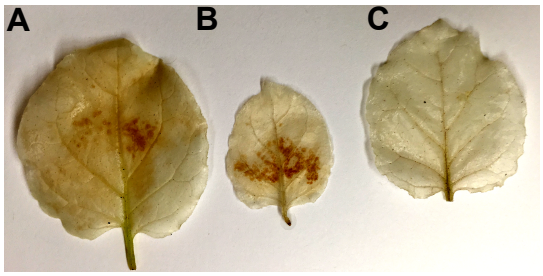


**Fig. 6. $H_2O_2$ is higher in leaves silenced for *NbISE3* and *NbIPR1.*** (**A**) *NbISE3.* (**B**) *NbAT1G04590*. (**C**) control.

specific mitochondrial RNAs. The *ise3* transcriptome did not indicate any mitochondrial encoded genes with reduced expression, but did identify a number with induced expression. Alternatively, ISE3 and IPR1 might have a more generalized retrograde signaling role, like GUN1.

ISE1 is found in the mitochondria and loss of *ISE1* induces an oxidative shift within the mitochondria and a reductive shift in plastids (**Stonebloom et al., 2009; Stonebloom et al., 2012**). Salicylhydroxamic acid (SHAM), which produces mitochondrial-generated ROS, increases PD transport (**Stonebloom et al., 2012**). SHAM specifically inhibits mitochondrial alternative oxidase (AOX), an enzyme that stabilizes the redox state of the cell (**Keunen et al., 2013; Keunen et al., 2015; Maxwell et al., 1999; Purvis and Shewfelt 1993**). Genes encoding proteins involved in retrograde signaling, including AOX1A, are induced in the *ise3* transcriptome. Further, *ise3* has altered expression of mETC proteins, proteins associated with ROS response (peroxidase, peroxisomal membrane, and PAP proteins), and other proteins with known involvement in ROS production, including RBOHA (**Keunen et al., 2013; Keunen et al., 2015; Maxwell et al., 1999; Purvis and Shewfelt 1993; Torres and Dangl, 2005; Torres et al., 2002; Yoshioka et al., 2003**). ROS are known retrograde signals and perhaps ROS can direct gene expression changes in the nucleus to affect PD transport in *ise3*. The cellular signals produced in the mitochondria that affect PD likely are part of retrograde signaling through ONPS. Alternatively, the mitochondria could play a more direct role in affecting PD by producing ROS near the cell wall, as ROS may induce cell wall loosening (**Cosgrove, 2005; Jones et al., 2006; Wolf et al., 2012**), or signaling between the ER and the mitochondria (**English and Voeltz, 2013**), which might influence the desmotuble to affect PD transport.

ROS have been implicated in PD transport. An emerging hypothesis is that the amount, type, and/or origin of the ROS that are generated influence PD differently. *gat1* is a mutation in the gene that encodes the THIOREDOXIN-m3 (TRX-m3) protein. Without TRX-m3, PD transport is restricted and $H_2O_2$ accumulates in the plant (**Benitez-Alfonso et al., 2009**). In contrast, *ise1* affects a mitochondrial protein and also over accumulates $H_2O_2$, but has increased PD transport (**Stonebloom et al., 2009**). **Stonebloom et al.** (**2012**) demonstrated that ROS produced by the mitochondria, through treatment with SHAM, increases PD transport, while ROS produced primarily in the plastid, through treatment with paraquat (PQ) reduces PD transport. Further, **Rutschow et al.** (**2011**) tested the effect of direct application of $H_2O_2$ on PD transport and found that small concentrations (0.6 mM) increases PD transport while ten times the concentration (6 mM) reduces PD transport. Here, we report that more $H_2O_2$ was detected in leaves silenced for *NbISE3* or *NbIPR1* compared to the control. This result is correlated with the increased PD transport observed in *NbISE3* or *NbIPR1* silenced tissues, and further suggests that $H_2O_2$ can affect PD transport (**Stonebloom et al., 2009; Stonebloom et al., 2012**).

Phenotypically, *ise3* has many similarities with *ise1* and *ise2*. All three mutants are embryo defective, cause increased PD transport in *A. thaliana* embryos, and loss of their encoded gene results in increased PD transport in leaves of a distantly related

eudicot species (**Stonebloom et al., 2009; Burch-Smith et al., 2011a; Burch-Smith et al., 2011b**). ISE1 and ISE3, along with its interactor IPR1, are proteins found in the mitochondria that may be involved in mitochondrial RNA processing and when *ISE1*, *ISE3*, or *IPR1* are silenced, they over accumulate $H_2O_2$ (results herein and in **Stonebloom et al.** (**2009**)). The *ise3* transcriptome indicates, however, that the individual genes affected by *ise3* do not strongly overlap with those affected by *ise1* or *ise2*. While the genes are not the same, some of the downstream processes and pathways are similar among the *ise* mutants. All three mutants exhibit changes to photosynthesis genes, cell wall restructuring, and ROS homeostasis.

Cell-cell transport is driven by many proteins that do not localize at PD (**Fig. 7**). We again show that retrograde signaling likely affects PD transport, further supporting the ONPS pathway (**Burch-Smith et al, 2011b**). Future studies will continue to dissect how processes critical to cellular homeostasis can alter cell-cell transport via PD.

## MATERIALS AND METHODS

### *ise3* identified as a plasmodesmata mutant

*ise3* was identified in a screen for mutants with increased PD transport as described (**Kim et al., 2002**). The *ise3* mutation was found at the genetic locus AT2G25570 using mapped-based cloning and sequencing as described (**Xu et al., 2012**). Complementation was verified by transforming *ise3* heterozygous plants with a construct containing the native *ISE3* promoter and the ISE3 coding sequence. The construct was cloned from *A. thaliana* seedling cDNA (ThermoFisher Scientific/Invitrogen, 18080051) using the primers in **Table S6** and restriction cloned into the promoter-modified pCAMBIA3300 binary vector (http://www.cambia.org/). Constructs were confirmed by sequencing, transformed into *Agrobacterium* (GV3101), and *A. thaliana* plants were transformed using the floral dip method as described (**Weigel and Glazebrook, 2006**).

Orthologs of *ISE3* and *IPR1* were identified with Ensembl Plants, release 32 - August 2016; http://plants.ensembl.org/) (**Kersey et al., 2016**). *N. benthamiana* orthologs of *ISE3* and *IPR1* were identified at Sol Genomics (https://solgenomics.net/) (**Bombarely et al., 2012**) for virus induced gene silencing (VIGS) constructs, and described in more detail below.

### Localization and Bimolecular Fluorescence Complementation studies of ISE3

ISE3 was tagged with the fluorescent protein GFP and transiently expressed along with a mitochondria-targeted CFP (mitoCFP) (**Niwa et al. 1999**) as described in (**Stonebloom et al., 2009**). The *ISE3* coding sequence was cloned from *A. thaliana* seedling cDNA (ThermoFisher Scientific/Invitrogen, 18080051) with the primers in **Table S6** and restriction cloned into the pRTL2-GFP vector (**Crawford and Zambryski, 2000**). Constructs were confirmed by sequencing, and transformed into *Agrobacterium* (GV3101). *N. benthamiana* plants were grown under 16-hours-light/8-hours-dark under

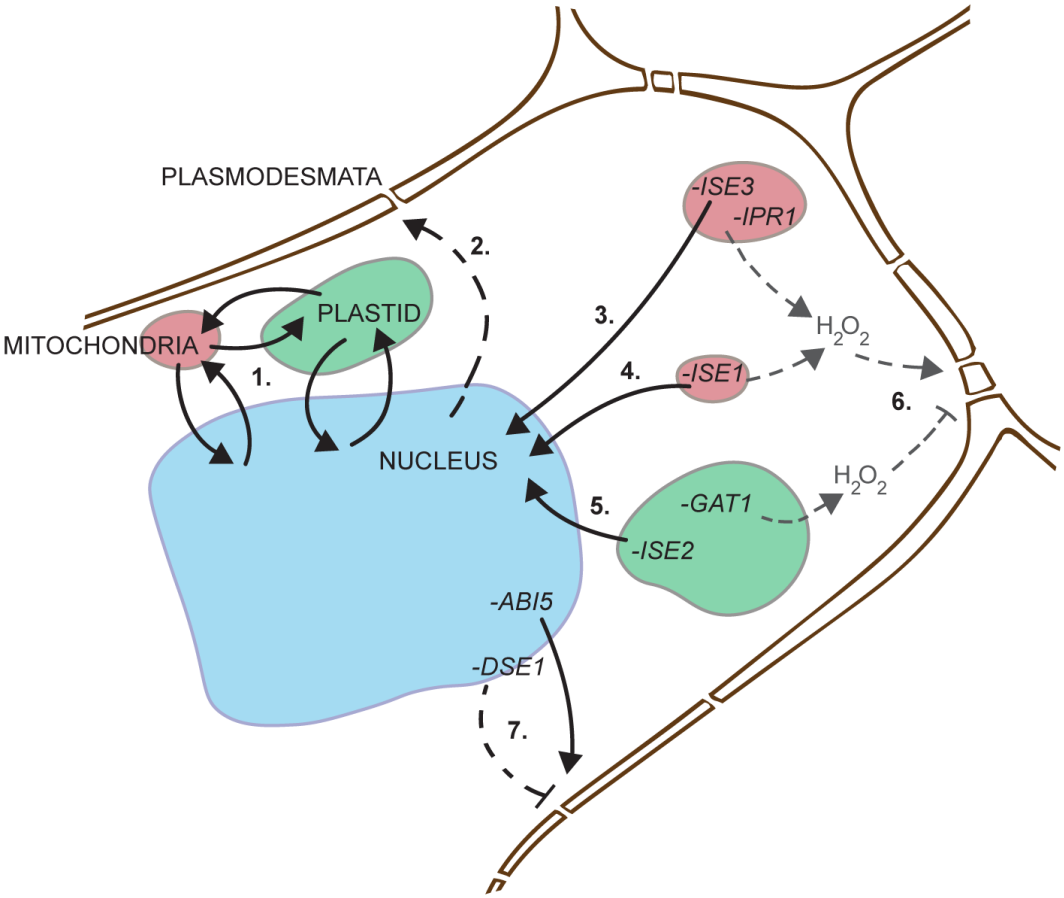


**Fig. 7. Cell-cell transport is driven by many proteins that do not localize at PD.** (**1**) Retrograde and anterograde signaling (arrows) coordinate organelles and the nucleus (**Kleine and Leister, 2016; Kleine et al., 2009**). (**2**) The nucleus affects the function of PD through unknown mechanisms (dotted arrow). (**3-5**) ISE1 is a mitochondrial protein, ISE2 is a plastid protein, and ISE3 is a mitochondrial protein; all affect the expression of nuclear genes encoding proteins that target to these organelles (**Burch-Smith et al., 2011b;** and results herein). (**6**) $H_2O_2$, affects PD transport (**Rutschow et al., 2011**; **Stonebloom et al., 2012**), and loss (shown with "-") of *ISE1*, *ISE3*, *IPR1*, or *GAT1* result in excessive $H_2O_2$ that may be generated by their respective organelles and may explain their PD transport phenotypes (**Benitez-Alfonso et al., 2009; Rutschow et al., 2011**; **Stonebloom et al., 2009; Stonebloom et al., 2012**). (**7**) Loss (shown with "-") of *DSE1* affects the expression of nuclear-encoded genes, including the transcription factor ABI5, and loss of *DSE1* and *ABI5* signal (unknown) events to affect PD transport (**Runkel et al., *submitted and under review***).

100 µmol photons $m^{-2}s^{-1}$ at room temperature. The fourth leaf (counting from the most recently emerged leaf downwards) of four-week old plants was simultaneously infiltrated with *A. tumefaciens* as described (**Brunkard et al., 2015b**), carrying constructs to express *ISE3-GFP* and mitoCFP. After 48 hours, the same region of each leaf was imaged as described (**Brunkard et al., 2015b**).

Bimolecular Fluorescence Complementation (BiFC) constructs were cloned from *A. thaliana* seedling cDNA (ThermoFisher Scientific/Invitrogen, 18080051) with the primers in **Table S6** and Gateway® cloned (ThermoFisher Scientific/Invitrogen K240020 and 11791-020) into the pBAT-TL-B-sYFP-C or N vectors (**Boevink et al., 2014; Uhrig et al., 2007**). Constructs were confirmed by sequencing, and transformed into *Agrobacterium* (GV3101). *N. benthamiana* plants were grown as described above and the fourth leaves of four-week old plants were simultaneously infiltrated as described above with *A. tumefaciens* (carrying constructs to express ISE3 and each potential interactor). After 48 hours, the same region of each leaf was imaged for BiFC.

**Virus Induced Gene Silencing and PD movement assays**

Virus Induced Gene Silencing construct design

pTRV2-*GUS* (pYC1) (**Stonebloom et al., 2009**) was designed previously. *NbISE3* and *NbIPR1* Virus Induced Gene Silencing (VIGS) constructs were designed after a BLAST search of the *A. thaliana ISE3* and *IPR1* at TAIR (http://www.arabidopsis.org/) to the *N. benthamiana* genome (v1.0.1) at Sol Genomics (https://solgenomics.net/) (**Bombarely et al., 2012**) using an e-value threshold of 10 and BLOSUM62 substitution matrix. The resulting *N. benthamiana* proteins were constructed into gene trees with other orthologs (**Kersey et al., 2016; Vilella et al., 2009;** Ensembl Plants, release 32 - August 2016; http://plants.ensembl.org/) (**Fig. S2A and S3A**). The gene trees were made with MAFFT (v7.273), using the robust L-INS-i method, with 100 bootstrap values (**Katoh et al., 2005**), and Archaeopteryx (version 0.9901, 2014-10-14, based on forester 1.038). The VIGS triggers were designed to silence the *N. benthamiana* orthologs of *ISE3* or *IPR1* by finding regions specific to the gene of interest, but not overlapping with related homologs. Each trigger was used as a BLAST query against the *N. benthamiana* genome (predicted cDNA v1.0.1) using an e-value threshold of 10 and BLOSUM62 substitution matrix to check for any off-target sequence matches. The constructs were checked again to be orthologs of *A. thaliana*, with BLAST in TAIR. There are two clear *NbISE3* and *NbIPR1* orthologs. The *pTRV2-NbISE3 and pTRV2-NbIPR1* VIGS triggers were designed to silence the orthologs. There is one additional gene that has significant DNA sequence overlap with the *NbIPR1* orthologs but it is not a predicted ortholog of *IPR1*; however, when the latter protein sequence is BLAST back to *A. thaliana,* it still identifies AtIPR1 as the best match in *A. thaliana* (**Fig. S3C**). Due to the significant sequence overlap of this gene, it may also be silenced by *pTRV2-NbIPR1.* This gene could be the result of an older duplication event in *N. benthamiana*, a pseudogene, or a gene related to *IPR1*.

The VIGS triggers were cloned from *N. benthamiana* genotype Nb-1 cDNA. RNA was extracted (Sigma-Aldrich, STRN250-1KT), treated with DNase (NEB, M0303S) and converted to cDNA (ThermoFisher Scientific/Invitrogen, 18080051). cDNA was treated with RNase H (ThermoFisher Scientific/Invitrogen: 18021071), and the product was restriction cloned (NEB, NcoI and XmaI) into pYL156 (empty TRV2 vector) with the primers designed for each construct (**Table S6**). VIGS triggers were aligned with the *N. benthamiana* genome (v1.0.1) sequence and the cloned cDNA sequence (**Figs. S2B and S3B-C**).

PD transport assay

VIGS, and imaging protocols were performed as described (**Brunkard et al., 2015b**). *N. benthamiana* plants were grown as above, silenced, and ten days after silencing, plants were infiltrated with *Agrobacterium* (GV3101) carrying a construct to express 1X-GFP, and imaged for PD transport 48 hours later.

### *ise3* transcriptome

Tissue collection and RNA sequencing analysis

Tissue collection was carried out as described (**Burch-Smith et al., 2011b**). Briefly, ~100 *ise3* or sibling WT mid-torpedo stage embryos were collected from siliques of *ise3*/+ heterozygous plants. Due to the difference in developmental age, the WT embryos were approximately ~8 DAF and *ise3* embryo age were ~12 DAF as described (**Burch-Smith et al., 2011b**). Three separate biological replicate samples were collected from multiple different plants grown on different days.

Total RNA was extracted from each replicate (Sigma-Aldrich, STRN250-1KT) and treated with DNase (NEB, M0303S). Library preps, ribosomal depletion, and Ion Torrent Proton sequencing were completed at the Functional Genomics Laboratory at UC Berkeley.

The Bowtie suite was used with modifications for analyzing Ion Torrent sequencing data. After filtering for quality (quality cut-off value = 20 with ≥75% bases meeting the cut-off value), TopHat v2.0.14, with parameters set to default except: max edit distance = 4, minimum intron length and minimum intron length found during split-segment (default) search = 20, number of mismatches allowed in each segment alignment for reads mapped independently = 3. The overall read mapping rates post filtering were between 64% and 76%. Over 10 million reads were mapped for each replicate (ranging from 10M to 15M reads).

The TopHat derived RNA sequencing alignments were analyzed using count-based differential expression analysis with edgeR in R (3.2.3), using a cutoff of an adjusted p-value of <0.05 and a log fold change of 2 and above, or -2 and below (**Fig. S4; Anders et al. 2013; Robinson et al., 2010**).

Transcriptome analysis of genes, pathways, and transcriptome comparisons

PANTHER Overrepresentation Test for Gene Ontology at http://pantherdb.org/ (release 2015-04-30, GO Ontology database released 2016-06-22), using the complete biological processes, molecular processes, and cellular component GO analyses were conducted using Bonferroni correction (**Mi et al., 2013; Mi et al., 2016**) to assess the *ise3* transcriptome. MapMan (http://mapman.gabipd.org/) (**Usadel et al., 2005**) was also used to assess the *ise3* transcriptome.

Hypergeometric probabilities were calculated as described (**Fury et al., 2006**) using R (3.2.3) and confirmed with a hypergeometric probability program that also calculates a gene overlap representation factor for transcriptomes (conducted on July 22, 2016, program at http://nemates.org/MA/progs/overlap_stats.html and program's statistics information at http://nemates.org/MA/progs/representation.stats.html).

**$H_2O_2$ detection with DAB staining**

$H_2O_2$ was detected using a 3,3-diaminobenzidine (DAB) (Sigma-Aldrich, D8001) following the staining protocol described (**Thordal-Christensen et al., 1997**) in *N. benthamiana* leaves silenced for *NbISE3, NbIPR1*, or the *GUS* control as described (**Stonebloom et al., 2009**).

**ACKNOWLEDGEMENTS**

This work initially was funded by the National Institutes of Health (NIH) Grant GM45244 (to P.C.Z.). A.M.R. was supported by a predoctoral fellowship from the National Science Foundation. This work used the Vincent J. Coates Genomics Sequencing Laboratory at UC Berkeley and the Ion Torrent Proton sequencing was funded by a grant from the California Institute for the Quantitative Biosciences (QB3). Our sincere thanks goes to D. Schichnes and S. E. Ruzin of the CNR Biological Imaging Facility at the University of California, Berkeley; fluorescence microscopy imaging reported in this publication was supported in part by the NIH S10 program under award number 1S10RR026866-01. The content is solely the responsibility of the authors and does not necessarily represent the official views of the NIH.

## REFERENCES

**Agarwal A, Koppstein D, Rozowsky J, Sboner A, Habegger L, Hillier LW, Sasidharan R, Reinke V, Waterston RH, and Gerstein M** (2010) Comparison and calibration of transcriptome data from RNA-Seq and tiling arrays. *BMC Genomics* **11**, 383.

**Alva V, Nam SZ, Söding J, and Lupas AN** (2016) The MPI bioinformatics Toolkit as an integrative platform for advanced protein sequence and structure analysis. *Nucleic Acids Res* **44**, W410-415.

**Amari K, Boutant E, Hofmann C, Schmitt-Keichinger C, Fernandez-Calvino L, Didier P, Lerich A, Mutterer J, Thomas CL, Heinlein M, et al.** (2010) A family of plasmodesmal proteins with receptor-like properties for plant viral movement proteins. *PLoS Pathog* **6**, e1001119.

**Anders S, McCarthy DJ, Chen Y, Okoniewski M, Smyth GK, Huber W, and Robinson MD** (2013) Count-based differential expression analysis of RNA sequencing data using R and Bioconductor. *Nat Protoc* **8**, 1765-1786.

**Apel K, and Hirt H** (2004) Reactive oxygen species: metabolism, oxidative stress, and signal transduction. *Annu Rev Plant Biol* **55**, 373-399.

**Barkan A, and Small I** (2014) Pentatricopeptide repeat proteins in plants. *Annu Rev Plant Biol* **65**, 415-442.

**Barros J, Serk H, Granlund I, and Pesquet E** (2015) The cell biology of lignification in higher plants. *Ann Bot* **115**, 1053-1074.

**Benitez-Alfonso Y, Cilia M, San Roman A, Thomas C, Maule A, Hearn S, and Jackson D** (2009) Control of *Arabidopsis* meristem development by thioredoxin-dependent regulation of intercellular transport. *Proc Natl Acad Sci USA* **106**, 3615-3620.

**Benitez-Alfonso Y, Faulkner C, Pendle A, Miyashima S, Helariutta Y, and Maule A** (2013) Symplastic intercellular connectivity regulates lateral root patterning. *Dev Cell* **26**, 136-147.

**Bentolila S, Oh J, Hanson MR, and Bukowski R** (2013) Comprehensive high-resolution analysis of the role of an *Arabidopsis* gene family in RNA editing. *PLoS Genet* **9**, e1003584.

**Bilska A, and Sowinski P** (2010) Closure of plasmodesmata in maize (Zea mays) at low temperature: a new mechanism for inhibition of photosynthesis. *Ann Bot* **106**, 675-686.

**Boerjan W, Ralph J, and Baucher M** (2003) Lignin biosynthesis. *Annu Rev Plant Biol* **54**, 519-546.

**Boevink P, McLellan H, Bukharova T, Engelhardt S, and Birch P** (2014) In vivo protein-protein interaction studies with BiFC: conditions, cautions, and caveats. *Methods Mol Biol* **1127**, 81-90.

**Bombarely A, Rosli HG, Vrebalov J, Moffett P, Mueller LA, and Martin GB** (2012) A draft genome sequence of *Nicotiana benthamiana* to enhance molecular plant-microbe biology research. *Mol Plant Microbe Interact* **25**, 1523-1530.

**Botha CEJ, Cross RHM, Bel AJE, and Peter CI** (2000) Phloem loading in the *sucrose-export-defective* (*SXD-1*) mutant maize is limited by callose deposition at plasmodesmata in bundle sheath–vascular parenchyma interface. *Protoplasma* **214**, 65-72.

**Brunkard JO, Runkel AM, and Zambryski PC** (2013) Plasmodesmata dynamics are coordinated by intracellular signaling pathways. *Curr Opin Plant Biol* **16**, 614-620.

**Brunkard JO, Runkel AM, and Zambryski PC** (2015a) The cytosol must flow: intercellular transport through plasmodesmata. *Curr Opin Cell Biol* **35**, 13-20.

**Brunkard JO, Burch-Smith TM, Runkel AM, and Zambryski PC** (2015b) Investigating plasmodesmata genetics with virus-induced gene silencing and an *Agrobacterium*-mediated GFP movement assay. *Methods Mol Biol* **1217**, 185-198.

**Burch-Smith TM, and Zambryski PC** (2010) Loss of *INCREASED SIZE EXCLUSION LIMIT (ISE)1* or *ISE2* increases the formation of secondary plasmodesmata. *Curr Biol* **20**, 989-993.

**Burch-Smith TM, and Zambryski PC** (2012) Plasmodesmata paradigm shift: regulation from without versus within. *Annu Rev Plant Biol* **63**, 239-260.

**Burch-Smith TM, and Zambryski PC** (2016) Regulation of plasmodesmal transport and modification of plasmodesmata during development and following infection by viruses and viral proteins. In *Plant-Virus Interactions* (ed. Tatjana Kleinow), pp. 87-122. Springer International Publishing Switzerland.

**Burch-Smith TM, Stonebloom S, Xu M, and Zambryski PC** (2011a) Plasmodesmata during development: re-examination of the importance of primary, secondary, and branched plasmodesmata structure versus function. *Protoplasma* **248**, 61-74.

**Burch-Smith TM, Brunkard JO, Choi YG, and Zambryski PC** (2011b) Organelle-nucleus cross-talk regulates plant intercellular communication via plasmodesmata. *Proc Natl Acad Sci USA* **108**, 1451-1460.

**Busi MV, Gomez-Lobato ME, Rius SP, Turowski VR, Casati P, Zabaleta EJ, Gomez-Casati DF, and Araya A** (2011) Effect of mitochondrial dysfunction on carbon metabolism and gene expression in flower tissues of *Arabidopsis thaliana*. *Mol Plant* **4**, 127-143.

**Calderwood A, Kopriva S, and Morris RJ** (2016) Transcript abundance explains mRNA mobility data in *Arabidopsis thaliana*. *Plant Cell* **28**, 610-605.

**Chapelle A, Morreel K, Vanholme R, Le-Bris P, Morin H, Lapierre C, Boerjan W, Jouanin L, and Demont-Caulet N** (2012) Impact of the absence of stem-specific β-glucosidases on lignin and monolignols. *Plant Physiol* **160**, 1204-1217.

**Cosgrove DJ** (2005) Growth of the plant cell wall. *Nat Rev Mol Cell Biol* **6**, 850-861.

**Crawford KM, and Zambryski PC** (2000) Subcellular localization determines the availability of non-targeted proteins to plasmodesmatal transport. *Curr Biol* **10**, 1032-1040.

**D'Auria JC, and Gershenzon J** (2005) The secondary metabolism of *Arabidopsis thaliana*: growing like a weed. *Curr Opin Plant Biol* **8**, 308-316.

**Daum G, Medzihradszky A, Suzaki T, and Lohmann JU** (2014) A mechanistic framework for noncell autonomous stem cell induction in *Arabidopsis*. *Proc Natl Acad Sci USA* **111**,14619-14624.

**De Storme N, and Geelen D** (2014) Callose homeostasis at plasmodesmata: molecular regulators and developmental relevance. *Front Plant Sci* **5**, 138.

**Dietz KJ, Mittler R, and Noctor G** (2016) Recent progress in understanding the role of reactive oxygen species in plant cell signaling. *Plant Physiol* **171**, 1535-1539.

**Emanuelsson O, Nielsen H, Brunak S, and von Heijne G** (2000) Predicting subcellular localization of proteins based on their N-terminal amino acid sequence. *J Mol Biol* **300**, 1005-1016.

**English AR, and Voeltz GK** (2013) Endoplasmic reticulum structure and interconnections with other organelles. *Cold Spring Harb Perspect Biol* **5**, a013227.

**Faulkner C, Petutschnig E, Benitez-Alfonso Y, Beck M, Robatzek S, Lipka V, and Maule AJ** (2013) LYM2-dependent chitin perception limits molecular flux via plasmodesmata. *Proc Natl Acad Sci USA* **110**, 9166-9170.

**Fichtenbauer D, Xu XM, Jackson D, and Kragler F** (2012) The chaperonin CCT8 facilitates spread of tobamovirus infection. *Plant Signal & Behav* **7**, 318-321.

**Fraser CM, and Chapple C** (2011) The phenylpropanoid pathway in *Arabidopsis*. *Arabidopsis Book* **9**, e0152.

**Fury W, Batliwalla F, Gregersen PK, and Li W** (2006) Overlapping probabilities of top ranking gene lists, hypergeometric distribution, and stringency of gene selection criterion. *Conf Proc IEEE Eng Med Biol Soc* **1**, 5531-5534.

**Giannoutsou E, Sotiriou P, Apostolakos P, and Galatis B** (2013) Early local differentiation of the cell wall matrix defines the contact sites in lobed mesophyll cells of *Zea mays*. *Ann Bot* **112**, 1067-1081.

**Gisel A, Barella S, Hempel FD, and Zambryski PC** (1999) Temporal and spatial regulation of symplastic trafficking during development in *Arabidopsis thaliana* apices. *Development* **126**, 1879-1889.

**Gisel A, Hempel FD, Barella S, and Zambryski P** (2002) Leaf-to-shoot apex movement of symplastic tracer is restricted coincident with flowering in *Arabidopsis*. *Proc Natl Acad Sci USA* **99**, 1713-1717.

**Huang J, Gu M, Lai Z, Fan B, Shi K, Zhou YH, Yu JQ, and Chen Z** (2010) Functional analysis of the *Arabidopsis* PAL gene family in plant growth, development, and response to environmental stress. *Plant Physiol* **153**, 1526-1538.

**Huang S, Van Aken O, Schwarzländer M, Belt K, and Millar AH** (2016) The roles of mitochondrial reactive oxygen species in cellular signaling and stress response in plants. *Plant Physiol* **171**, 1551-1559.

**Hückelhoven R** (2007) Cell wall-associated mechanisms of disease resistance and susceptibility. *Annu Rev Phytopathol* **45**, 101-127.

**Jones DL, Blancaflor EB, Kochian LV, and Gilroy S** (2006) Spatial coordination of aluminium uptake, production of reactive oxygen species, callose production and wall rigidification in maize roots. *Plant Cell Environ* **29**, 1309-1318.

**Kaija H, Alatalo SL, Halleen JM, Lindqvist Y, Schneider G, Väänänen HK, and Vihko P** (2002) Phosphatase and oxygen radical-generating activities of mammalian purple acid phosphatase are functionally independent. *Biochem Biophys Res Commun* **292**, 128-132.

**Karpenahalli MR, Lupas AN, and Söding J** (2007) TPRpred: a tool for prediction of TPR-, PPR- and SEL1-like repeats from protein sequences. *BMC Bioinformatics* **8**, 2.

**Katoh K, Kuma K, Toh H, and Miyata T** (2005) MAFFT version 5: improvement in accuracy of multiple sequence alignment. *Nucleic Acids Res* **33**, 511-518.

**Keunen E, Jozefczak M, Remans T, Vangronsveld J, and Cuypers A** (2013) Alternative respiration as a primary defence during cadmium-induced mitochondrial oxidative challenge in *Arabidopsis thaliana. Environmental and Experimental Botany* **91**, 63-73.

**Keunen E, Schellingen K, Van Der Straeten D, Remans T, Colpaert J, Vangronsveld J, and Cuypers A** (2015) ALTERNATIVE OXIDASE1a modulates the oxidative challenge during moderate Cd exposure in *Arabidopsis thaliana* leaves. *J Exp Bot* **66**, 2967-2977.

**Kersey PJ, Allen JE, Armean I, Boddu S, Bolt BJ, Carvalho-Silva D, Christensen M, Davis P, Falin LJ, Grabmueller C, et al.** (2016) Ensembl Genomes 2016: more genomes, more complexity. *Nucleic Acids Res* **44**, D574-580.

**Kim I, Hempel FD, Sha K, Pfluger J, and Zambryski PC** (2002) Identification of a developmental transition in plasmodesmatal function during embryogenesis in *Arabidopsis thaliana*. *Development* **129**, 1261-1272.

**Kim I, Cho E, Crawford K, Hempel FD, and Zambryski PC** (2005a) Cell-to-cell movement of GFP during embryogenesis and early seedling development in *Arabidopsis*. *Proc Natl Acad Sci USA* **102**, 2227-2231.

**Kim I, Kobayashi K, Cho E, and Zambryski PC** (2005b) Subdomains for transport via plasmodesmata corresponding to the apical-basal axis are established during *Arabidopsis* embryogenesis. *Proc Natl Acad Sci USA* **102**, 11945-11950.

**Kleine T, and Leister D** (2016) Retrograde signaling: Organelles go networking. *Biochim Biophys Acta* **1857**, 1313-1325.

**Kleine T, Maier UG, and Leister D** (2009) DNA transfer from organelles to the nucleus: the idiosyncratic genetics of endosymbiosis. *Annu Rev Plant Biol* **60**, 115-138.

**Klie S, and Nikoloski Z** (2012) The choice between MapMan and Gene Ontology for automated gene function prediction in plant science. *Frontiers in Genetics* **3**, 115.

**Koussevitzky S, Nott A, Mockler TC, Hong F, Sachetto-Martins G, Surpin M, Lim J, Mittler R, and Chory J** (2007) Signals from chloroplasts converge to regulate nuclear gene expression. *Science* **316**, 715-719.

**Lee JY, Wang X, Cui W, Sager R, Modla S, Czymmek K, Zybaliov B, van Wijk K, Zhang C, Lu H, et al.** (2011) A plasmodesmata-localized protein mediates crosstalk between cell-to-cell communication and innate immunity in *Arabidopsis*. *Plant Cell* **23**, 3353-3373.

**Levy A, Erlanger M, Rosenthal M, and Epel BL** (2007) A plasmodesmata-associated beta-1,3-glucanase in *Arabidopsis*. *Plant J* **49**, 669-82.

**Lurin C, Andrés C, Aubourg S, Bellaoui M, Bitton F, Bruyère C, Caboche M, Debast C, Gualberto J, Hoffmann B, et al.** (2004) Genome-wide analysis of *Arabidopsis* pentatricopeptide repeat proteins reveals their essential role in organelle biogenesis. *Plant Cell* **16**, 2089-2103.

**Maule A, Gaudioso-Pedraza R, and Benitez-Alfonso Y** (2013) Callose deposition and symplastic connectivity are regulated prior to lateral root emergence. *Commun Integr Biol* **6**, e26531.

**Maxwell DP, Wang Y, and McIntosh L** (1999) The alternative oxidase lowers mitochondrial reactive oxygen production in plant cells. *Proc Natl Acad Sci USA* **96**, 8271-8276.

**McElver J, Tzafrir I, Aux G, Rogers R, Ashby C, Smith K, Thomas C, Schetter A, Zhou Q, Cushman MA, et al.** (2001) Insertional mutagenesis of genes required for seed development in *Arabidopsis thaliana*. *Genetics* **159**, 1751-1763.

**Mi H, Muruganujan A, Casagrande JT, and Thomas PD** (2013) Large-scale gene function analysis with the PANTHER classification system. *Nat Protoc* **8**, 1551-1566.

**Mi H, Poudel S, Muruganujan A, Casagrande JT, and Thomas PD** (2016) PANTHER version 10: expanded protein families and functions, and analysis tools. *Nucleic Acids Res* **44**, 336-342.

**Millar AH, Small ID, Day DA, and Whelan J** (2008) Mitochondrial biogenesis and function in *Arabidopsis*. *Arabidopsis Book* **6**, e0111.

**Mitchell A, Chang HY, Daugherty L, Fraser M, Hunter S, Lopez R, McAnulla C, McMenamin C, Nuka G, Pesseat S, et al.** (2015) The InterPro protein families database: the classification resource after 15 years. *Nucleic Acids Res* **43**, D213-D221.

**Mittl PR, and Schneider-Brachert W** (2007) Sel1-like repeat proteins in signal transduction. *Cell Signal* **19**, 20-31.

**Moghadam AA, Ebrahimie E, Taghavi SM, Niazi A, Babgohari MZ, Deihimi T, Djavaheri M, and Ramezani A** (2013) How the nucleus and mitochondria communicate in energy production during stress: nuclear MtATP6, an early-stress responsive gene, regulates the mitochondrial $F_1F_o$-ATP synthase complex. *Mol Biotechnol* **54**, 756-769.

**Nakatsubo T, Mizutani M, Suzuki S, Hattori T, and Umezawa T** (2008) Characterization of *Arabidopsis thaliana* pinoresinol reductase, a new type of enzyme involved in lignan biosynthesis. *J Biol Chem* **283**, 15550-15557.

**Niwa Y, Hirano T, Yoshimoto K, Shimizu M, and Kobayashi H** (1999) Non-invasive quantitative detection and applications of non-toxic, S65T-type green fluorescent protein in living plants. *Plant J* **18**, 455-463.

**Patton DA, Franzmann LH, and Meinke DW** (1991) Mapping genes essential for embryo development in *Arabidopsis thaliana*. *Mol Gen Genet* **227**, 337-47.

**Pollastri S, and Tattini M** (2011) Flavonols: old compounds for old roles. *Ann Bot* **108**, 1225-1233.

**Prikryl J, Rojas M, Schuster G, and Barkan A** (2011) Mechanism of RNA stabilization and translational activation by a pentatricopeptide repeat protein. *Proc Natl Acad Sci USA* **108**, 415-20.

**Provencher LM, Miao L, Sinha N, and Lucas WJ** (2001) *Sucrose export defective1* encodes a novel protein implicated in chloroplast-to-nucleus signaling. *Plant Cell* **13**, 1127-1141.

**Purvis AC, and Shewfelt RL** (1993) Does the alternative pathway ameliorate chilling injury in sensitive plant tissues? *Physiologia Plantarum* **88**, 712-718.

**Ravichandran S, Stone SL, Benkel B, Zhang J, Berrue F, and Prithiviraj B** (2015) Optimal level of purple acid phosphatase5 is required for maintaining complete resistance to *Pseudomonas syringae*. *Front Plant Sci* **6**, 568.

**Rim Y, Huang L, Chu H, Han X, Cho WK, Jeon CO, Kim HJ, Hong JC, Lucas WJ, and Kim JY** (2011) Analysis of *Arabidopsis* transcription factor families revealed extensive capacity for cell-to-cell movement as well as discrete trafficking patterns. *Mol Cells* **32**, 519-526.

**Rinne PL, and van der Schoot C** (1998) Symplasmic fields in the tunica of the shoot apical meristem coordinate morphogenetic events. *Development* **125**, 1477-1485.

**Robinson MD, McCarthy DJ, and Smyth GK** (2010) edgeR: a Bioconductor package for differential expression analysis of digital gene expression data. *Bioinformatics* **26**, 139-140.

**Runkel AM, Brunkard JO, Ahern, MA, Xu, M, and Zambryski PC** (*submitted and under review*, 2016) The *dse1* transcriptome reveals that ABI5 down-regulates plasmodesmatal transport.

**Rutschow HL, Baskin TI, and Kramer EM** (2011) Regulation of solute flux through plasmodesmata in the root meristem. *Plant Physiol* **155**, 1817-1826.

**Sanger R, and Lee JY** (2014) Plasmodesmata in integrated cell signalling: insights from development and environmental signals and stresses. *J Exp Bot* **65**, 6337-6358.

**Schmid M, Davison TS, Henz SR, Pape UJ, Demar M, Vingron M, Schölkopf B, Weigel D, and Lohmann JU** (2005) A gene expression map of *Arabidopsis thaliana* development. *Nat Genet* **37**, 501-506.

**Stonebloom S, Burch-Smith T, Kim I, Meinke D, Mindrinos M, and Zambryski P** (2009) Loss of the plant DEAD-box protein *ISE1* leads to defective mitochondria and increased cell-to-cell transport via plasmodesmata. *Proc Natl Acad Sci USA* **106**, 17229-17234.

**Stonebloom S, Brunkard JO, Cheung AC, Jiang K, Feldman L, and Zambryski P** (2012) Redox states of plastids and mitochondria differentially regulate intercellular transport via plasmodesmata. *Plant Physiol* **158**, 190-199.

**Thordal-Christensen H, Zhang Z, Wei Y, and Collinge DB** (1997) Subcellular localization of $H_2O_2$ in plants. $H_2O_2$ accumulation in papillae and hypersensitive response during the barley—powdery mildew interaction. *Plant J* **11**, 1187-1194.

**Tilsner J, Nicolas W, Rosado A, and Bayer EM** (2016) Staying Tight: Plasmodesmal membrane contact sites and the control of cell-to-cell connectivity in plants. *Annu Rev Plant Biol* **29**, 337-364.

**Torres MA, and Dangl JL** (2005) Functions of the respiratory burst oxidase in biotic interactions, abiotic stress and development. *Curr Opin Plant Biol* **8**, 397-403.

**Torres MA, Dangl JL, and Jones JDG** (2002) *Arabidopsis* gp91phox homologues *AtrbohD* and *AtrbohF* are required for accumulation of reactive oxygen intermediates in the plant defense response. *Proc Natl Acad Sci USA* **99**, 517–22.

**Uhrig JF, Mutondo M, Zimmermann I, Deeks MJ, Machesky LM, Thomas P, Uhrig S, Rambke C, Hussey PJ, and Hülskamp M** (2007) The role of *Arabidopsis* SCAR genes in ARP2-ARP3- dependent cell morphogenesis. *Development* **134**, 967–977.

**Usadel B, Nagel A, Thimm O, Redestig H, Blaesing OE, Palacios-Rojas N, Selbig J, Hannemann J, Piques MC, Steinhauser D, et al.** (2005) Extension of the visualization tool MapMan to allow statistical analysis of arrays, display of corresponding genes, and comparison with known responses. *Plant Physiol* **138**, 1195-11204.

**Van Aken O, Zhang B, Carrie C, Uggalla V, Paynter E, Giraud E, and Whelan J** (2009) Defining the mitochondrial stress response in *Arabidopsis thaliana*. *Mol Plant* **2**, 1310-1324.

**Van Aken O, Zhang B, Law S, Narsai R, and Whelan J** (2013) AtWRKY40 and AtWRKY63 modulate the expression of stress-responsive nuclear genes encoding mitochondrial and chloroplast proteins. *Plant Physiol* **162**, 254-271.

**Vatén A, Dettmer J, Wu S, Stierhof YD, Miyashima S, Yadav SR, Roberts CJ, Campilho A, Bulone V, Lichtenberger R, et al.** (2011) Callose biosynthesis regulates symplastic trafficking during root development. *Dev Cell* **21**, 1144-1155.

**Veljanovski V, Vanderbeld B, Knowles VL, Snedden WA, and Plaxton WC** (2006) Biochemical and molecular characterization of AtPAP26, a vacuolar purple acid phosphatase up-regulated in phosphate-deprived *Arabidopsis* suspension cells and seedlings. *Plant Physiol* **142**, 1282–1293.

**Vilella AJ, Severin J, Ureta-Vidal A, Heng L, Durbin R, and Birney E** (2009) EnsemblCompara GeneTrees: Complete, duplication-aware phylogenetic trees invertebrates. *Genome Res* **19**, 327-335.

**Vogt T** (2010) Phenylpropanoid biosynthesis. *Mol Plant* **3**, 2-20.

**Weigel D, and Glazebrook J** (2006) In planta transformation of *Arabidopsis. Cold Spring Harb Protoc* doi:10.1101/pdb.prot4668.

**Wolf S, Hématy K, and Höfte H** (2012) Growth control and cell wall signaling in plants. *Ann Review Plant Biol* **63**, 381-407.

**Woodson JD, Perez-Ruiz JM, Schmitz RJ, Ecker JR, and Chory J** (2013) Sigma factor-mediated plastid retrograde signals control nuclear gene expression. *Plant J* **73**, 1-13.

**Wu S, and Gallagher KL** (2012) Transcription factors on the move. *Curr Opin Plant Biol* **15**, 645-651.

**Xu M, Cho E, Burch-Smith TM, and Zambryski PC** (2012) Plasmodesmata formation and cell-to-cell transport are reduced in *decreased size exclusion limit 1* during embryogenesis in *Arabidopsis*. *Proc Natl Acad Sci USA* **109**, 5098-5103.

**Xu XM, Wang J, Xuan Z, Goldshmidt A, Borrill PG, Hariharan N, Kim JY, and Jackson D** (2011) Chaperonins facilitate KNOTTED1 cell-to-cell trafficking and stem cell function. *Science* **26**, 1141-1144.

**Yoshioka H, Numata N, Nakajima K, Katou S, Kawakita K, Rowland O, Jones JD, and Doke N** (2003) *Nicotiana benthamiana* gp91phox homologs *NbrbohA* and *NbrbohB* participate in H2O2 accumulation and resistance to *Phytophthora infestans*. *Plant Cell* **15**, 706-718.

**Zavaliev R, Ueki S, Epel BL, and Citovsky V** (2011) Biology of callose (β-1,3-glucan) turnover at plasmodesmata. *Protoplasma* **248**, 117-130.

**Zhang HD, Cui YL, Huang C, Yin QQ, Qin XM, Xu T, He XF, Zhang Y, Li ZR, and Yang ZN** (2015) PPR protein PDM1/SEL1 is involved in RNA editing and splicing of plastid genes in *Arabidopsis thaliana*. *Photosynth Res* **126**, 311-321.

**Zhou R, Jackson L, Shadle G, Nakashima J, Temple S, Chen F, and Dixon RA** (2010) Distinct cinnamoyl CoA reductases involved in parallel routes to lignin in *Medicago truncatula*. *Proc Natl Acad Sci USA* **107**, 17803-17808.

## SUPPLEMENTARY MATERIALS

### Supplementary Figures

**A**

| ISE3 (AT2G25570) | Len | cTP | mTP | SP | other | Loc | RC |
|---|---|---|---|---|---|---|---|
| Sequence | 288 | 0.030 | 0.719 | 0.113 | 0.087 | M | 2 |
| cutoff | | 0.000 | 0.000 | 0.000 | 0.000 | | |

**B**

| IPR1 (AT1G04590) | Len | cTP | mTP | SP | other | Loc | RC |
|---|---|---|---|---|---|---|---|
| Sequence | 384 | 0.093 | 0.667 | 0.033 | 0.076 | M | 3 |
| cutoff | | 0.000 | 0.000 | 0.000 | 0.000 | | |

**C**

| Repeat | Begin | Alignment from IPR1 (AT1G04590) | End | P-value |
|---|---|---|---|---|
| PPR | 180 | ASLKIVIASLEKEHQWHRMVQVIKWILSKGQGNTM | 214 | 2.5e-04 |
| PPR | 215 | GTYGQLIRALDMDRRAEEAHVIWRKKVGNDLHSVP | 249 | 1.1e-05 |
| PPR | 251 | QLCLQMMRIYFRNNMLQELVKVMKLFKDLESYDRK | 285 | 4.9e-03 |
| PPR | 290 | HIVQTVADAYELLGMLDEKERVVTKYSHLLLGTPS | 324 | 2.4e-03 |

**Fig. S1. IPR1 contains PPR repeats, and both ISE3 and IPR1 are predicted to localize to the mitochondria.** (**A**) ISE3 has a predicted mitochondrial targeting peptide (mTP) and is not expected to have a chloroplast transit peptide (cTP) or a secretory signal peptide (SP); this prediction has a reliability class (RC) of 2, meaning there is a strong measure of the difference between the highest and the second highest output score (0.800 > diff > 0.600) suggesting the localization prediction is likely correct (**Emanuelsson et al., 2000**). (**B**) IPR1 (AT1G04590) has a predicted mTP and is not expected to have cTP or a SP; this prediction has a RC of 3, meaning there is a good measure of the difference between the highest and the second highest output score (0.600 > diff > 0.400) suggesting the localization prediction is likely correct (**Emanuelsson et al., 2000**). (**C**) IPR1 may be a pentatricopeptide repeats (PPR) protein; TPRpred (**Alva et al., 2016; Karpenahalli et al., 2007**) predicts IPR1 is a PPR protein with a probability of 68% (p = 2.2e-08).

A

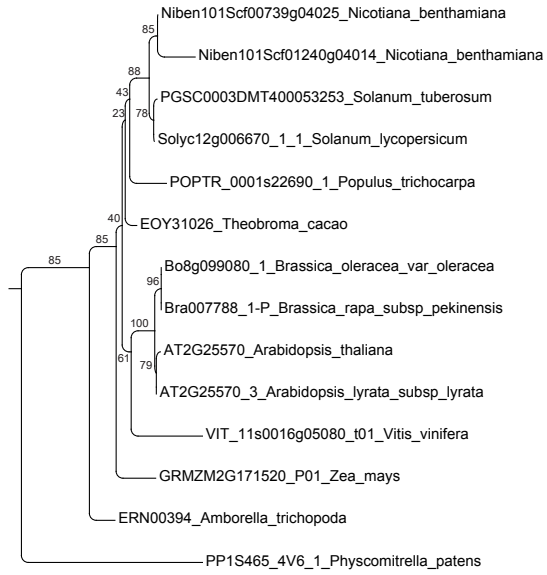


B

```
NbISE3_VIGS_trigger    --------------------------cgattccttgcctgaattggtaattggcgctcttt
Niben101Scf00739g04025 gtcaa--atagcaatagacaaacgccgattccttgcctgaattggcaattggcgctcttt
Niben101Scf01240g04014 gtcaaatatagcaatagtcaaacgccgattccttgcctgaattggtaattggcgctcttt
                                           ********************.**************

NbISE3_VIGS_trigger    gccctccatttttcttcaatccctttcgaaaagctgcgatcagtgttctttgtagttcgga
Niben101Scf00739g04025 gccctccatttttcttcggccccttttcgaaaagctgcgatcagagttctctttagttcgga
Niben101Scf01240g04014 gccctccatttttcttcaatccctttcgaaaagctgcgatcagtgttctttgtagttcgga
                       ****************...********************** *****.* *********

NbISE3_VIGS_trigger    gcgaccactatt---------------------gaaggcagataatgtttagatcattcct
Niben101Scf00739g04025 gcgaccaccattggccgagcttcagttgctaagaaggcagataatgtttagatcattcct
Niben101Scf01240g04014 gcgaccactatt---------------------gaaggcagataatgtttagatcattcct
                       ********.***                     ****************************

NbISE3_VIGS_trigger    tctaaaggctgtcattaaacagcttacttatcatccagctatcactaaacagctctgtcg
Niben101Scf00739g04025 tctaaaggctgtcattaaacagcttacttatcatccagctgtcactaaacagctatgtcg
Niben101Scf01240g04014 tctaaaggctgtcattaaacagcttacttatcatccagctatcactaaacagctctgtcg
                       ****************************************.************* *****

NbISE3_VIGS_trigger    tcatcctttccagttccatctagagagaggaatgcacagcagaaataagaaggcgatgga
Niben101Scf00739g04025 tcatcctttccagtaccatctagagagaggaatgcacagcagaaataagaaggcgatgga
Niben101Scf01240g04014 tcatcctttccagttccatctagagagaggaatgcacagcagaaataagaaggcgatgga
                       ************* ************************************************

NbISE3_VIGS_trigger    atacatagctaggggggtggaatgctctgcaggaagttgatagagtaattgattattgtga
Niben101Scf00739g04025 gtacatagctaggggggtggaatgctctgcaggaagttgatagagtaattgattattgtga
Niben101Scf01240g04014 atacatagctaggggggtggaatgctctgcaggaagttgatagagtaattgattattgtga
                       .************************************************************

NbISE3_VIGS_trigger    gcttaatgacaaacgtctcattccttcacttaggacagcaaaggagaattttgagttggc
Niben101Scf00739g04025 gcttaatgacaaacgtctcattccttcacttaggacagcaaaagagaattttgaattggc
Niben101Scf01240g04014 gcttaatgacaaacgtctcattccttcacttaggacagcaaaggagaattttgagttggc
                       ****************************************.***********.*****

NbISE3_VIGS_trigger    tctggaagtagacaattcaaatacccatgcaagatattggctttcaaaactgcatctcaa
Niben101Scf00739g04025 tctggaagcagacaactcaaatacccatgcaagatattggctttcaaaactgcatctcaa
Niben101Scf01240g04014 tctggaagtagacaattcaaatacccatgcaagatattggctttcaaaactgcatctcaa
                       ********.*******.************************************************

NbISE3_VIGS_trigger    gtaccatgtccctggggcgtgtagtgctgtaggggctgctttattagtggaagctgcaga
Niben101Scf00739g04025 gtaccatgtccctggggcgtgcaaagctgtaggggctgctttattagtggaagctgcaga
Niben101Scf01240g04014 gtaccatgtccctggggcgtgtagtgctgtaggggctgctttattagtggaagctgcaga
                       **********************.*. ************************************

NbISE3_VIGS_trigger    gatgggtgatccagatgctcaatttgaattagggtgccgtctaagagttgagaacgaata
Niben101Scf00739g04025 gatgggtgatcccgatgctcaatttgaattaggttgccgtctaagagttgagaacaacta
Niben101Scf01240g04014 gatgggtgatccagatgctcaatttgaattagggtgccgtctaagagttgaggtggttt-
                       ************ ******************** ******************.  .  *

NbISE3_VIGS_trigger    tgtgcaatcggatcagcaagcattttactacttggagaaagctgttgaccagttgcatcc
Niben101Scf00739g04025 tgtgcaatcagatcagcaagcattttactacttggagaaggctgttgaccagttgcatcc
Niben101Scf0124        -------tcttttcggaacatattaattttgtcaagaagaatggttacaccacctatga
                              **   *. * **    ** *.* . * .****.. ** * **    . .**

NbISE3_VIGS_trigger    aggtgcactttacctcttaggtgctgtgtatcttactggggattgcgtgaaaanggatg-
Niben101Scf00739g04025 aggtgcactttacctcttaggtgctgtgtatcttactggggattgcgtgaaaagggatg-
Niben101Scf01240g04014 gctcgtatgatgttaaagattctctgttggtttagtgacaaataatctgaacgtctatgc
                       .  .*.*.  *...    *  . **** .*.* .. . ..** .. **** .   ***

NbISE3_VIGS_trigger    -------ttggctctgcattgtggtgtttccatagagcatctgagaagggtcatgctgga
Niben101Scf00739g04025 -------ttggctctgcattgtggtgtttccatagagcatctga----------------
Niben101Scf01240g04014 agctagtttgggtttagaactcaaactttggctaacgtcactttgatatctgaaacaagg
                              **** *.*. * . ...  ***   **. *.  **

NbISE3_VIGS_trigger    gcagctatagcttatggatccctttctactccaaggtg------tggaacttccagaatca
Niben101Scf00739g04025 ------------------------------------------------------------
Niben101Scf01240g04014 ttagct-----tgttggatctcccttaccgtggtatgacttgtgaactcctctagtgtaa


NbISE3_VIGS_trigger    ataacgaa-----atttttagtgaagagggggtcctcaagcagaatatc---gaggagtc
Niben101Scf00739g04025 ----------------------gaagcgggggtcctcaagcagaatatcaaggaggaatg
Niben101Scf01240g04014 actacaaatgaacaatttttataaaatgggcgttactgctgacaccttc---tcgattt-
                                 .**. *** **. ...   * * . **     *.  *

NbISE3_VIGS_trigger    gagctgatccggagcttaatccgattgagctggccagagaacaatttgaaattgctgcaa
Niben101Scf00739g04025 gagttgatcctgagcttaatccgattgagctggccagagaacaatttgaaattgctgcaa
Niben101Scf01240g04014 --gattttacaatgtttatcttagccacttttggttggccaatataatcatatatctg---
                         * *  * * . *.*** ........  .***...*  **.*   * * **  ***

NbISE3_VIGS_trigger    aagcaggatctgaccttggatttagatggttaagaagacttgaggaggaagaanaaacgtc
Niben101Scf00739g04025 aagcaggatctgaccttggatttagatggttaaaaagacttgaggaggaagagaaacgtc
Niben101Scf01240g04014 aagccttttcacatattctattgcagtagtggagaattattgtgttaaa-----------
                       ****    **  *. **  ***  ..*.** .*.**   *** *  ..*

NbISE3_VIGS_trigger    tgttgtcttcctagttcatgaatatcaga-----------------------------
Niben101Scf00739g04025 tgctgtcgtcc-------------------------------------------------
Niben101Scf01240g04014 ccttgttctattagtatttggatgtcagaaaagtctgtataaatcatgctgtcagctcag
                       . .***. * .
```

C

(continued from previous page)

**D**

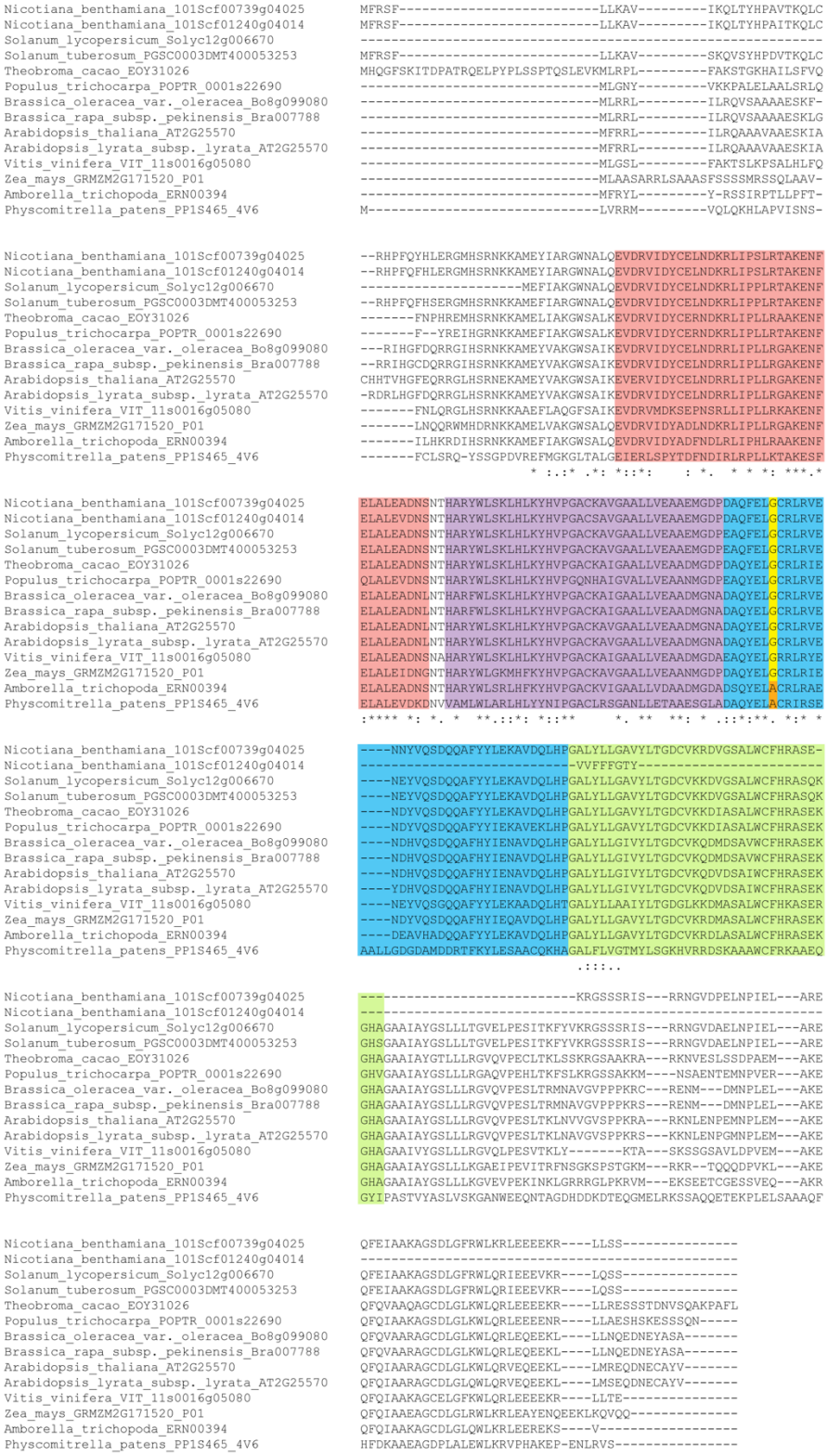

(continued from previous page)

**Fig. S2. VIGS trigger designed for *ISE3* in *N. benthamiana.*** Putative orthologs of *ISE3* were found through Ensembl Plants and aligned with the *N. benthamiana ISE3* putative orthologs (identified by BLAST in SolGenomics with the *A. thaliana* ISE3 protein). (**A**) Protein sequences were aligned by MAFFT (L-INS-i with 100 bootstrap values) to produce gene trees with Archaeopteryx. There are two *ISE3* genes in *N. benthamiana*, which often has two homeologues for each gene in its genome. (**B**) An alignment of the two *N. benthamiana ISE3* orthologs (cDNA) with the designed pTRV2-*NbISE3* VIGS trigger shows alignment to the *N. benthamiana ISE3* genes (*Niben101Scf00739g04025* and *Niben101Scf01240g04014*). (**C**) Predicted structure of *A. thaliana* ISE3 using Phyre2 with 92% of sequence modelled with 100% confidence by the single highest scoring template (**Kelley et al., 2015**). Coloring is based on tertiary structure and the amino acid affected by the *ise3-1* mutation is noted on the model with a white arrow. (**D**) The amino acid affected by the *ise3-1* mutation is conserved in most of the *ISE3* orthologs (yellow) of the gene tree in (**A**) except in the more basal species shown in (**A**), which include *Amborella trichopoda* (the most basal extant flowering plant) and *Physcomitrella patens* (a bryophyte), which have an alanine (A) substituted for a glycine (G) at this position (orange). Amino acid conservation can be observed among the *ISE3* orthologs in (**A**), especially within the SEL1 repeats (repeat 1 = red, repeat 2 = purple, repeat 3 = blue, repeat 4 = green). The labeled SEL1 repeats were identified with TPRpred (**Fig. 1E**) using the *A. thaliana* ISE3 protein sequence.

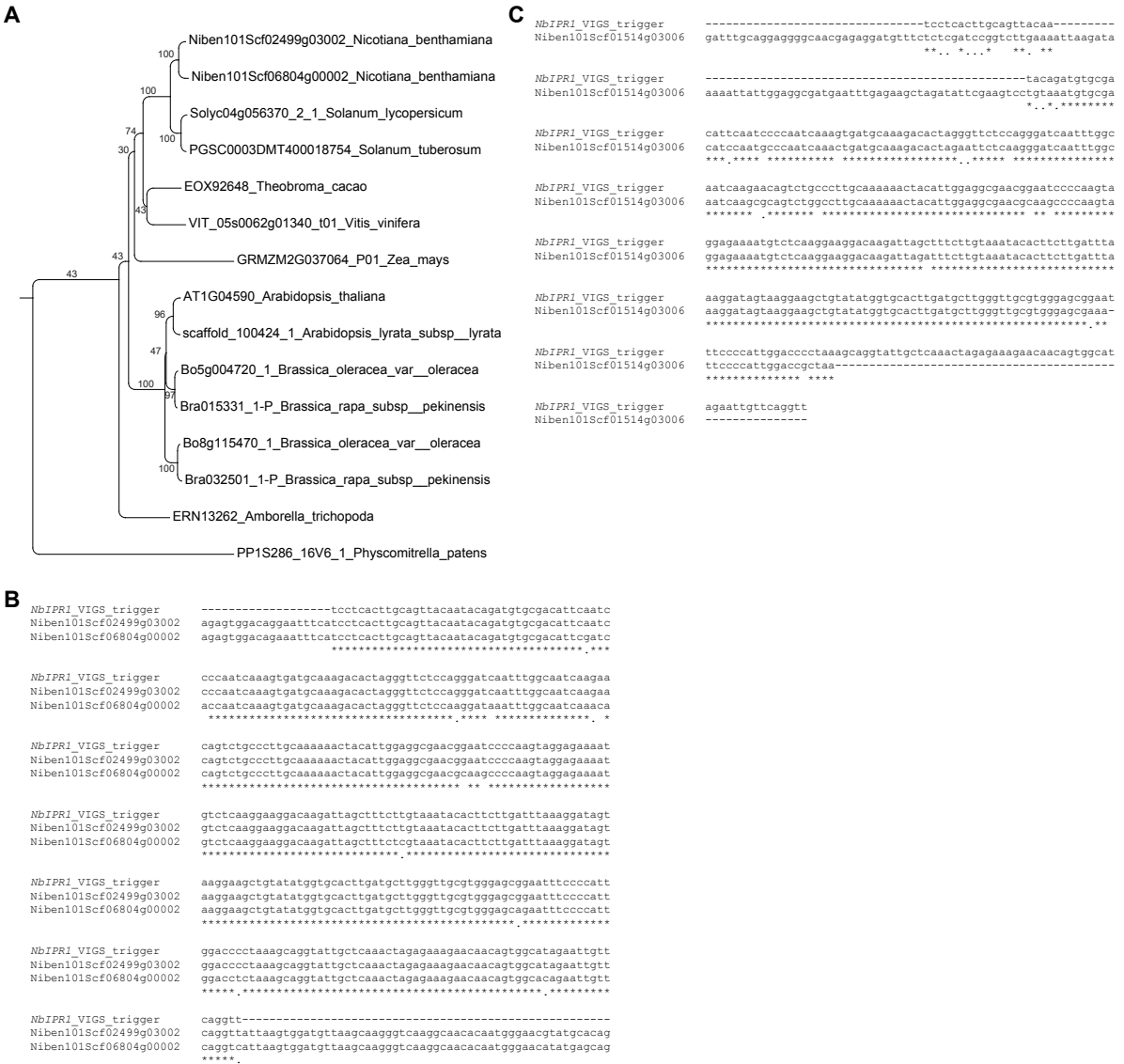


**Fig. S3. VIGS trigger design for *IPR1* in *N. benthamiana.*** Putative orthologs of *IPR1* proteins were found through Ensembl Plants and aligned with the *N. benthamiana IPR1* putative orthologs (identified by BLAST in SolGenomics with the *A. thaliana* IPR1 protein sequence). (**A**) Protein sequences were aligned using MAFFT (L-INS-i with 100 bootstrap values) to produce gene trees in Archaeopteryx. There are two *IPR1* genes in the *N. benthamiana* genome. (**B**) An alignment of the two *N. benthamiana IPR1* orthologs (cDNA) with the designed pTRV2-*NbIPR1* VIGS trigger shows alignment to the *N. benthamiana* genes (*Niben101Scf02499G03002* and *Niben101Scf06804g00002*). (**C**) An alignment of the pTRV2-*NbIPR1* VIGS trigger with a possible off-target gene (*Niben101Scf01514g03006*), which has significant DNA sequence overlap with the *NbIPR1* genes, but is not a predicted *NbIPR1* ortholog. When the protein sequence of this gene is BLAST to the *A. thaliana* genome, however, *AtIPR1* is the best match.

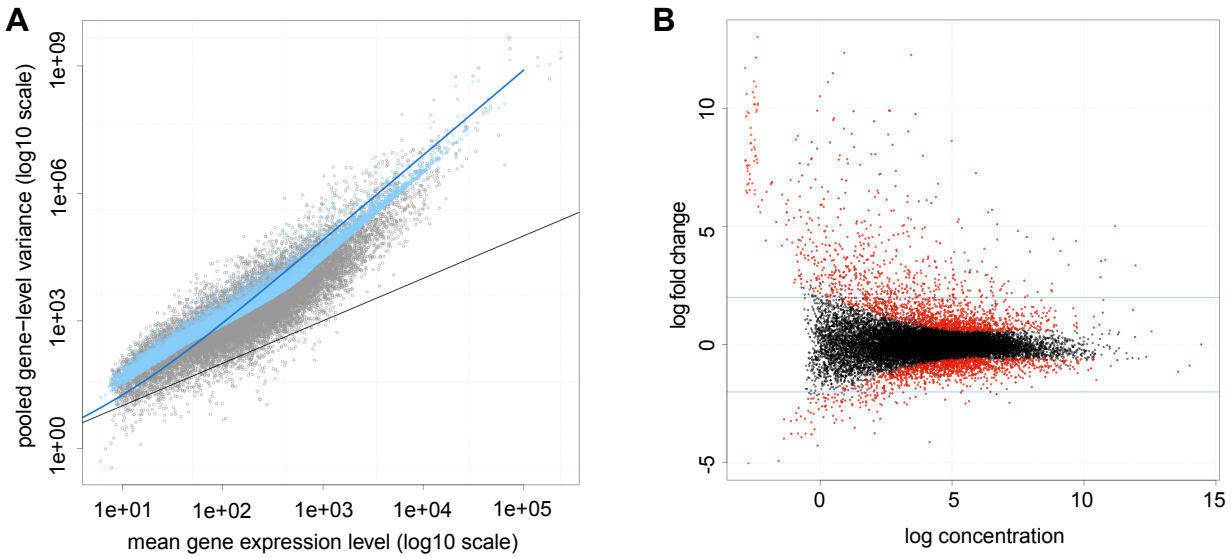


**Fig. S4. EdgeR analysis of the *ise3* transcriptome.** (**A**) Mean-variance relationship plot shows the raw variances of the counts (gray dots), the variances using the gene wise dispersions (light blue dots), the variances using the common dispersion (solid blue line), and the Poisson variance (black line). (**B**) Plot of the log-fold change (FC) against the log counts per million (CPM). Genes that are not differentially expressed ($p>0.05$, black dots) and differentially expressed genes ($p<0.05$, red dots) are shown in plot with blue lines that delineate genes above or below the logFC cutoff.

## Supplementary Materials References

**Kelley LA, Mezulis S, Yates CM, Wass MN, and Sternberg MJ** (2015) The Phyre2 web portal for protein modeling, prediction and analysis. *Nat Protoc* **10**, 845-858.

## Supplementary Tables

Note: Supplementary Table 1 is in a separate document due to size, and is available upon request.

## Table S2. A GO analysis of the up-regulated genes in the *ise3* _RNAseq transcriptome.

| GO biological process complete | Ref (#) | Found (#) | Expected (#) | Enrichment | Fold | p-value |
|---|---|---|---|---|---|---|
| suberin biosynthetic process (GO:0010345) | 16 | 9 | 0.37 | up | 24.34 | 4.98E-07 |
| phenylpropanoid biosynthetic process (GO:0009699) | 103 | 16 | 2.38 | up | 6.72 | 9.74E-06 |
| phenylpropanoid metabolic process (GO:0009698) | 129 | 19 | 2.98 | up | 6.37 | 8.52E-07 |
| response to chitin (GO:0010200) | 108 | 12 | 2.5 | up | 4.81 | 2.38E-02 |
| response to organonitrogen compound (GO:0010243 | 130 | 14 | 3 | up | 4.66 | 6.49E-03 |
| response to water deprivation (GO:0009414) | 230 | 18 | 5.31 | up | 3.39 | 2.20E-02 |
| response to water (GO:0009415) | 235 | 18 | 5.43 | up | 3.31 | 2.92E-02 |
| secondary metabolite biosynthetic process (GO:0044 | 251 | 19 | 5.8 | up | 3.28 | 2.00E-02 |
| secondary metabolic process (GO:0019748) | 361 | 26 | 8.34 | up | 3.12 | 1.23E-03 |
| response to acid chemical (GO:0001101) | 860 | 47 | 19.87 | up | 2.37 | 1.79E-04 |
| response to oxygen-containing compound (GO:19017 | 1122 | 58 | 25.93 | up | 2.24 | 3.58E-05 |
| response to organic substance (GO:0010033) | 1453 | 69 | 33.57 | up | 2.06 | 4.07E-05 |
| response to endogenous stimulus (GO:0009719) | 1270 | 58 | 29.34 | up | 1.98 | 2.03E-03 |
| response to chemical (GO:0042221) | 2053 | 87 | 47.44 | up | 1.83 | 8.81E-05 |
| single-organism metabolic process (GO:0044710) | 3163 | 111 | 73.08 | up | 1.52 | 1.20E-02 |
| response to stimulus (GO:0050896) | 4612 | 151 | 106.57 | up | 1.42 | 8.34E-03 |
| Unclassified (UNCLASSIFIED) | 7502 | 183 | 173.34 | up | 1.06 | 0.00E+00 |
| cellular protein metabolic process (GO:0044267) | 2412 | 28 | 55.73 | down | 0.5 | 3.25E-02 |

| GO cellular component complete | Ref (#) | Found (#) | Expected (#) | Enrichment | Fold | p-value |
|---|---|---|---|---|---|---|
| extracellular region (GO:0005576) | 2560 | 100 | 59.15 | up | 1.69 | 8.52E-05 |
| Unclassified (UNCLASSIFIED) | 5153 | 143 | 119.07 | up | 1.2 | 0.00E+00 |
| cell part (GO:0044464) | 18881 | 374 | 436.27 | down | 0.86 | 4.87E-05 |
| cell (GO:0005623) | 18883 | 374 | 436.31 | down | 0.86 | 4.76E-05 |
| intracellular membrane-bounded organelle (GO:0043 | 15117 | 285 | 349.3 | down | 0.82 | 8.56E-05 |
| membrane-bounded organelle (GO:0043227) | 15117 | 285 | 349.3 | down | 0.82 | 8.56E-05 |
| intracellular organelle (GO:0043229) | 15362 | 287 | 354.96 | down | 0.81 | 1.72E-05 |
| organelle (GO:0043226) | 15362 | 287 | 354.96 | down | 0.81 | 1.72E-05 |
| cytoplasm (GO:0005737) | 10931 | 203 | 252.57 | down | 0.8 | 1.27E-02 |
| intracellular part (GO:0044424) | 17197 | 319 | 397.36 | down | 0.8 | 6.68E-08 |
| intracellular (GO:0005622) | 17216 | 319 | 397.8 | down | 0.8 | 5.26E-08 |
| nucleus (GO:0005634) | 8385 | 142 | 193.75 | down | 0.73 | 1.29E-03 |
| organelle part (GO:0044422) | 3688 | 47 | 85.22 | down | 0.55 | 5.45E-04 |
| intracellular organelle part (GO:0044446) | 3679 | 46 | 85.01 | down | 0.54 | 3.07E-04 |
| intracellular non-membrane-bounded organelle (GO:( | 1142 | 9 | 26.39 | down | 0.34 | 3.18E-02 |
| non-membrane-bounded organelle (GO:0043228) | 1142 | 9 | 26.39 | down | 0.34 | 3.18E-02 |
| macromolecular complex (GO:0032991) | 1884 | 11 | 43.53 | down | 0.25 | 8.41E-07 |

| | | | | | | |
|---|---|---|---|---|---|---|
| protein complex (GO:0043234) | 1330 | 7 | 30.73 | down | 0.23 | 8.67E-05 |

| **GO molecular function complete** | **Ref (#)** | **Found (#)** | **Expected (#)** | **Enrichment** | **Fold** | **p-value** |
|---|---|---|---|---|---|---|
| nutrient reservoir activity (GO:0045735) | 54 | 12 | 1.25 | up | 9.62 | 1.16E-05 |
| Unclassified (UNCLASSIFIED) | 7204 | 158 | 166.46 | down | 0.95 | 0.00E+00 |
| RNA binding (GO:0003723) | 802 | 3 | 18.53 | down | < 0.2 | 1.23E-02 |

## Table S3. A GO analysis of the down-regulated genes in the *ise3*_RNAseq transcriptome.

| GO biological process complete | Ref (#) | Found (#) | Expected (#) | Enrichment | Fold | p-value |
|---|---|---|---|---|---|---|
| Unclassified (UNCLASSIFIED) | 7502 | 25 | 32.09 | down | 0.78 | 0.00E+00 |

| GO cellular component complete | Ref (#) | Found (#) | Expected (#) | Enrichment | Fold | p-value |
|---|---|---|---|---|---|---|
| extracellular region (GO:0005576) | 2560 | 28 | 10.95 | up | 2.56 | 1.33E-03 |
| Unclassified (UNCLASSIFIED) | 5153 | 13 | 22.04 | down | 0.59 | 0.00E+00 |

| GO molecular function complete | Ref (#) | Found (#) | Expected (#) | Enrichment | Fold | p-value |
|---|---|---|---|---|---|---|
| Unclassified (UNCLASSIFIED) | 7204 | 26 | 30.82 | down | 0.84 | 0.00E+00 |

## Table S4. MapMan analysis of overrepresented pathways in the *ise3* transcriptome.

| Bin | MapMan category name | # of genes | p-value[1] |
|---|---|---|---|
| 1 | Photosynthesis | 5 | 7.5E-04 |
| 1.1 | Photosynthesis: lightreaction | 3 | 7.4E-03 |
| 1.3 | Photosynthesis: calvin cycle | 2 | 4.1E-02 |
| 10.8 | Cell wall: pectinesterases | 8 | 3.1E-02 |
| 11.3 | Lipid metabolism: phospholipid synthesis | 3 | 1.5E-02 |
| 16.1 | Secondary metabolism: simple phenols | 4 | 3.4E-03 |
| 20.2 | Stress: abiotic | 20 | 3.5E-03 |
| 21.4 | Redox: glutaredoxins | 2 | 4.2E-02 |
| 26 | Miscellaneous | 75 | 3.3E-03 |
| 26.28 | Miscellaneous: GDSL-motif lipase | 4 | 2.1E-02 |
| 27 | RNA | 85 | 1.4E-02 |
| 27.3 | RNA: regulation of transcription | 81 | 3.8E-02 |
| 28.2 | DNA: repair | 2 | 2.2E-02 |
| 29 | Protein | 64 | 3.3E-02 |
| 29.2 | Protein: synthesis | 7 | 2.3E-03 |
| 30.8 | Signalling: miscellaneous | 2 | 4.5E-02 |
| 35.1 | Not assigned: no ontology | 59 | 1.8E-02 |
| 1.3.2 | Photosynthesis: calvin cycle - rubisco small subunit | 2 | 4.1E-02 |
| 11.9.4.13 | Lipid metabolism: lipid degradation - beta-oxidation, acyl CoA reductase | 3 | 3.0E-02 |
| 20.1.7.12 | Stress: biotic - PR-proteins, plant defensins | 5 | 3.2E-02 |
| 20.2.99 | Stress: abiotic - unspecified | 12 | 2.5E-03 |
| 27.3.32 | RNA: regulation of transcription - WRKY domain transcription factor family | 11 | 4.8E-02 |
| 27.3.67 | RNA: regulation of transcription - putative transcription regulator | 4 | 4.1E-02 |
| 29.2.7 | Protein: synthesis - transfer RNA | 2 | 3.1E-02 |
| 29.2.7.2 | Protein: synthesis - transfer RNA, plastid | 2 | 3.1E-02 |
| 35.1.41 | Not assigned: no ontology - hydroxyproline rich proteins | 7 | 1.3E-02 |

[1] The MapMan Bins listed have a p-value <0.05, however, the p-values are not adjusted (Wilcoxon Rank-Sum Test without Benjamini Hochberg correction for false discovery rate). With p-value adjustment, MapMan does not pick up any Bins with a p-value <0.05.

## Table S5. Transcriptome analysis of *ise3* with the *ise1*, *ise2*, and *dse1* transcriptomes - similarly regulated genes among *ise1, ise2,* and *ise3.*

| Locus (1) | Gene Description (1) | Primary Gene Symbol (1) | *ise3*_Ion | *ise1*_Tiling | *ise2*_Tiling | *dse1*_Tiling |
|---|---|---|---|---|---|---|
| AT1G01070 | nodulin MtN21-like tra | | 3 | 3.6 | 3.2 | - |
| AT1G03630 | Encodes for a protein | PROTOCHLOROPHYLLIDE OXIDC | -2.3 | -2.4 | -6.6 | -7.7 |
| AT1G08990 | plant glycogenin-like s | PLANT GLYCOGENIN-LIKE STAR( | 2.6 | 3.8 | 3.6 | 2.8 |
| AT1G10640 | Pectin lyase-like supe | | -2.2 | -3.3 | -7.6 | - |
| AT1G17030 | unknown protein; FUN | | 2.1 | 6.2 | 3.2 | 2.7 |
| AT1G17960 | Threonyl-tRNA synthe | | 3.7 | 6.1 | 2.4 | - |
| AT1G19200 | Protein of unknown fu | | 3.3 | 4.2 | 2.6 | 2.6 |
| AT1G22910 | RNA-binding (RRM/RI | | -2.1 | -2.1 | -2.7 | - |
| AT1G23570 | Domain of unknown fu | | 3.1 | 7.9 | 14.9 | - |
| AT1G23800 | Encodes a mitochondi | ALDEHYDE DEHYDROGENASE 2I | 4.6 | 2.5 | 3.5 | - |
| AT1G26820 | Encodes ribonuclease | RIBONUCLEASE 3 (RNS3) | 2.9 | 2.4 | 3.7 | - |
| AT1G28470 | NAC domain containir | NAC DOMAIN CONTAINING PROT | 4.6 | 2.3 | 2.1 | 4.1 |
| AT1G30170 | Protein of unknown fu | | 6.6 | 4.2 | 36.6 | - |
| AT1G30660 | nucleic acid binding;nu | | 2.7 | 3.9 | 3.8 | - |
| AT1G35290 | Thioesterase superfar | | -3.5 | -2.1 | -5.1 | - |
| AT1G65900 | unknown protein; FUN | | -2.1 | -2.5 | -2.2 | - |
| AT1G80180 | unknown protein; FUN | | 2.1 | 2.1 | 2 | - |
| AT2G01890 | Encodes a purple acid | PURPLE ACID PHOSPHATASE 8 ( | 8.9 | 4 | 2 | - |
| AT2G41400 | Pollen Ole e 1 allerger | | 12.3 | 9.7 | 8.2 | - |
| AT3G01600 | NAC domain containir | NAC DOMAIN CONTAINING PROT | 2.4 | 3.6 | 12 | - |
| AT3G03650 | embryo sac developm | EMBRYO SAC DEVELOPMENT AF | 4.7 | 6.8 | 4.5 | 2.9 |
| AT3G05390 | FUNCTIONS IN: mole | | 2.5 | 3.5 | 2.6 | - |
| AT3G13672 | TRAF-like superfamily | | 2.3 | 4 | 2 | - |
| AT3G22400 | Encodes lipoxygenase | (LOX5) | 5.7 | 2 | 3.6 | 15.5 |
| AT3G27400 | Pectin lyase-like supe | | 3 | 4.4 | 3.2 | - |
| AT3G52810 | purple acid phosphata | PURPLE ACID PHOSPHATASE 21 | 5.2 | 6.8 | 4.9 | - |
| AT4G13680 | Protein of unknown fu | | 8.5 | 9.1 | 8.4 | - |
| AT4G16640 | Matrixin family protein | | 4.9 | 2.1 | 3.2 | 6.2 |
| AT4G29110 | unknown protein; FUN | | 3 | 7.8 | 5.7 | 6.1 |
| AT4G30530 | Encodes a gamma-glu | GAMMA-GLUTAMYL PEPTIDASE | 2.8 | 3 | 6.9 | 2.3 |
| AT4G37030 | unknown protein; FUN | | 4.4 | 6 | 4 | - |
| AT4G37370 | member of CYP81D | CYTOCHROME P450, FAMILY 81, | 2.9 | 2.7 | 5.1 | - |
| AT4G37690 | Galactosyl transferase | | 2.6 | 7 | 4.2 | 3 |
| AT5G02140 | Pathogenesis-related | | 8 | 2.6 | 2.9 | - |
| AT5G06720 | Encodes a peroxidase | PEROXIDASE 2 (PA2) | 3.3 | 3.6 | 4.5 | 4.8 |
| AT5G07550 | member of Oleosin-lik | GLYCINE-RICH PROTEIN 19 (GRF | 4 | 3.3 | 3 | - |
| AT5G10930 | Encodes CBL-interact | CBL-INTERACTING PROTEIN KIN/ | 2.5 | 2.9 | 2 | - |

| | | | | | |
|---|---|---|---|---|---|
| AT5G11410 | Protein kinase superfa | 4.6 | 4.6 | 2.5 | - |
| AT5G14130 | Peroxidase superfamil | 3.5 | 2.9 | 2 | 2.4 |
| AT5G14490 | NAC domain containir NAC DOMAIN CONTAINING PROT | 4.5 | 5.8 | 2.4 | - |
| AT5G16030 | unknown protein; FUN | -2.6 | -5 | -3.2 | - |
| AT5G22800 | A locus involved in em EMBRYO DEFECTIVE 1030 (EMB1 | 2.1 | 12.3 | 4.4 | - |
| AT5G24860 | encodes a small prote FLOWERING PROMOTING FACTC | 2.1 | 5.6 | 3.7 | - |
| AT5G25190 | encodes a member of ETHYLENE AND SALT INDUCIBLE | 2.7 | 6.9 | 10 | - |
| AT5G40720 | CONTAINS InterPro D | 3.7 | 2.2 | 2.1 | - |
| AT5G54585 | unknown protein; Has | 2.9 | 3.7 | 4.1 | - |
| AT5G61420 | Encodes a nuclear loc MYB DOMAIN PROTEIN 28 (MYB2 | 3.8 | 6.8 | 3.5 | - |
| AT5G61890 | encodes a member of | 3.3 | 2.4 | 2.7 | - |
| AT5G64060 | NAC domain containir NAC DOMAIN CONTAINING PROT | 2.9 | 2.4 | 3.4 | 2 |

(1) TAIR annotation.

## Table S6. Primers for complementation, localization, BiFC, and VIGS experiments

| Name | Gene Locus (F/R) | Sequence 5' - 3' | Purpose | Cloning Method |
|---|---|---|---|---|
| XM_355 | promoter_AT2G25570_F | ttaaggcctgcaGGAACAGTTCATCATTCTCAGG | complementation | StuI-SbfI site |
| XM_356 | promoter_AT2G25570_R | gaaccatggTTTAGCCGGAGAAGAAACC | complementation | NcoI site |
| XM_357 | AT2G25570_F | aaaccatggcaTTTCGTCGTTTAATCTCCGGCAAG | localization | NcoI site |
| XM_358 | AT2G25570_R | aatccatggcaccTACATAGGCACATTCGTTATC | localization | NcoI site |
| AR_202 | AT2G25570_F | caccATGTTTCGTCGTTTAATTCTCCG | BiFC | Gateway® cloned |
| AR_203 | AT2G25570_R | TACATAGGCACATTCGTTATCTTGTTCC | BiFC | Gateway® cloned |
| AR_204 | AT2G30920_F | caccATGTTGGCGTCGGTACGG | BiFC | Gateway® cloned |
| AR_205 | AT2G30920_R | TATGTCTCCAAGATCCTTCCTTTTCG | BiFC | Gateway® cloned |
| AR_206 | AT3G17910_F | caccATGGCGACCTCGCTTTCC | BiFC | Gateway® cloned |
| AR_207 | AT3G17910_R | TCTGCGGACAGGCTTTGCC | BiFC | Gateway® cloned |
| AR_208 | AT1G15220_F | caccATGGAGAAAACAGACGAAGAGAG | BiFC | Gateway® cloned |
| AR_209 | AT1G15220_R | CCGGTTGAGCCATCTCCTCAAT | BiFC | Gateway® cloned |
| AR_210 | AT4G16800_F | caccATGAGCTTCGTCAAGTATCTCC | BiFC | Gateway® cloned |
| AR_211 | AT4G16800_R | ATTGCCAGTGTACAGAGGCTTAC | BiFC | Gateway® cloned |
| AR_212 | AT1G04590_F | caccATGGCGGGTTTCAGTTCTCTAA | BiFC | Gateway® cloned |
| AR_213 | AT1G04590_R | CGCTCCATGTTCGAATTGTTTTTCA | BiFC | Gateway® cloned |
| AR_247 | AT1G12770_F | caccATGGCGGCATCAACTTCAAC | BiFC | Gateway® cloned |
| AR_246 | AT1G12770_R | CCTTATAATAGCTTTATCTTCCTCAGTGAC | BiFC | Gateway® cloned |
| AR_159 | pTRV2_NbISE3_F | gagccatggCGATTCCTTGCCTG | VIGS gene silencing | NcoI site |
| AR_158 | pTRV2_NbISE3_R | gctcccgggAATCAACTCTTTTATAAACTCTG | VIGS gene silencing | XmaI site |
| AR_274 | pTRV2_NbIPR1_F | gagccatggTCCTCACTTGCAGTTACAATAC | VIGS gene silencing | NcoI site |
| AR_275 | pTRV2_NbIPR1_R | gatcccgggAACCTGAACAATTCTATGCCAC | VIGS gene silencing | XmaI site |

## Chapter 4: Chloroplasts extend stromules independently and in response to internal redox signals

**Previously published as:**

**Brunkard JO**[†]**, Runkel AM**[†]**, and Zambryski PC** (2015) Chloroplasts extend stromules independently and in response to internal redox signals. *Proc Natl Acad Sci USA* **112**, 10044-10049.

[†] J.O.B. and A.M.R. contributed equally to this work

## ABSTRACT

A fundamental mystery of plant cell biology is the occurrence of “stromules,” stroma-filled tubular extensions from plastids (such as chloroplasts) that are universally observed in plants but whose functions are, in effect, completely unknown. One prevalent hypothesis is that stromules exchange signals or metabolites between plastids and other subcellular compartments, and that stromules are induced during stress. Until now, no signaling mechanisms originating within the plastid have been identified that regulate stromule activity, a critical missing link in this hypothesis. Using confocal and superresolution 3D microscopy, we have shown that stromules form in response to light-sensitive redox signals within the chloroplast. Stromule frequency increased during the day or after treatment with chemicals that produce reactive oxygen species specifically in the chloroplast. Silencing expression of the chloroplast NADPH-dependent thioredoxin reductase, a central hub in chloroplast redox signaling pathways, increased chloroplast stromule frequency, whereas silencing expression of nuclear genes related to plastid genome expression and tetrapyrrole biosynthesis had no impact on stromules. Leucoplasts, which are not photosynthetic, also made more stromules in the daytime. Leucoplasts did not respond to the same redox signaling pathway but instead increased stromule formation when exposed to sucrose, a major product of photosynthesis, although sucrose has no impact on chloroplast stromule frequency. Thus, different types of plastids make stromules in response to distinct signals. Finally, isolated chloroplasts could make stromules independently after extraction from the cytoplasm, suggesting that chloroplast-associated factors are sufficient to generate stromules. These discoveries demonstrate that chloroplasts are remarkably autonomous organelles that alter their stromule frequency in reaction to internal signal transduction pathways.

## INTRODUCTION

Chloroplasts, the descendants of ancient bacterial endosymbionts, exert impressive influence over processes that are not directly related to their metabolic roles. In recent years, forward genetic screens have led to the discoveries that chloroplasts are critical regulators of leaf shape, cell–cell signaling through plasmodesmata, pathogen defense, and even alternative splicing in the nucleus (**Avendaño-Vázquez et al., 2014; Burch-Smith et al., 2011; Estavillo et al., 2011; Koussevitzky et al., 2007; Nomura et al., 2012; Petrillo et al., 2014; Stonebloom et al., 2012; Xiao et al., 2012**) however, in almost all of these pathways, the signaling route between the chloroplast and the nucleus is unknown. This is a pressing question for plant biology and cell biology in general: how do organelles communicate with the nucleus to coordinate genetic programs and cellular function? One possible route for this communication is through “stromules,” stroma-filled tubular extensions of unknown function from plastids (**Hanson and Sattarzadeh, 2011; Köhler et al., 1997; Schattat et al., 2012a**).

Stromules were first observed in spinach cells (**Wildman et al., 1962**), and have since been observed in every cell type and land plant species investigated to date (**Natesan**

**et al., 2005**). Several studies have identified conditions that can induce or decrease stromule formation (**Erickson et al., 2014; Gray et al., 2012; Holzinger et al., 2007; Natesan et al., 2009; Schattat and Klösgen, 2011**), concluding that stromule frequency can change in response to abiotic stress, phytohormone signaling, and massive disruption of cellular function (e.g., strong inhibition of cytosolic translation or of actin microfilament dynamics). Almost nothing is known about the genetics of stromules; some mutants with strong morphological defects in plastids, such as mutants with improper plastid division or lacking plastid mechanosensitive channels, cannot form stromules at normal frequencies, but these plastids are so severely misshapen that their stromule frequencies cannot be directly compared with wild-type plastids (**Holzinger et al., 2008; Veley et al., 2012**). To date, few experiments have tested whether signals inside plastids can affect stromule frequency, and all of those experiments (e.g., treatment with antibiotics that interfere with plastid genome expression; **Gray et al.** (**2012**)) have suggested that stromule frequency is not regulated by internal plastid biology. Here we test whether light-sensitive redox signaling pathways initiated within chloroplasts regulate stromule activity.

## RESULTS AND DISCUSSION

### Chloroplasts make more stromules during the day

We began our study by conducting a time course to determine the effects of light on chloroplast stromule formation. For all in planta experiments (except where noted otherwise), we observed stromules in the proximal abaxial epidermis of cotyledons of young *N. benthamiana* or *A. thaliana* plants, or in the proximal abaxial epidermis of young leaves at 2 wk after silencing gene expression with virus-induced gene silencing (VIGS). We collected a single z-stack of confocal images of only one leaf of each plant, and considered plants to be independent samples. (The number of plants observed for each treatment for an experiment is designated “n” throughout.) Thus, each experiment considered the stromule frequency determined from hundreds, thousands, or even tens of thousands of plastids.

Over the course of 2 d, we measured stromule frequency in cotyledons from young *N. benthamiana* seedlings every 4 h, and found significantly more stromules during the daytime than at nighttime; 20.8 ± 1.8% of chloroplasts had stromules in the day, compared with only 12.8 ± 0.9% at night ($n \geq 22$, $p < 0.0005$) (**Fig. 1 and Fig. S1**). (Throughout the paper, stromule frequency is reported as percentage ± SE.) There was no significant difference in stromule frequency between the first and second days or between the first and second nights, indicating that the observed changes were reactions to the changing light environment rather than a progressive developmental change over 48 h.

Previous studies investigating the relationship between chloroplast stromule frequency and light reported that light decreases stromule frequency in seedling hypocotyls during de-etiolation after skotomorphogenesis, and that constant darkness or exposure to only

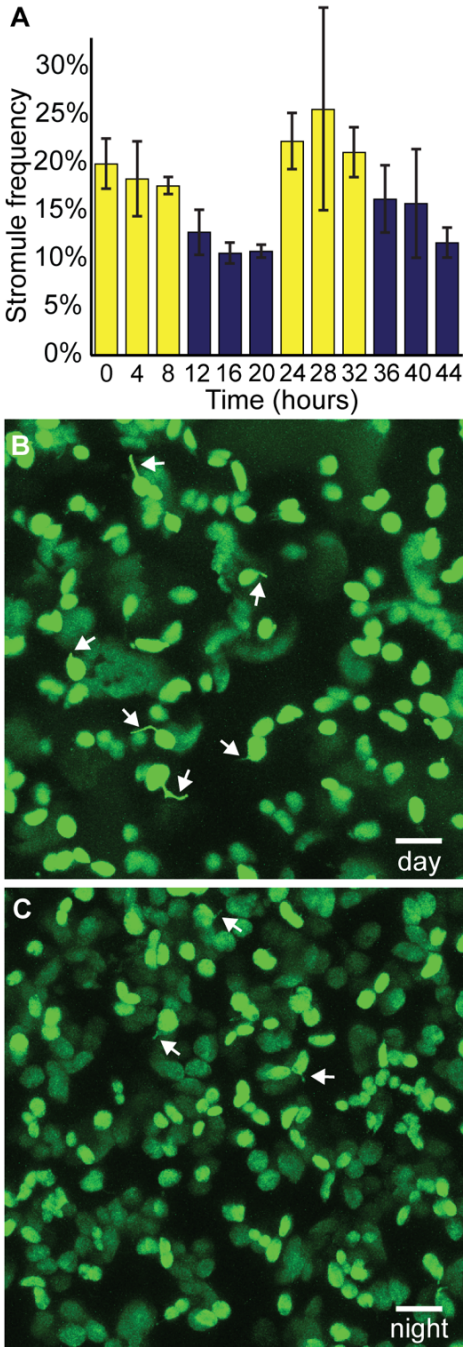


**Fig. 1. Chloroplast stromule frequency varies with diurnal cycles**. (**A**) Stromule frequency rises in the day (yellow bars) and decreases at night (blue bars) in chloroplasts of *N. benthamiana* seedlings ($n \geq 22$, $p < 0.0005$). (**B and C**) Representative images of *N. benthamiana* epidermal chloroplasts labeled with stromal GFP (green) in the day (**B**) and at night (**C**). Some stromules are indicated by white arrows. As a visual aid, here and in other figures; not all stromules are indicated, and the indicated stromules were selected at random. Error bars indicate ± SE. (Scale bars: 10 μm.)

blue light increases stromule frequency after photomorphogenesis (**Gray et al., 2012**). The apparent discrepancy between those conclusions and our results showing that light promotes chloroplast stromule formation is explained by the different plastid types used in the de-etiolation experiment (etioplasts transitioning to become chloroplasts) and the dramatic developmental and physiological transitions used in both experiments (constant darkness to constant light, or vice versa), which are not reflective of typical chloroplast stromule behavior in normal, healthy plants. We conclude that light promotes chloroplast stromule formation during the day.

**Reactive oxygen species inside chloroplasts promote stromule formation**

Plants sense light with the pigments of the photosynthetic electron transport chain (pETC) in the chloroplast or with photoreceptors elsewhere in the cell (**Hughes, 2013**). We tested whether stromule frequency responds specifically to light sensed by the chloroplast itself by chemically inhibiting pETC activity. We used two pETC inhibitors, 3-(3,4-dichlorophenyl)-1,1-dimethylurea (DCMU) and 2,5-dibromo-6-isopropyl-3-methyl-1,4-benzoquinone (DBMIB). DCMU prevents reduction of plastoquinone at photosystem II and generates singlet oxygen, whereas DBMIB prevents plastoquinols from reducing the cytochrome b6f complex and generates superoxide (**Petrillo et al., 2014**).

We measured the effects of DCMU and DBMIB on the chloroplast stromal redox status, as monitored by a stromal redox-sensitive transgenic GFP biosensor, pt-roGFP2 (**Stonebloom et al., 2012**), to find very low active concentrations of each compound with our treatment technique, and found that 10 μM DCMU or 12 μM DBMIB was sufficient to strongly oxidize redox buffers in the chloroplast stroma. The normalized proportion of oxidized pt-roGFP2 rose from 20.0 ± 3.5% in control conditions to 68.9 ± 3.0% after 10 μM DCMU treatment and to 41.5 ± 7.1% after 12 μM DBMIB treatment ($n \geq 28$, $p < 0.01$) (**Fig. S2**).

We assessed stromule frequency at 2 h after treating *N. benthamiana* cotyledons with either of the photosynthesis inhibitors (**Fig. 2 A-C and Fig. S2 A-C**). In the epidermal chloroplasts of mock-treated cotyledons, the average chloroplast stromule frequency was 9.2 ± 1.4%. After treatment with DCMU or DBMIB, stromule frequency increased by more than 50%, to 15.5 ± 2.6% with DCMU and 16.8 ± 2.9% with DBMIB ($n \geq 20$, $p < 0.05$). This finding suggests that stromule formation responds to light-sensitive redox signals inside the chloroplast, to our knowledge the first demonstration that internal chloroplast pathways may regulate stromules.

Unlike *N. benthamiana*, the epidermis of *A. thaliana* has two distinct types of plastids: chloroplasts in the guard cells and leucoplasts in the pavement cells (**Fig. S3**). Leucoplasts are not photosynthetic, but like chloroplasts, they have many other roles in metabolism and storage. As in *N. benthamiana* epidermal chloroplasts, DCMU and DBMIB promote stromule formation in guard cell chloroplasts of *A. thaliana* cotyledons, raising stromule frequency from 15.7 ± 3.8% to 28.1 ± 4.0% for DCMU ($n \geq 16$, $p < 0.05$) and to 48.1 ± 6.3% for DBMIB ($n \geq 10$, $P < 0.0005$) (**Fig. 2D**). This demonstrates that

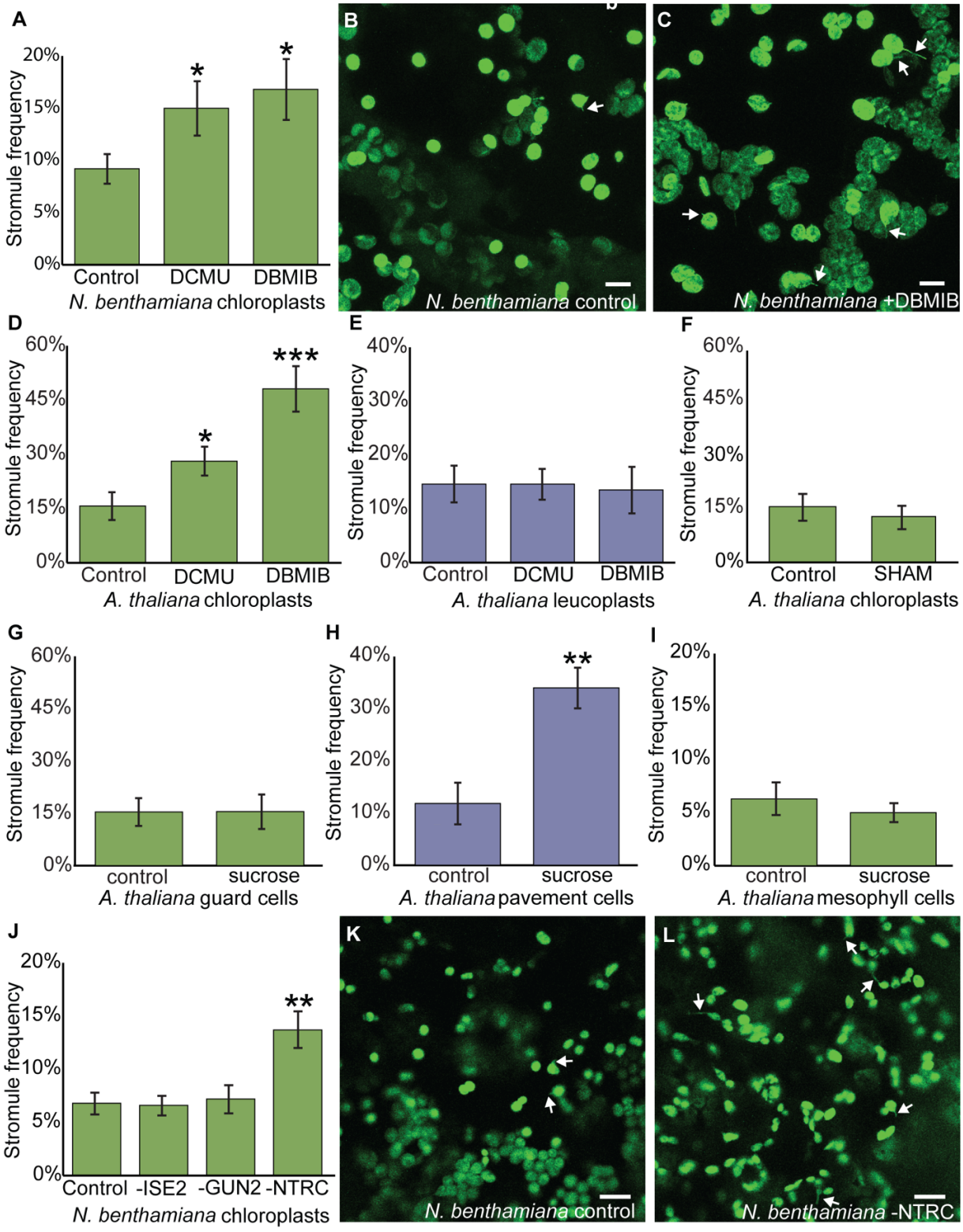
A
Stromule frequency
20%
15%
10%
5%
0%
*
*
Control
DCMU
DBMIB
N. benthamiana chloroplasts
B
N. benthamiana control
C
N. benthamiana +DBMIB
D
Stromule frequency
60%
45%
30%
15%
0%
*
***
Control
DCMU
DBMIB
A. thaliana chloroplasts
E
Stromule frequency
40%
30%
20%
10%
0%
Control
DCMU
DBMIB
A. thaliana leucoplasts
F
Stromule frequency
60%
45%
30%
15%
0%
Control
SHAM
A. thaliana chloroplasts
G
Stromule frequency
60%
45%
30%
15%
0%
control
sucrose
A. thaliana guard cells
H
Stromule frequency
40%
30%
20%
10%
0%
**
control
sucrose
A. thaliana pavement cells
I
Stromule frequency
20%
15%
10%
5%
0%
control
sucrose
A. thaliana mesophyll cells
J
Stromule frequency
20%
15%
10%
5%
0%
**
Control
-ISE2
-GUN2
-NTRC
N. benthamiana chloroplasts
K
N. benthamiana control
L
N. benthamiana -NTRC

(continued from previous page)

**Fig. 2. ROS in the chloroplast induce stromules.** (**A**) DCMU and DBMIB treatments both increase stromule frequency in chloroplasts of *N. benthamiana* seedlings ($n \geq 20$, $p < 0.05$). (**B and C**) Representative images of *N. benthamiana* chloroplasts treated with control (**B**) or with DBMIB (**C**). (**D**) *A. thaliana* epidermal chloroplast stromule frequency increases after DCMU or DBMIB treatment (DCMU, $n \geq 16$, $p < 0.05$; DBMIB, $n \geq 10$, $p < 0.0005$). (**E**) Stromule frequency in *A. thaliana* epidermal leucoplasts is unaffected by DCMU or DBMIB treatment (DCMU, $n \geq 16$, $p = 0.98$; DBMIB, $n \geq 10$, $p = 0.84$). (**F**) *A. thaliana* epidermal chloroplast stromule frequency is unaffected by SHAM ($n \geq 13$, $p = 0.57$). (**G**) *A. thaliana* epidermal chloroplast frequency is similar in chloroplasts with or without sucrose treatment ($n \geq 8$, $p = 0.96$). (**H**) *A. thaliana* epidermal leucoplast stromule frequency increases after sucrose treatment ($n \geq 8$, $p < 0.01$). (**I**) Stromule frequency is not affected by sucrose treatment in *A. thaliana* mesophyll chloroplasts ($n \geq 8$, $p = 0.52$). (**J**) Silencing *NbNTRC* increases stromule frequency in *N. benthamiana* leaves ($n = 8$, $p < 0.01$), but silencing *NbISE2* or *NbGUN2* does not affect stromule frequency ($n = 8$, $p > 0.82$). (**K and L**) Representative images of *N. benthamiana* chloroplasts in control (**K**) or after silencing *NbNTRC* (**L**). Chloroplasts and stromules in are labeled with GFP. Some stromules are indicated by white arrows. Error bars indicate ± SE. *$p < 0.05$; **$p < 0.01$; ***$p < 0.0005$. (Scale bars: 10 μm.)

the induction of chloroplast stromules by DCMU and DBMIB is conserved in evolutionarily divergent plants, since *N. benthamiana* is an asterid and *A. thaliana* is a rosid, with the last common ancestor of the two species living more than 100 million years ago (**Bell et al., 2010**). In contrast, leucoplasts in the epidermis of *A. thaliana* were unaffected by DCMU and DBMIB treatment [14.6 ± 3.4% in control conditions vs. 14.6 ± 2.8% with DCMU ($n \geq 16$, $p = 0.98$) and 13.5 ± 4.3% with DBMIB ($n \geq 10$, $p = 0.84$)], showing that the effects of DCMU and DBMIB are specific responses to their roles interfering with the pETC (**Fig. 2E**).

To further test whether stromules form in response to the chloroplast redox status specifically, as opposed to any oxidative stress in the cell, we also treated *A. thaliana* cotyledons with salicylhydroxamic acid (SHAM). SHAM inhibits the mitochondrial alternative oxidase, which leads to rapid and strong oxidation of mitochondrial redox buffers (**Stonebloom et al., 2012**). SHAM did not impact chloroplast stromule formation in *A. thaliana* (15.7 ± 3.8% in control vs. 12.8 ± 3.3% with SHAM; $n \geq 13$, $p = 0.57$), supporting the hypothesis that chloroplast stromule frequency is specifically regulated by the redox status of the chloroplast (**Fig. 2F and Fig. S4**).

In summary, low concentrations of DCMU or DBMIB are sufficient to induce significant increases in stromule frequency within only 2 h. This is apparently not a secondary effect of broad disruption of cellular metabolism or redox homeostasis, because leucoplasts, which are not photosynthetic, are unaffected by the treatments, and disrupting mitochondrial function and generating reactive oxygen species (ROS) in mitochondria by SHAM treatment does not affect chloroplast stromule frequency. Thus, light-sensitive redox cues inside chloroplasts specifically affect stromule frequency.

**NADPH-Dependent Thioredoxin Reductase c regulates chloroplast stromule frequency**

Signaling from chloroplasts to other organelles within the plant cell is critical for plant survival and development (**Chi et al., 2013; Woodson et al., 2008**). Chloroplast-to-nucleus signaling is transduced through several pathways, some of which are light-sensitive. We used VIGS in *N. benthamiana* as a reverse genetic approach (**Brunkard et al., 2015**) to determine whether disrupting the light-sensitive chloroplast-to-nucleus signal transduction pathways impacts stromule formation. VIGS strongly reduces gene expression in young leaves within 1–2 wk of infection by generating small RNAs that specifically target a gene for posttranscriptional silencing (**Brunkard et al., 2015**).

Chloroplasts contain their own genomes encoding approximately 80 proteins (mostly related to photosynthesis or transcription and translation), and light exerts control over plastid genome expression (PGE) at transcriptional and posttranscriptional levels (**Barkan, 2011**). Thus, we first focused on *NbISE2*, an essential plastid RNA helicase required for healthy chloroplast biogenesis and PGE (**Burch-Smith et al., 2011**). Without ISE2, hundreds of nuclear genes involved in photosynthesis are strongly down-regulated (**Burch-Smith et al., 2011**). Silencing *NbISE2* gene expression had no impact

on stromule frequency, however (6.8 ± 1.0% in controls vs. 6.6 ± 0.9% after silencing *NbISE2*; n = 8, p = 0.85) (**Fig. 2J and Fig. S5**), in agreement with previous reports that antibiotics directly interfering with PGE, such as lincomycin, have no effect on stromule frequency (**Gray et al., 2012**).

PGE coordinates the expression of photosynthesis-associated nuclear genes through a signal transduction pathway mediated by tetrapyrrole metabolism (**Chi et al., 2013; Terry and Smith, 2013; Woodson and Chory, 2008**). Genetic disruptions to tetrapyrrole metabolism, specifically defects in the branch point between heme and chlorophyll biosynthesis, interfere with chloroplast biogenesis and photosynthesis (**Terry and Smith, 2013**). We next tested whether loss of NbGUN2, a chloroplast heme oxygenase that participates in chloroplast-to-nucleus communication, impacts stromule formation. As with *NbISE2*, silencing *NbGUN2* gene expression had no impact on chloroplast stromule frequency (7.2 ± 1.3% after silencing *NbGUN2*; n = 8, p = 0.82) despite causing clear physiological stress and chlorosis (**Fig. 2J and Figs. S5, S6, and S7**).

We then silenced the expression of the chloroplast NADPH-Dependent Thioredoxin Reductase (*NbNTRC*) (**Figs. S8 and S9**), which regulates the redox status and activity of myriad chloroplast proteins and is a critical hub in chloroplast redox signal transduction (**Michalska et al., 2009**). Silencing *NbNTRC* more than doubled the stromule frequency (13.7 ± 1.7%; n = 8, p < 0.01), providing genetic evidence that redox signaling within the chloroplast regulates stromule formation (**Fig. 2 J-L and Figs. S5, S8, and S9**). Moreover, to our knowledge, *NbNTRC* is now the first gene identified that regulates stromule frequency without other apparent effects on chloroplast shape.

**Sucrose promotes stromule formation in epidermal leucoplasts, but not in chloroplasts**

**Schattat et al.** (**2012b**) reported that stromule frequency increases during the day in the epidermal leucoplasts of *A. thaliana*. Because leucoplasts do not contain pigments and do not respond to DCMU or DBMIB, we sought another hypothesis to explain why leucoplast stromule frequency is light-responsive. Physiologically, one of the major impacts of light on epidermal pavement cells is an increase in sucrose imported from underlying cells that contain photosynthesizing chloroplasts. Previous reports have indicated that stromule frequency is sensitive to sugar levels, but with inconsistent conclusions (**Schattat and Klösgen, 2011**). We found that epidermal leucoplast stromule frequency rises remarkably following sucrose treatments in *A. thaliana* (33.9 ± 3.8% with sucrose vs. 11.8 ± 3.9% without sucrose; n ≥ 8, p < 0.01) (**Fig. 2H and Fig. S10**). In contrast, chloroplast stromule frequency did not respond to sucrose treatments in either the epidermal guard cells or mesophyll of *A. thaliana* [in the epidermis, 15.4 ± 3.9% with sucrose vs. 15.7 ± 3.8% without (n ≥ 8, p = 0.96); in the mesophyll, 5.0 ± 0.9% with sucrose vs. 6.3 ± 1.7% without (n ≥ 8, p = 0.52)] (**Fig. 2 G and I and Fig. S10**). These results imply that different plastid types use separate signaling pathways to induce stromule formation.

## Isolated chloroplasts can form stromules

With the finding that signals originating within the chloroplast can trigger stromule formation, we then explored whether stromule formation is dependent on cytosolic structures (e.g., the cytoskeleton), as has been suggested previously (**Hanson and Sattarzadeh, 2011; Natesan et al., 2009**), or if chloroplasts can make stromules on their own. Previous studies have argued that stromule formation is guided and supported by the cytoskeleton and endoplasmic reticulum, but whether stromule formation requires these external factors is unknown (**Hanson and Sattarzadeh, 2011**, **Schattat et al., 2011**). To address this question, we extracted chloroplasts from leaves of *N. benthamiana*, *A. thaliana*, and *Spinacia oleracea* using well-established methods for isolating functional, undamaged chloroplasts (**Joly and Carpentier, 2011**). We visualized chloroplast stroma either with GFP by extracting chloroplasts from leaves expressing plastid-targeted GFP or with a supravital stain, carboxyfluorescein diacetate (CFDA), which fluoresces only after hydrolysis by carboxylesterases in the chloroplast stroma (**Schulz et al., 2004**). We readily found isolated chloroplasts with intact stromules in all three species and regardless of staining technique (**Fig. 3 and Fig. S11**). The stromules were dynamic and could grow very long, sometimes extending more than 150 µm from chloroplasts only 4–6 µm in diameter (**Fig. S11**). As in plant cells, many stromules were bent and curved along their length, whereas some were very long and straight (**Fig. 3 and Fig. S11**). Using time-lapse microscopy, we repeatedly observed isolated chloroplasts form apparently new stromules, validating that chloroplasts can generate stromules independently. Stromules are absent in the first frames of chloroplasts shown in **Fig. 3D and E**, but they appear and lengthen over the course of 8 min (**Movies S1 and S2**).

## Superresolution microscopy illuminates stromule ultrastructure

Because stromules can form in isolation after extraction of chloroplasts from their cellular context, we decided to further investigate stromules using superresolution microscopy to gain new insight into their ultrastructure, which will inform future efforts at identifying the chloroplast-associated structural components responsible for stromule formation. The diameter of stromules is postulated to be <200 nm, but this is below the diffraction limit of conventional light microscopy (**Hanson and Sattarzadeh, 2011; Shaw and Ehrhardt, 2013**), even under optimal conditions. Visualizing stromules by transmission electron microscopy is challenging, because stromule membranes are not easily distinguished from other membranes in thin sections required for conventional electron microscopy. We used 3D structured illumination microscopy (3D-SIM) to obtain the highest-resolution images of wild-type stromules to date (**Hanson and Sattarzadeh, 2011; Shaw and Ehrhardt, 2013**), and present some representative examples in **Figure 4** and **Movie S3**. The improved resolution of 3D-SIM is illustrated by the well-defined thylakoid grana in 3D-SIM images (**Fig. 4 B-E**) compared with thylakoids visualized by more conventional confocal scanning laser microscopy (**Fig. 4A**).

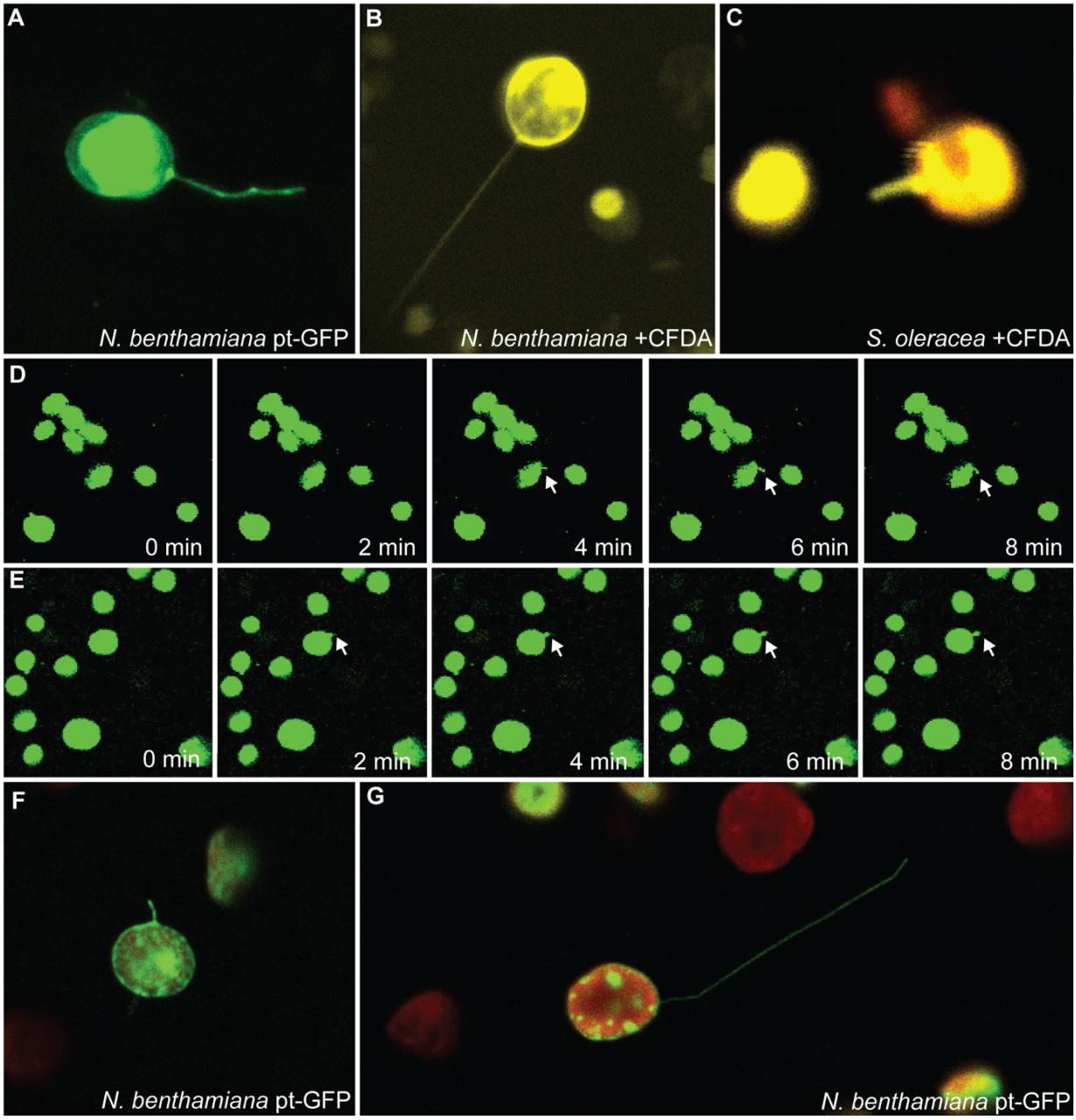


**Fig. 3. Isolated chloroplasts form stromules.** *N. benthamiana* chloroplasts labeled with stromal GFP (**A**, green) or CFDA staining (**B**, yellow) show stromules after isolation from their cellular environment. (**C**) Chloroplasts isolated from *S. oleracea* and stained with CFDA (yellow; chlorophyll autofluorescence, red) also have stromules. (**D and E**) Isolated *N. benthamiana* chloroplasts labeled with stromal GFP form new stromules over time. Newly forming stromules are indicated by white arrows. (**F and G**) *N. benthamiana* chloroplasts isolated with a Percoll purification step and labeled with stromal GFP (green; chlorophyll autofluorescence, red) also have stromules.

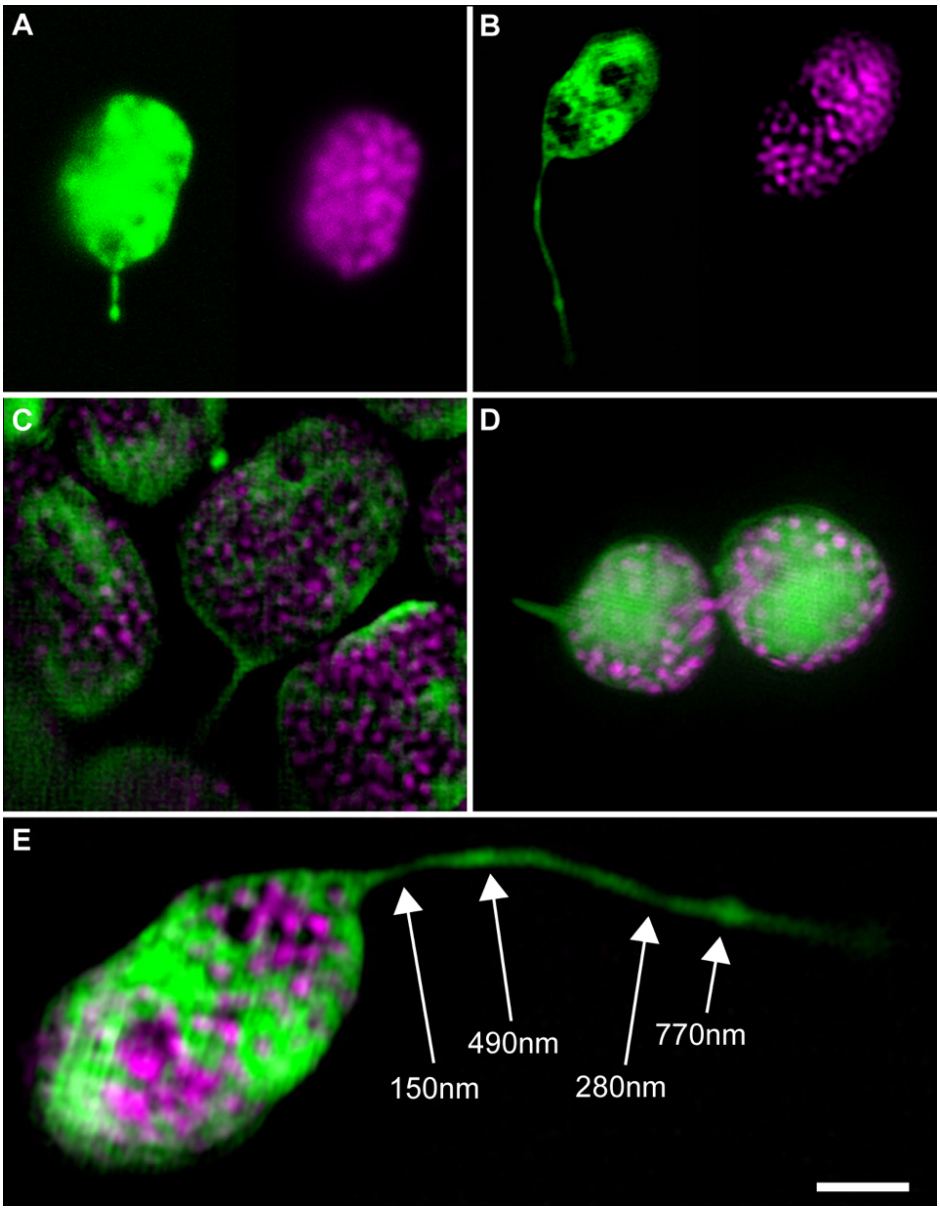


**Fig. 4. Examples of fluorescent stromules in *N. benthamiana* chloroplasts visualized by 3D structured illumination microscopy (3D-SIM).** (**A and B**) Comparison of confocal laser scanning microscopy (**A**; also shown in **Fig. S11**) and 3D-SIM (**B**; also shown in **E** and in **Movie S3**) to visualize chloroplast structure (Left: stromal GFP, green; Right: thylakoid chlorophyll, magenta). In particular, note the improved resolution of stromule width and the clarity of the thylakoid grana in the 3D-SIM z-slice (**B**). (**C**) 3D-SIM z-slice image of mesophyll chloroplasts with stromules. (**D**) An epidermal chloroplast connected by a thin bridge that contains both stroma and thylakoids also has a stromule (Left), as shown by SIM. (**E**) 3D-SIM reveals variability in stromule width. Stromal GFP, green; chlorophyll autofluorescence, magenta. (Scale bar: 2 μm.) One z-slice from a 3D-SIM reconstruction is shown, with measured stromule diameters labeled at indicated positions (white arrows).

At their smallest, we observed stromules <150 nm in diameter (**Fig. 4E**); given that this is approximately the resolution of 3D-SIM, stromules could be even narrower. 3D-SIM also revealed striking variability in stromule diameter along the length of an individual stromule. Stromules often were narrowest near the chloroplast body, and then typically varied between approximately 200 and 600 nm wide at different positions along their lengths, as shown in **Figure 4E**. The variability in stromule width was apparent whether we observed chloroplasts in planta or after isolation, suggesting that structural factors inside the chloroplast could be responsible for the heterogeneous diameter of stromules.

## CONCLUSIONS

Chloroplasts are extraordinarily independent organelles with their own genomes, as many as 3,000 different proteins, and an array of biochemical activities ranging from photosynthesis and carbon fixation to the synthesis of amino acids, fatty acids, hormones, and pigments. Here we have shown that chloroplasts are even more independent, generating stromules in response to changes in the internal chloroplast redox status in a pathway regulated by the chloroplast NADPH-dependent thioredoxin reductase, NTRC. Leucoplasts, nonphotosynthetic plastids, do not make stromules in response to the same redox cues as chloroplasts, but instead are responsive to sucrose concentration, demonstrating that different types of plastids form stromules in response to different signals. We propose a model consistent with these findings that light promotes stromule formation in leaves by increasing ROS in chloroplasts (**Lai et al., 2012**) and by increasing sucrose levels in cells with leucoplasts (**Fig. 5**).

Previous reports have investigated stromules using a variety of plastid types in a broad range of species and tissues, generally assuming that stromules act similarly in all cells (**Erickson et al., 2014; Gray et al., 2012; Hanson and Sattarzadeh, 2011; Holzinger et al., 2007; Holzinger et al., 2008; Köhler et al., 1997; Natesan et al., 2005; Natesan et al., 2009; Schattat et al., 2011; Schattat et al., 2012b; Wildman et al., 1962**). In light of the clear differences in signals that influence leucoplast and chloroplast stromule formation (**Figs. 2 and 5**), future work will need to carefully consider the biological context of stromule activity. With the discovery that stromules extend from chloroplasts independently of external structures, analogies to cytonemes could help reveal the roles of stromules, because cytonemes are comparable thin, tubular projections that extend from animal cells to facilitate intercellular communication during development (**Bischoff et al., 2013; Roy et al., 2014**). Although the function of stromules remains unknown, it may be speculated that they similarly facilitate signal transduction between organelles, given that stromules have been observed associating with the nucleus, plasma membrane, endoplasmic reticulum, and other plastids (**Hanson and Sattarzadeh, 2011; Schattat et al., 2011; Schattat et al., 2012a**).

Numerous studies in just the past few years have demonstrated the vital importance of chloroplast-to-nucleus signaling in plant growth and responses to stress (**Avendaño-Vázquez et al., 2014; Burch-Smith et al., 2011; Chi et al., 2013; Estavillo et al.,**

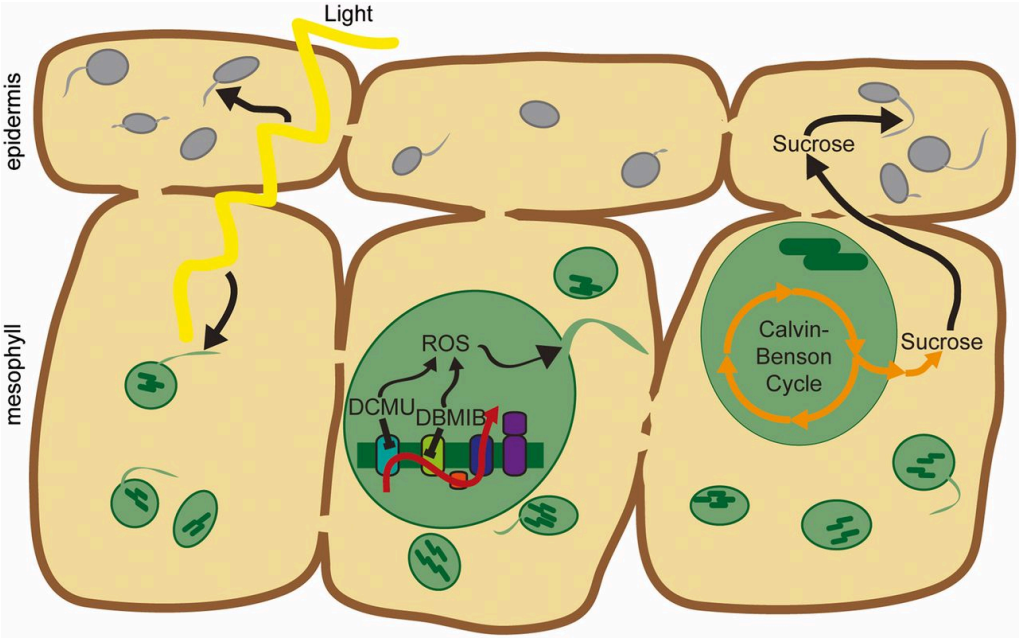


**Fig. 5. Stromules are initiated by signals within the chloroplast.** (Left) Stromule frequency increases in the light (daytime) in both chloroplasts and leucoplasts. (Center) ROS generated from the pETC trigger stromule formation in chloroplasts. (Right) Sucrose promotes stromule formation in leucoplasts, but not chloroplasts. Sucrose is synthesized in the cytosol from products of the Calvin–Benson cycle in chloroplasts and then moves into neighboring heterotrophic pavement cells via plasmodesmata. For simplicity of presentation, only photosynthetic mesophyll cells are shown (and not photosynthetic guard cells), because there is no evidence suggesting that stromules in these cell types behave differently.

**2011; Koussevitzky et al., 2007; Nomura et al., 2012; Petrillo et al., 2014; Stonebloom et al., 2012; Terry and Smith, 2013; Woodson and Chory, 2008; Xiao et al., 2012**), with critical agricultural implications, but the structural pathways underlying this signal transduction remain largely uncharacterized. Stromules may contribute to these pathways, because they dynamically respond to physiological signals inside the chloroplast. Continued study of stromules may illuminate how chloroplasts physically interact with their environment to coordinate cellular function.

## MATERIALS AND METHODS

### Plant and chemical materials

For most *N. benthamiana* studies, we used a stable transgenic stromal fluorescent marker line, 35SPRO:FNRtp:EGFP, designated pt-GFP herein (**Schattat et al., 2011**). We also used the *N. benthamiana* wild-type accession Nb-1 for isolation of wild-type chloroplasts. For *A. thaliana* studies, we used a stable transgenic stromal fluorescent marker line (**Stonebloom et al., 2012**), 35SPRO:RbcStp:roGFP2, designated pt-roGFP2 herein. pt-roGFP2 was also used for measuring stromal redox status.

We obtained DCMU (also known as Diuron; product no. D2425), DBMIB (product no. 271993), and SHAM (product no. S607) from Sigma-Aldrich. Concentrated stock solutions were prepared in DMSO.

### Microscopy

All standard stromule visualization experiments were performed using a Zeiss LSM 710 confocal microscope equipped with an acousto-optical tunable filter to tightly control laser power. GFP was excited with a 488-nm laser with <0.25 mW original power, and emissions from 500 to 530 nm were detected. The 3D-SIM was performed using a Zeiss Elyra PS.1 microscope equipped with standard GFP and Cy5 filter sets.

### Diurnal time course experiment

*N. benthamiana* stably expressing pt-GFP was grown for 5 d under 100 µmol of photons m−2s−1 (measured with a LI-COR 250A light meter with a LI-190R quantum sensor that detects photosynthetically active radiation, 400–700 nm) with 12-h day length. Epidermal chloroplasts of cotyledons of intact plants were observed every 4 h over the course of 48 h. A green light-emitting diode was used during night time points to prevent exposure to photosynthetically active radiation.

### pETC inhibitor treatments

*A. thaliana* pt-roGFP2 plants were stratified for 3 d at 4 °C and then grown for 14 d under 100 µmol of photons m−2s−1 of light with 16 h day length. The redox status of pt-roGFP2 in *A. thaliana* cotyledons was measured after treatment with 10 µM DCMU, 12

μM DBMIB, or 0.1% DMSO (control treatment), following the protocol described by **Stonebloom et al.** (**2012**) but using a Zeiss LSM 710 confocal microscope with 405-nm and 488-nm lasers, collecting emissions ranging from 500 to 530 nm.

*N. benthamiana* stably expressing pt-GFP was grown for 14 d under 100 μmol of photons m−2s−1 of light with a 16-h day length. Cotyledons were painted with DCMU (10 μM from 10 mM stock solution in DMSO), DBMIB (12 μM from 12 mM stock solution in DMSO), or control 2 h before observation of epidermal chloroplasts.

To measure stromule frequency in *A. thaliana* (grown as above to measure redox status), pt-roGFP2 cotyledons were removed and placed on 0.5X Murashige and Skoog plates (0.8% agar, pH 5.6) with DCMU (10 μM from 10 mM stock solution in DMSO), DBMIB (12 μM from 12 mM stock solution in DMSO), SHAM (200 μM in DMSO), sucrose (30 mM, or 1% wt/vol), or control for 2 h before imaging of cotyledon epidermal leucoplasts (of pavement cells) and chloroplasts (of guard cells).

**Virus Induced Gene Silencing**

pt-GFP plants were grown for 3 wk under 100 μmol of photons m−2s−1 of light with a 16-h day length before agroinfiltration with the appropriate VIGS vectors. Details of Virus Induced Gene Silencing (VIGS) vector construction are provided in SI Methods. Two weeks later, young leaves with silenced gene expression were cut, and the epidermal chloroplasts of the basal region of the leaf were visualized immediately.

**Chloroplast extraction**

Intact chloroplasts were extracted from mature leaves of pt-GFP (N. benthamiana), Nb-1 (wild-type N. benthamiana), pt-roGFP2 (*A. thaliana*), and spinach by grinding leaves in extraction buffer (50 mM Hepes NaOH, 330 mM sorbitol, 2 mM EDTA, 1 mM MgCl2, 1 mM MnCl2, pH 6.9), filtering the homogenate through several layers of cheesecloth, and then pelleting by centrifugation and resuspending in isolation buffer (50 mM Hepes NaOH, 330 mM sorbitol, 2 mM EDTA, 1 mM MgCl2, 1 mM MnCl2, 10 mM KCl, 1 mM NaCl, pH 7.6) as described previously (**Joly and Carpentier, 2011**). More complex protocols, such as inclusion of a Percoll gradient for purification (35% vol/vol), had no discernable effect on chloroplast stromule formation. Isolated spinach or wild-type *N. benthamiana* chloroplasts were incubated with an equal volume of 25 mg/L 5 (6)-carboxyfluorescein diacetate (Sigma-Aldrich, product no. 21879) for 5 min (**Schulz et al., 2004**), centrifuged at 700 × g for another 60 s, and resuspended in isolation buffer. Chloroplasts were visualized by confocal or structured illumination microscopy immediately after isolation.

**Data analysis**

Stromule frequencies were counted using ImageJ software (imagej.nih.gov/ij/) to scan through z-stacks of confocal images using a focal depth of 1 Airy unit, which allowed us

to visualize stromules extended in any axis from the plastid. Stromules were counted regardless of length but only if <1 μm in diameter, as described by **Hanson and Sattarzadeh** (**2011**). Most previous studies reported stromule frequencies per cell, considering multiple cells from a single leaf as independent samples. **Schattat and Klösgen** (**2011**), for example, found little variation in stromule frequencies within an individual leaf, but dramatic variation in stromule frequencies between different leaves. This led them to treat separate fields of view within a single leaf as distinct samples, reducing the apparent variation and effectively increasing statistical power. We also found that stromule frequency varied very little among cells within a leaf, but varied notably among leaves of the same age and condition from different plants. Therefore, we considered one leaf per plant as an individual sample (n), and observed many plants for each experiment. Throughout an experiment, all of the analyzed leaves experienced the same growth conditions and were observed at the same age and size.

We conducted power analysis ($\alpha = 0.05$; $\beta = 0.20$) on pilot studies under our growth conditions to determine the sufficient sample size to confidently assert whether or not a treatment caused changes in stromule frequency, and found an approximate minimal n ≥16 for *N. benthamiana* time course and chemical treatment experiments, and n ≥ 8 for all other experiments. Per treatment, we counted more than 5,000 plastids, at least 100 cells, and ~20 plants for each chemical treatment or 8 plants for each silencing experiment. Mean stromule frequencies were compared with the Student t test, with significance indicated at $p < 0.05$.

We also analyzed all data using angular transformations to account for differences in variation in datasets with very high or low stromule frequencies, but the transformation had no impact on the statistical significance of our results, so we present the data as raw frequencies for the purpose of clear presentation. SEs are presented throughout to describe stromule frequencies. R (www.r-project.org) was used for all statistical analyses.

## ACKNOWLEDGEMENTS

We thank J. Mathur for the generous gift of pt-GFP N. benthamiana seeds, M.A. Ahern for corroborating stromule counts, and S.E. Ruzin and D. Schichnes of the University of California Berkeley College of Natural Resources Biological Imaging Facility for microscopy support. Research reported in this publication was supported in part by the National Institutes of Health S10 program under award numbers 1S10RR026866-01 and 1S10OD018136-01. The content is solely the responsibility of the authors and does not necessarily represent the official views of the National Institutes of Health. J.O.B. and A.M.R. were supported by predoctoral fellowships from the National Science Foundation.

## REFERENCES

**Avendaño-Vázquez AO, Cordoba E, Llamas E, San Román C, Nisar N, De la Torre S, Ramos-Vega M, Gutiérrez-Nava MD, Cazzonelli CI, Pogson BJ, et al.** (2014) An uncharacterised apocarotenoid-derived signal generated in ζ-carotene desaturase mutants controls leaf development and the expression of chloroplast and nuclear genes in *Arabidopsis*. *Plant Cell* **26**, 2524-2537.

**Barkan A** (2011) Expression of plastid genes: Organelle-specific elaborations on a prokaryotic scaffold. *Plant Physiol* **155**, 1520-1532.

**Bell CD, Soltis DE, and Soltis PS** (2010) The age and diversification of the angiosperms re-revisited. *Am J Bot* **97**, 1296-1303.

**Bischoff M, Gradilla AC, Seijo I, Andrés G, Rodríguez-Navas C, González-Méndez L, and Guerrero I** (2013) Cytonemes are required for the establishment of a normal Hedgehog morphogen gradient in *Drosophila* epithelia. *Nat Cell Biol* **15**, 1269-1281.

**Brunkard JO, Burch-Smith TM, Runkel AM, and Zambryski PC** (2015b) Investigating plasmodesmata genetics with virus-induced gene silencing and an *Agrobacterium*-mediated GFP movement assay. *Methods Mol Biol* **1217**, 185-198.

**Burch-Smith TM, Brunkard JO, Choi YG, and Zambryski PC** (2011) Organelle-nucleus cross-talk regulates plant intercellular communication via plasmodesmata. *Proc Natl Acad Sci USA* **108**, E1451-E1460.

**Chi W, Sun X, and Zhang L** (2013) Intracellular signaling from plastid to nucleus. *Annu Rev Plant Biol* **64**, 559-582.

**Erickson JL, Ziegler J, Guevara D, Abel S, Klösgen RB, Mathur J, Rothstein SJ, and Schattat MH** (2014) Agrobacterium-derived cytokinin influences plastid morphology and starch accumulation in *Nicotiana benthamiana* during transient assays. *BMC Plant Biol* **14**, 127.

**Estavillo GM, Crisp PA, Pornsiriwong W, Wirtz M, Collinge D, Carrie C, Giraud E, Whelan J, David P, Javot H, et al.** (2011) Evidence for a SAL1-PAP chloroplast retrograde pathway that functions in drought and high light signaling in *Arabidopsis*. *Plant Cell* **23**, 3992-4012.

**Gisk B, Yasui Y, Kohchi T, and Frankenberg-Dinkel N** (2010) Characterization of the haem oxygenase protein family in *Arabidopsis thaliana* reveals a diversity of functions. *Biochem J* **425**, 425-434.

**Gray JC, Hansen MR, Shaw DJ, Graham K, Dale R, Smallman P, Natesan SK, and Newell CA** (2012) Plastid stromules are induced by stress treatments acting through abscisic acid. *Plant J* **69**, 387-398.

**Hanson MR, and Sattarzadeh A** (2011) Stromules: Recent insights into a long neglected feature of plastid morphology and function. *Plant Physiol* **155**, 1486-1492.

**Holzinger A, Buchner O, Lütz C, and Hanson MR** (2007) Temperature-sensitive formation of chloroplast protrusions and stromules in mesophyll cells of *Arabidopsis thaliana*. *Protoplasma* **230**, 23-30.

**Holzinger A, Kwok EY, and Hanson MR** (2008) Effects of *arc3*, *arc5* and *arc6* mutations on plastid morphology and stromule formation in green and nongreen tissues of *Arabidopsis thaliana*. *Photochem Photobiol* **84**, 1324-1335.

**Hughes J** (2013) Phytochrome cytoplasmic signaling. *Annu Rev Plant Biol* **64**, 377-402.

**Joly D, and Carpentier R** (2011) Rapid isolation of intact chloroplasts from spinach leaves. *Photosynthesis Research Protocols*, ed Carpentier R (Humana, New York), pp 321-325.

**Köhler RH, Cao J, Zipfel WR, Webb WW, and Hanson MR** (1997) Exchange of protein molecules through connections between higher plant plastids. *Science* **276**, 2039-2042.

**Koussevitzky S, Nott A, Mockler TC, Hong F, Sachetto-Martins G, Surpin M, Lim J, Mittler R, and Chory J** (2007) Signals from chloroplasts converge to regulate nuclear gene expression. *Science* **316**, 715-719.

**Lai AG, Doherty CJ, Mueller-Roeber B, Kay SA, Schippers JH, and Dijkwel PP** (2012) CIRCADIAN CLOCK-ASSOCIATED 1 regulates ROS homeostasis and oxidative stress responses. *Proc Natl Acad Sci USA* **109**, 17129-17134.

**Michalska J, Zauber H, Buchanan BB, Cejudo FJ, and Geigenberger P** (2009) NTRC links built-in thioredoxin to light and sucrose in regulating starch synthesis in chloroplasts and amyloplasts. *Proc Natl Acad Sci USA* **106**, 9908-9913.

**Natesan SK, Sullivan JA, and Gray JC** (2005) Stromules: A characteristic cell-specific feature of plastid morphology. *J Exp Bot* **56**, 787-797.

**Natesan SK, Sullivan JA, and Gray JC** (2009) Myosin XI is required for actin-associated movement of plastid stromules. *Mol Plant* **2**, 1262-1272.

**Nomura H, Komori T, Uemura S, Kanda Y, Shimotani K, Nakai K, Furuichi T, Takebayashi K, Sugimoto T, Sano S, et al.** (2012) Chloroplast-mediated activation of plant immune signalling in *Arabidopsis*. *Nat Commun* **3**, 926.

**Petrillo E, Godoy Herz MA, Fuchs A, Reifer D, Fuller J, Yanovsky MJ, Simpson C, Brown JW, Barta A, Kalyna M, et al.** (2014) A chloroplast retrograde signal regulates nuclear alternative splicing. *Science* **344**, 427-430.

**Reichheld JP, Khafif M, Riondet C, Droux M, Bonnard G, and Meyer Y** (2007) Inactivation of thioredoxin reductases reveals a complex interplay between thioredoxin and glutathione pathways in *Arabidopsis* development. *Plant Cell* **19**, 1851-1865.

**Roy S, Huang H, Liu S, and Kornberg TB** (2014) Cytoneme-mediated contact-dependent transport of the Drosophila decapentaplegic signaling protein. *Science* **343**, 1244624.

**Schattat MH, and Klösgen RB** (2011) Induction of stromule formation by extracellular sucrose and glucose in epidermal leaf tissue of *Arabidopsis thaliana*. *BMC Plant Biol* **11**, 115.

**Schattat M, Barton K, Baudisch B, Klösgen RB, and Mathur J** (2011) Plastid stromule branching coincides with contiguous endoplasmic reticulum dynamics. *Plant Physiol* **155**, 1667-1677.

**Schattat MH, Griffiths S, Mathur N, Barton K, Wozny MR, Dunn N, Greenwood JS, and Mathur J** (2012a) Differential coloring reveals that plastids do not form networks for exchanging macromolecules. *Plant Cell* **24**, 1465-1477.

**Schattat MH, Klösgen RB, and Mathur J** (2012b) New insights on stromules: Stroma filled tubules extended by independent plastids. *Plant Signal Behav* **7**, 1132-1137.

**Schulz A, Knoetzel J, Scheller HV, and Mant A** (2004) Uptake of a fluorescent dye as a swift and simple indicator of organelle intactness: Import-competent chloroplasts from soil-grown *Arabidopsis*. *J Histochem Cytochem* **52**, 701-704.

**Shaw SL, and Ehrhardt DW** (2013) Smaller, faster, brighter: Advances in optical imaging of living plant cells. *Annu Rev Plant Biol* **64**, 351-375.

**Stonebloom S, Brunkard JO, Cheung AC, Jiang K, Feldman L, and Zambryski P** (2012) Redox states of plastids and mitochondria differentially regulate intercellular transport via plasmodesmata. *Plant Physiol* **158**, 190-199.

**Terry MJ, and Smith AG** (2013) A model for tetrapyrrole synthesis as the primary mechanism for plastid-to-nucleus signaling during chloroplast biogenesis. *Front Plant Sci* **4**, 14.

**Veley KM, Marshburn S, Clure CE, and Haswell ES** (2012) Mechanosensitive channels protect plastids from hypoosmotic stress during normal plant growth. *Curr Biol* **22**, 408-413.

**Wildman SG, Hongladarom T, and Honda SI** (1962) Chloroplasts and mitochondria in living plant cells: Cinephotomicrographic studies. *Science* **138**, 434-436.

**Woodson JD, and Chory J** (2008) Coordination of gene expression between organellar and nuclear genomes. *Nat Rev Genet* **9**, 383-395.

**Xiao Y, Savchenko T, Baidoo EE, Chehab WE, Hayden DM, Tolstikov V, Corwin JA, Kliebenstein DJ, Keasling JD, and Dehesh K** (2012) Retrograde signaling by the plastidial metabolite MEcPP regulates expression of nuclear stress-response genes. *Cell* **149**, 1525-1535.

**SUPPLEMENTARY MATERIALS**
**Supplementary Figures**

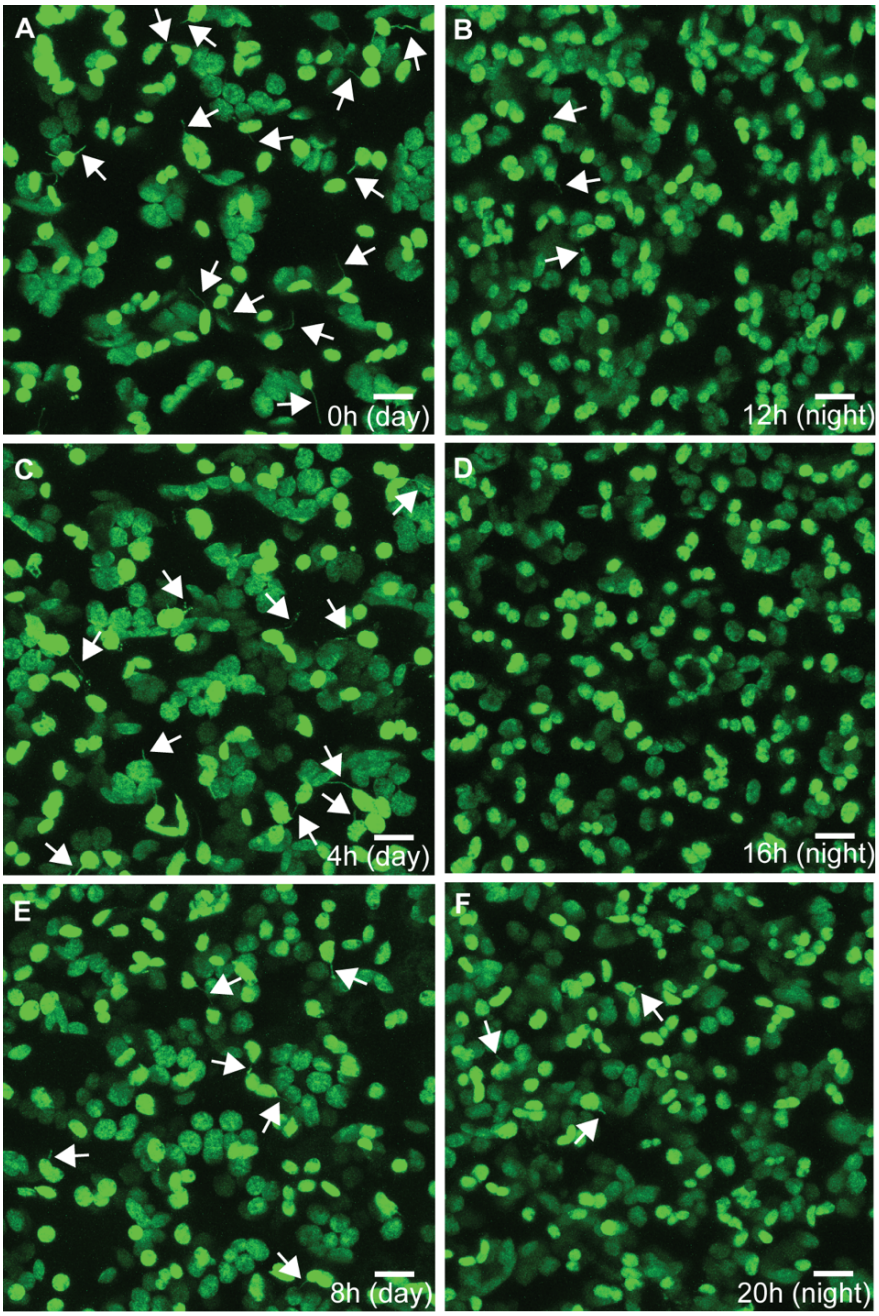


**Fig. S1**. **Representative images of stromule frequency over the course of 48 h during a 12-h light/12-h dark cycle.** *N. benthamiana* chloroplast stromule frequency is high throughout the day (**A**, dawn; **C**, 4 h after dawn; **E**, 8 h after dawn) and low throughout the night (**B**, dusk; **D**, 4 h after dusk; **F**, 8 h after dusk). Chloroplasts and stromules are labeled with stromal GFP. Some stromules are indicated by white arrows. (Scale bars: 10 μm.)

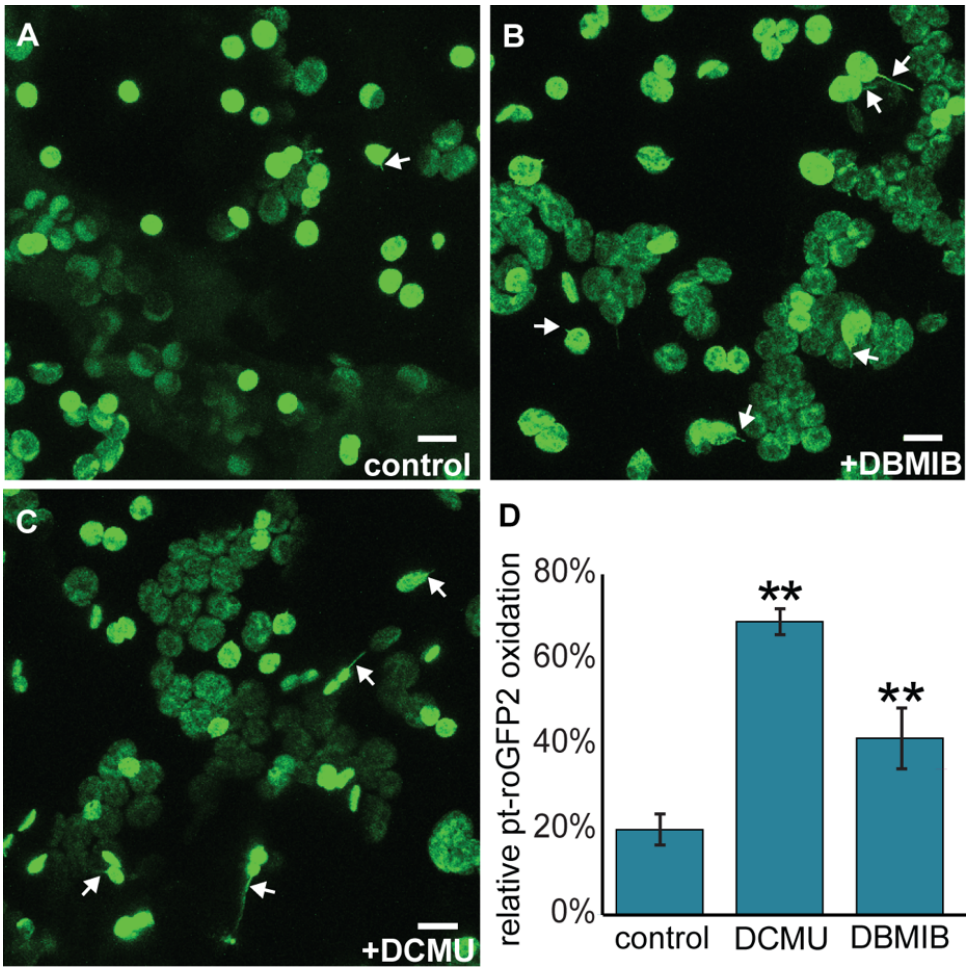


**Fig. S2**. **Oxidation of stromal redox buffers by ROS from photosynthesis induces stromules in chloroplasts.** (**A-C**) Representative images of stromule formation with control (**A**), DBMIB (**B**), and DCMU (**C**) treatments in *N. benthamiana* chloroplasts. (**D**) Both DBMIB and DCMU cause strong oxidation of chloroplast redox buffers, as measured by pt-roGFP2 in *A. thaliana* cotyledons. n ≥28. **p < 0.01. Chloroplasts and stromules are labeled with stromal GFP. Some stromules are indicated by white arrows. Error bars indicate ± SE. (Scale bars: 10 μm.)

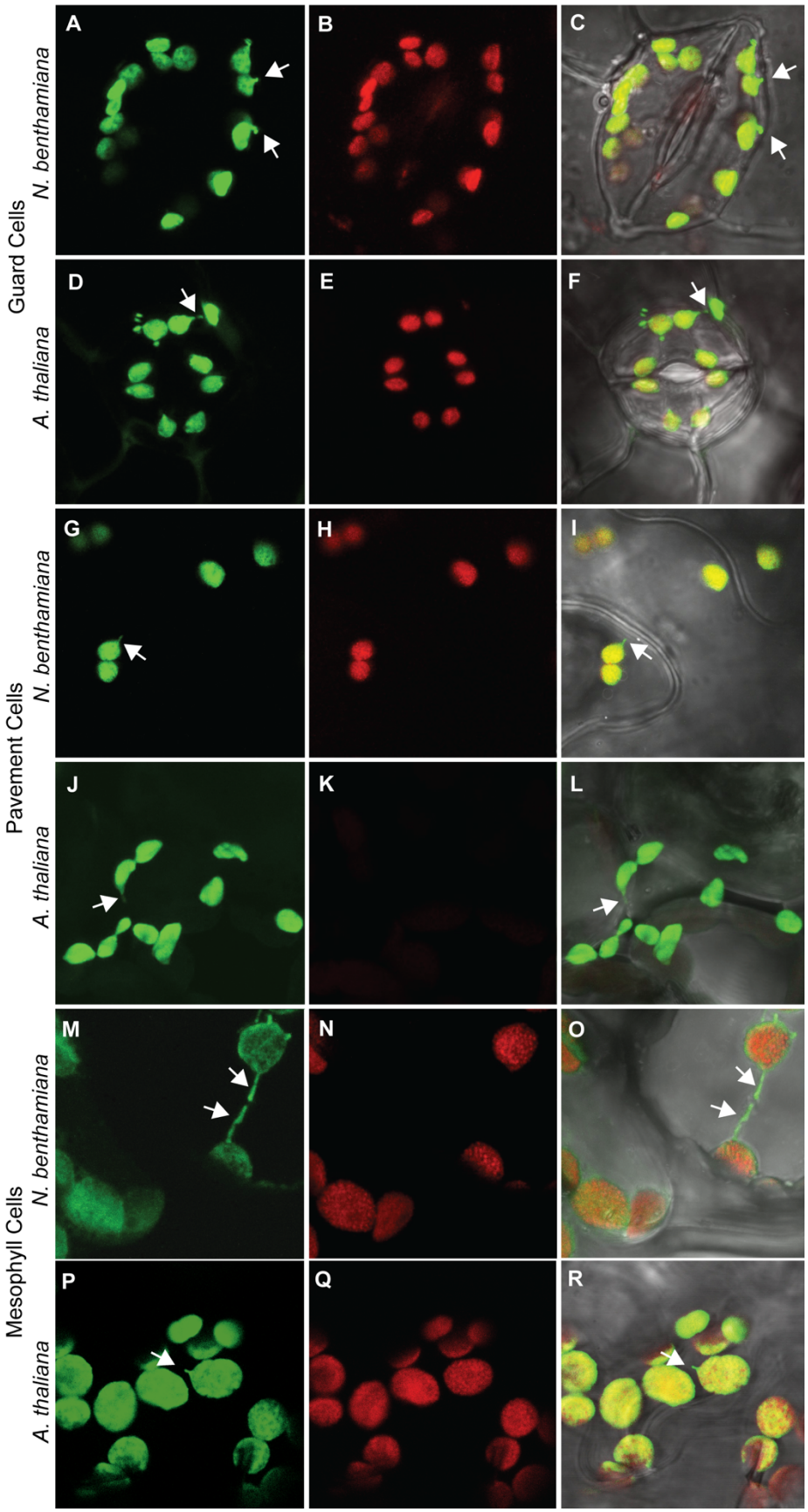
Guard Cells
Pavement Cells
Mesophyll Cells
N. benthamiana
A. thaliana
N. benthamiana
A. thaliana
N. benthamiana
A. thaliana
A
B
C
D
E
F
G
H
I
J
K
L
M
N
O
P
Q
R

(continued from previous page)

**Fig. S3**. **Representative images of chloroplasts and leucoplasts in *N. benthamiana* and *A. thaliana* visualized with confocal laser scanning microscopy.** Guard cells (**A-C** and **D-F**), pavement cells (**G-I** and **J-L**), and mesophyll cells (**M-O** and **P-R**) all contain chloroplasts in *N. benthamiana*, as do *A. thaliana* guard cells (**E**) and mesophyll cells (**Q**); however, *A. thaliana* pavement cells (**J-L**) have leucoplasts that lack chlorophyll (**K**). Green, stromal GFP; red, chlorophyll autofluorescence; gray, transmitted light. Some stromules are indicated by white arrows.

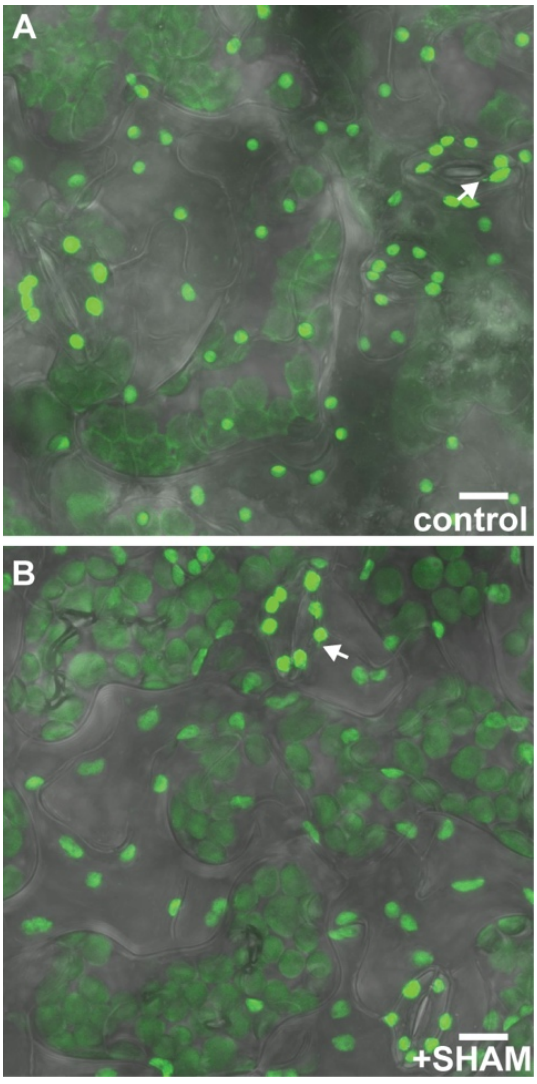


**Fig. S4**. **SHAM does not impact stromule frequency in *A. thaliana* guard cells.** Stromule frequency is similar in guard cells with control treatment (**A**) and those with SHAM treatment (**B**). Green, stromal GFP; gray, transmitted light. Some stromules are indicated by white arrows. (Scale bars: 10 μm.)

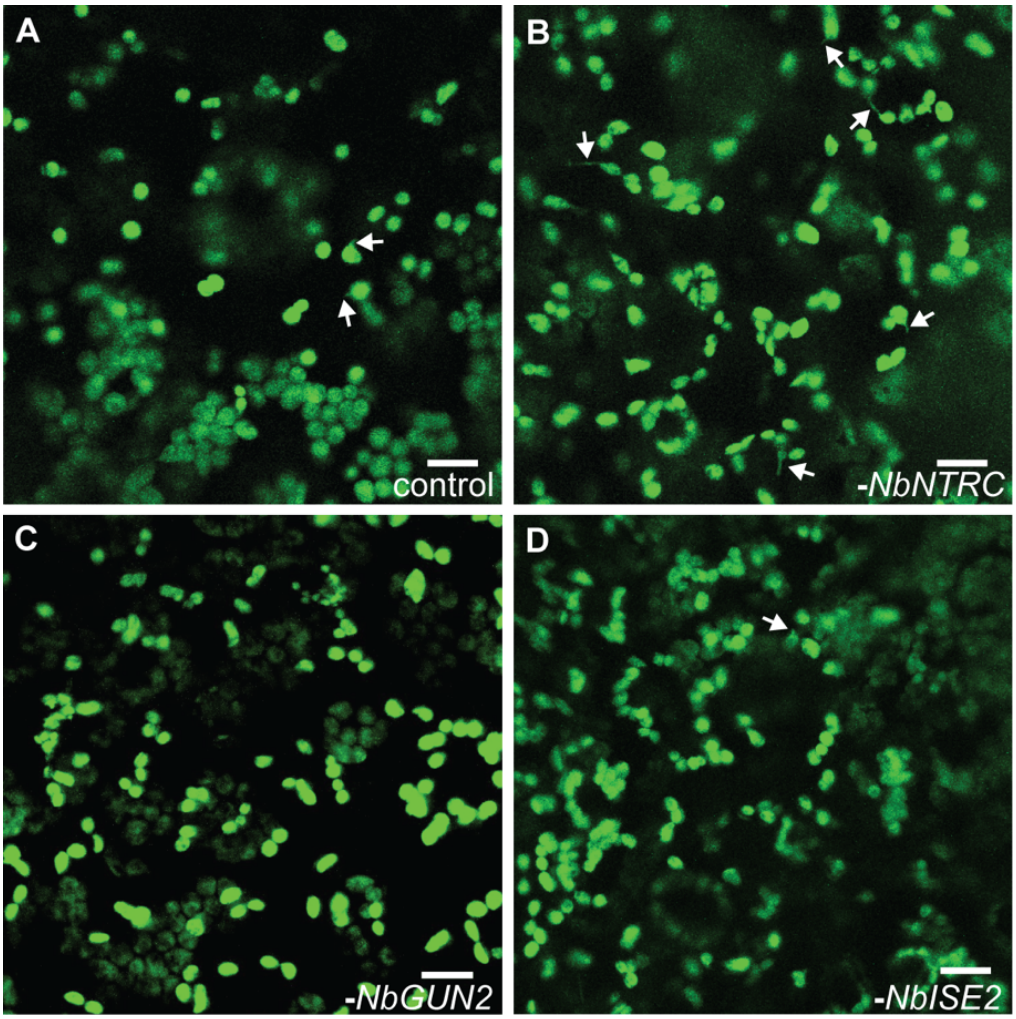


**Fig. S5**. **Representative images of stromule frequency in *N. benthamiana* after silencing.** VIGS of *NbNTRC* (**B**), *NbGUN2* (**C**), or *NbISE2* (**D**), versus control (**A**). Green, stromal GFP. Some stromules are indicated by white arrows. (Scale bars: 10 μm.)


86_N_benthamiana_NbS00002296g0006_1
87_N_benthamiana_NbS00031948g0007_1
67_S_tuberosum_PGSC0003DMP400052173
81_S_lycopersicum_Solyc12g009470_1_1
2_S_bicolor_Sb10g023510_1
40_Z_mays_GRMZM2G101004_T01
37_Z_mays_GRMZM2G043277_T02
30_S_italica_Si007047m
39_Z_mays_GRMZM2G157936_T01
3_S_bicolor_Sb10g023550_1
31_S_italica_Si008723m
45_B_distachyon_Bradi1g36640_1
66_O_sativa_LOC_Os06g40080_1
21_P_patens_Pp1s158_129V6_2
22_P_patens_Pp1s47_217V6_1
4_S_moellendorfii_97989
48_A_coerulea_Aquca_001_00890_1
25_A_thaliana_AT2G26670_1
5_A_lyrata_481532
41_C_rubella_Carubv10023804m
28_A_thaliana_AT1G69720_1
7_A_lyrata_315973
43_C_rubella_Carubv10021525m
27_A_thaliana_AT1G58300_1
6_A_lyrata_475436
44_C_rubella_arubv10021693m
34_E_salsugineum_Thhalv10024084m
53_B_rapa_Bra027878
33_E_salsugineum_Thhalv10002061m
52_B_rapa_Bra012054
55_B_rapa_Bra040771
14_C_sativus_Cucsa_292760_1
49_Malus_x_domestica_MDP0000271045
50_Malus_x_domestica_MDP0000700015
15_P_persica_ppa009633m
69_G_max_Glyma06g29530_1
70_G_max_Glyma04g19030_1
78_P_vulgaris_Phvul_009G198100_1
80_F_vesca_mrna31036_1-v1_0-hybrid
24_C_sinensis_orange1_1g023201m
36_C_clementina_Ciclev10009114m
61_Egr_Eucgr_C04219_1
71_G_raimondii_Gorai_010G063800_1
82_T_cacao_Thecc1EG038078t1
57_L_usitatissimum_Lus10030092
58_L_usitatissimum_Lus10005718
11_R_communis_28320_m001133
19_M_esculenta_cassava4_1_013127m
75_Ptr_Potri_006G069700_1
76_P_trichocarpa_Potri_018G131700_1
74_G_raimondii_Gorai_013G234100_1
72_G_raimondii_Gorai_009G017800_1
18_V_vinifera_GSVIVT01015535001
9_C_papaya_evm_model_supercontig_75_25
60_E_grandis_Eucgr_C01176_1
88_N_benthamiana_NbS00001374g0008_1
89_N_benthamiana_NbS00052272g0009_1
85_S_tuberosum_PGSC0003DMP400014047
84_S_lycopersicum_Solyc04g079290_2_1
17_V_vinifera_GSVIVT01009554001
47_A_coerulea_Aquca_015_00123_1
26_A_thaliana_AT2G26550_1
8_A_lyrata_481515
42_C_rubella_Carubv10023752m
32_E_salsugineum_Thhalv10008345m
54_B_rapa_Bra023283
16_P_persica_ppa009873m
51_Malus_x_domestica_MDP0000231307
73_G_raimondii_Gorai_009G275400_1
83_Tca_Thecc1EG033890t2
62_E_grandis_Eucgr_F02368_1
23_C_sinensis_orange1_1g021151m
35_C_clementina_Ciclev10001892m
20_M_esculenta_cassava4_1_014396m
12_R_communis_30170_m013919
56_L_usitatissimum_Lus10021748
59_L_usitatissimum_Lus10042666
13_C_sativus_Cucsa_123530_1
10_C_papaya_evm_TU_contig_24415_14
77_P_trichocarpa_Potri_014G034200_1
65_Osa_LOC_Os03g27770_1
46_B_distachyon_Bradi1g60540_1
29_S_italica_Si036671m
1_S_bicolor_Sb01g033330_1
38_Z_mays_GRMZM2G004222_T01
63_P_virgatum_Pavirv00024077m
64_P_virgatum_Pavirv00006617m
68_G_max_Glyma14g08880_1
79_P_vulgaris_PhvuT_001G019900_1
0.1
HO1-like Family
HO2-like Family

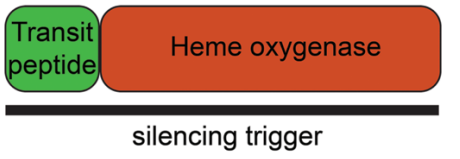
Transit peptide
Heme oxygenase
silencing trigger


TRV-GUS
TRV-GUN2

(continued from previous page)

**Fig. S6**. **Identification of *GUN2* orthologs in *N. benthamiana*. A gene tree of heme oxygenases arranged homologs into two clades: *HO1* (or *GUN2*)-like and *HO2*-like.** (Upper) *N. benthamiana* has two *HO1* homeologs. (Lower Left) The silencing trigger against *NbGUN2* was designed to cover the entire gene sequence (837 bp). (Lower Right) Silencing *NbGUN2* caused expected phenotypes, such as chlorosis.

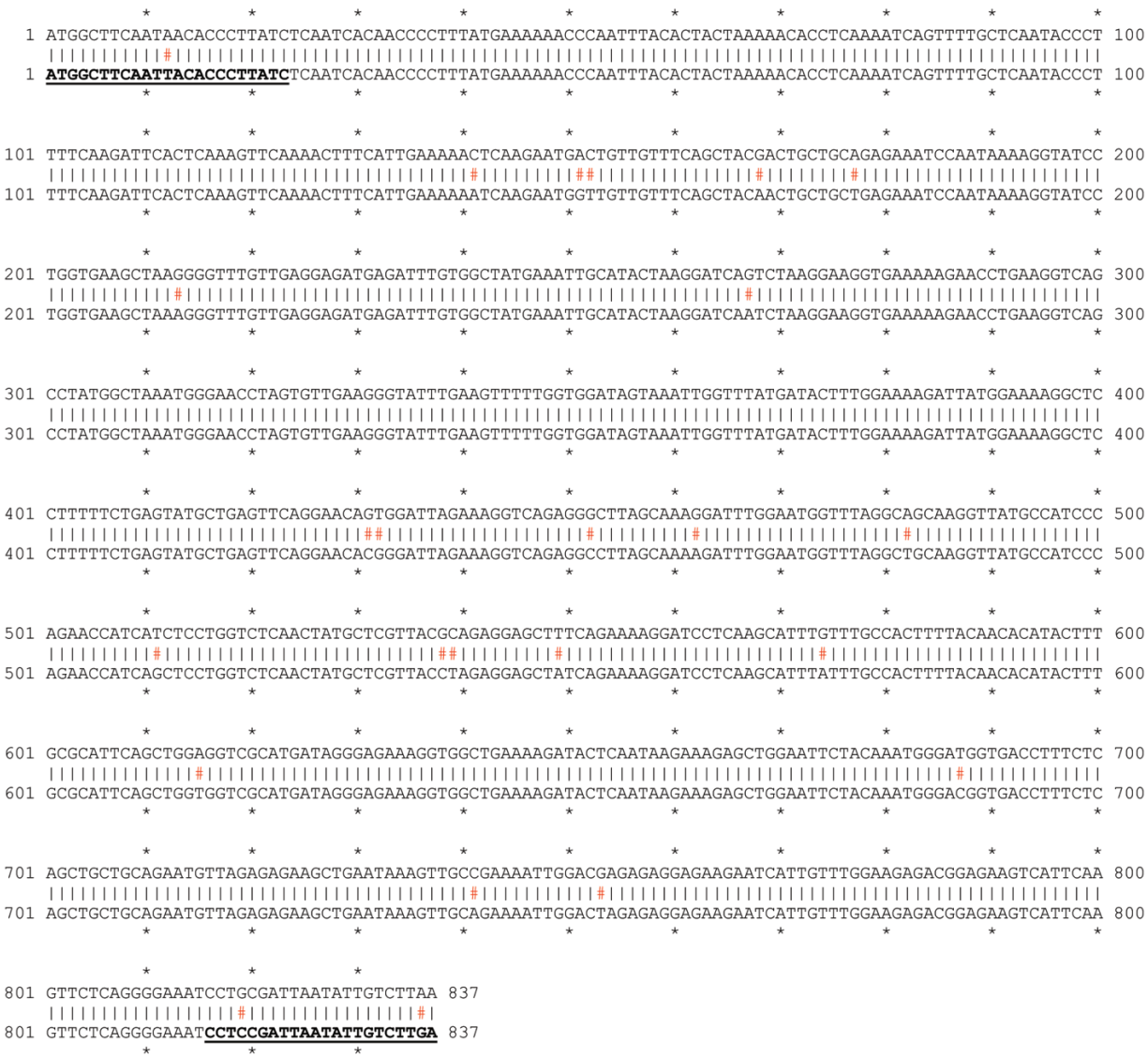


**Fig. S7**. **The silencing trigger for *NbGUN2* (bottom line) was cloned using primers specific to *NbGUN2a* (NbS00031948g0007).** Here, the silencing trigger is aligned against the homeologous gene, *NbGUN2b* (NbS00002296g0006). Mismatches are indicated with red hashtags, aligned primer sequences are in bold type and underscored.

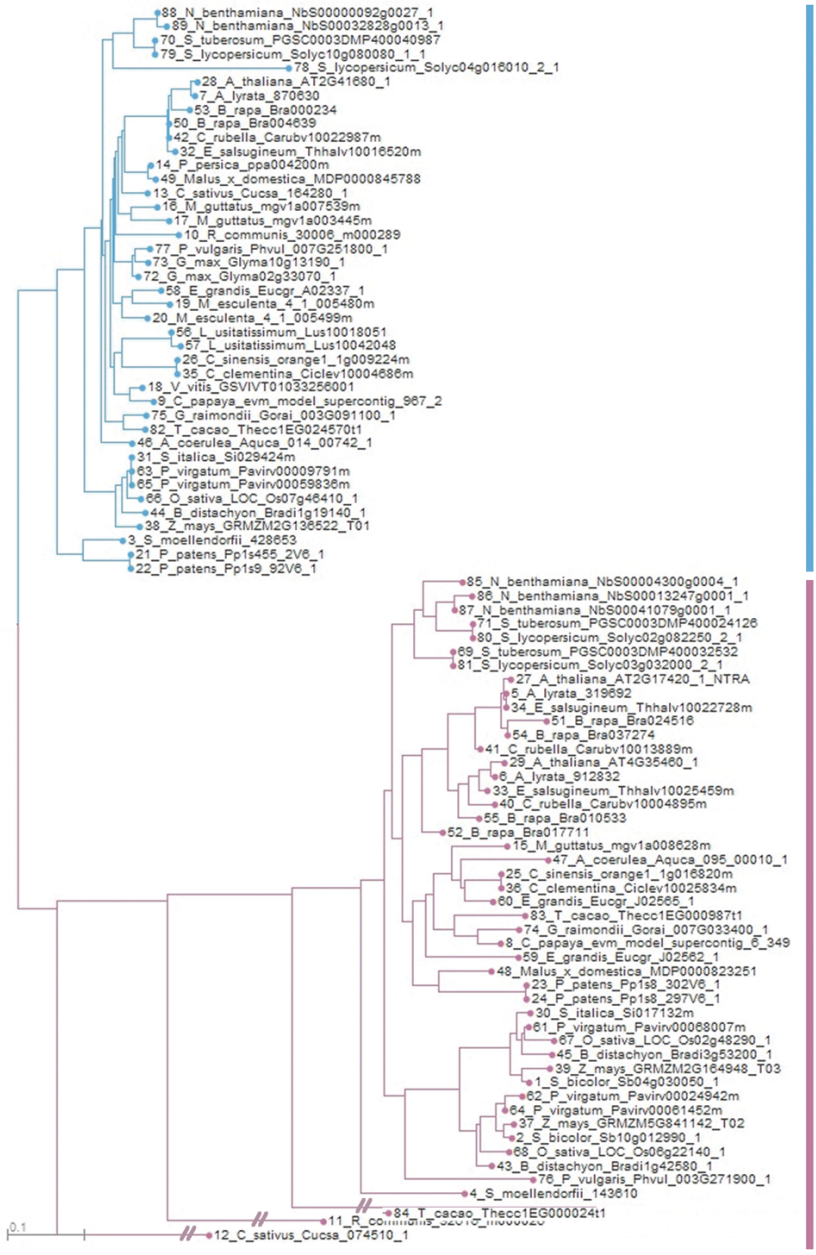
88_N_benthamiana_NbS00000092g0027_1
89_N_benthamiana_NbS00032828g0013_1
70_S_tuberosum_PGSC0003DMP400040987
79_S_lycopersicum_Solyc10g080080_1_1
78_S_lycopersicum_Solyc04g016010_2_1
28_A_thaliana_AT2G41680_1
7_A_lyrata_870630
53_B_rapa_Bra000234
50_B_rapa_Bra004639
42_C_rubella_Carubv10022987m
32_E_salsugineum_Thhalv10016520m
14_P_persica_ppa004200m
49_Malus_x_domestica_MDP0000845788
13_C_sativus_Cucsa_164280_1
16_M_guttatus_mgv1a007539m
17_M_guttatus_mgv1a003445m
10_R_communis_30006_m000289
77_P_vulgaris_Phvul_007G251800_1
73_G_max_Glyma10g13190_1
72_G_max_Glyma02g33070_1
58_E_grandis_Eucgr_A02337_1
19_M_esculenta_4_1_005480m
20_M_esculenta_4_1_005499m
56_L_usitatissimum_Lus10018051
57_L_usitatissimum_Lus10042048
26_C_sinensis_orange1_1g009224m
35_C_clementina_Ciclev10004686m
18_V_vitis_GSVIVT01033256001
9_C_papaya_evm_model_supercontig_967_2
75_G_raimondii_Gorai_003G091100_1
82_T_cacao_Thecc1EG024570t1
46_A_coerulea_Aquca_014_00742_1
31_S_italica_Si029424m
63_P_virgatum_Pavirv00009791m
65_P_virgatum_Pavirv00059836m
66_O_sativa_LOC_Os07g46410_1
44_B_distachyon_Bradi1g19140_1
38_Z_mays_GRMZM2G136522_T01
3_S_moellendorfii_428653
21_P_patens_Pp1s455_2V6_1
22_P_patens_Pp1s9_92V6_1
NTRC family
85_N_benthamiana_NbS00004300g0004_1
86_N_benthamiana_NbS00013247g0001_1
87_N_benthamiana_NbS00041079g0001_1
71_S_tuberosum_PGSC0003DMP400024126
80_S_lycopersicum_Solyc02g082250_2_1
69_S_tuberosum_PGSC0003DMP400032532
81_S_lycopersicum_Solyc03g032000_2_1
27_A_thaliana_AT2G17420_1_NTRA
5_A_lyrata_319692
34_E_salsugineum_Thhalv10022728m
51_B_rapa_Bra024516
54_B_rapa_Bra037274
41_C_rubella_Carubv10013889m
29_A_thaliana_AT4G35460_1
6_A_lyrata_912832
33_E_salsugineum_Thhalv10025459m
40_C_rubella_Carubv10004895m
55_B_rapa_Bra010533
52_B_rapa_Bra017711
15_M_guttatus_mgv1a008628m
47_A_coerulea_Aquca_095_00010_1
25_C_sinensis_orange1_1g016820m
36_C_clementina_Ciclev10025834m
60_E_grandis_Eucgr_J02565_1
83_T_cacao_Thecc1EG000987t1
74_G_raimondii_Gorai_007G033400_1
8_C_papaya_evm_model_supercontig_6_349
59_E_grandis_Eucgr_J02562_1
48_Malus_x_domestica_MDP0000823251
23_P_patens_Pp1s8_302V6_1
24_P_patens_Pp1s8_297V6_1
30_S_italica_Si017132m
61_P_virgatum_Pavirv00068007m
67_O_sativa_LOC_Os02g48290_1
45_B_distachyon_Bradi3g53200_1
39_Z_mays_GRMZM2G164948_T03
1_S_bicolor_Sb04g030050_1
62_P_virgatum_Pavirv00024942m
64_P_virgatum_Pavirv00061452m
37_Z_mays_GRMZM5G841142_T02
2_S_bicolor_Sb10g012990_1
68_O_sativa_LOC_Os06g22140_1
43_B_distachyon_Bradi1g42580_1
76_P_vulgaris_Phvul_003G271900_1
4_S_moellendorfii_143610
84_T_cacao_Thecc1EG000024t1
11_R_communis_32016_m000020
12_C_sativus_Cucsa_074510_1
0.1
NTRA/B family


Transit peptide
NADPH oxidoreductase domain
Thioredoxin domain
silencing trigger


TRV-GUS
TRV-NbNTRC

(continued from previous page)

**Fig. S8**. **Identification of *NTRC* orthologs in *N. benthamiana*.** (Upper) A gene tree based on *AtNTRC* arranged homologs into two clades: *NTRA/NTRB-like* and *NTRC-like. N. benthamiana* has two *NTRC* homeologs. (Lower Left) The silencing trigger against *NbNTRC* was designed against a sequence that encodes part of the NADPH oxidoreductase domain. (Lower Right) Plants without gene silencing (*TRV-GUS*) appeared similar to plants silencing *NbNTRC* expression (*TRV-NbNTRC*).

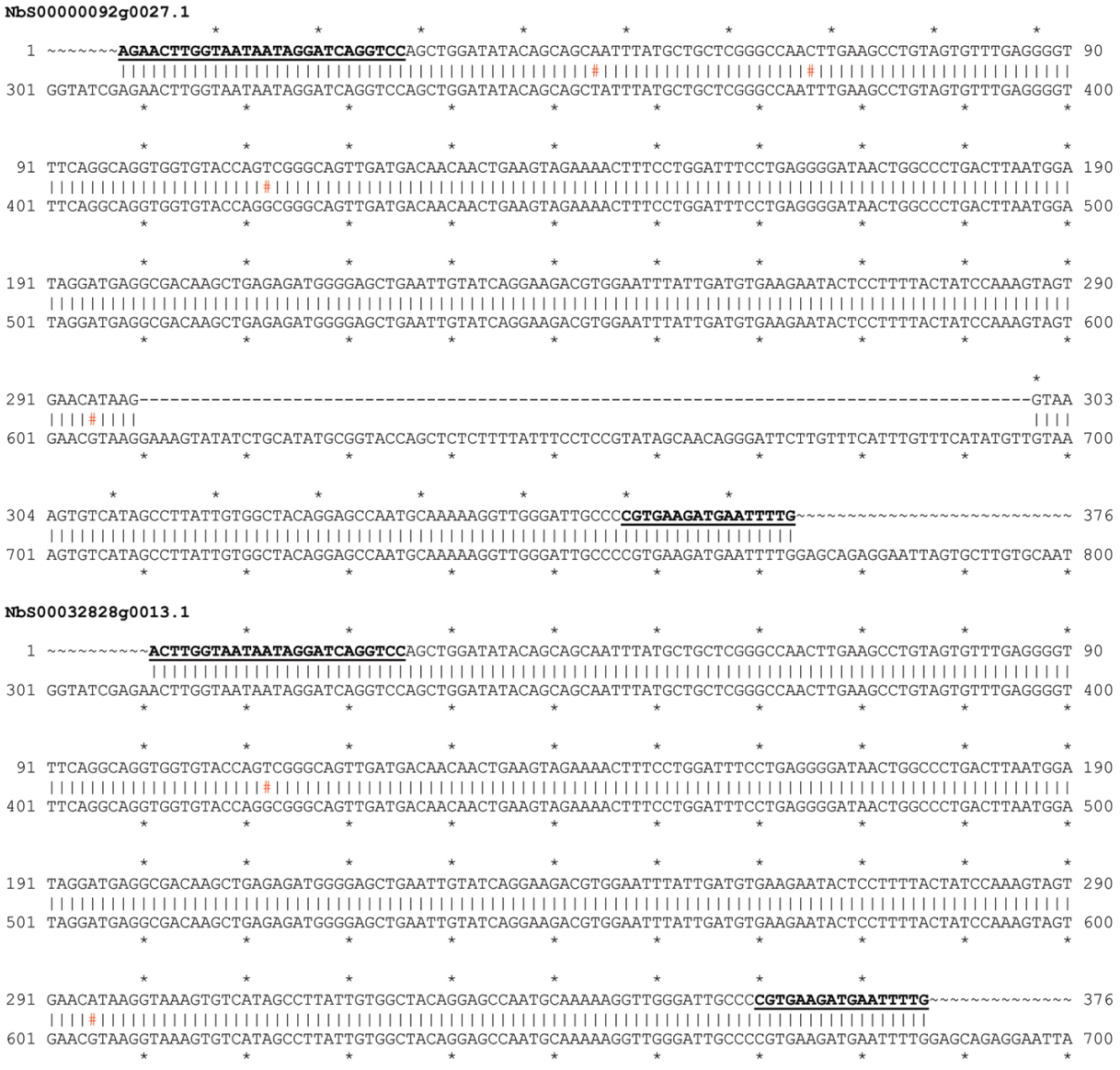


**Fig. S9**. **The silencing trigger for *NbNTRC* (top line) was cloned using primers specific to either *NbNTRC* homeolog.** The annotated cDNA sequence of Nb00000092g0027.1 includes an intron (numbered here as nucleotides 610–696; bottom row, top alignment) that was not detected in any of the sequences we cloned, and is thus likely a misannotation or rare isoform. Accounting for this discrepancy, the silencing trigger is ~99% identical to both *NbNTRC* homeologs. Mismatches are indicated with red hashtags; aligned primer sequences are in bold type and underscored.

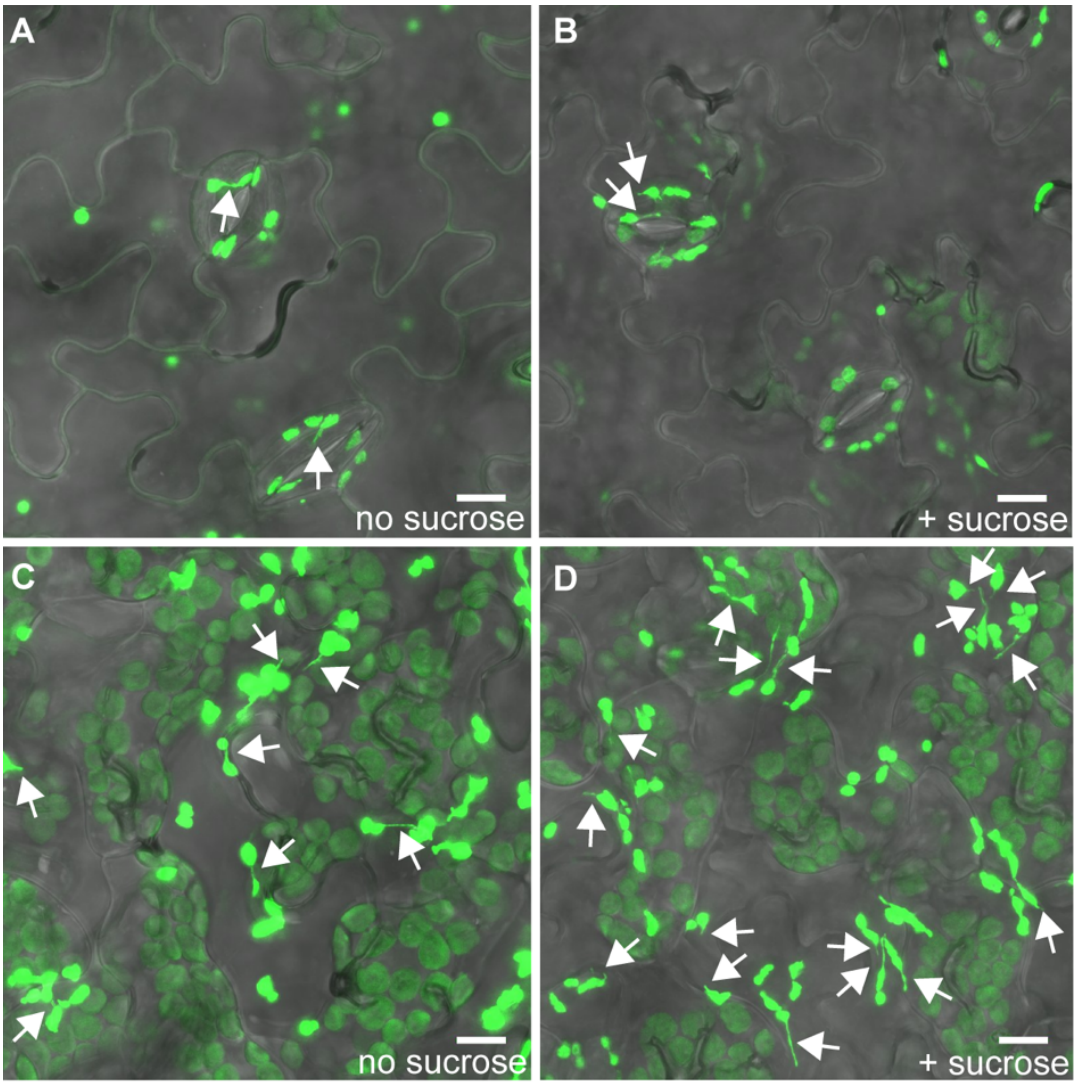


**Fig. S10**. **Sucrose increases leucoplast but not chloroplast stromule frequency.** Representative images of stromule frequency with and without sucrose treatment in *A. thaliana* epidermal cells. Stromule frequency is similar in chloroplasts (found in guard cells in the epidermis) without sucrose treatment (**A**) or with sucrose treatment (**B**). Sucrose treatment increases stromule frequency in leucoplasts (**D**) compared with control (**C**). Plastids and stromules are labeled with stromal GFP (green). Some stromules are indicated by white arrows. (Scale bars: 10 μm.)

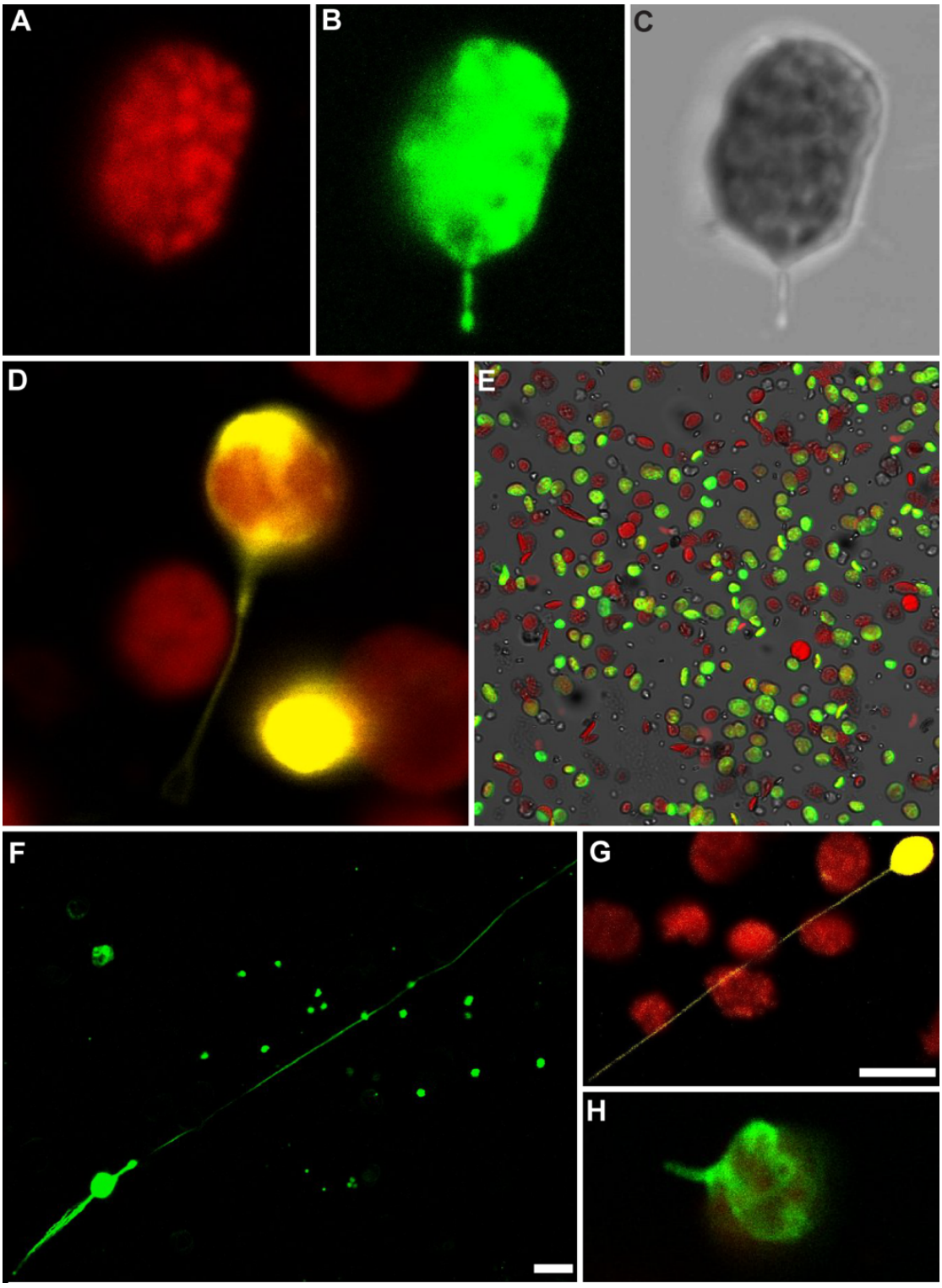
A
B
C
D
E
F
G
H

(continued from previous page)

**Fig. S11. Stromules of isolated chloroplasts visualized by confocal microscopy and 3D-SIM.** (**A-C**) After extraction from cells, isolated chloroplasts of *N. benthamiana* have stromules, as visualized by either stromal GFP fluorescence (**B**) or transmitted light (**C**), whereas chlorophyll autofluorescence remains restricted to the thylakoids (**A**). (**D**) CFDA also labels stromules in isolated *N. benthamiana* chloroplasts (CFDA, yellow; chlorophyll, red). (**E**) Representative example of sample purity after chloroplast isolation protocol. Many chloroplasts are fully intact, with stromal GFP (green); some were damaged during extraction and have lost stromal GFP, but retain the thylakoid membranes (chlorophyll autofluorescence, red); and very small quantitites of nonfluorescent materials remain with the sample (transmitted light, gray). (**F and G**) After isolation, some *N. benthamiana* chloroplasts have stromules that are very long, as visualized by GFP (**F**, in green) or CFDA staining (**G**, in yellow; chlorophyll autofluorescence, red). (**H**) Isolated *A. thaliana* chloroplasts expressing stromal roGFP2 (green) also have stromules after extraction from cells. (Scale bars: 5 μm.)

**Supplementary Videos**

Note: Supplementary Videos are in separate files.

**Video S1. Time lapse video of an isolated *N. benthamiana* chloroplast forming a new stromule.** The video is 66× accelerated at 6 frames/s, covering a total of 22 min. Chloroplasts are labeled with stromal GFP.

**Video S2. Time lapse video of an isolated *N. benthamiana* chloroplast forming a new stromule.** The video is 66× accelerated at 6 frames/s, covering a total of 22 min. Chloroplasts are labeled with stromal GFP.

**Video S3. Superresolution z-stack sections of a *N. benthamiana* chloroplast visualized with live cell 3D-SIM showing that stromule width varies along the length of the stromule.** Each frame progresses the focal plane 100 nm through the z axis of the 3D-SIM reconstruction.

**Supplementary Materials and Methods**

Virus Induced Gene Silencing

*GUN2* (TAIR ID AT2G26670) and *NTRC* (TAIR ID AT2G41680) orthologs in *N. benthamiana* were identified from gene trees generated by BLAST searches using *A. thaliana* protein sequence queries (Figs. S6–S9*). N. benthamiana* is an allotetraploid resulting from the hybridization of two *Nicotiana* species, and thus often has two homeologs of genes that are single copy in *A. thaliana*. Moreover, both *GUN2* and *NTRC* are members of larger gene families. In *A. thaliana*, there are three NADPH-dependent thioredoxin reductases (*NTRA* and *NTRB* in the cytosol and mitochondria,

and *NTRC* in plastids) and four heme oxygenases (*HO1*, *HO3*, and *HO4* are closely related and partially redundant, whereas *HO2* serves a distinct function) (**Gisk et al., 2010; Reichheld et al., 2007**).

To identify all true orthologs of *NTRC* and *HO1* and design silencing constructs targeting these genes, but not orthologs of *NTRA*/*NTRB* or *HO2*, we used *A. thaliana* protein sequences in a BLAST search against the *N. benthamiana* genome (v0.4.4 predicted cDNAs) from the Sol Genomics Network (solgenomics.net) and also against the land plant genomes available at Phytozome (www.phytozome.net). Amino acid sequences of these putative homologs were aligned with MAFFT (mafft.cbrc.jp) using the highly accurate L-INS-i algorithm. Aligned residues were used to generate a gene tree with the neighbor-joining method using 100 samples for bootstrapping. Silencing triggers were then designed to silence all copies of the target genes but no other genes in the *N. benthamiana* genome, using BLAST searches to confirm that no genomic sequence between 20 and 24 nucleotides long matched the silencing trigger with fewer than three mismatches.

*NbISE2*, *NbGUN2*, and *NbNTRC* were silenced using VIGS as described by **Brunkard et al. (2015)** alongside a viral negative control, pYC1 [Tobacco rattle virus (TRV) with a mock silencing trigger against β-glucoronidase]. In brief, to prepare the silencing constructs, RNA was extracted from *N. benthamiana* genotype Nb-1 (Spectrum Plant Total RNA Kit; Sigma-Aldrich) and treated with DNase I (New England Biolabs). This RNA was used to synthesize cDNA with SuperScript III Reverse Transcriptase (Invitrogen) and oligo(dT)20 primers. Silencing triggers were then amplified and inserted into the TRV-derived VIGS vector, pYL156, using standard restriction enzyme-based methods (**Brunkard et al., 2015**).

Oligonucleotides

Oligonucleotides used to clone silencing triggers are shown with restriction sites underscored and nucleotides matching the genomic sequences in upper case:

*NbGUN2*_F: 5'gattctagaATGGCTTCAATTACACCCTTATC3'

*NbGUN2*_R: 5'gatctcgagTCAAGACAATATTAATCGGAGG3'

*NbNTRC*_F: 5'gtatctAGAACTTGGTAATAATAGGATCAGGTCC3'

*NbNTRC*_R: 5'ctgctcgagCAAAATTCATCTTCACG3'

**Supplementary Materials References**

**Gisk B, Yasui Y, Kohchi T, and Frankenberg-Dinkel N** (2010) Characterization of the haem oxygenase protein family in *Arabidopsis thaliana* reveals a diversity of functions. *Biochem J* **425**, 425-434.

**Reichheld JP, Khafif M, Riondet C, Droux M, Bonnard G, and Meyer Y** (2007) Inactivation of thioredoxin reductases reveals a complex interplay between thioredoxin and glutathione pathways in *Arabidopsis* development. *Plant Cell* **19**, 1851-1865.

**Brunkard JO, Burch-Smith TM, Runkel AM, and Zambryski PC** (2015b) Investigating plasmodesmata genetics with virus-induced gene silencing and an *Agrobacterium*-mediated GFP movement assay. *Methods Mol Biol* **1217**, 185-198.